DEVELOPMENT OF PH-RESPONSIVE NANO-POLYPLEXES FOR INTRACELLULAR DELIVERY OF THERAPEUTIC BIOMACROMOLECULES

By

Brian Connor Evans

Dissertation

Submitted to the Faculty of the

Graduate School of Vanderbilt University

in Partial Fulfillment of the Requirements

for the Degree of

DOCTOR OF PHILOSOPHY

in

Biomedical Engineering

May, 2015

Nashville, Tennessee

Approved:

Craig. L. Duvall, Ph.D.

Hak-Joon Sung, Ph.D.

Todd D. Giorgio, Ph.D.

Colleen M. Brophy, M.D.

James R. Goldenring, M.D., Ph.D.

To my parents, Debbie and David, who have given me every opportunity in life to succeed,

to my family, Nanny, Eric, Rachel, Cash, and Dax who have supported and loved me through all that I do,

and Melissa, my munchkin,

ACKNOWLEDGEMENTS

First and foremost, I would like to thank my advisor and mentor Dr. Craig Duvall. His drive, intelligence, and unwavering devotion to his work and his students are all traits that I will strive to emulate throughout the rest of my career. His guidance, insight, and friendship have seen me through my failures and my successes, and I will forever be grateful to Craig for driving me to succeed throughout graduate school. I would also like to thank Dr. Colleen Brophy for her patience and oversight during the past five years. She, along with her lab, has provided me with invaluable resources and guidance that made this work possible. I would also like to thank my other committee members, Dr. Todd Giorgio, Dr. Hak-joon Sung, and Dr. James Goldenring for their feedback and advisement that have helped to shape this work and better myself as a researcher.

I would like to especially thank Dr. Kyle Hocking for the immense amount of work he contributed to this project and for his friendship and encouragement throughout graduate school. I would also like to thank Drs. Michael Osgood and Igor Voskresensky for their countless hours completing rabbit surgeries. I would also like to thank Drs. Joyce Cheung-Flynn and Padmini Komalavilas for their aid in designing and carrying out experiments and Dr. Eric Wise for his help in obtaining human tissue for experiments. I would also like to thank Kameron Kilchrist for his aid in this work, and the undergraduate researchers that I have had the pleasure of mentoring over the past five years and who have all made significant contributions to these studies: Julia Dmowska, Mitchell Weisenberger, Cristina Contreras, and Sayali Belsare.

Additionally, I would like to thank my fellow lab mates, specifically Mukesh Gupta, Chris Nelson, Kameron Kilchrist, Martina Miteva, Kelsey Beavers, Lucas Hofmeister, Angela Zachman, Spencer Crowder, Shann Yu, Samantha Sarett, and John Martin for their feedback on this project and for their comradery throughout graduate school.

Confocal imaging was performed using a Zeiss LSM 710 Inverted Confocal Microscope through the use of the VUMC Cell Imaging Shared Resource, (supported by NIH Grants CA68485, DK20593, DK58404, HD15052, DK59637, and Ey008126). Dynamic light scattering and TEM were conducted through the use of the core facilities of the Vanderbilt Institute of Nanoscale Sciences and Engineering (VINSE). Histological sectioning and immunostaining were performed in part by the Vanderbilt

Translational Pathology Shared Resource (TPSR). This work was supported by NIH grant 1R21HL110056-01, AHA scientist development grant 11SDG4890030, and the NSF graduate research fellowship program.

TABLE OF CONTENTS

Page

LIST OF TABLES

Table Page

LIST OF EQUATIONS

Equation

LIST OF FIGURES

LIST OF ABBREVIATIONS

ANG II – angiotensin II
CR – charge ratio
CREB – cyclic adenosine monophosphate element binding protein
CVD – cardiovascular disease
D_6MSO – deuterated dimethyl sulfoxide
DLS – dynamic light scattering
DMF – dimethyl formamide, LiBR – lithium bromide
EEA1 – early endosomal antigen 1
ESI-MS – electrospray ionization mass spectrometry
F-actin – filamentous actin
G-actin – globular actin
GAPDH – glyceraldehyde 3-phosphate dehydrogenase
GPC – gel permeation chromatography
HCAVSMC – human coronary artery vascular smooth muscle cell
HIV – human immunodeficiency virus
hnRNP A0 – heterogeneous nuclear ribonucleoprotein A0
HSP20 – heat shock protein 20
HSP27 – heat shock protein 27
HSV – human saphenous vein
HUVEC – human umbilical vein endothelial cells
IL-6 – Interleukin 6
IV – intravenous
LAMP1 – lysosomal associated protein 1
LDH – lactate dehydrogenase
LDPI – laser Doppler perfusion imaging
LIM-K – Lim Kinase
MCP – monocyte chemoattractant protein
MEK ½ - mitogen activated protein kinase kinase ½
MIP – macrophage inflammatory protein
MK2 – mitogen activated protein kinase activated protein kinase II
MK2i – MK2 inhibitory peptide
NMR – nuclear magnetic resonance
NO – nitrous oxide
NP – nano-polyplex
NP – nano-polyplex
p38 MAPK – p38 mitogen activated protein kinase
PE - phenylephrine
p-HSP20 – phosphorylated HSP20 mimetic peptide,
PKA – protein kinase A
PKG – protein kinase G
SAH – subarachnoid hemorrhage
SNP – sodium nitroprusside
TAT – transactivator of transcription
TNF-α – tumor necrosis factor alpha
TTP – tristetraprolin,

CHAPTER I

INTRODUCTION

Peptide Delivery Barriers

The therapeutic potential of peptides, proteins, and antibodies in applications ranging from cancer treatments to vascular pathologies has become more apparent as the fundamental etiology of these disease states becomes more comprehensively characterized [Wilson, 2009 #321;Alexander, 2005 #120;Craik, 2013 #273;Ewing, 2011 #178;Gizard, 2008 #203;Ni, 2010 #263;Hata, 2005 #206]. However, major *in vivo* barriers exist to effective intracellular delivery of peptide-based, biomacromolecular therapeutics for specific applications: proteolysis of the peptide in the *in vivo* environment prior to or following cellular internalization, circumvention of non-specific binding and/or side-effects, translocation across the lipid bilayer that constitutes the cell membrane, escape from the intracellular endo-lysosomal and exocytosis trafficking pathways, and achieving an effective peptide dose within the intracellular micro-environment where the therapeutic target is located (**fig. 1.1**) [5-8]. A wide array of approaches have been investigated to address these delivery barriers ranging from the utilization of drug delivery vehicles that improve

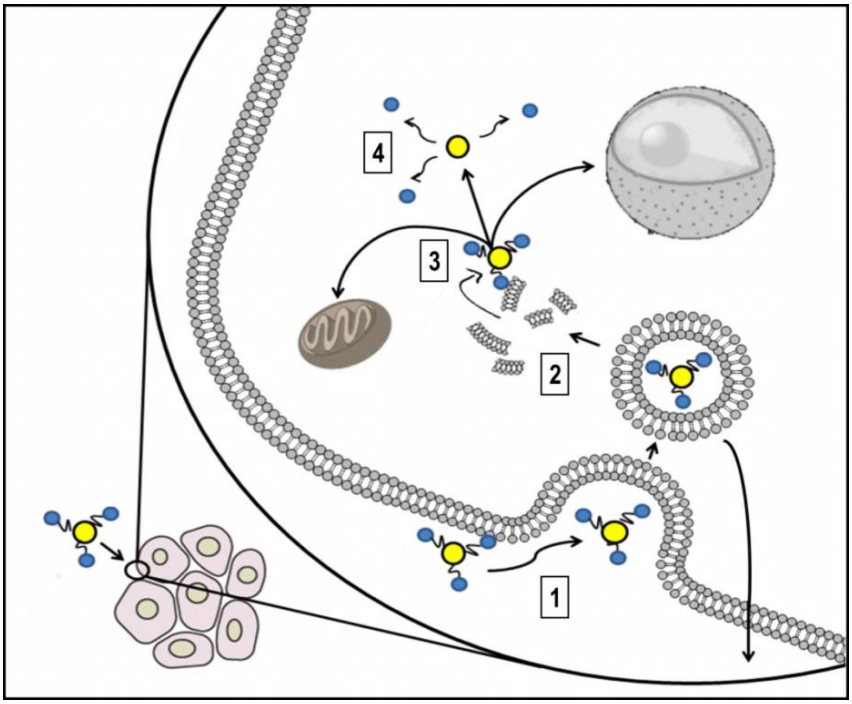

Figure 1.1 - Intracellular peptide delivery barriers: 1) Biomacromolecular therapeutics like peptides must first translocate the cellular membrane and become internalized in the cell. 2) Once internalized, the therapeutic must escape from the endo-lysosomal pathway or consequently face degradation in lysosomes and/or trafficking for exocytosis out of the cell. 3) Finally, if a drug delivery vehicle is utilized to deliver the therapeutic then the vehicle must contain an inherent mechanism to release the therapeutic in order to avoid steric hindrance of bioactivity in the cytosol. Figure adopted with permission from [4].

proteolytic resistance and in vivo half-life [9-11] to the use of electroporation, or cell-penetrant/fusogenic peptides to increase cellular internalization [12-14]. In addition to these approaches, the study and use of colloidal drug carriers such as liposomes, micelles, and nanoparticles to deliver biomacromolecular therapeutics has increased dramatically in the past decade [15-17]. These colloidal drug carriers are attractive because they can be modified to be multi-functional in terms of containing targeting moieties [18], cell penetrating and/or fusogenic peptides [19, 20], and environmentally responsive 'smart' polymers that can facilitate escape from the endo-lysosomal trafficking pathway or trigger site-specific, release of the therapeutic payload [21-25]. Despite the advances made in overcoming these delivery barriers, substantial synthetic and functional limitations still exist in terms of multi-functional drug carriers that simultaneously address the key delivery barriers of stability, cellular uptake, escape from the endo-lysosomal pathway, and an effective means to 'un-package' or release the desired therapeutic into the proper intracellular micro-environment.

The Role of p38/MAPK Signaling in Vein Graft Failure

Cardiovascular disease (**CVD**) is the leading cause of death in the United States, with coronary heart disease responsible for more than 50% of CVD-related mortality (i.e., causing 1 of every 6 deaths) [26]. In terms of financial burden, the direct and indirect cost of coronary heart disease in the US were ~$200 billion in 2009, with a projected price increase of 100% between 2013 and 2030 [26] Coronary artery bypass grafting with autologous conduits remains the standard treatment for multi-vessel coronary heart disease. However, almost half of saphenous vein grafts fail within the first 18 months due to intimal hyperplasia (**IH**) [27]. Although intimal hyperplasia occurs normal physiologic conditions in the closing of the ductus arteriosus[28], pathologic intimal hyperplasia (also known as accelerated intimal hyperplasia) occurs in a variety of disease states, specifically in the context of vascular bypass grafting with autologous vein. Vein graft intimal hyperplasia is characterized by the migration and proliferation of smooth muscle cells into the intima and is associated with excess deposition of extracellular matrix [29]. This process results in the formation of a highly cellular lesion (i.e., neointima) that reduces vascular lumen area and ultimately leads to thrombosis and/or complete occlusion. No therapeutic approaches are sufficient to inhibit IH and improve graft patency in humans. Antithrombotic and antiplatelet agents, such

as warfarin, clopidogrel, and aspirin, have little or no effect on IH [30]. Two large clinical trials tested delivery of an E2F transcription factor decoy, designed to prevent smooth muscle proliferation, to coronary and peripheral vascular vein grafts, but these trials were unsuccessful at preventing graft failure [27, 31].

One of the underlying causes of IH is activation of the p38 mitogen activated protein kinase (p38 MAPK) pathway in vascular smooth muscle cells (VSMCs) owing to mechanical and biochemical stresses experienced by the graft during harvest as well as during post-transplant adaptation to arterial pressure (i.e., vein graft arterialization) [32]. p38 MAPK activates multiple pro-inflammatory and pro-fibrotic effectors implicated in IH (**fig. 1.22**) [33-35]. However, inhibitors of p38 MAPK have failed clinical trials because of the adverse effects associated with blocking this pleotropic, upstream mediator [36]. p38 phosphorylation of MK2 triggers its translocation from the nucleus to the cytosol [37]. Activated MK2 signals through downstream targets such as heat shock protein 27 (HSP-27), heterogeneous nuclear ribonucleoprotein A0 (hnRNP A0), and cyclic AMP response element binding protein (CREB) to promote VSMC migration [38], proliferation [39], and inflammatory cytokine production [35]—which combined lead to graft IH and failure. Although logical therapeutics, small molecule inhibitors of MK2 have failed to gain FDA approval owing to lack of specificity and solubility [40]. A highly specific, cell-penetrating peptide-based MK2 inhibitor (MK2i) has been developed [41] that is currently in phase I clinical trials for treatment of idiopathic pulmonary fibrosis and shows potential to reduce IH in vein transplants [42]. However, like

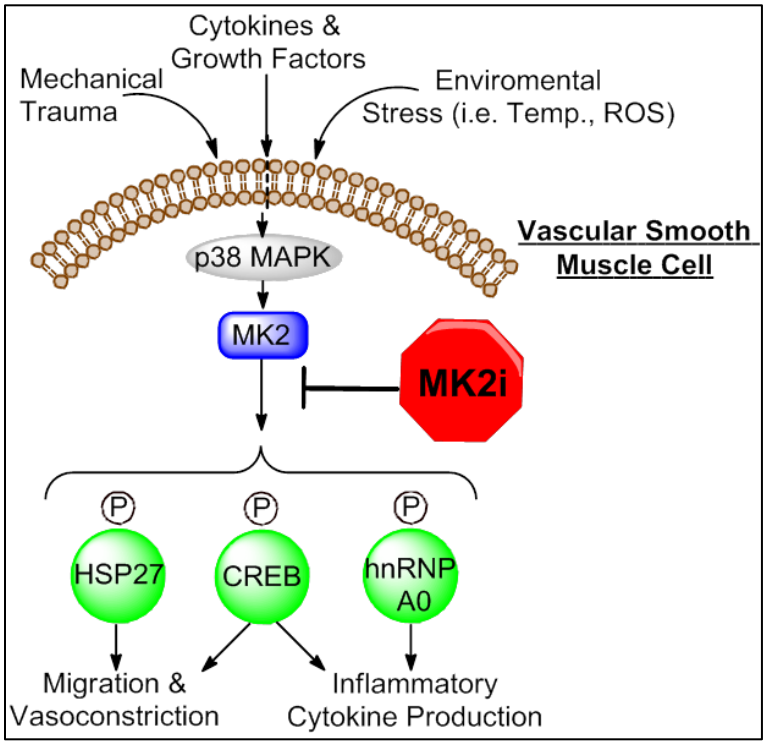

Figure 1.2 - P38/MAPK signaling cascade: Overview of the p38 MAPK-MK2 pathway that is activated in vascular smooth muscle cells during surgical resection and transplantation resulting in a pathological, synthetic vascular smooth muscle cell phenotype. From [2], reprinted with permission from AAAS.

many intracellular-acting biologics, MK2i bioavailability within the cytoplasm (where activated MK2 is localized) is limited by sequestration/degradation within late endosomes and early lysosomes [8].

The Role of HSP20 and MK2 in Vasospasm

Vasospasm refers to the pathological constriction of human vascular tissue that can lead to downstream tissue ischemia and, ultimately, tissue necrosis. The clinical burden of vasospasm can be highlighted in two areas: **1)** Coronary vasospasm (both acute vasospasm following coronary artery bypass grafting and Prinzmetal's angina) and **2)** subarachnoid hemorrhage-induced symptomatic cerebral vasospasm. There are approximately 1.6 million coronary artery bypass procedures performed annually in the United States [43], and acute coronary vasospasm occurs in 1-8% of all patients undergoing to coronary artery bypass grafting [44]. Treatment of coronary vasospasm includes immediate, invasive intracoronary administration of vasodilators such as nitroglycerin or verapamil [45]. Coronary vasoaspasm also occurs outside the context of coronary bypass grafting and is referred to as Prinzmetal's, or "variant" angina [46]. The prevalence of Prinzmetal's angina ranges from ~4% of patients undergoing coronary angiography in the United states [47] to ~30% of patients in Japan [48]. Again, treatment involves administration of vasodilators (i.e., nitrates such as nitroglycerin and calcium channel blockers such as verapamil) and β-blockers and high doses of aspirin are contraindicated. Similarly, the current treatments for symptomatic cerebral vasospasm following subarachnoid hemorrhaging are also limited. Subarachnoid hemorrhages (**SAH**) affect 30,000 people annually and cause up to 7% of all strokes [49]. Nearly all cases of SAH are due to rupture of a cerebral aneurysm, and 40-50% of post-SAH mortality is attributed to symptomatic vasospasm (i.e., delayed cerebral ischemia) [50]. Current therapeutic approaches (i.e. triple H therapy [51]) have yielded no significant improvement in mortality rates. Since cerebral perfusion pressure is directly proportional to mean arterial pressure systemically-delivered vasodilators are avoided as they result in systemic hypotension, thereby exacerbating cerebral ischemia. Thus, there exists a significant clinical need for therapeutic interventions for vasospasm that avoid systemic effects by selectively targeting vasospastic vessels.

At the ultrastructural level, vasospasm is mediated by the contraction of vascular smooth muscle. Smooth muscle contraction is caused by the sliding of actin and myosin filaments past each other within smooth muscle cells. As a result, actively depolymerizing or destabilizing actin filaments results in

inhibition of smooth muscle contraction and enhancement of relaxation as the myosin filaments no longer have an intact substrate to bind to and utilize to generate force. Thus, the destabilization of actin filaments in smooth muscle may be a promising therapeutic approach to preventing and treating vasospasm. Vasospasm is associated with a down-regulation of heat shock protein 20 (**HSP20,** also known as HSPB6) and concomitant increases in the expression and phosphorylation of heat shock protein 27 (**HSP27**, also known as HSPB1). Both HSP20 and HSP27 have been shown to be key regulators of actin dynamics and contraction in smooth muscle [38, 52]. HSP20 is activated through nucleotide-dependent protein kinases and is thought to interact with with the 14-3-3 scaffolding protein leading to the dissociation, dephosphorylation, and activation of the actin disassembly protein cofilin [52] (**fig. 1.3**). Activation of MAPKAP Kinase II (**MK2**) by p38 MAPK is also believed to contribute to vasoconstriction through the formation of filamentous actin (**F-actin**) stress fibers within smooth muscle cells. MK2 phosphorylates HSP27, which associates with filamentous actin to prevent actin depolymerization and inhibit tissue vasorelaxation [34, 53]. Activated MK2 also phosphorylates LIM kinase which phosphorylates and deactivates cofilin, thereby inhibiting actin depolymerization[33]. Thus, both HSP20 and MK2 play key roles in actin dynamics and represent promising targets to treat and prevent vasospasm[54]. In fact, a peptide mimetic of phosphorylated HSP20 (**p-HSP20**) was recently developed and shown to prevent SAH-induced macrovascular vasospasm in a non-craniotomy model of SAH-induced vasospasm[55] and a MK2 inhibitory peptide (**MK2i**), derived from a sequence shown by Hayess and Benndorf to inhibit MK2 in vitro[41], was optimized[40] and shown to enhance sodium nitroprusside induced vasorelaxation of vascular smooth muscle[56]. However, sequestration and accumulation of both the p-HSP20 and MK2i peptides in the endo-lysosomal trafficking pathway remains a fundamental barrier to achieving optimal bioactivity on the actin regulatory machinery located in the cytoplasm[8]: previous studies have required extremely high doses to achieve therapeutic bioactivity, limiting the practicality of clinical translation.

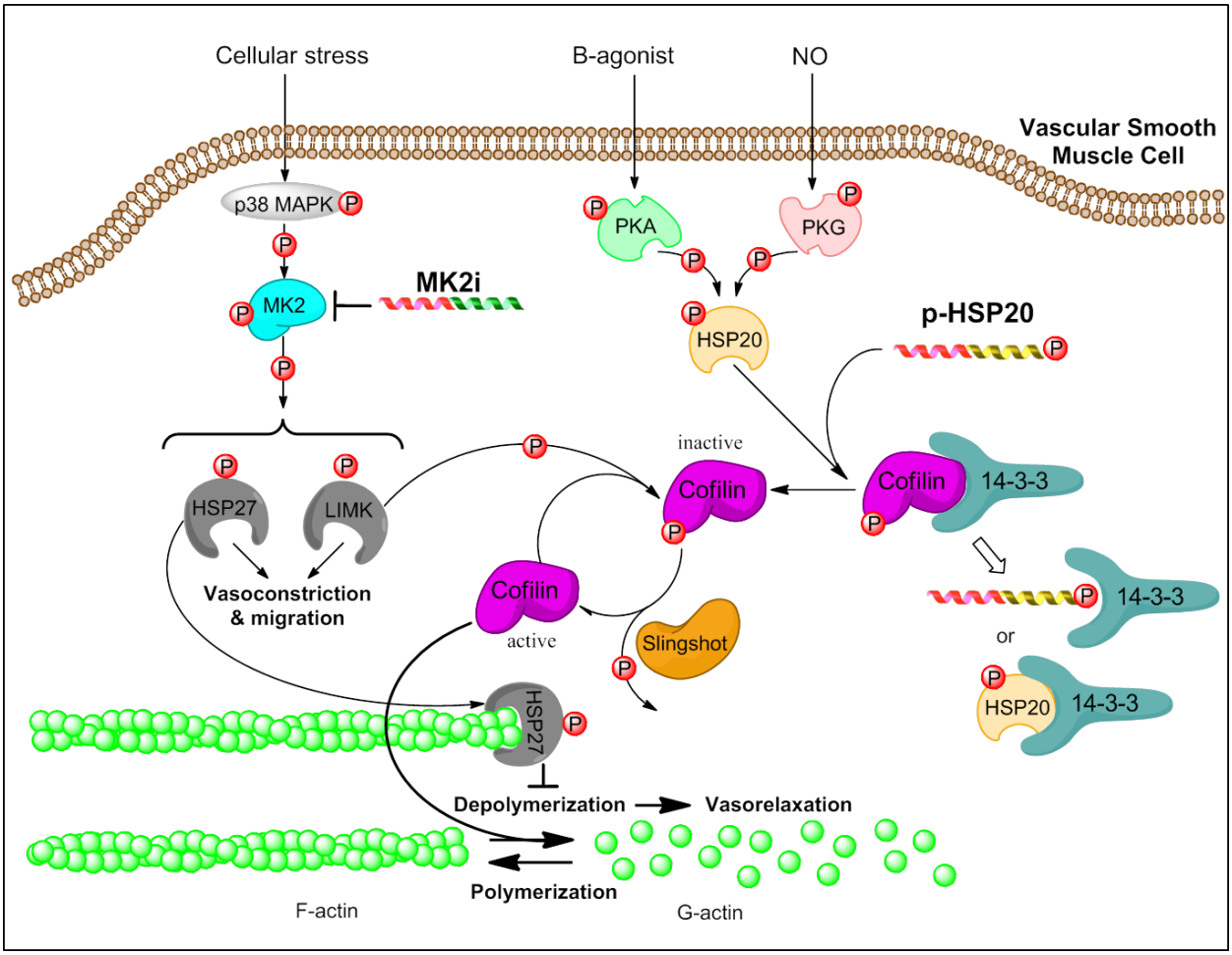

Figure 1.3 - The role of MAPKAP Kinase 2 (MK2) and Heat Shock Protein 20 (HSP20) in actin mediated regulation of smooth muscle tone: MK2 is activated by cellular stress (e.g. mechanical trauma, cytokines, ROS, etc.) through p38 MAPK. Activated MK2 activates a number of downstream effectors: 1) phosphorylation of heat shock protein 27 (**HSP27**) results in capping of filamentous actin thereby inhibiting actin depolymerization and vasorelaxation. 2) phosphorylation of Lim Kinase (**LIMK**) results in phosphorylation and deactivation of cofilin which prevents actin degradation and inhibits vasorelaxation. The MK2 inhibitory peptide (**MK2i**) binds to MK2 preventing the activation of these downstream effectors and promoting vasorelaxation. HSP20 is phosphorylated by cyclic nucleotide-dependent protein kinases (PKA and PKG) resulting in binding to and displacement of phosphorylated coflin from the 14-3-3 protein. This displacement causes cofilin to become dephosphorylated and activated by phosphatases such as slingshot, resulting in depolymerization of filamentous actin. The phospho-HSP20 peptide mimetic (**p-HSP20**) recapitulates the activity of phosphorylated HSP20, ultimately leading to vasorelaxation. Reprinted with permission from [1]. Copyright 2015 American Chemical Society.

A Translational Approach to Intracellular Peptide Delivery

Peptide based biomacromolecular therapeutics have significant potential for use in a variety of clinical applications ranging from cancer treatment to cardiovascular disease. In comparison to small-molecule drugs, peptide based therapies are advantageous in terms of specificity, potency, and biocompatibility. However, major *in vivo* barriers exist to effective intracellular delivery of biomacromolecular therapeutics for translational applications. Many delivery platforms have been

developed and studied to increase *in vivo* stability and facilitate cellular uptake and endosomal escape, but these approaches are typically costly, involve complex synthesis schemes, can be cytotoxic, and can suffer from relatively limited therapeutic enhancement. **The overall goal of this project is to develop a simple, biocompatible drug delivery platform to enhance intracellular delivery of therapeutic peptides by enhancing cellular uptake, facilitating endosomal escape and cytoplasmic release of the drug payload thereby increasing the duration of therapeutic efficacy.**

Cell penetrating peptides (**CPPs**), which are generally cationic and interact with the negative charge of cell membranes, are commonly conjugated to biologic therapeutics such as peptides, DNA, and siRNA to increase cell uptake. The use of CPPs can significantly increase cellular uptake of therapeutics, however, CPPs do not address the delivery barrier of escaping the endo-lysosomal trafficking pathways subsequent to cellular internalization. The cationic nature of CPPs makes them amenable to electrostatic complexation with anionic polymers for the development of novel drug delivery systems. Electrostatic complexation of therapeutics into a nanomedicine is desirable in that it circumvents the need for chemical conjugation of the therapeutic to the carrier which can result in steric hindrance of the therapeutic payload's bioactivity. Furthermore, complex synthesis schemes that are characteristic of colloidal drug carriers (e.g. liposomes and micellar constructs) usually suffer from poor yields due to the need for multiple rounds of synthesis and purification necessary to achieve the desired product. As a result, **the development of a simple, cost-effective platform to address the delivery barriers that biomacromolecules face will allow for the translation of highly-specific and potent biologic therapeutics and research tools for a wide range of applications.** The following specific aims are designed to test the *hypothesis* that endosomolytic nano-polyplexes can serve as a general platform technology for the intracellular delivery of CPP-based therapeutic peptides for a variety of applications in *in vitro*, *ex vivo*, and *in vivo* mechanistic studies, with strong potential for translation toward treatment of human disease.

Specific Aim 1: *Synthesize and characterize a library of nano-polyplexes (**NPs**) formulated with a MAPKAP Kinase 2 inhibitor peptide (**MK2i-NPs**).* An MK2i cell penetrating peptide will be formulated with an anionic, endosomolytic polymer at a range of charge ratios (**CRs**). The size, polydispersity, surface

charge, and pH-responsive behavior of the resulting nano-polyplexes (**NPs**) will be characterized to determine optimal conditions for formulation of a nanomedicine with ideal physico-chemical properties.

Specific Aim 2: *Assess uptake, retention, endosomal escape, and bioactivity of an optimized MK2i-NP formulation in relevant in vitro models.* Flow cytometry will be performed to compare the cellular uptake and retention of fluorescently labeled MK2i-NPs vs. free peptide. Microscopic analysis of fluorescently labeled MK2i uptake in conjunction with an endo-lysosomal dye will be used to verify enhanced endosomal escape of NPs compared to the peptide alone. The bioactivity and duration of efficacy of the MK2i-NPs will be compared to the free peptide through functional readouts relevant to IH in human coronary artery vascular smooth muscle cells (**HCAVSMCs**).

Specific Aim 3: *Assess the therapeutic efficacy of MK2i-NPs* ex vivo *in human saphenous vein and* in vivo *in a rabbit vein graft interposition model.* MK2i-NP vessel penetration and peptide retention will be assessed in human saphenous vein (HSV) explants. The ability of MK2i-NPs to inhibit intimal hyperplasia (**IH**) will be evaluated *ex vivo* in human saphenous vein (**HSV)** explants. Western blot analysis of protein expression will be used to verify underlying therapeutic mechanisms. The ability of MK2i-NPs to prevent IH and improve vein graft patency will be evaluated *in vivo* in a rabbit jugular vein graft interposition model. Immunohistochemical analyses will be utilized to assess the effect of MK2 inhibition on vascular smooth muscle cell phenotype both *ex vivo* and *in vivo*.

Specific Aim 4: *Assess nano-polyplexes as a platform technology.* Nano-polyplex formulations will be optimized for two therapeutic CPPs and applied to prevent and treat vasospasm. The uptake and retention of the optimized NPs will be assessed through flow cytometry and endosomal escape will be assessed through subcellular fractionation. The bioactivity of each NP formulation will be assessed *in vitro* through the analysis of F-actin stress fiber formation in vascular smooth muscle cells and *ex vivo* through smooth muscle physiology studies performed on viable human vascular tissue explants.

CHAPTER II

DEVELOPMENT, OPTIMIZATION, & CHARACTERIZATION OF MK2I-NPS

Introduction

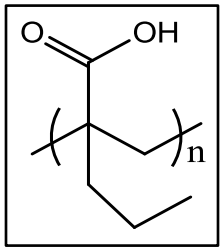

Figure 2.1 - PPAA chemical structure

Therapeutic peptides are generally modified with a cell penetrating peptide sequence to promote cell internalization via endocytosis and/or micropinocytosis n[54, 57-59]. However, CPP-modified peptides suffer from poor bioactivity due to entrapment in endosomal vesicles that are trafficked for lysosomal degradation or exocytosis as opposed to cytoplasmic peptide release [5, 7, 8, 58, 60, 61]. We and other have shown that co-delivery of an endosomolytic polymer with a CPP-internalized therapeutic increases cytoplasmic delivery and bioacitivity [7, 21, 62-65]. Poly(ethylacrylic acid) (PEAA) was first described for pH-dependent disruption of lipid vesicles [66, 67], and the related polymer PPAA was subsequently shown to have membrane disruptive properties in a pH range that is ideally tuned for endosomal escape and intracellular delivery [68, 69]. Early endosomes are continuously acidified through ion exchange and ATP-dependent proton pumps in the vesicle membrane [70-72], and in this environment, the pendant carboxylic acid moieties on PPAA (**fig. 2.1**) become more protonated / deionized. This deionization reversibly transitions PPAA into a more hydrophobic, membrane-interactive conformation that results in disruption of the endosomal membrane and enables cytoplasmic delivery of endosomal cargo. The pKa of the pendant carboxylic acids is roughly 6.7, so at higher pH values, such as physiologic pH, the carboxylic acid groups are predominately deprotonated / ionized, conferring a net negative charge to the polymer. In contrast, the pKa of certain amino acid side chains that typically constitute CPPs, namely arginine and lysine, is much higher (pKa~10-12.5 depending on amino acid). As a result, peptides that contain a high number of these polar side chains such as CPPs are primarily protonated and cationic at physiologic pH. Consequently, CPP-based peptide therapeutics can be electrostatically complexed at an intermediate pH between the pKa of cationic amino acid side chains of CPPs and anionic carboxylic acids on PPAA.

This generalizable electrostatic complexation approach will be utilized for the formulation of nano-polyplexes with a cell permeant peptide inhibitor of MAPKAP Kinase 2 (**Table 2.1**). The MK2i peptide will be made through solid phase peptide synthesis with standard Fmoc chemistry, purified by RP-HPLC, and verified via ESI-MS. Poly(propylacrylic acid) will be synthesized through RAFT polymerization utilizing 4-cyano-4-(ethylsulfanylthiocarbonyl) sulfanylvpentanoic acid (ECT) as the chain transfer agent. Polyplexes will be formed by mixing the PPAA homopolymer with the MK2i peptide in aqueous buffer with a defined pH between the pKa values of the primary amines present on MK2i and the carboxylic acid moieties in the PPAA polymer. To determine an optimal nanoparticle formulation, a library of nano-polyplexes (**NPs**) will be prepared at a range of charge ratios (i.e. **CR** = $([NH_3^+]_{MK2i}/[COO^-]_{PPAA})$ from 10:1 to 1:10.

Peptide	Sequence	MW	Function
MK2i (MMI-0100)	YARAAARQARAKALARQLGVAA	2283.67	MAPKAP Kinase II inhibitor

Table 2.1 - MK2i peptide. Red amino acid abbreviations indicate the presence of polar amino groups in the amino acid side chain that potentiate electrostatic interaction with PPAA: R (arginine), K (lysine) - primary amines (strong base); N (asparagine), Q (glutamine) - amides (weak bases).

To provide a vehicle control for biological studies, non-endosomolytic MK2i-NPs (NE-MK2i-NPs) will be formulated with poly(acrylic acid) (**PAA, fig. 2.2**), a structurally similar polymer that does not have a pH response in a physiologically relevant range due to the pKa of the carboxylic acid group being lower (pKa~4.3) than the pH range encountered in the endo-lysosomal pathway. MK2i peptide will be fluorescently labeled with an amine-reactive Alexa-488 or Alexa-568 succinimidyl ester for the formulation of fluorescent MK2i-NPs for uptake studies.

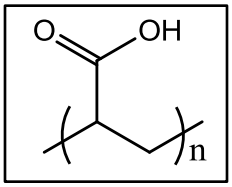

Figure 2.2 - PAA chemical structure

MK2iNP size and surface charge based on ζ-potential will be analyzed through dynamic light scattering (**DLS**) analysis. An optimal charge ratio will be chosen based upon three criteria: **1)** consistently yields a unimodal particle size distribution with hydrodynamic diameter in the nanometer size range, **2)** minimal size, and **3)** minimal polydispersity. Optimized MK2i-NP size and morphology will be further characterized through TEM analysis of uranyl-acetate counterstained samples. DLS analysis of pH-dependent MK2i-NP size will be used to verify NP dissociation in acidic, endosomal conditions. pH-dependent membrane disruptive activity (i.e. endosomolytic potential) will be assayed through a red blood

cell hemolysis assay at pH values mimicking physiologic (pH 7.4), early endosomal (pH 6.8), late endosomal (pH 6.2), and lysosomal (pH 5.6) pH values.

Methods

Materials

All reagents were purchased from Sigma and were of analytical grade unless otherwise stated. PD10 desalting columns were purchased from GE healthcare. Diethyl propylmalonate was purchased from Alfa Aesar (Ward Hill, MA). All monomers were filtered through a basic alumina column to remove inhibitors prior to use in polymerizations. Dioxane was distilled prior to use in polymerizations. 2,2'-Azobis(2-methylpropionitrile) (AIBN) was recrystallized twice from methanol prior to use.

Synthesis of 4-cyano-4-(ethylsulfanylthiocarbonyl) sulfanylvpentanoic acid (ECT)

The RAFT chain transfer agent ECT was synthesized following protocols previously described by Convertine et al. [64] and adapted from Moad et al. [73]. Briefly, Ethanethiol (76 mmol, 4.72 g) was reacted with carbon disulfide (79 mmol, 6.0 g) in the presence of sodium hydride (79 mmol, 3.15 g) in diethyl ether for 1h. The resulting sodium S-ethyl trithiocarbonate was further reacted with iodine (25 mmol, 6.3 g) to obtain bis(ethylfulfanyl-thiocarbonyl) disulfide, which was further refluxed with 4,4'-azobis(4-cyanopentanoic acid) in ethylacetate for 18 h. The crude ECT was purified by column chromatography using silica gel as the stationary phase and a gradient of ethyl acetate:hexane (40:60 to 70:30) as the mobile phase. ^{1}H NMR (400MHz, $CDCl_3$): δ 1.36 t ($SCH_2C\mathbf{H}_3$); δ 1.88 s ($CCNC\mathbf{H}_3$); δ 2.3–2.65 m ($C\mathbf{H}_2C\mathbf{H}_2$); δ 3.35 q ($SC\mathbf{H}_2CH_3$).

Synthesis of 2-propylacrylic acid (2-PAA)

The synthesis of 2-PAA was adapted from existing methods developed by Ferrito et al. [74]. Briefly, diethyl propylmalonate (200 mmol, 40.45 g) was stirred in 1M KOH in 95% ethanol and acidified with HCl to yield 2-carbopropoxybutyric acid, which was reacted with diethylamine (200 mmol, 14.62 g) and formalin (200 mmol, 16.11 g) at room temperature for 24h, followed by reflux at 60°C for 8 hours. Following acidification with sulfuric acid, the resulting 2-propylacrylate was extracted 3x with diethyl ether

and dried over magnesium sulfate. The pure 2-propylacrylate was then refluxed in 2M KOH for 20 h to yield 2-propyl acrylic acid, which was extracted 3x with diethyl ether, dried, and vacuum distilled under vacuum to yield a colorless oil. ^{1}H NMR (400 MHz, $CDCl_3$) δ 0.97 t (CH_3CH_2); δ 1.55 m ($CH_3CH_2CH_2$); δ 2.31 t ($CH_3CH_2CH_2$); δ 5.69-6.32 q (CH_2=C); δ 12 s (CCOOH).

Synthesis and characterization poly(propylacrylic acid) (PPAA) and poly(acrylic acid) (PAA)

The ECT chain transfer agent (CTA) was utilized in the RAFT polymerization of a poly(2-propylacrylic acid) homopolymer (PPAA) that was carried out in bulk under a nitrogen atmosphere at 70°C for 48 hours using AIBN as the free radical initiator. The reaction mix was put through three freeze-vacuum-thaw cycles and purged with nitrogen for thirty minutes prior to polymerization. The molar ratio of CTA to AIBN was 1 to 1 and the monomer to CTA ratio was set so that a degree of polymerization (DP) of 190 would be achieved at 100% conversion. Following polymerization, the resultant polymer was dissolved in DMF and precipitated into ether 5 times before drying overnight *in vacuo*. The RAFT polymerization of a poly(acrylic acid) homopolymer (PAA) was carried out in distilled dioxane under a nitrogen atmosphere at 70°C for 18 hours using AIBN as the free radical initiator and ECT as the CTA. The reaction mix was purged with nitrogen for thirty minutes prior to polymerization. The molar ratio of CTA to AIBN was 5 to 1 and the monomer to CTA ratio was set so that a DP of 150 would be achieved at 100% conversion. Following polymerization, the resultant polymer was dissolved in dioxane and precipitated into ether 5 times before drying overnight *in vacuo*. Gel permeation chromatography (GPC, Agilent) was used to determine molecular weight and polydispersity (M_w/M_n, PDI) of the PPAA and PAA homopolymers using HPLC-grade DMF containing 0.1% LiBr at 60°C as mobile phase. Molecular weight calculations were calculated with ASTRA V software (Wyatt Technology) and were based on calculated dn/dc values for PPAA determined through injection of serial dilutions of the polymer in conjunction with off-line refractive index monitoring.

Synthesis cell permeant MAPKAP Kinase 2 inhibitory peptide (MK2i)

A cell penetrant MK2 inhibitor peptide (MK2i, sequence YARAAARQARAKALARQLGVAA, MW = 2283.67) was synthesized on a PS3 3 channel serial peptide synthesizer (Protein Technologies, Inc.

Tucson, AZ) utilizing standard Fmoc Chemistry. N-methylpyrrolidone (NMP, Fischer Scientific) was utilized as a solvent in all peptide syntheses. HCTU was used as an activator (Chempep, Wellington, FL) in the presence of N-methylmorpholine. All amino acids were double coupled in order to maximize yield and purity. Peptides were cleaved/deprotected in Reagent B: TFA/Phenol/H_2O/triisopropylsilane (88/5/5/2). Successful peptide synthesis was verified through LC-MS analysis on a Waters Synapt ESI-MS. Peptides were then further purified by reverse phase HPLC on a Waters 1525 binary HPLC pump outfitted with an extended flow kit, a Waters 2489 UV/Visible detector and a phenomenex Luna C18(2) AXIA packed column (100A, 250 x 21.2 mm, 5 micron). **A)** HPLC grade water with 0.05% formic acid and **B)** HPLC grade acetonitrile were used as the mobile phases and the peptide was purified utilizing a 90% A to 90% B gradient over 25 minutes (16 mL/min). Acetonitrile was removed from purified fractions with a rotary evaporator and the purified fractions were then frozen, lyophilized, and peptide purity was verified through electrospray ionization mass spectrometry (ESI-MS) on a Waters Synapt ESI-MS.

MK2i nano-polyplex (MK2i-NP) synthesis and characterization

PPAA was dissolved in 1 M NaOH and diluted into a phosphate buffer (pH 8) to obtain a stock solution. MK2i was dissolved in phosphate buffer (pH 8). The MK2i peptide and PPAA polymer were mixed at a range of CRs from $[NH_3^+]$:$[COO^-]$ = 10:1 to 1:10 to form MK2i-NPs. The resulting polyplexes were syringe filtered through 0.45 μm PTFE filter, and the hydrodynamic diameter and ζ-potential were characterized on a Malvern Zetasizer Nano-ZS.

A CR of 1:3 was then chosen as the optimal formulation and used in subsequent studies. Nano-polyplexes formulated at the same CR with the non-endosomolytic polymer PAA (i.e., NE-MK2i-NPs) were analyzed by DLS and used as a vehicle control in all subsequent studies. MK2i-NPs were visualized through transmission electron microscopy (TEM) imaging. TEM samples were prepared by inverting carbon film-backed copper grids onto a droplet of aqueous polyplex suspensions (1 mg/mL) and blotted dry. All samples were then counterstained with 3% uranyl acetate. Samples were desiccated *in vacuo* for 2 h prior to TEM imaging. The pH-dependent size changes of polypexes at a CR of 1:3 were then quantified by DLS analysis at various pH values in PBS.

PH-dependent membrane disruption hemolysis assay

In order to assess the polyplexes' potential for enhancing endosomal escape, a red blood cell hemolysis assay was utilized as previously described [75] to measure the capacity of polyplexes to cause pH-dependent disruption of lipid bilayers. Briefly, following approval by Vanderbilt Medical Center's Institutional Review Board, whole human blood from an anonymous donor was drawn and plasma was aspirated following centrifugation of the red blood cells. The remaining erythrocytes were washed three times with 150 mM NaCl and re-suspended into phosphate buffers corresponding to physiologic (pH 7.4), early endosome (pH 6.8), early/late endosome (pH 6.2), and late endosome/lysosomal (pH 5.8) environments. The polyplexes and peptides (1-40 μg/mL), PBS (negative control), or 1% Triton X-100 (positive control) was added to the erythrocyte suspensions and incubated at 37 °C for 1 hour. Intact erythrocytes were pelleted via centrifugation, and supernatant was carefully transferred to a new 96-well plate. The hemoglobin content within the supernatant was then measured via absorbance at 541 nm. Percent hemolysis was determined relative to Triton X-100 and PBS controls.

Results

Polymer synthesis and characterization

RAFT polymerization was used to synthesize a poly(propylacrylic acid) and poly(acrylic acid) homopolymers that were subsequently analyzed by gel permeation chromatography [calculated PPAA dn/dc = 0.087 ml/g DP = 193 (GPC), PDI = 1.47 (GPC) (**fig. 2.3 A**); calculated PAA dn/dc = 0.09 ml/g DP = 150 (GPC), PDI = 1.27 (GPC) (**fig. 2.3 B**). Polymer purity and molecular weight were then verified through NMR spectroscopy utilizing D_6MSO as a solvent. (PPAA DP = 190 (H^1 NMR) (**fig. 2.3 C**); PAA DP = 106 (H^1 NMR) (**fig. 2.3 D**).

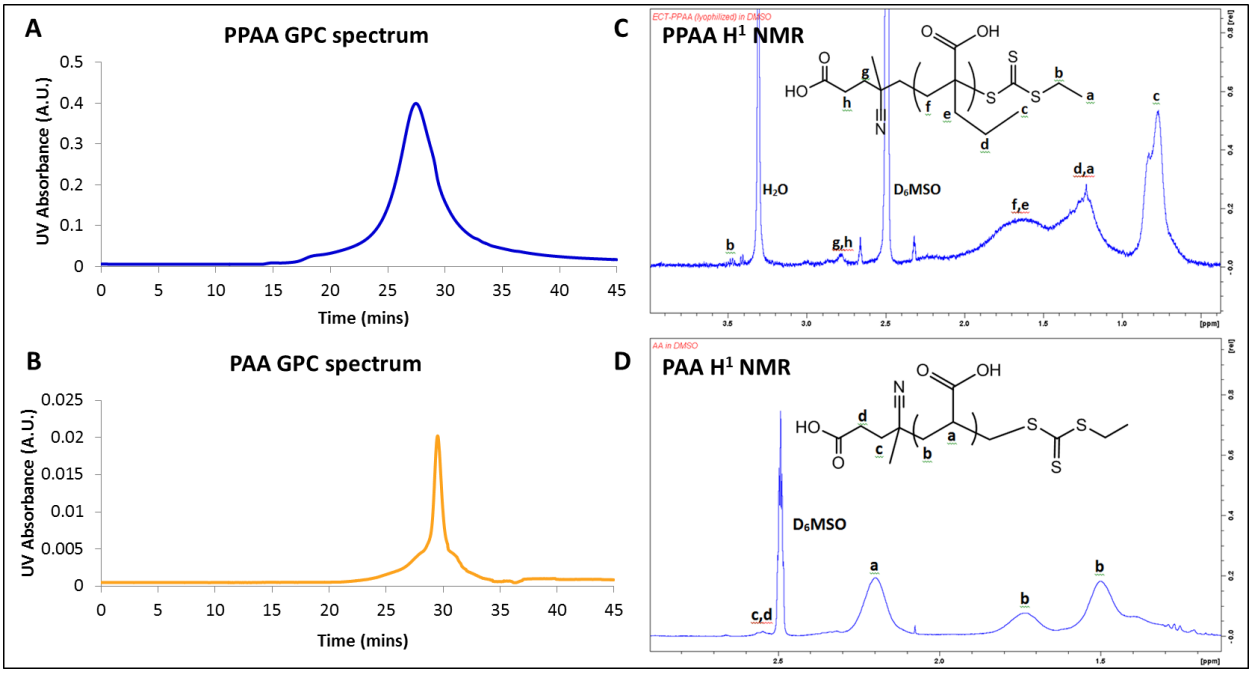

Figure 2.3 - Polymer characterization. GPC chromatograms of **(A)** poly(propylacrylic acid) (PPAA) [degree of polymerization = 193, PDI =1.471, dη/dC = 0.087 (ml/g)] and **(B)** poly(acrylic acid) (PAA) [degree of polymerization = 150, PDI = 1.27, dη/dC = 0.09 (ml/g)] polymers in DMF. The trace shows UV absorbance at the characteristic absorption peak of the trithiocarbonate moiety (310 nm) present in the 4-cyano-4-(ethylsulfanylthiocarbonyl) sulfanylvpentanoic acid (ECT) chain transfer agent utilized in the polymerization. ^{1}H NMR spectrum of **(C)** poly(propylacrylic acid) (PPAA) and **(D)** poly(acrylic acid) (PAA) in D_6MSO. Molecular weight was determined by comparing the area of peaks associated with the chain transfer agent (i.e. peaks c,d for PAA and peak b for PPAA) to peaks associated acrylic acid/propylacrylic acid (i.e. peak a for PAA and peak c for PPAA): PAA degree of polymerization = 106, PPAA degree of polymerization = 190. From [2], reprinted with permission from AAAS.

Peptide synthesis and purification

The Purity of the HPLC-Purified MK2i peptide was verified through electrospray ionization mass spectrometry (MK2i MW = 2283.67 g/mol, (**fig. 2.4**).

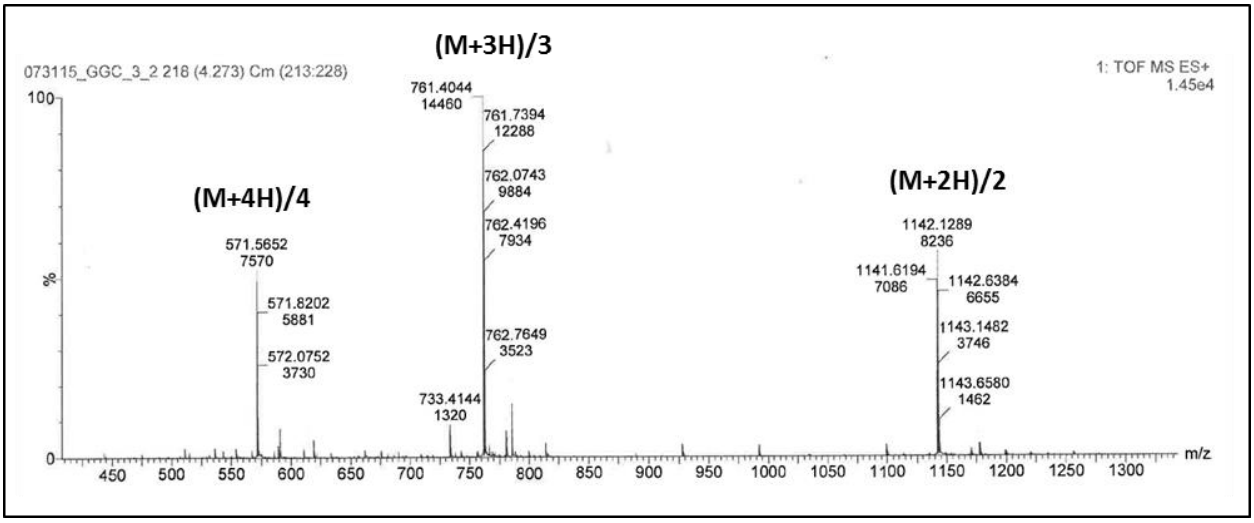

Figure 2.4 – MK2i peptide characterization. Electrospray-ionization mass spectrometry (ESI-MS) mass spectrum for the HPLC-purified CPP-MK2i fusion peptide. sequence: YARAAARQARA-KALARQLGVAA, MW = 2283.67 g/mol. The mass spectrum shows three major peaks each corresponding to the fragmentation of the full peptide sequence. From [2], reprinted with permission from AAAS.

MK2i nano-polyplex (MK2i-NP) synthesis and characterization

NPs were formed by simple mixing of the poly(acrylic acid) (**PAA**) or poly(propylacrylic acid) (**PPAA**) homopolymers with the MK2i peptide in PBS at pH 8.0, which is between the pKa values of the primary amines present on the MK2i peptide and the carboxylic acid moieties in the PPAA polymer; this ensures optimal solubility and net charge on both the cationic peptide and anionic polymers (**fig. 2.5 A**). PPAA was utilized in the lead MK2i-NP formulation because of its well-defined pH-dependent membrane disruptive activity (schematically illustrated in **fig. 2.5 B**) [21, 76, 77] and previous safe use in animal models [78, 79]. PAA was utilized as a vector control as it is an anionic polymer with structural similarity to PPAA but lacks pH-responsiveness in a physiologically relevant range due to its lower pKa (pKa~4.3) (**fig. 2.5 C**).

To determine optimal nanoparticle formulation conditions, a library of MK2i-NPs was prepared at a range of charge ratios [i.e. **CR** = ($[NH_3^+]_{MK2i}$:$[COO^-]_{PPAA}$)], and the size distribution and particle surface charge were characterized. MK2i-NP ζ-potential was directly proportional to the CR, with an apparent isoelectric point at CR ~ 2:1 (**fig. 2.5 D**). A CR of 1:3 was chosen as the optimal formulation as this ratio yielded a unimodal size distribution with minimal particle size and polydispersity (**table 2.2**). Non-endosomolytic MK2i nano-polyplexes (**NE-MK2i-NPs**) were formulated with PAA as a vehicle control for biological studies. NE-MK2i-NPs prepared at CR=1:3 with PAA had size and ζ-potential statistically

equivalent to the endosomolytic MK2i-NPs. Interestingly, optimized NPs formulated at a CR of 1:3 yielded a negative surface charge (ζ-potential = -11.9 mV), indicating that the cationic peptide is primarily packaged into the core of the nanoparticles and that the anionic polymer PPAA is the primary component exposed at the surface of the NPs in aqueous environments.

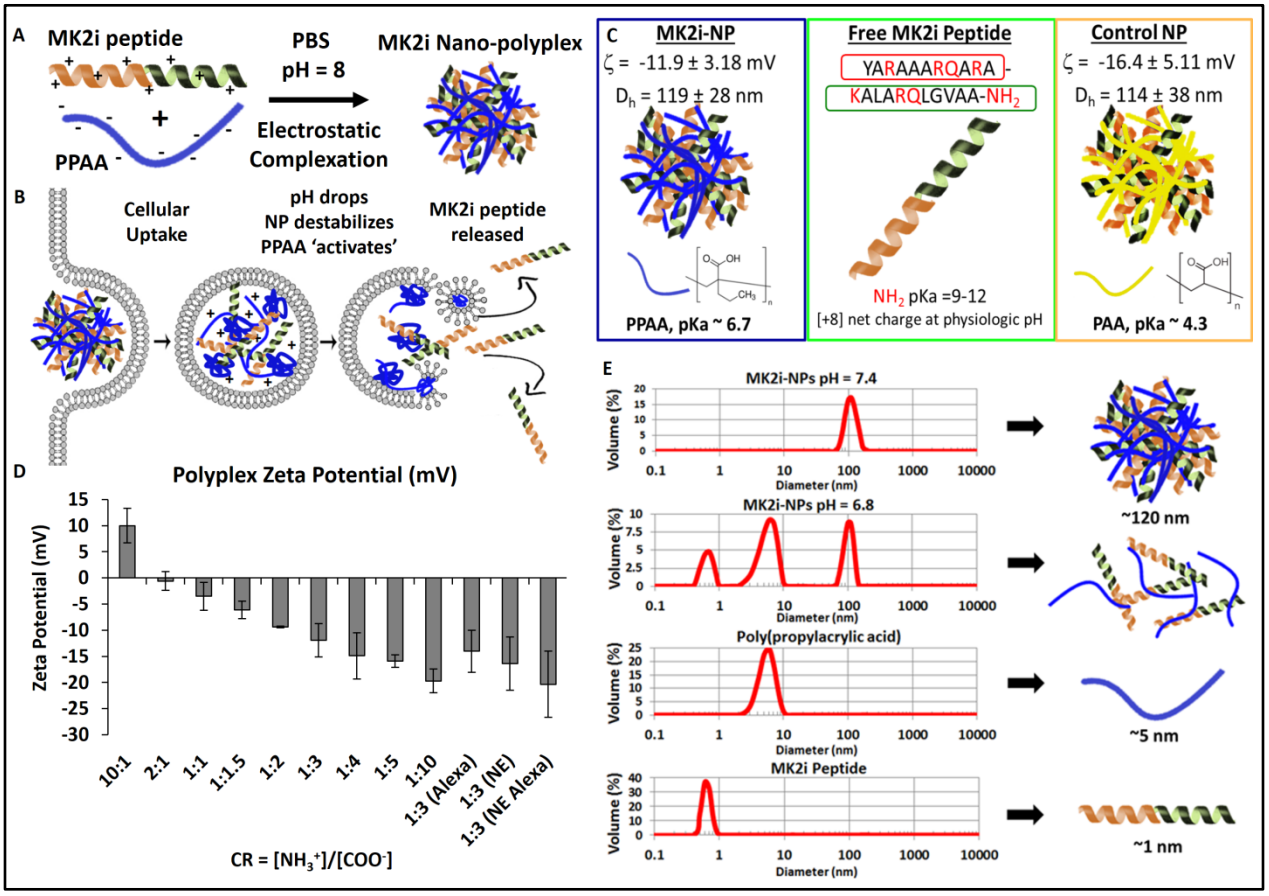

Figure 2.5 - MK2i-NP synthesis and characterization. (A) MK2i-NP synthesis scheme. **(B)** MK2i-NPs hypothesized mechanism of endosomal escape. **(C)** Treatment comparison summary: Endosomolytic MK2i-NPs formulated with poly(propylacrylic acid), non-endosomolytic (NE) NE-MK2i-NPs formulated with poly(acrylic acid). MK2i-NPs and NE-MK2i-NPs are made with the MK2i peptide with the sequence shown (red = modified TAT mimetic cell penetrating peptide sequence, green = MK2 inhibitory sequence). **(D)** Zeta potential of polyplexes prepared at different charge ratios ($[NH_3^+]/[COO^-]$). Alexa denotes NPs formulated with an Alexa-488 conjugated MK2i peptide. NE denotes NE-MK2i-NPs. Data are represented as mean ± SEM (*n* = 3 independent measurements). **(E)** DLS analysis of pH-dependent MK2i-NP disassembly. From [2], reprinted with permission from AAAS.

MK2i-NP unpackaging under endolysosomal conditions was assessed at a range of pHs revealing that the MK2i-NPs dissociated as the pH was lowered from extracellular pH toward the pKa of the carboxylic acids (pH~6.7) on PPAA, which also correlates to early endosomal conditions [80] (**fig. 2.5 E**). It is hypothesized that at the lower pH, the PPAA polymer becomes protonated/deionized, and the net positive charge on the peptide causes electrostatic repulsion and disassembly of the MK2i-NPs. NP

disassembly under early endosome-like conditions reduces the likelihood that peptide bioactivity and/or PPAA endosomal membrane disruptive function is sterically hindered by polymer-peptide interactions.

NH2:COOH	Z-ave diameter (nm)
10:1	10.32 ± 2.63*
2:1	52.1 ± 46.86*
1:1	970.6 ± 662.4
1:1.5	465.1 ± 138.4*
1:2	474.2 ± 32.59
1:3	118.8 ± 26.76
1:4	607.4 ± 285.2*
1:5	213.0 ± 67.95*
1:10	21.57 ± 9.89*
1:3 (Alexa)	168.5 ± 24.63
1:3 (NE)	113.7 ± 14.47
1:3 (NE Alexa)	197.4 ± 12.85

Table 2.2 – MK2i nano-polyplex library characterization. Size summary of MK2i-NPs prepared at different charge ratios ($[NH_3^+]/[COO^-]$) as determined by DLS analysis. Asterisks (*) indicate multimodal size distributions (multiple peaks present). 1:3 (Alexa) polyplexes were formulated with an Alexa488-conjugated MK2i peptide to use in cellular uptake studies. 1:3 (NE) polyplexes were formulated with a non-endosomolytic (NE) poly(acrylic acid) polymer that does not exhibit pH-dependent membrane disruptive activity in the endosomal pH range as a vehicle control. Data are mean ± peak width. From [2], reprinted with permission from AAAS.

In order to verify DLS results, uranyl acetate counter-stained nano-polyplexes (at a charge ratio = 1:3) were imaged using transmission electron microscopy. TEM images revealed particle sizes in agreement with results from DLS analysis (**fig. 2.6**).

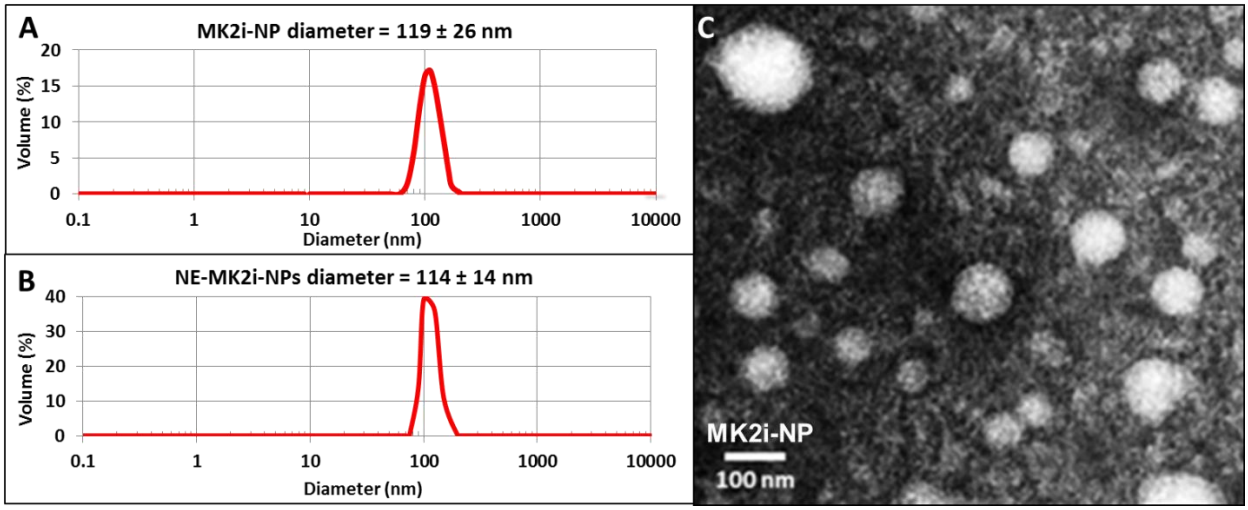

Figure 2.6 - NP size and morphology. Dynamic light scattering analysis of **(A)** MK2i-NP and **(B)** NE-MK2i-NP size distributions. **(C)** Representative TEM images of uranyl acetate counterstained MK2i-NPs. Scale bar = 100 nm. From [2], reprinted with permission from AAAS.

In order to verify that the pH-responsive behavior of the PPAA polymer is maintained when electrostatically complexed with the MK2i peptide a red blood cell hemolysis assay was used to measure pH-dependent membrane disruption activity of polyplexes at pH values mimicking physiologic (pH 7.4), early endosome (pH 6.8), early/late endosome (pH 6.2), and late endosome/lysosomal (pH 5.8) environments (**fig. 2.7**).

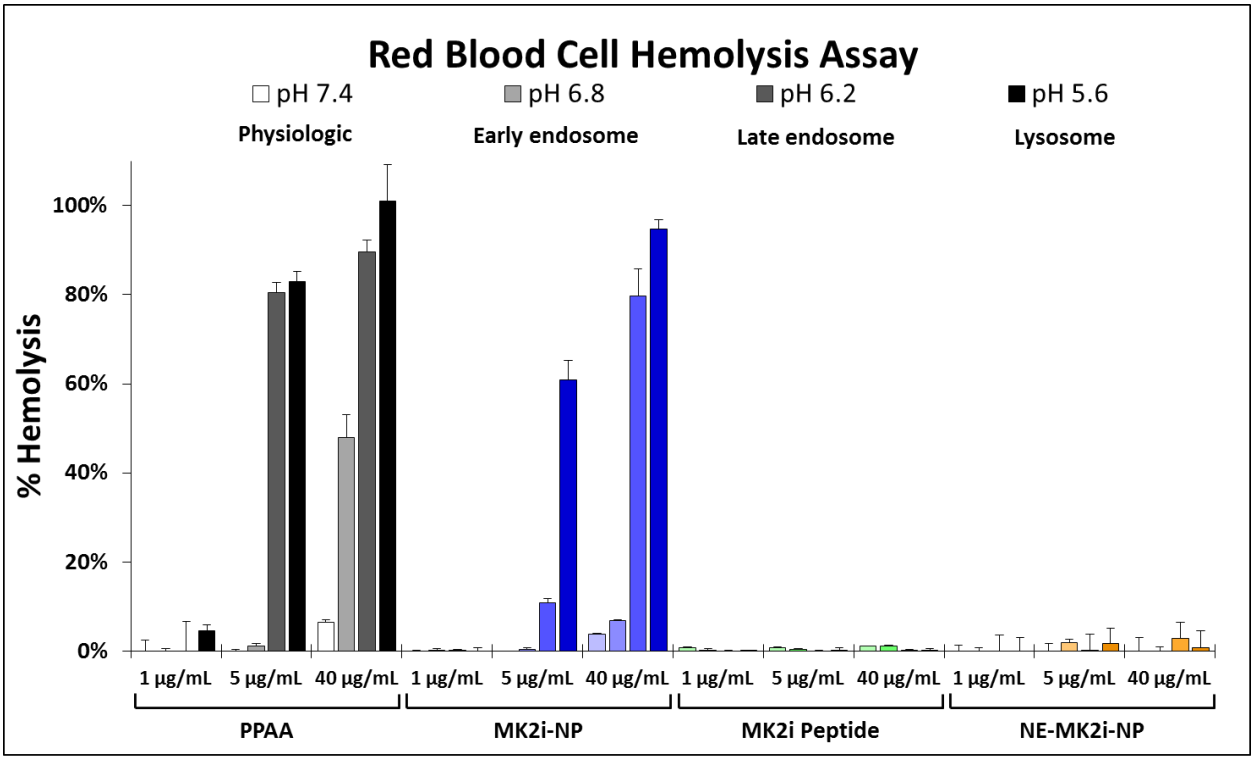

Figure 2.7 - pH-dependent red blood cell membrane disruption. Red blood cell hemolysis assay shows that MK2i-NPs have similar, albeit slightly masked, pH-dependent and dose-dependent membrane disruptive activity to the PPAA polymer but NE-MK2i-NPs and the MK2i peptide alone do not.

At physiologic and even early endosomal pH, no significant red blood cell membrane disruption was observed even at polymer concentrations as high as 40 µg/mL. However, as the pH was lowered to late endosomal values, a significant increase in hemolysis was observed, with greater membrane disruption at pH 5.8 compared to 6.6. The hemolytic behavior of the polymer was directly proportional to polymer concentration, with over 90% erythrocyte lysis occurring at 40 µg/mL polymer in pH 5.8 buffer. This switch-like transition to a membrane disruptive conformation at late endosomal pH combined with negligible membrane disruptive activity in the physiologic pH range demonstrates the desired functionality of the polyplexes and further indicates their potential as non-toxic, endosomolytic intracellular delivery vehicles. Interestingly, the polyplexes demonstrated less hemolytic capacity than the pH responsive

polymer alone, indicating that the formation of an electrostatic complex with the MK2i peptide slightly masks the membrane-disruptive activity of the polymer. This finding is consistent with the pH-dependent size changes monitored by DLS, which evinced polyplex dissociation at early endosomal pH values (i.e. pH 6.8), indicating that as the endosomal pH decreases the polyplexes will first dissociate and subsequently disrupt the endosomal membrane. This behavior is advantageous in that it effectively "un-packages" the therapeutic peptide from the electrostatic complexes prior to cytoplasmic release, ensuring that peptide bioactivity is not hindered due to steric hindrance from the pH-responsive polymer.

Discussion

Methods to enable the efficient intracellular delivery of peptide-based therapeutics are a potentially high-impact but relatively unmet need. This shortcoming is primarily due to multiple delivery barriers that exist in terms of delivering biomacromolecular therapeutics, each of which must be addressed to optimize bioactivity. The data presented herein demonstrate the successful synthesis and optimization of electrostatically complexed, pH-responsive nanoparticles that are ~100 nm in size and show pH-responsive unpackaging and membrane disruptive behavior ideal for endosomal escape and intracellular pay-load delivery.

The RAFT synthesized PPAA polymer serves as the key component of this nanotechnology platform for intracellular peptide delivery. The carboxylic acid groups present in the PPAA repeating unit has a pKa ~6.7, causing it to become protonated and membrane-disruptive at pH values encountered in the endo-lysosomal pathway as shown in **fig. 2.7**. [62]. These carboxylic acid groups are deprotonated at pH values above the pKa of 6.7, rendering the polymer anionic at slightly basic pH values. This anionic behavior allows for electrostatic complexation with cationic peptides due to the presence of primary amines in specific amino acid side chains (pKa ~9-12 depending on the amino acid) and results in well-defined nano-polyplexes as shown in **figs. 2.5** and **2.6**. Furthermore, the electrostatic complexation of a cationic therapeutic and the anionic 'smart' polymer is reversible, allowing for 'de-complexation' and release of the peptide once the PPAA polymer becomes protonated due to electrostatic repulsion as shown in **2.5A**. Most peptide based therapeutics, as well as many nucleic acid, protein and small molecule based therapeutics, utilize a cell penetrating peptide to facilitate cellular uptake, and the majority

of these cell penetrating peptides are cationic in nature (e.g. oligoarginines, oligolysines, TAT, penetratin, etc.) [12, 13, 81, 82]. As a result, this approach has the potential to serve as a platform technology for the intracellular delivery of a wide range of therapeutics for a myriad of applications.

Conclusion

The utilization of RAFT polymerization enabled the synthesis of a relatively monodisperse endosomolytic, pH-responsive poly(propylacrylic acid) homopolymer and a control non-endosomolytic poly(acrylic acid) homopolymer. Solid-phase peptide synthesis utilized in conjunction with reverse phase HPLC yielded a pure MK2i peptide. These components were utilized to formulate pH-responsive, endosomolytic MK2i nano-polyplexes (**MK2i-NPs**) and control, non-endosomolytic nano-polyplexes (**NE-MK2i-NPs**). MK2i-NPs demonstrated ideal pH-responsive behavior both in terms of pH-responsive decomplexation to allow for payload release after cellular internalization and in demonstrating switch-like, pH-dependent membrane disruptive activity (whereas the control NE-MK2i-NPs did not). As a result, two separate NP formulations have been synthesized, characterized, and optimized for further study as peptide-delivery carriers *in vitro*.

CHAPTER III

MK2I-NP UPTAKE, RETENTION, ENDOSOMAL ESCAPE, & BIOACTIVITY

Introduction

It is widely reported in literature that peptides, as well as other biomacromolecular therapeutics, suffer from poor uptake as they are not inherently membrane permeable [83]. Thus, many therapeutic biologics are modified with cell penetrating peptide sequences to increase peptide uptake and bioactivity. However, the choice of CPP sequence significantly influences peptide potency, and CPPs can cause nonspecific effects independent of the therapeutic sequence. The original MK2 inhibitory peptide sequence was discovered and optimized as a substrate peptide based on the sequence surrounding the serine 86 phosphorylation site of heat shock protein 27 (*13*). Testing various MK2 inhibitory peptides revealed that the inclusion of many CPP sequences caused nonspecific kinase inhibitory activity that was associated with cytotoxicity *in vitro* (*12*). These findings led to the discovery that the CPP sequence utilized in the current studies (i.e., YARAAARQARA, a modified version of the HIV transactivator of transcription, or TAT, cell penetrating peptide) produces optimal specificity against MK2 and motivated our goal of developing a translational delivery technology to enhance the therapeutic potential of this optimized MK2i peptide. The optimized MK2i-NP formulation formulated with this cell permeant MK2i peptide yielded a nanoparticle with a negative surface (ζ-potential of -11.9 ± 3.2 mV). Current approaches to non-specifically increase cellular uptake are almost universally focused on imparting a positive charge to the drug formulation in order to interact with the inherent negative charge of the cellular membrane [19, 58, 84]. In order to ensure that formulation into a negatively charged nanoparticle does not hinder cellular uptake, cellular uptake studies will be performed to compare uptake of free peptide to the MK2i-NP and NE-MK2i-NP formulations. Furthermore, since multiple cell-types are present in vein grafts, cell type-specific uptake will be investigated through the quantification of MK2i uptake in both vascular smooth muscle and endothelial cells.

MK2i-NPs evinced ideal membrane disruptive activity as demonstrated through a red blood cell hemolysis assay. However, the lipid bilayer that constitutes the membrane of red blood cells is merely a

biological model and does not accurately replicate the endosomal membrane. Thus, endosomal escape will be further investigated and verified *in vitro* through colocalization studies using microscopic analysis of fluorescently labeled MK2i-NP uptake in conjunction with an endosomal dye over time. Escape from endosomal trafficking is a promising approach to extending the duration of efficacy of peptide-based therapeutics as it circumvents trafficking for lysosomal degradation and/or trafficking for exocytosis. To this end, the intracellular retention of MK2i when delivered in an endosomolytic NP formulation will be measured over time following treatment removal in vascular smooth muscle cells.

NP formulation is designed to optimize uptake, retention, and endosomal escape of the MK2i peptide; hence, it is hypothesized that NP formulation will concomitantly increase MK2i bioactivity and duration of therapeutic efficacy. MK2 inhibition has demonstrated promise in inhibiting cell migration and inflammatory cytokine production which are both hallmarks of IH pathogenesis. As a result, the ability of MK2i-NPs to inhibit inflammatory cytokine production and migration will be assessed in both vascular smooth muscle and endothelial cells. To assess the duration of therapeutic efficacy, inflammatory cytokine production will be assessed over time following treatment removal in cells stimulated with an inflammatory agonist. Furthermore, due to the inherent membrane disruptive activity of PPAA, there is potential that NP formulation may have deleterious effects on cell viability. Consequently, cell viability will be assessed in cells treated with a range of concentrations of the NP formulations to ensure biocompatibility.

Methods

Cell culture

Primary HCAVSMCs and HUVECs were obtained from Lonza; HCAVSMCs were cultured in vascular cell basal medium (ATCC) supplemented with a vascular smooth muscle cell growth kit, 1% penicillin-streptomycin and plasmocin (5 µg/mL)]. HUVECs were cultured in endothelial basal medium (Lonza) supplemented with an EGM-2 bullet kit, 1% penicillin-streptomycin and plasmocin (5 µg/mL).

All cultures were maintained in 75cm^2 polystyrene tissue culture flasks in a 37°C and 5% CO_2 environment with cell culture media refreshed every other day. Cells were grown to 80-90% confluence prior to being harvested and passaged. All cells were seeded at a density of 20,000-30,000 cells/cm^2, as

required for each specific experiment. Only cells from early passages (numbers 3-8) were used in experiments.

Microscopic analysis of MK2i-NP uptake and intracellular trafficking

An amine-reactive Alexa-488 succinimidyl ester was dissolved in DMSO and mixed at a 1 to 3 molar ratio with the MK2i peptide in 100 mM sodium bicarbonate buffer (pH 8.3). Unreacted fluorophore and organic solvent were removed using a PD-10 miditrap G-10 desalting column, and the fluorescently labeled peptide was lyophilized. PPAA and PAA polymers were mixed with fluorescently labeled MK2i peptide at a CR 1:3 and syringe filtered through a 0.45 µm PTFE filter to form fluorescent MK2i-NPs and control NE-MK2i-NPs, respectively. Fluorescent MK2i-NPs, NE-MK2i-NPs, or MK2i peptide alone were applied to HCAVSMCs grown on Lab-Tek II 8-well chambered coverglass at a concentration of 10 µM MK2i peptide in low serum media for 2 hours. Cells were then washed 2x with PBS, and subsequently incubated in fresh medium for an additional 0, 2, 4, 10, or 22 hours. For the final two hours of incubation, 50 nM Lysotracker Red DND-99 was added to each well in order to visualize acidic endo/lysosomal vesicles. Cells were then washed with 0.1% Trypan blue to quench extracellular fluorescence followed by 2 additional washes with PBS. Cells were then imaged using a LSM 710 META confocal fluorescence microscope with ZEN imaging software. Gain settings were kept constant for all images acquired.

All images were processed using imageJ and colocalization was analyzed using Just Another Colocalization Plugin (JACoP) [85]. Mander's overlap coefficients were then calculated for $n \geq 3$ separate images for each treatment group to quantify colocalization. To determine treatment effects on the size of the compartments where the peptide was found, the free hand selection tool in ImageJ was used to outline $n \geq 50$ individual intracellular compartments for each treatment group, and the area of each was quantified and averaged.

Flow cytometric quantification of MK2i-NP uptake and intracellular retention

HCAVSMCs or HUVECs were grown to 80-90% confluence, harvested, and seeded at 20,000 cells/well in a 24 well plate and allowed to adhere overnight in low serum media (DMEM, 1% FBS, and 1% P/S). Fluorescent MK2i peptide, MK2i-NPs, and NE-MK2i-NPs were synthesized as noted above for

microscopy analysis, and HCAVSMCs were treated at a concentration of 10 μM MK2i for 2 hours. Following treatment, cells were washed with PBS, washed with CellScrub buffer for 10 minutes at room temperature to remove extracellular polyplexes and/or peptide, washed 2x in PBS, and given fresh complete growth media. ECs were immediately harvested and VSMCs were incubated for an additional 0, 12, 24, 72, or 120 hours. Cells were then washed with PBS, trypsinized, and resuspended in 0.1% Trypan blue in PBS for analysis on a FACSCalibur flow cytometer BD CellQuest Pro software (v 5.2). Data was exported and analyzed with FlowJo software (V 7.6.4). All samples were run in triplicate.

The intracellular MK2i half-life ($t_{1/2}$) was calculated by exponential decay nonlinear regression analysis of intracellular peptide fluorescence at 0 and 5 days following treatment removal using the exponential decay function [where N= intracellular fluorescence and λ = the decay rate]:

$$N(t) = N_o e^{-\lambda t} \qquad (eq. 1)$$

And calculating the $t_{1/2}$ from the decay constant of each exponential decay function as follows:

$$t_{1/2} = {\ln(2)}/{\lambda} \qquad (eq. 2)$$

Boyden chamber chemotaxis assay

HCAVSMCs or HUVECs were seeded in a 24 well plate at a density of 30,000 cells/well in low serum media and allowed to adhere overnight. Cells were treated for 30 mins with MK2i-NPs, NE-MK2i-NPs, MK2i peptide, or PBS. For 5 day post-treatment migration assays VSMCs were washed 2x with PBS and then cultured in fresh medium for 5 days with the media being replaced every 2 days. Following treatment or 5 days of post-treatment incubation, each well was washed 2x with PBS , trypsinized, resuspended in 100 μl low serum growth media, and plated onto 6.5-mm, 8-μm pore polycarbonate inserts (Corning) in a 24-well plate with 600 μl low serum growth media containing either 50 ng/ml PDGF-BB (VSMCs) or 25 ng/ml VEGF (ECs) in the lower chamber. Cells were allowed to migrate for 8 hours, and then cells on the upper side of each insert were gently removed with a cotton swab. Cells on the lower side of each insert were then fixed and stained using a Modified Giemsa Differential Quik Stain Kit. After staining, 4 images were taken from the four quadrants of each insert, and the number of cells per high-power field were quantified in ImageJ by thresholding each image and manually counting the cells.

Scratch wound chemokinesis assay

HCAVSMCs were seeded in Lab-TEK II 8-well chambered coverglass at a density of 20,000 cells/well in 250 µl low serum growth media and allowed to adhere overnight to achieve a nearly confluent (90-95%) monolayer. Cells were treated with MK2i-NPs, NE-MK2i-NPs, MK2i peptide or PBS -/- for 30 minutes. Following treatment, scratch wounds were made with a 10 uL pipette tip through the middle of each cell monolayer. The media was then replaced with low serum growth media containing a CellTracker Green BODIPY dye for 30 minutes to enable visualization of migrating cells. Following treatment with the dye, media was replaced with low serum growth media containing 50 ng/ml PDGF-BB (or with PBS for the negative control). Scratch wound areas were then imaged at 24 hours using a Nikon Eclipse Ti inverted fluorescence microscope with NIS Elements imaging software. Wound closure was calculated with ImageJ software by quantifying the scratch wound area around the periphery of migrating cells normalized to the original scratch wound area. Scratch wound assays for each treatment group were performed in 3 independent experiments.

Cell proliferation assay

To confirm that VSMC migration results were not influenced by treatment effects on cellular growth rates, a cellular proliferation assay was performed. HCAVSMCs were seeded at 10,000 cells/well in a 96-well plate in low serum media and allowed to adhere overnight. Cells were treated for 30 minutes with MK2i-NPs, NE-MK2i-NPs, MK2i peptide or PBS. Each treatment was then aspirated and replaced with 100 µl low serum growth media ± 50 ng/ml PDGF-BB. After 24 hours of incubation, a CellTiter 96 Aqueous Non-Radioactive Cell Proliferation Assay (Promega) was performed according to the manufacturer's protocol.

MK2i-NP cytotoxicity in stimulated HCAVSMCs

The CytoTox-ONE Homogenous Membrane Integrity assay (Promega) was used to assess the cytotoxicity of MK2i, MK2i-NP, and NE-MK2i-NP treatments according to the manufacturer's instructions. Briefly, HCAVSMCs from early passage were grown to 80-90% confluence in a 75 cm^2 tissue culture flask in a 37°C/5% CO_2 incubator prior to harvest. 200 µL of cell suspension (at 10,000 cells/well) was seeded

onto 96-well plates to yield an approximate 70% confluence per well. Cells were allowed to adhere to the plate overnight. Cells were stimulated with either 10 μM angiotensin-II or 20 ng/ml TNF-α for 4 hours followed by treatment with MK2i-NPs, MK2i, or NE-MK2i-NPs for 2 hours. Following treatment, cells were aspirated and 200 μL of fresh medium was added to each well. After 24 hours of incubation in fresh media cells were washed 2x with PBS and re-suspended in 100 μL lysis buffer. Each well was then supplemented with 100 μL Lactate dehydrogenase (**LDH**) substrate and incubated at RT for 10 minutes prior to the addition of 50 μL stop solution. LDH-induced fluorescence (excitation 550 nm, emission 600 nm) was then quantified with a TECAN Infinite M1000 Pro plate reader and used to determine cell viability compared to untreated control groups.

Inflammatory Cytokine Analysis

In order to evaluate the ability of MK2i-NPs to inhibit Interleukin-6 (**IL-6**) production, HCAVSMCs were cultured and seeded onto a 96-well plate using the methods described in the LDH cytotoxicity assay above. Cells were treated with 20 ng/mL tumor necrosis factor-α (**TNFα**) for 4 hours followed by treatment with MK2i-NPs or MK2i alone for 2 hours. Following treatment, each well was aspirated and supplemented with fresh medium. After 12 and 24 hours, 100 μL of supernatant was collected and frozen at -80°C until cytokine analysis could be performed.

Similarly, to evaluate the ability of MK2i-NPs to inhibit TNFα production, HCAVSMCs were cultured and seeded onto a 96-well plate using the methods described in the LDH cytotoxicity assay above. Cells were treated with 10 μM ANG II for 4 hours followed by treatment with MK2i-NPs, NE-MK2i-NPs, or free MK2i peptide alone for 2 hours. Following treatment, each well was aspirated and supplemented with fresh medium. After 12 and 24 hours, 100 μL of supernatant was collected and frozen at -80°C until cytokine analysis could be performed.

To longitudinally assess the duration of NP effects on production of the inflammatory cytokine monocyte chemoattractant protein 1 (**MCP-1**) in vascular cells, HCAVSMCs and HUVECs were treated in low serum media with MK2i-NPs, MK2i, or NE-MK2i-NPs for 2 hours. Following treatment, each well was aspirated and supplemented with fresh medium. After 3 or 5 days cells were stimulated with TNFα (20

ng/ml) for 24 hours. Following stimulation 100 µl of supernatant was collected and frozen at -80°C until cytokine analysis could be performed.

Human IL-6 (cat # 900-K16), Human TNFα (cat # 900-K25), and Human MCP-1 (cat # 900-K31) ELISA development kits (Peprotech; Rocky Hill, NJ) were used to measure cytokine levels in supernatant collected from treated cells. For both assays 9 standards were prepared according to the manufacturer's protocol. 40 µL of supernatant was diluted with 60 µL diluent; quadruplicates of each sample were used. Absorbance at 405 nm with wavelength correction at 650 nm was monitored for 1 hour with readings taken every 5 minutes. Concentrations of IL-6 and TNFα were determined through extrapolation from a 4 parameter logistic fit of the standard curve. All data were then normalized to cell viability determined through a LDH-based cytotoxicity assay (Promega). Data are expressed as mean ± SEM.

Statistics

Statistical analysis was performed with one-way analysis of variance (ANOVA) followed by Tukey's post-hoc test to validate statistical significance of mean differences between experimental groups. Analyses were done with OriginPro 8 software or Minitab 16 software. Statistical significance was accepted within a normal-based 95% confidence limit (α=0.05). Results are presented as arithmetic mean ± SEM graphically, and p-values are included within figures or in the figure legends.

Results

MK2i-NP uptake and Intracellular retention

Measurement of MK2i uptake and intracellular retention over a 5 day period after treatment removal in human vascular smooth muscle cells (**VSMCs**) revealed that MK2i-NPs significantly increased peptide internalization by over an order of magnitude and increased intracellular MK2i retention over 5 days after treatment removal (**fig. 3.1**).

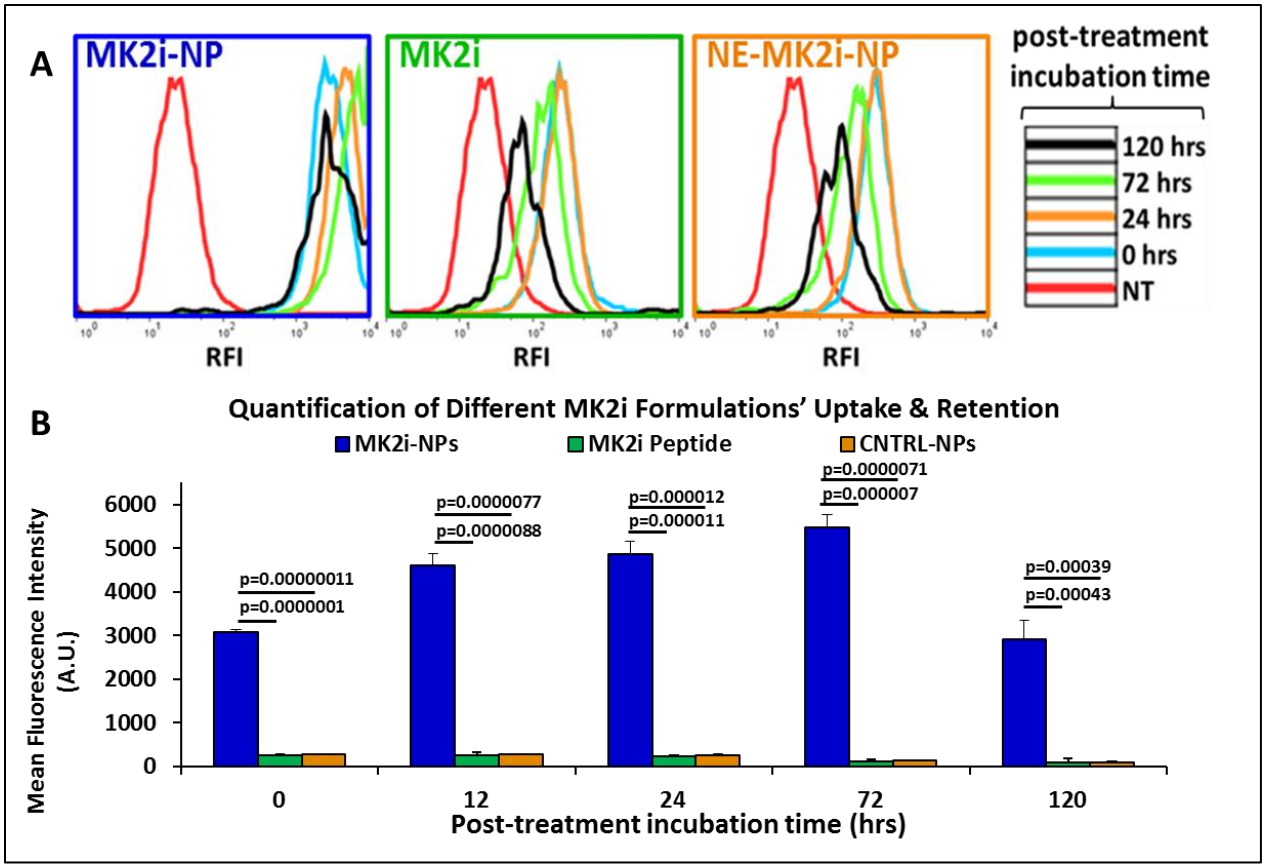

Figure 3.1 - MK2i-NP formulations increase cellular uptake and extend intracellular retention. (A) Representative flow histograms of MK2i internalization when delivered as a free peptide, via MK2i-NPs, and via NE-MK2i-NPs. **(B)** Flow cytometric quantification of HCAVSMC uptake and retention of fluorescently labeled MK2i, MK2i-NPs, and NE-MK2i-NPs. Data are mean ± SEM, *n* =3. *P* values determined via single factor ANOVA. From [2], reprinted with permission from AAAS.

Interestingly, MK2i-NPs showed an increase in peptide-associated fluorescence over the first 72 hours of incubation following treatment/washing. It was verified that this effect was not due to delayed internalization of MK2i-NPs bound to the outer membrane of the cells (**fig. 3.2**) but that this increase in fluorescence is due to an Alexa-488 self-quenching mechanism[86]; increased fluorescence over time may be due to diminished quenching as the MK2i is unpackaged from the NPs intracellularly.

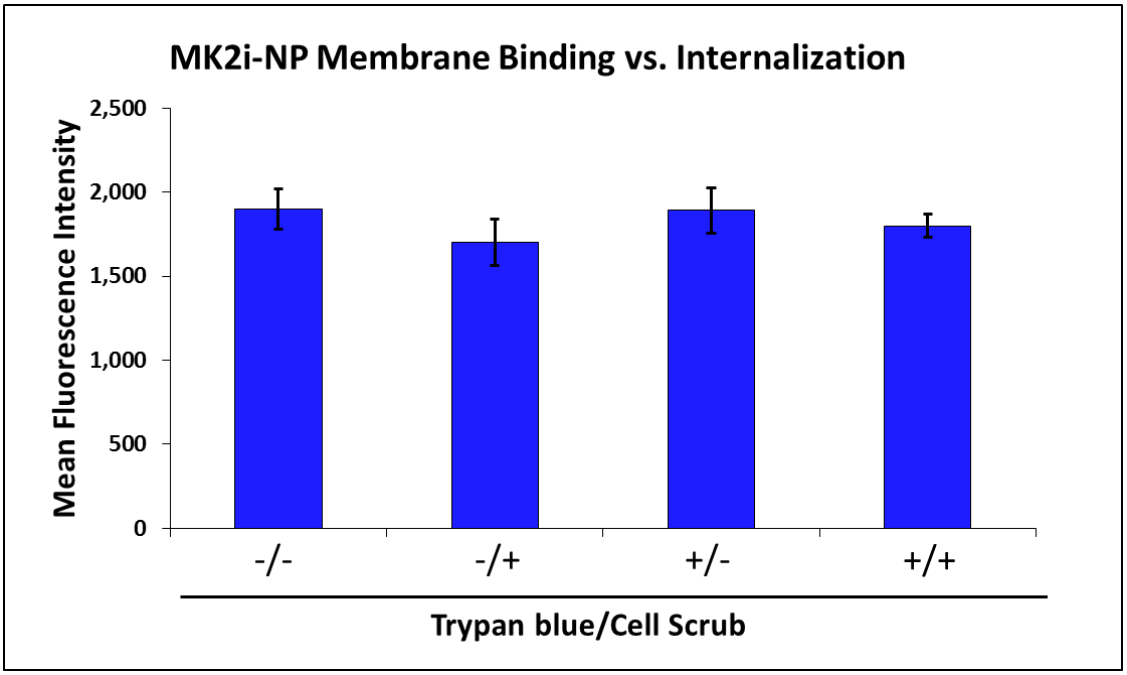

Figure 3.2 - MK2i-NP membrane binding. MK2i-NP internalization is not affected by membrane bound NPs as shown by minimal differences in MK2i-NP uptake in VSMCs that either had extracellular fluorescence quenched by trypan blue and/or were extensively washed with cell scrub buffer to remove any extracellular NPs following treatment removal.

Because NE-MK2i-NP uptake was equivalent to the free peptide, these data indicate that differences in cell internalization are due to NP composition and independent of particle morphology and charge. Notably, enhanced peptide delivery via the MK2i-NP formulation was also detected in analogous studies on endothelial cells suggesting that this is not a cell type-specific observation (**fig. 3.3**). Furthermore, considering that uptake was similar between separate cell types further suggest that increased internalization may be the result of a non-specific interaction/uptake mechanism or potentially mediated through a specific cell receptor present on both vascular smooth muscle and endothelial cells.

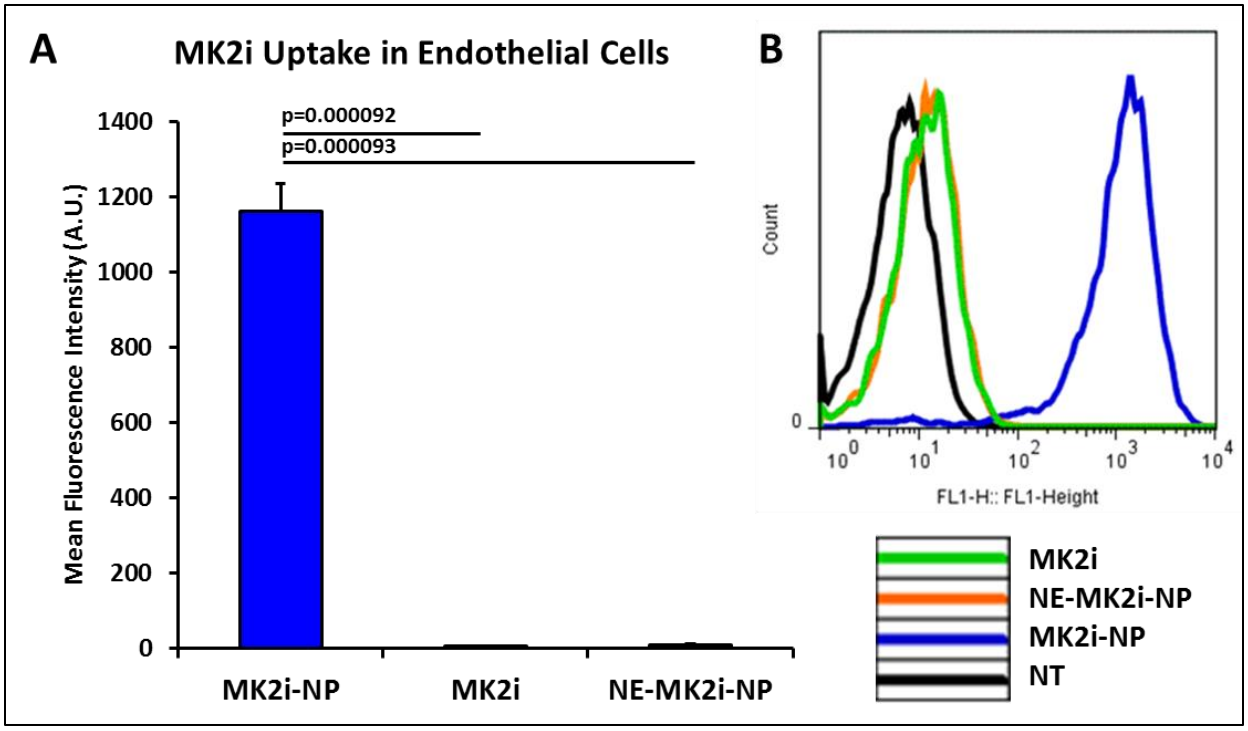

Figure 3.3 - MK2i uptake in endothelial cells. (A) Flow cytometric quantification and **(B)** representative flow histograms of endothelial cell uptake of fluorescently labeled MK2i, MK2i-NPs, and NE-MK2i-NPs. Data are mean ± SEM, *n* =3. *P* values determined via single factor ANOVA. From [2], reprinted with permission from AAAS.

Half-life calculations (**fig. 3.4 A**) showed that MK2i-NPs increased the intracellular half-life of the MK2i peptide by over an order of magnitude from 4 days to 58 days. However, it must be noted that these calculations may be skewed by the increase in intracellular fluorescence in cells treated with MK2i-NPs after treatment removal, which is why half-life calculations were performed solely on 0 and 5 day time points after the amount of MK2i fluorescence decreased below initial uptake levels. Considering that increased fluorescence over time may be due to diminished fluorescent quenching as the MK2i is unpackaged from the NPs intracellularly further supports that Increased peptide intracellular half-life following delivery via MK2i-NP formulations is likely due to decreased rate of peptide degradation in the endolysosomal pathway and/or the rate of exocytotic recycling out of the cell [87]. In addition to increasing uptake and intracellular retention, NP formulation also increased the percentage of treated cells positive for internalization following treatment (**fig. 3.4 B and C**). Furthermore, the percentage of VSMCs positive for internalization of the free MK2i peptide decreased over time (from 52% to 4% over 5 days) whereas VSMCs treated with the NP formulation stayed relatively constant (from 88% to 96% over

5 days). These findings further support that formulation into endosomolytic NPs increases the intracellular half-life of the MK2i peptide and shows potential to increase the duration of MK2i therapeutic efficacy.

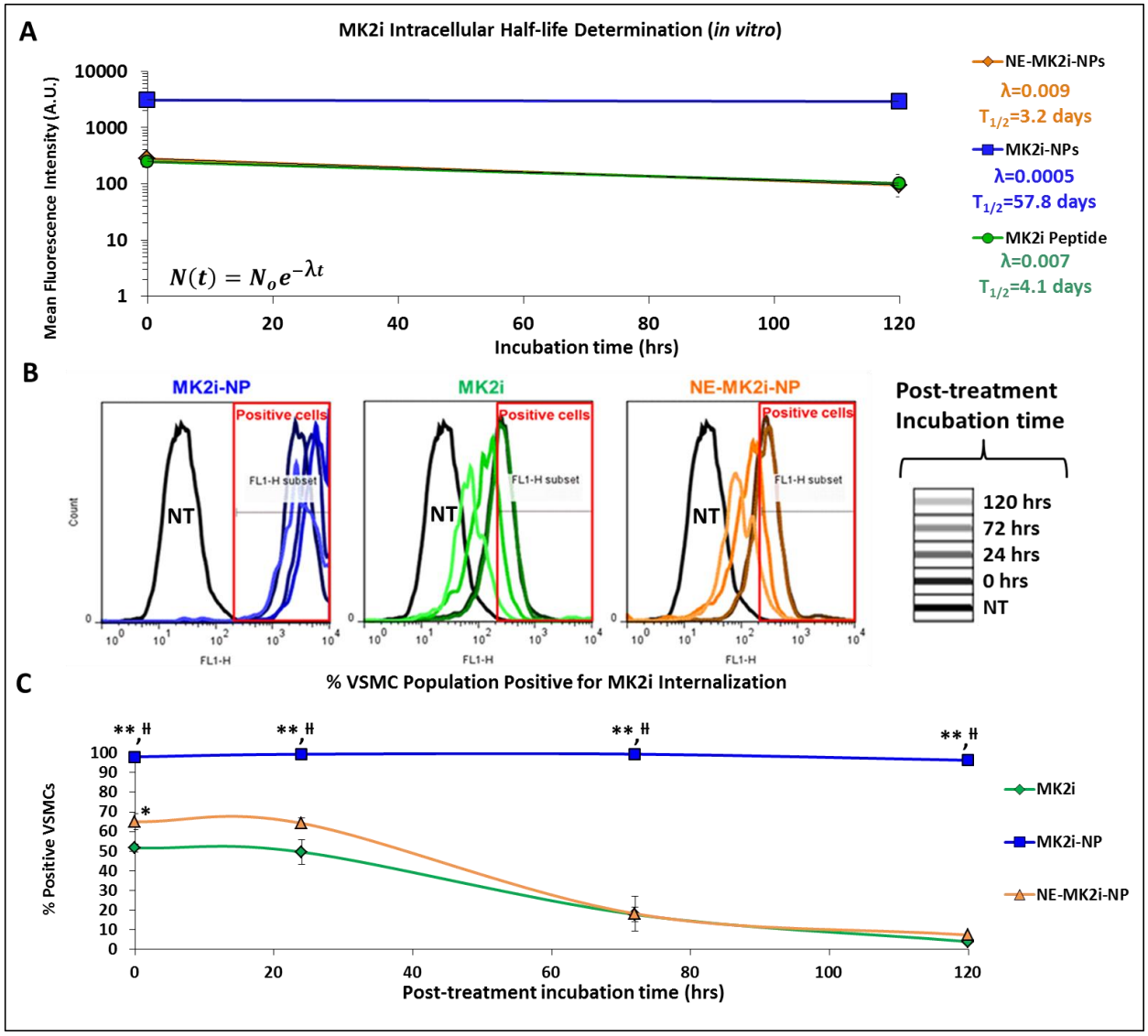

Figure 3.4 - MK2i uptake and intracellular retention. (A) Quantification of intracellular MK2i half-life ($t_{1/2}$) by exponential decay nonlinear regression analysis of intracellular peptide fluorescence at 0 and 5 days following treatment removal. **(B)** Longitudinal quantification and **(C)** Representative flow histograms and subsets used to calculate the percentage of HCAVSMCs positive for MK2i internalization following removal of treatment with free MK2i, MK2i-NPs, or NE-MK2i-NPs. Data are mean ± SEM, n =3. * P<0.01, ** P<0.001 vs. MK2i, ǂ P<0.01, ǂǂ P<0.001 vs. NE-MK2i-NPs. P values determined via single factor ANOVA. From [2], reprinted with permission from AAAS.

To elucidate the mechanism responsible for the observed increase in MK2i intracellular retention, microscopy/colocalization studies were used to assess endosomal escape of MK2i-NPs. Imaging and quantification of MK2i-NP endosomal escape in VSMCs demonstrated that MK2i-NP formulation significantly reduced MK2i endolysosomal colocalization (**fig. 3.5 A**). Longitudinal quantification of

MK2i/Lysotracker colocalization following treatment revealed significantly reduced MK2i/lysotracker colocalization for the MK2i-NP treated cells, and MK2i delivered via the NP formulation showed decreased colocalization over time, suggesting an active endosomal escape mechanism (**figure 3.5 B**). Interestingly, quantification of compartment size revealed that NE-MK2i-NP or MK2i treated cells showed MK2i localization within smaller vesicles representative of endosomes, whereas MK2i delivered via MK2i-NPs was found within larger compartments, potentially representative of the cytosol or disrupted vesicles (**fig. 3.5 C**).

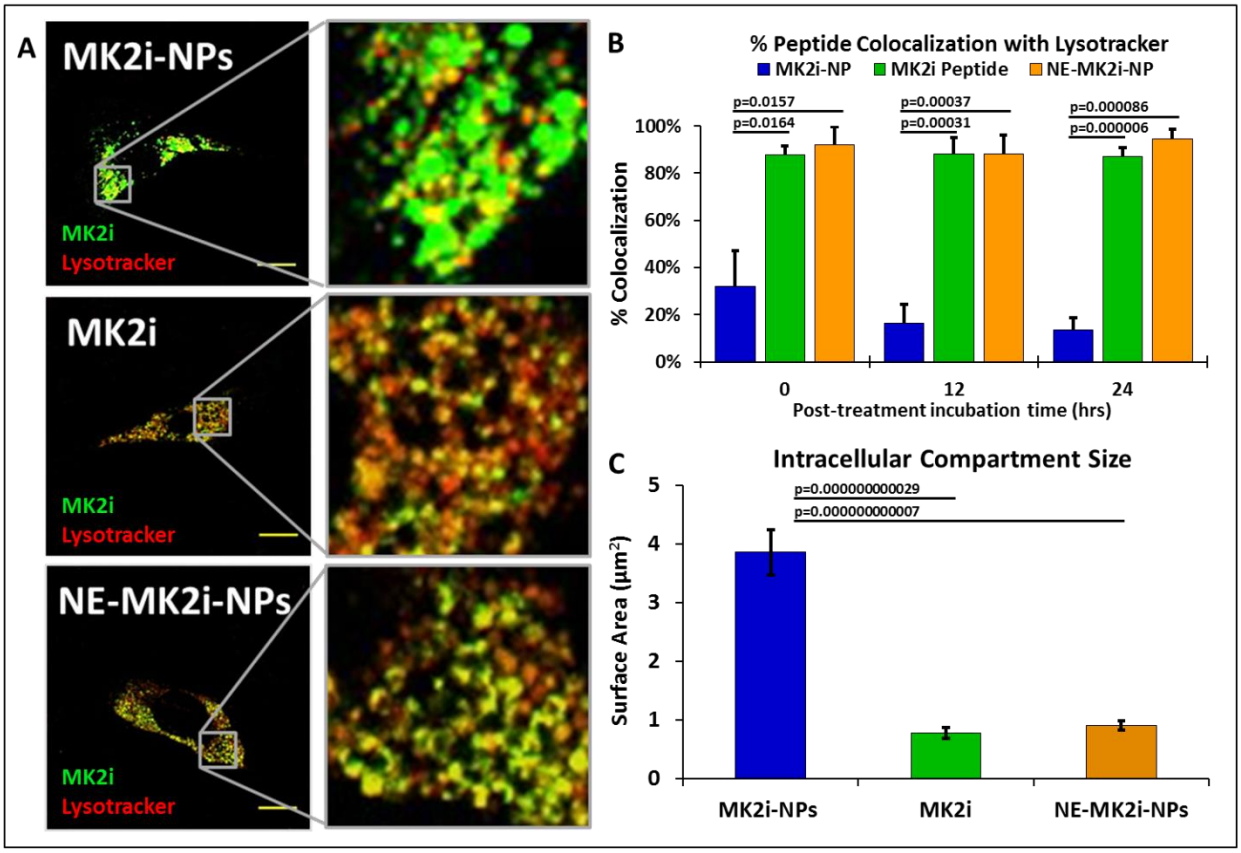

Figure 3.5 - MK2i-NPs reduce endo-lysosomal colocalization of MK2i. (A) Representative confocal microscopy images of Alexa-488 labeled MK2i (green) colocalization (yellow) with Lysotracker (red). Scale bars = 20 μm. **(B)** Quantification of MK2i Alexa-488 labeled MK2i colocalization with Lysotracker red in HCAVSMCs 24 hours after 2 hours of treatment determined via calculation of Mander's coefficients. Data are mean ± SEM (n≥3 separate images). *P* values determined via one way ANOVA. **(C)** Quantification of intracellular compartment size of HCAVSMCs treated with Alexa-488 labeled MK2i. Data are mean ± SEM (n≥50 separate intracellular compartments per treatment group). *P* values determined via one way ANOVA. From [2], reprinted with permission from AAAS.

In order to assess the *in vitro* therapeutic efficacy and cytocompatibility of NPs compared to the free MK2i peptide, TNFα and ANG II-stimulated HCAVSMCs were treated with a range of MK2i-NP or MK2i peptide concentrations for 2 hours and incubated in fresh media for 24 hours. Following incubation,

supernatant was collected for cytokine analysis and an LDH assay was used to quantify cell viability. None of the treatments displayed significant cytotoxicity at any of the concentrations tested (**fig. 3.6**).

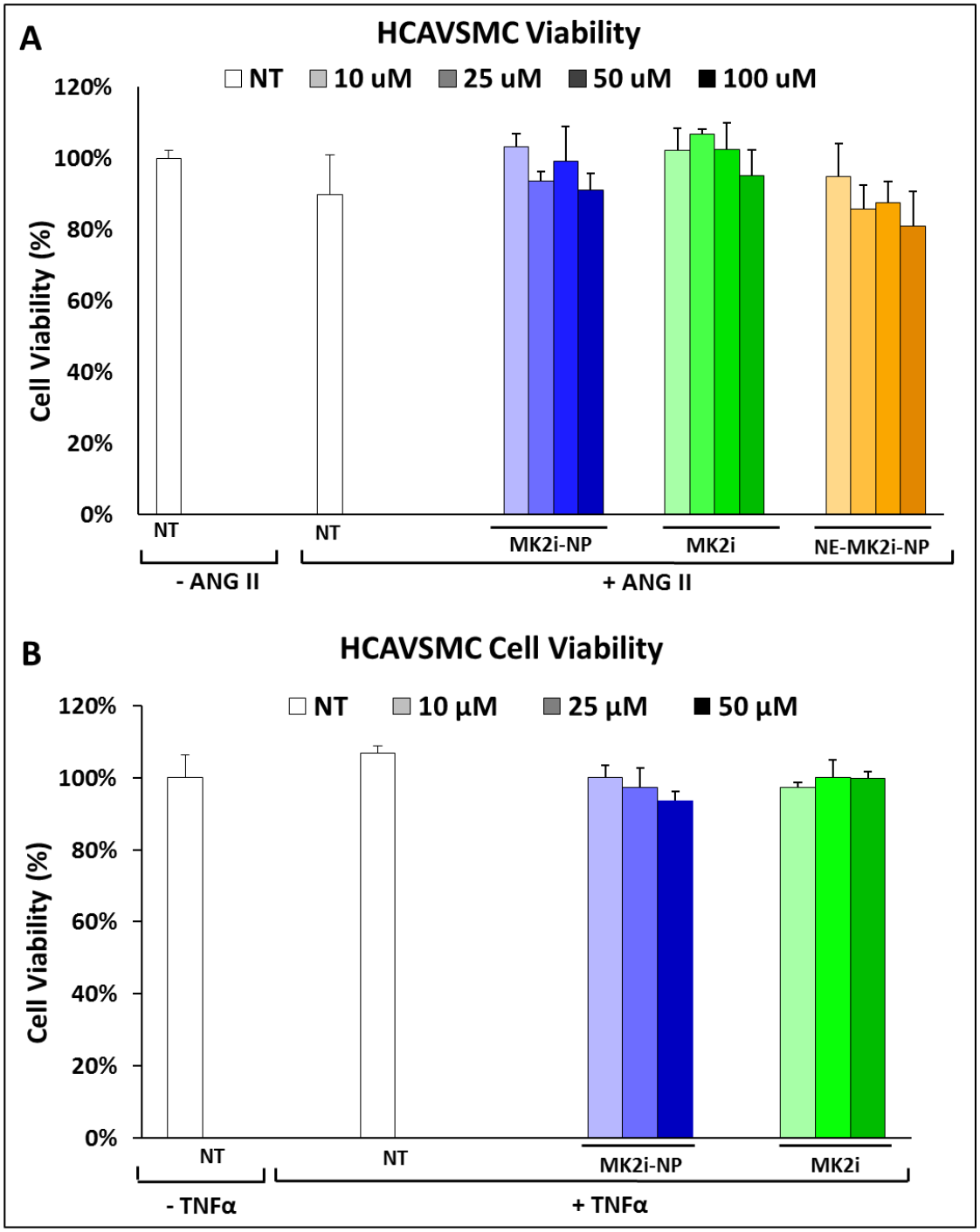

Figure 3.6 - Cell viability in treated HCAVSMCs. Cell viability in HCAVSMCs stimulated with **a)** 10 µM ANG II or **b)** 20 ng/ml TNFα for 6 hours, treated for two hours with MK2i-NPs, NE-MK2i-NPs, or the MK2i peptide alone (concentrations in figure legends) and cultured for 24 hours in fresh media as determined by an LDH cytotoxicity assay. NT = No treatment, data are mean ± SEM, *n* = 4. No statistically significant differences were observed. From [2], reprinted with permission from AAAS.

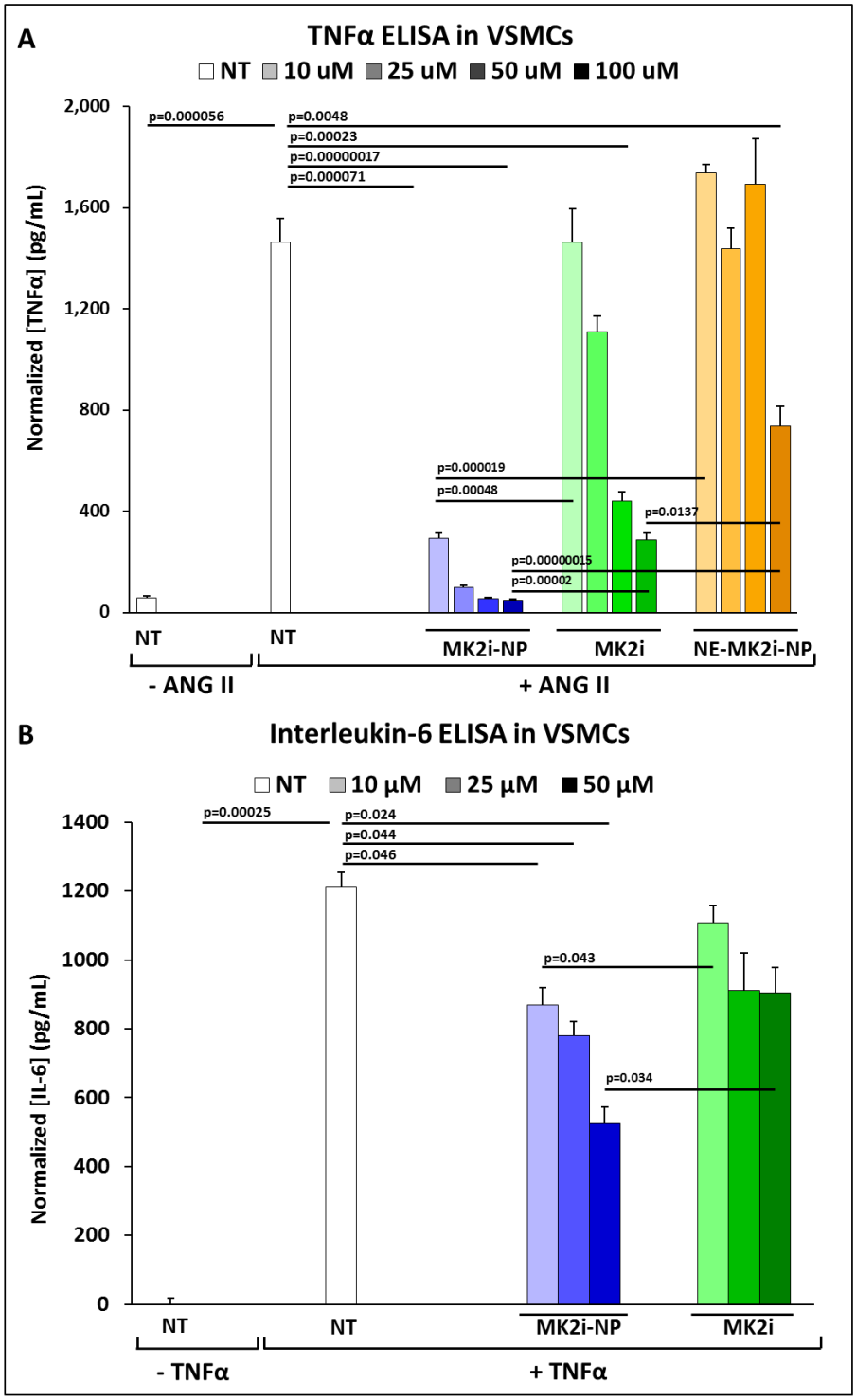

Figure 3.7 - MK2i-NP formulation enhances MK2i bioactivity *in vitro*. (A) Quantification of ANG-II-induced TNFα production in HCAVSMCs. Data are mean ± SEM (n = 4 technical replicates). *P* values determined via one way ANOVA. **(B)** Quantification of TNFα-induced IL-6 production in HCAVSMCs. Data are mean ± SEM (*n* = 4 technical replicates). *P* values determined via one way ANOVA. From [2], reprinted with permission from AAAS.

Subsequent to verification of cell viability, ELISAs were performed on collected supernatants to quantify IL-6 secretion and TNFα production in TNFα and ANG II-stimulated HCAVSMCs, respectively. Both IL-6 and TNFα are inflammatory cytokines that are activated downstream of MK2 and, thus, provide an indirect measure of MK2 inhibition [88-90]. MK2i-NPs were found to significantly inhibit TNFα production in ANG-II stimulated HCAVSMCs at all concentrations in a dose-dependent manner compared to the untreated control (f**ig. 3.7A**). In fact, MK2i-NPs were found to inhibit TNFα production at a 10-fold lower dose than the free peptide (10 µM

MK2i-NPs vs. 100 μM free MK2i). MK2i-NPs were also found to significantly enhance MK2i-mediated inhibition of IL-6 production compared to the MK2i peptide alone (**fig. 3.7 B**). Interestingly, measurement of TNFα secretion in ANG II-stimulated HCAVSMCs proved to be a more robust readout of NP activity relative to inhibition of IL-6 production in response to TNFα. As expected based upon uptake and endosomal escape studies, NE-MK2i-NPs made with a poly(acrylic acid) as a vehicle control did not demonstrate any enhancement in MK2i mediated inhibition of TNFα production.

In addition to inflammatory processes, vascular smooth muscle cell migration into the intima is also integral in the pathogenesis of IH [91]; Thus, both Boyden transwell chemotaxis and scratch wound chemokinesis assays were performed in treated HCAVSMCs in the presence of the chemoattractant platelet derived growth factor (**PDGF**). The Boyden transwell chemotaxis assay demonstrated that MK2i inhibition significantly inhibited VSMC chemotaxis (**fig. 3.8**).

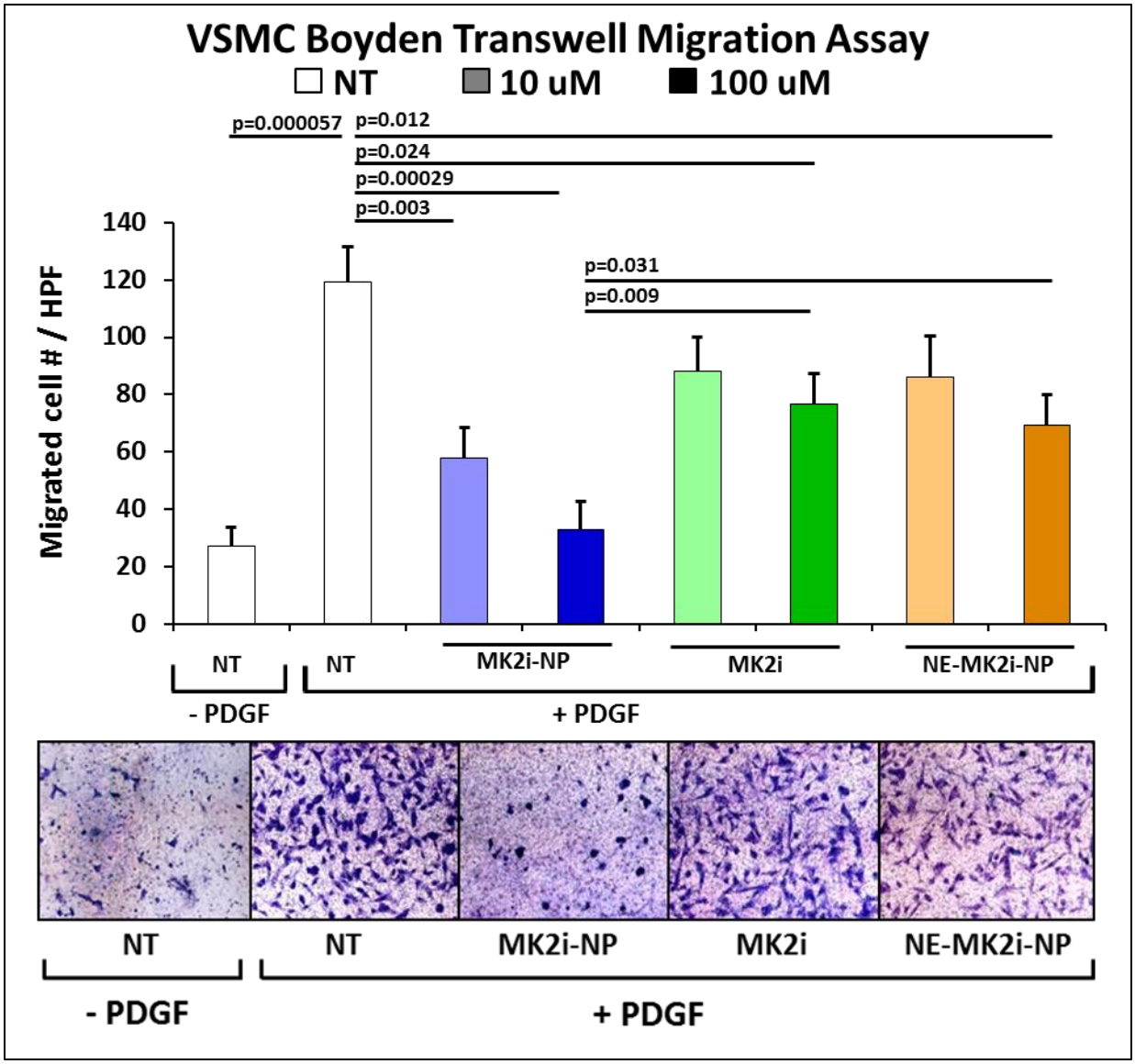

Figure 3.8 - MK2i-NPs inhibit VSMC chemotaxis *in vitro*. Quantification and representative images of HCAVSMC migration immediately after treatment removal determined via a Boyden transwell migration assay. Data are mean ± SEM (*n* = 3 technical replicates from 2 separate experiments). *P* values determined via one way ANOVA. From [1], reprinted with permission from AAAS.

In agreement with MK2i-NP inhibition of TNFα production, MK2i-NPs were found to equivalently inhibit directional VSMC migration at an order of magnitude lower dose than the free MK2i peptide. To further investigate the effects of MK2i-NPs on vascular smooth msucle cell migration, a scratch wound chemokinesis assay was performed (**fig. 3.9**). Similar to results yielded by chemotaxis assays, chemokinesis was also inhibited by MK2i and MK2i-NPs were able to inhibit migration at a significantly (i.e., >10-fold) lower dose than the free MK2i peptide. These results suggest that MK2 inhibition not only

inhibits directional vascular smooth muscle cell migration but also inhibits vascular smooth muscle cell motility.

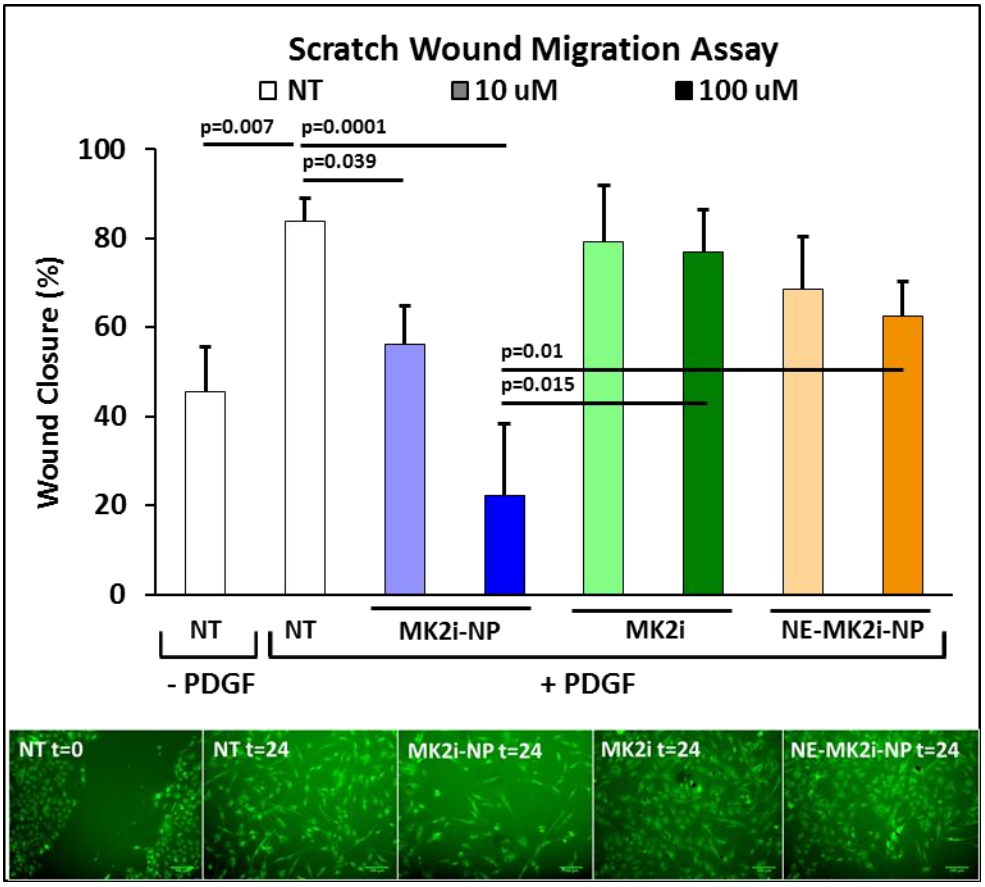

Figure 3.9 - MK2i-NPs inhibit VSMC chemokinesis *in vitro*. Quantification and representative images of HCAVSMC migration immediately after treatment removal determined via scratch wound migration assay. Scale bars = 100 μm, all images are of cells in the presence of PDGF. Data are mean ± SEM (n = 3). P values determined via one way ANOVA. From [1], reprinted with permission from AAAS.

In light of the significant effects of MK2i on cell migration, a proliferation assay was performed to ensure that inhibition of migration was not attributable to treatment effects on cell proliferation. The same treatment protocol and time points from the scratch wound migration assay were utilized for analysis of cellular proliferation with and without the addition of PDGF-BB. None of the treatments were found to produce significant effects on HCAVSMC proliferation although PDGF appeared to slightly increase proliferation and MK2 inhibition trended towards dose dependent inhibition of migration (**fig. 3.10**).

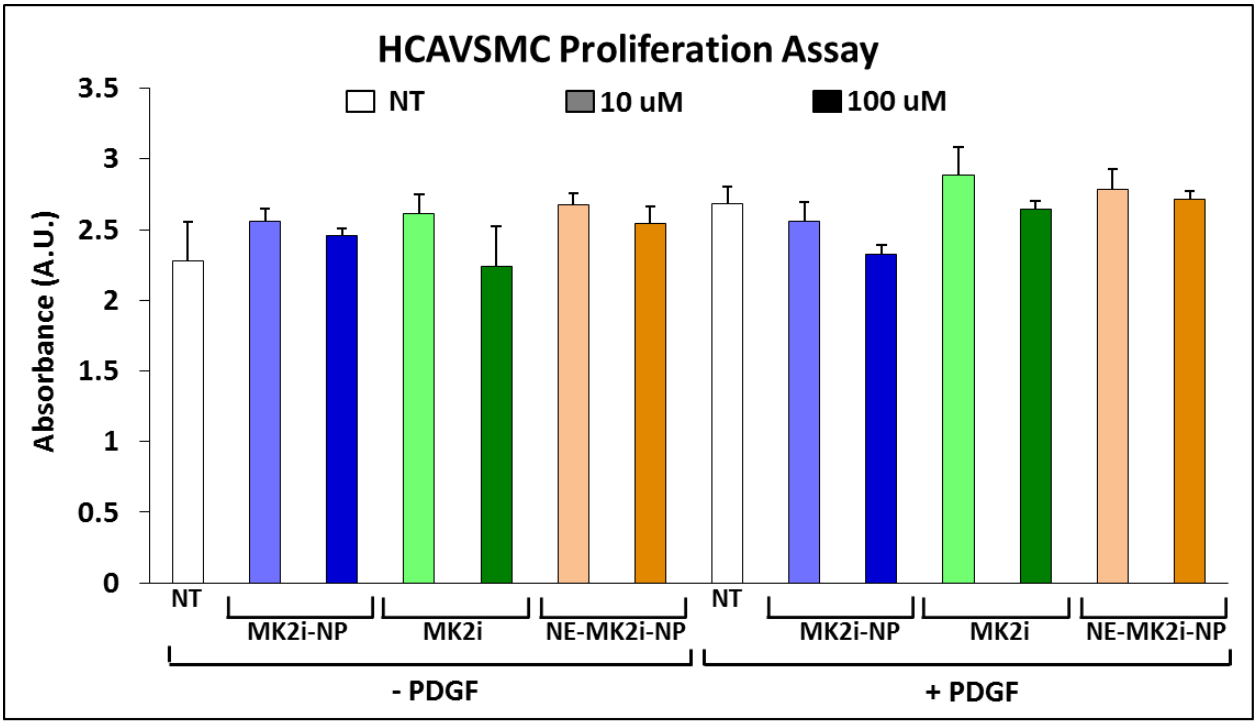

Figure 3.10 - Cell proliferation assay. Cell proliferation in HCAVSMCs treated for 30 minutes with MK2i peptide alone, MK2i-NPs, or NE-MK2i-NPs and cultured for 24 hours in fresh media with (+) or without (-) 50 ng/mL PDGF-BB. NT = no treatment, n = 4. No statistically significant differences were found. *P* values determined via one way ANOVA. From [1], reprinted with permission from AAAS.

Endothelial cells as well as vascular smooth muscle cells displayed increased uptake of the MK2i peptide when formulated into NPs, motivating inquiry into the effects of MK2 inhibition in endothelial cells. In order evaluate MK2i-NP effects on endothelial migration, a Boyden transwell migration assay was performed on endothelial cells in the presence of the chemoattractant vascular endothelial growth factor (**VEGF**) revealing that MK2 inhibition reduced cellular migration independent of cell type (**fig. 3.11**). Furthermore, it appears that MK2i-NPs were more effective at inhibiting migration in endothelial cells as well as vascular smooth muscle cells.

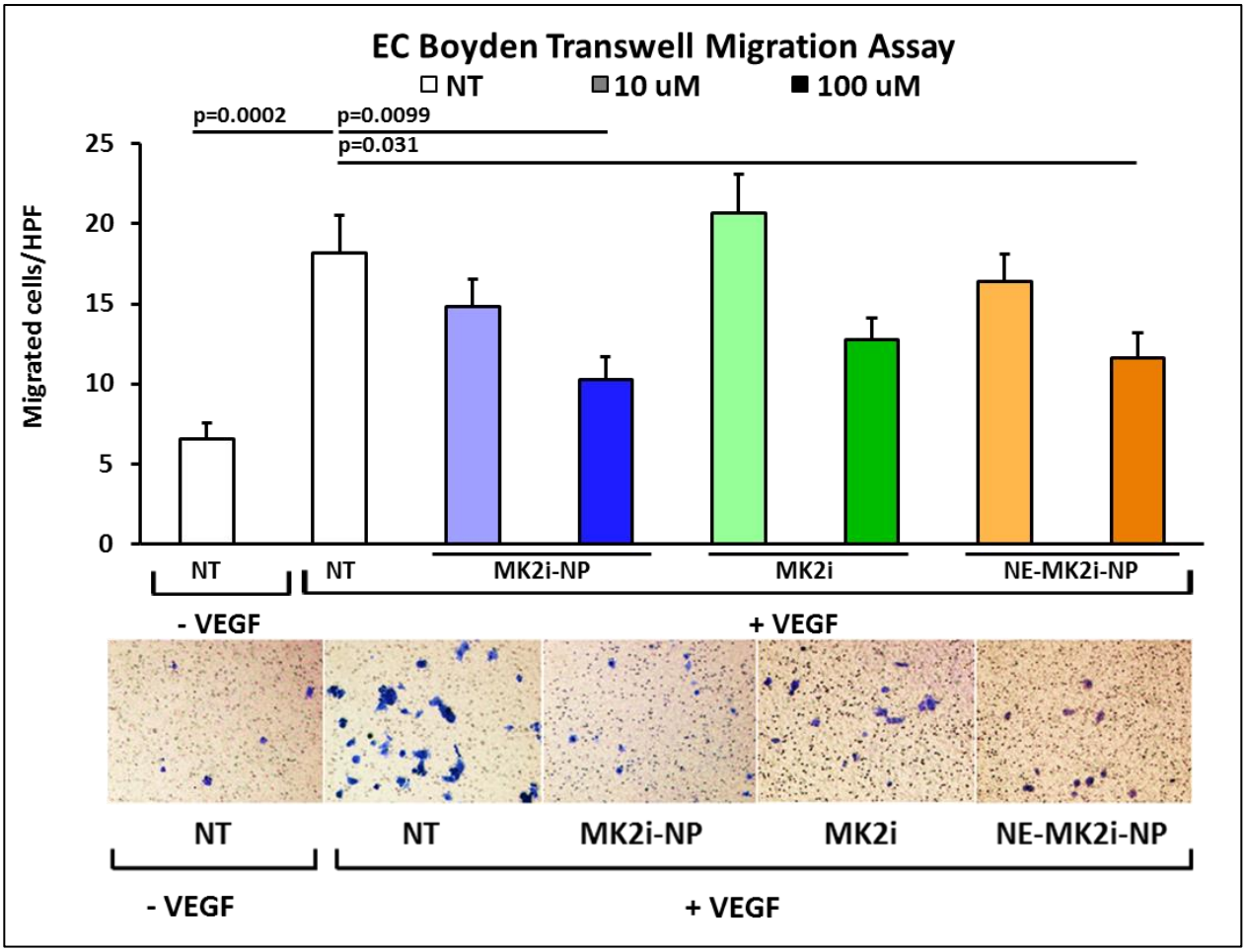

Figure 3.11 - MK2i effects on endothelial migration.
Quantification and representative images of HUVEC migration immediately after treatment removal determined via a Boyden transwell migration assay. Data are mean ± SEM (n = 3 technical replicates from 2 separate experiments). *P* values determined via one way ANOVA. From [2], reprinted with permission from AAAS.

Because the intracellular half-life of MK2i was significantly higher when delivered via MK2i-NPs, *in vitro* bioactivity assays were also carried out at 5 days post-treatment to assess the impact of the NP formulation on longevity of peptide therapeutic action. A 5 day time point was chosen as it is outside the calculated intracellular half-life of MK2i (i.e., 3.2 days), indicating that the bioactivity of the free peptide will be significantly reduced compared to MK2i-NPs. Indeed, investigation of Inhibition of VSMC migration 5 days post-treatment via a Boyden transwell chemotaxis assay revealed that MK2i-NPs sustained inhibitory activity at all concentrations whereas free MK2i or NE-MK2i-NPs showed no significant effects (**fig. 3.12**).

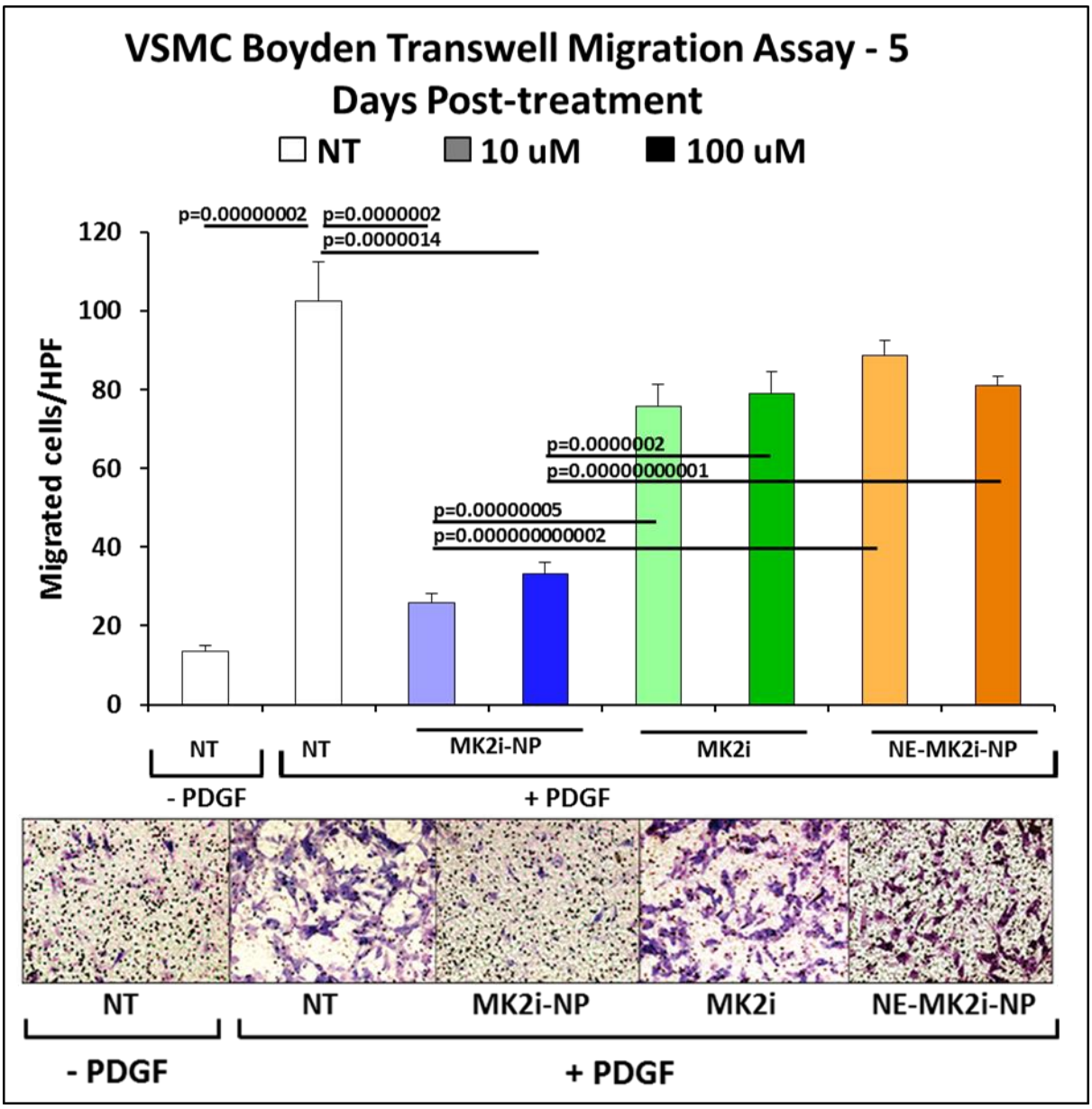

Figure 3.12 - MK2i-NPs prolong inhibition of VSMC migration *in vitro*. Quantification and representative images of HCAVSMC migration 5 days after treatment removal determined via a Boyden transwell migration assay. Data are mean ± SEM (n = 3 technical replicates). P values determined via one way ANOVA. From [2], reprinted with permission from AAAS.

In order to further investigate the effect of NP formulation on the duration of MK2i bioactivity, the ability of MK2i-NPs to sustain inhibition of inflammatory cytokine production was also investigated. In accord with intracellular half-life calculations for the MK2i-NP formulation compared to the free MK2i peptide, the ability of the free MK2i peptide to inhibit TNFα-stimulated production of monocyte chemoattractant protein-1 (**MCP-1**, which attracts inflammatory cells and is implicated in vein graft IH [92])

was significantly decreased at 5 days post-treatment in vascular smooth muscle cells (**fig. 3.13 A**) whereas MK2i-NPs demonstrated sustained inhibitory bioactivity at 5 days post-treatment. To clarify if this prolonged duration of bioactivity is cell type dependent the TNFα-stimulated production of MCP-1 in endothelial cells was also investigated at 3 and 5 days after treatment removal (**fig. 3.13 B**). MK2i-NPs were found to significantly inhibit endothelial MCP-1 production compared to both untreated and MK2i treated cells at both time points, further corroborating the intracellular half-lives calculated for the free peptide compared to the NP formulation.

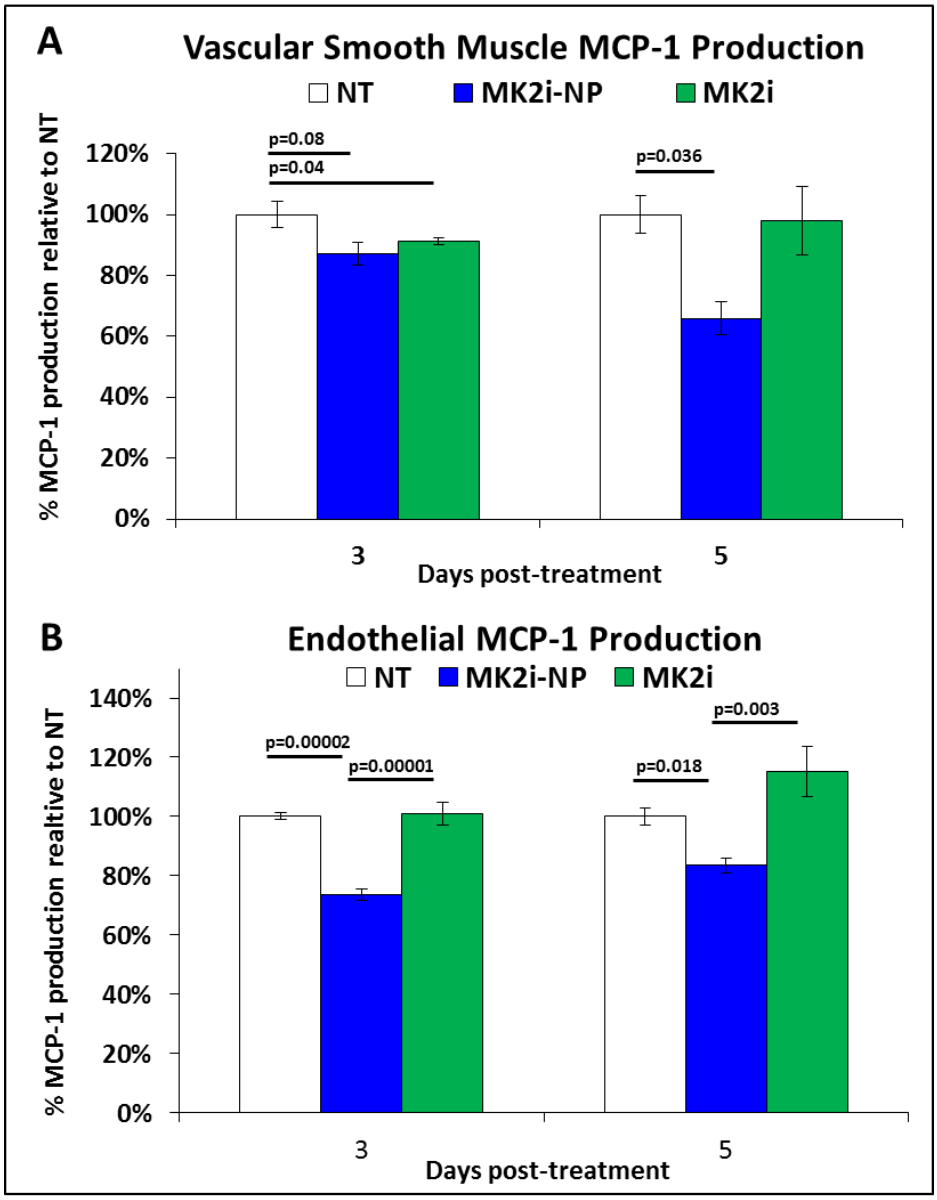

Figure 3.13 - Vascular smooth muscle and endothelial MCP-1 production over time. Quantification of MCP-1 production relative to untreated controls in both **(A)** vascular smooth muscle and **(B)** endothelial cells following 24 hours of stimulation with 20 ng/ml TNFα at 3 and 5 days after treatment removal. All treatments used a 10 μM dose of MK2i, Data are mean ± SEM, *n* = 4. *P* values determined via one way ANOVA. From [2], reprinted with permission from AAAS.

Discussion

Upon activation, MAPKAP Kinase II translocates from the nucleus to the cytoplasm [37] and, as a result, an antagonist of activated MK2 such as the MK2i peptide used herein must be efficiently internalized and delivered into the cytosol in order to optimize bioactivity. However, when delivered in its free form the MK2i peptide becomes entrapped in late endosomes [8] and is restricted from accessing activated MK2 in the cytoplasm. Formulation of the positively charged, CPP-based MK2i peptide with the anionic, endosomolytic polymer PPAA was conceptualized as a method to enhance peptide endolysosomal escape and therapeutic potency. This approach was inspired by the convention for nonviral delivery of nucleic acids, which is based on electrostatic formation of polyplexes between anionic nucleic acids and positively charged CPP sequences, lipids, or polymeric transfection agents to enhance uptake and endosomal escape [45, 93, 94]. NP formulation yielded net negatively charged particle; serendipitously, the NP formulation significantly increased peptide uptake by VSMCs relative to the free, CPP-based MK2i peptide. Notably, the *in vitro* comparisons of MK2i-NPs and NE-MK2i-NPs suggest that the high level of MK2i-NP cell internalization was dependent on the specific composition of PPAA, rather than purely dictated by NP morphology and surface charge. The α-alkyl substitution of the propyl moiety makes PPAA more lipophilic/hydrophobic relative to acrylic acid, suggesting that the observed differences in uptake may be the result of increased hydrophobic interactions of MK2i-NPs with the cell membrane. Hydrophobic interactions may nonspecifically trigger MK2i-NP cell internalization, or MK2i-NP internalization could be mediated through a more specific interaction, for example by VSMC scavenger receptors that are upregulated in settings of vascular stress and that internalize negatively charged/hydrophobic particles [95, 96].

Avoiding endolysosomal degradation and extracellular recycling is vital to optimizing potency and longevity of action of cytosolically-active peptides[7]. A sustained therapeutic effect is of particular importance for a peptide-based vein graft therapeutic where it is desirable for a single, intraoperative treatment to achieve prolonged bioactivity throughout the post-transplant inflammatory and healing phases. To this end, NP formulation improved the potency, intracellular retention and duration of bioactivity of the MK2i peptide in multiple vascular cell types through the pH-dependent membrane disruptive activity of PPAA, which is ideally tuned for directing endolysosomal escape. Furthermore, the

buffering capacity of the NPs may provide a means of cargo protection, since more acidic environments are typically more prone to degradation of biologic drugs. Once internalized, the duration of efficacy of the delivered peptide is dependent on rates of exocytosis, endo-lysosomal degradation, and cytoplasmic degradation. It is well established that free peptides in the cytosol are short-lived and rapidly broken down by intracellular proteolytic complexes (e.g. the ATP-dependent 26 S proteasome) [97]; the presented intracellular retention and duration of bioactivity data suggest that complexation with the PPAA polymer may not only facilitate endosomal escape but may also cytosolically stabilize the MK2i peptide and help sustain its bioactivity.

The data presented herein firmly establish the anti-migratory and anti-inflammatory mechanisms of action of MK2i-NPs in VSMCs *in vitro* and confirm the utility of targeting the p38-MK2 pathway to inhibit multiple factors underlying IH pathogenesis. Although VSMCs are considered the primary target cell for therapeutically blocking IH, vascular endothelial cells also efficiently internalized the MK2i-NPs. Considering focal disruption of the endothelium occurs during vein graft harvest even under optimal conditions [98], one potential concern is that MK2i-NP inhibition of endothelial migration may have deleterious effects on vein graft re-endothelialization. However, evidence suggests that ECs responsible for vein graft re-endothelialization are predominantly derived from the surrounding artery [99]. This concern does, however, further justify the use of an *ex vivo* topical treatment scheme that will avoid non-specific effects on cells outside the graft. Although not assessed here, the p38 MAPK pathway has also recently been implicated in TGF-β–mediated endothelial-to-mesenchymal transdifferentiation [32], which is believed to be a key mechanism underlying IH [100]. Recent studies have also demonstrated that MK2 deficiency promotes endothelial healing and prevents endothelial recruitment of inflammatory cells in an arterial injury model [80]. Although the role of endothelial MK2 inhibition in IH remains unclear, our data support that MK2 inhibition decreases endothelial production of inflammatory cytokines. These findings motivate further investigation into the role of endothelial MK2 inhibition in IH.

Conclusion

In vitro uptake, retention, and endosomal colocalization studies established that formulation into NPs drastically increases both cellular uptake and intracellular retention in both endothelial and vascular

smooth muscle cells. MK2i-NPs were found to facilitate endosomal escape and cytosolic delivery of a fluorescently labeled MK2i peptide. *In vitro* analysis of vascular smooth muscle and endothelial cell migration and inflammatory cytokine production revealed that MK2i-NPs significantly increased both the anti-migratory and anti-inflammatory potency and duration of therapeutic efficacy of the MK2i peptide. These results correlate well with the observed increase in uptake, intracellular retention, and endosomal escape facilitated by NP formulation with a pH-responsive, endosomolytic polymer.

It is hypothesized that when the MK2i-NP nanotechnology presented here is translated *in vivo*, that the enhanced uptake and intracellular half-life demonstrated *in vitro* will results in optimized peptide delivery that minimizes the therapeutic dose required and will prolong the duration of efficacy of the treatment. However, further *ex vivo* studies will be necessary to elucidate the underlying molecular mechanisms responsible for the observed bioactivity and to verify that the preliminary *in vitro* results presented will hold true in the more complex, 3-dimensional architecture of human vascular tissue. Ultimately, *in vivo* studies in a relevant animal model will be required to verify that MK2i-NPs can inhibit multiple processes underyling IH pathogenesis in a clinically relevant, dynamic flow environment. These studies will provide further insight into the role that MK2 plays in the transdifferentiation of vascular smooth muscle cells from a contractile (i.e., healthy) to a synthetic (i.e., pathological) phenotype and establish the clinical translatability of this approach as a platform technology for intracellular peptide delivery.

CHAPTER IV

MK2I-NPS AS A THERAPEUTIC FOR INTIMAL HYPERPLASIA

Introduction

Ex vivo, intraoperative treatment of grafts with MK2i-NPs is an ideal therapeutic strategy to enhance delivery to the target tissue and avoid potential for off-target effects or systemic toxicity. MK2 may represent an ideal target because of its involvement in inflammation, cell migration, and phenotypic modulation. A recent study on mouse vein grafts showed that while the free MK2i peptide prevented early intimal thickening, the rate of intimal thickening during weeks 1-4 post-transplant was similar between the treated and untreated control grafts [56]. Thus, there is a clinical need for both a therapeutic that comprehensively addresses the processes involved in IH and a delivery method that achieves potent and sustained therapeutic efficacy following a single treatment. I*n vitro* bioactivity assays revealed that MK2i-NPs sustained potent inhibition of multiple factors underlying IH: migration and inflammation. However, many promising drug delivery technologies lack *in vitro* to *in vivo* translatability [101], as the highly dynamic and highly complex 3-dimensional *in vivo* environment presents new delivery barriers that alter therapeutic pharmacokinetics. In order to elucidate if the increases in uptake seen *in vitro* will translate to increased uptake in human vascular tissue, fluorescently labeled MK2i will be utilized to visualize *ex vivo* uptake and vessel penetration in viable human saphenous vein (**HSV**) explants. Counterstaining with endothelial and vascular smooth muscle cell markers will be utilized to assess uptake in different vascular cell populations.

To provide insight into the underlying molecular changes in p38-MAPK/MK2 signaling responsible for the anti-migratory and anti-inflammatory effects demonstrated *in vitro*, western blot analysis of the phosphorylation state of known MK2 substrates (i.e., hnRNP A0, CREB, and HSP27, see **fig. 1.2**) will be investigated *ex vivo* in viable HSV. Moreover, an *ex vivo* organ culture model of IH in will be utilized in conjunction with vessel morphometrical analysisto assess the ability of MK2i-NPs versus free MK2i to inhibit neointimal thickening. In addition to assessing tissue following organ culture, immunohistochemical analysis of treated HSV explants will be used to assess differences in vascular smooth muscle cell

phenotype. Tissue viability will be assessed in HSV to ensure that *ex vivo* results are not affected by tissue toxicity due to NP formulation.

Finally, to assess the clinical translatability of this NP approach to peptide delivery an *in vivo* rabbit model of bilateral jugular vein graft interposition into the common carotid artery that employs a polymeric cuff method to induce turbulent blood flow and accelerate graft IH will be undertaken (**fig. 4.1**). In this model, jugular vein grafts will be treated or given vehicle control for 30 minutes *ex vivo*, which is representative of the amount of time that grafts are explanted during human revascularization procedures. Grafts will be harvested 28 days post-operatively and histological sections prepared to measure intimal thickening. In addition, immunohistochemical analysis of intimal cellular proliferation, macrophage recruitment/persistence, and contractile versus synthetic vascular smooth muscle cell phenotypic markers will also be used to provide further insight into treatment effects on various aspects of IH pathogenesis.

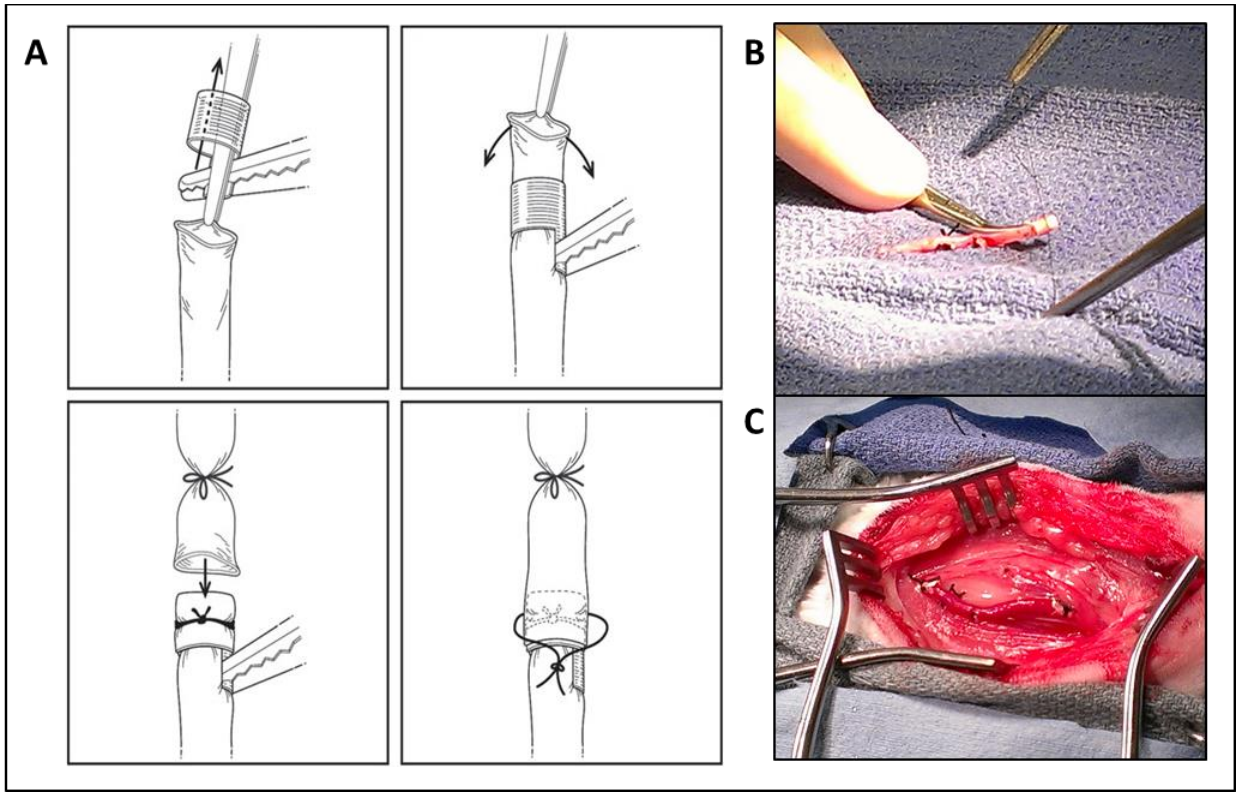

Figure 4.1 – Anastomotic cuff technique for bilateral jugular vein grafting into the carotid artery. (A) Schematic of the anastomotic cuff technique for vein graft interposition: a) The vein graft is pulled through the cuff and then b) everted, c) fixed, and d) inserted into the artery and secured around the cuff. Reproduced from [3]. **(B)** A vein graft with ends everted around polymeric cuffs. **(C)** Interpositioned vein graft with reconstituted blood flow.

Methods

Study design

For *ex vivo* studies, HSV histology samples were blinded to the treatment group for all analyses. For *in vivo* studies, an a prior power analysis based upon pilot data determined a sample size of 4 rabbits (8 grafts) per treatment group to provide 95% power to detect significant difference in our primary endpoints with α=0.05. Endpoints and peptide dosage were selected based upon existing precedents for the evaluation of IH. Failed grafts (i.e., due to partial or complete thrombosis) and grafts in which the contralateral graft failed were excluded due to the compensatory changes in blood flow following contralateral graft occlusion. Contralateral treatments in each rabbit were randomized and samples were blinded prior to histological analyses. One rabbit was euthanized at day 14 due to thrombosis of both grafts. The incidence of graft failure was: NT - 10 grafts harvested, 2 failed due to thromboses, 1 excluded due to contralateral failure, 7 patent; MK2i – 16 grafts harvested, 8 grafts failed due to thromboses, 0 excluded due to contralateral thrombosis, 8 patent; MK2i-NP – 14 grafts harvested, 2 failed due to thrombosis, 3 excluded due to contralateral thrombosis, 9 patent. Altogether, $n \geq 7$ patent grafts without contralateral occlusion per treatment group were included in the reported data.

Human saphenous vein

Upon approval by Vanderbilt Medical Center's institutional Review Board, de-identified, discarded segments of HSV were collected from consented patients undergoing coronary or peripheral vascular bypass surgeries. Following surgical resection, HSV segments were stored in saline solution until the end of the surgical procedure, at which time they were placed in cold transplant harvest buffer (100 mM potassium lactobionate, 25 mM KH_2PO_4, 5 mM $MgSO_4$, 30 mM raffinose, 5 mM adenosine, 3 mM glutathione, 1 mM allopurinol, 50 g/L hydroxyethyl starch, pH 7.4). All HSV segments were used within 24 hours of harvest. Utilizing sterile technique, HSV segments were transferred to a 60 mm Petri dish. The end of each segment (0.5 mm) was removed with a blade, and excess adventitial and adipose tissue was removed with minimal manipulation. HSV segments were cut into consecutive rings with an approximate width of 1.0 mm to be utilized in organ culture experiments. Two rings from each segment were

immediately fixed in 10% formalin at 37°C for 30 min to obtain pre-culture intimal thickness measurements.

Prior to organ culture experiments, HSV viability was confirmed. HSV rings were weighed and their lengths recorded. HSV rings were then suspended in a muscle bath containing a bicarbonate buffer (120mM NaCl, 4.7 mM KCl, 1.0 mM $MgSO_4$, 1.0 mM NaH_2PO_4, 10 mM glucose, 1.5 mM $CaCl_2$, and 25 mM Na_2HCO_3, pH 7.4) equilibrated with 95% O2 and 5% CO2 at 37 °C. The rings were stretched and the length progressively adjusted until maximal tension was obtained. Normalized reactivity was obtained by determining the passive length–tension relationship for each vessel segment. Rings were maintained at a resting tension of 1 g, which produces maximal responses to contractile agonists, as previously determined, and equilibrated for 2 h in buffer. Force measurements were obtained using a Radnoti Glass Technology force transducer (159901A) interfaced with a Powerlab data acquisition system and Chart software. HSV rings were initially contracted with 110 mM KCl (with equimolar replacement of NaCl in bicarbonate buffer) and the force generated was measured. 110 mM KCl causes membrane depolarization, leading to contraction of vessels containing functionally viable smooth muscle.

Microscopic Analysis of MK2i delivery to HSV

An Alexa-568 labeled MK2i peptide was prepared as stated in section 4.9. After verifying viability, HSV rings were treated with 100 µM labeled MK2i peptide, MK2i-NPs, or NE-MK2i-NPs for 30 minutes while suspended in a muscle bath, washed 2x in PBS -/-, and immediately embedded in OCT compound and frozen over dry ice. 5 µm cryosections were cut from the middle of each treated vessel and mounted on microscope slides. Immunofluorescence staining was then carried out with CD31 and α-SMA primary antibodies and a FAM labeled secondary antibody. Microscopy images were obtained using a Nikon Eclipse Ti inverted fluorescence microscope. Gain settings were kept constant for all images acquired for all samples.

HSV organ culture and assay for ex vivo IH

After vessel viability was verified with multiple KCl challenges, additional rings were cut and placed in a 24 well plate and maintained in RPMI 1640 medium supplemented with 30% FBS, 1% L-

glutamine and 1% penicillin/streptomycin for 14 days at 37 °C in an atmosphere of 5% CO2 in air. The rings were treated with MK2i-NPs, NE-MK2i-NPs, MK2i peptide, or buffer alone for 2 hours, washed, and given fresh media. The culture medium without treatments was replaced every 2 days for 14 days.

HSV viability

To ensure that treatments did not impact tissue viability, an MTT assay was performed on HSV rings at 1 and 14 days post-treatment (**supplementary fig. 15**). HSV rings were prepared and treated as noted above, and following 1 or 14 days of organ culture, HSV rings were weighed and then placed in 250 µL of 0.01% methyl tetrazolium dissolved in DPBS for 1 hour. The reaction was stopped by placing the rings into distilled water. The rings were then placed into 1 mL of CelloSolve and incubated at 37°C overnight. Following incubation, rings were mixed in solution, and the CelloSolve was extracted and placed into a cuvette where the optical density at 570 nm was determined. Relative viability calculations were based on the optical density normalized to the wet weight of the ring.

Vessel morphometry and immunohistochemical analyses

After 14 days of organ culture, vein segments were fixed in 0.5 ml of 10% formalin at 37 °C for 30 min and embedded in paraffin for sectioning. Beginning at the midportion of each ring, 5 transverse sections, spaced 5 µm apart, were cut from each specimen. Histological sections were prepared and separate sections were stained with Verhoeff–van Gieson (VVG, elastin fibers), Ki67 (cellular proliferation), caspase 3 (apoptosis), α-smooth muscle acting (α-SMA, contractile vascular smmoth muscle cell phenotypic marker), or vimentin (synthetic vascular smooth muscle cell phenotypic marker). Histology sections were imaged using a Nikon Eclipse Ti inverted fluorescence microscope, and 6 radially parallel measurements of intimal and medial thickness were randomly taken from each section using NIS Elements imaging software (total of 6–12 measurements per ring, n≥3 rings per treatment group from separate donors) to quantify intimal thickness. Intima was defined as tissue on the luminal side of the internal elastic lamina or the chaotic organization of the cells contained within it, whereas the medial layer was contained between the intimal layer and the external elastic lamina. Ki67-, caspase 3-, α-SMA–, and vimentin-positive staining in the intima was quantified by free form selecting the intima in imageJ and

using a color deconvolution method as previously described [102] and normalized to the number of intimal cell nuclei. 8 histological images from grafts from 2 different donors were analyzed for each treatment group.

Western blot analysis of protein *phosphorylation in HSV*

Following 2 hours of treatment, a portion of the treated HSV rings were snap-frozen with liquid nitrogen, pulverized, and homogenized using urea-DTT-CHAPS buffer. For analysis of hnRNP A0 phosphorylation treated HSV rings were maintained in organ culture in fresh media for 24 hours prior to homogenization. For analysis of CREB and HSP27 phosphorylation HSV rings were frozen immediately after treatment removal. Lysates were centrifuged (6000 g, 20 minutes), and the supernatant was collected for each sample for evaluation of HnRNP A0, CREB, and HSP27 phosphorylation. Equal amounts of protein (20 µg per lane) were loaded on 15, 10, or 4–20% SDS–PAGE gels; proteins were electrophoretically separated and then transferred to Immobilon membranes. For hnRNP A0 phosphorylation, membranes were probed overnight at 4°C with primary antibodies for phospho-hnRNP A0 (Millipore) and unphosphorylated hnRNP A0 (Santa Cruz). For CREB phosphorylation, membranes were probed overnight at 4°C with primary antibodies for phospho-CREB (abcam) and unphosphorylated CREB (abcam). For HSP27 phsophorylation membranes were probed overnight at 4°C with primary antibodies for phospho-HSP27 (Epitomics) and unphosphorylated HSP27 (Santa Cruz). After washing, the membranes were incubated with appropriate secondary antibodies (Li-Cor) for 1 hour at room temperature. The secondary antibody was imaged using the Odyssey direct infrared fluorescence imaging system and densitometrically quantified with LiCor Odyssey software v2.1 at 800 and 680 nm wavelengths.

Rabbit bilateral jugular vein graft interposition model

This study was approved by the Vanderbilt Institutional Animal Care and Use Committee and conforms to the *Guide for the Care and Use of Laboratory Animals.* Male New Zealand White rabbits (3.0–3.5 kg; n = 24) were anesthetized through an intramuscular injection with ketamine hydrochloride (1.4 mg/kg) and xylazine (0.2 mg/kg). Anesthesia was maintained with endotracheal intubation and

inhaled isoflurane (2.0–5.0%). A high-dose IV heparin bolus (250 U/kg) was administered immediately prior to carotid cross clamp. The operative procedure was performed with aseptic technique under 2.5x optical magnification.

Vein bypass grafts were constructed with an anastomotic cuff technique as previously described[103]. Briefly, polymer cuffs consisting of a 2.0-mm body loop were fashioned from a 4-Fr introducer sheath. Following ligation of smaller tributary vessels, the external jugular veins were harvested (3.0-4.0 cm in length) for creation of an interposition graft into the common carotid artery. Jugular vein ends were passed through a cuff, everted, and fixed with 6-0 silk. Vein grafts were subsequently treated for 30 minutes in 2 mL of either 30 μM MK2i-NP, 30 μM MK2i peptide, or PBS (no treatment). Following treatment, the carotid artery lumen was exposed with a 2.0-cm arteriotomy, and the cuffed, reversed vein ends were inserted. A 3-0 silk was used to secure the artery around the cuff. Finally, 1.0 cm of carotid artery back wall was cut away between the cuffs to permit vein graft extension.

Rabbits were euthanized at 28 days post-operatively, and vein grafts were perfusion fixed *in situ* with 10% neutral buffered formalin under ~50 mm Hg pressure with a roller pump. Vein grafts were subsequently excised and sectioned into four segments avoiding the tissue overlying the cuff in order to allow for evaluation of morphological variation along the length of the graft. Histological sections were prepared and separate sections were stained with Verhoeff-van Gieson (**VVG**) , PCNA (abcam), α-SMA (abcam), vimentin (abcam), or RAM-11 (Dako). Intimal and medial thicknesses were quantified by taking 3 measurements from each quadrant of each VVG stained vessel section (12 measurements/segment = 48 measurements/graft). PCNA, α-SMA, vimentin, and RAM-11 positive staining in the intima was quantified by free form selecting the intima in imageJ and using a color deconvolution method as previously described[102] and normalized to the number of intimal cell nuclei. 16 histological images from 4 different graft sections were analyzed for each treatment group.

Results

MK2i-NP delivery of peptide into intact human saphenous vein (**HSV**) was assessed revealing that uptake occurs in both endothelial and smooth muscle cells. As expected, MK2i-NPs, MK2i, and NE-MK2i-NPs all showed more concentrated uptake at the luminal and adventitial surfaces that act as

diffusion barriers (**fig. 4.2**); Although MK2i was colocalized with the endothelial marker CD31 on the luminal surface of the vessel (**fig. 4.2 B**), MK2i penetration into the intimal and medial layers was verified by MK2i distribution through tissue layers that stained positively for the smooth muscle marker α-SMA (**fig. 4.2 A**). Furthermore, in accordance with in vitro results, MK2i-NPs increased the overall peptide uptake within the vessel wall (**fig. 4.2 C**).

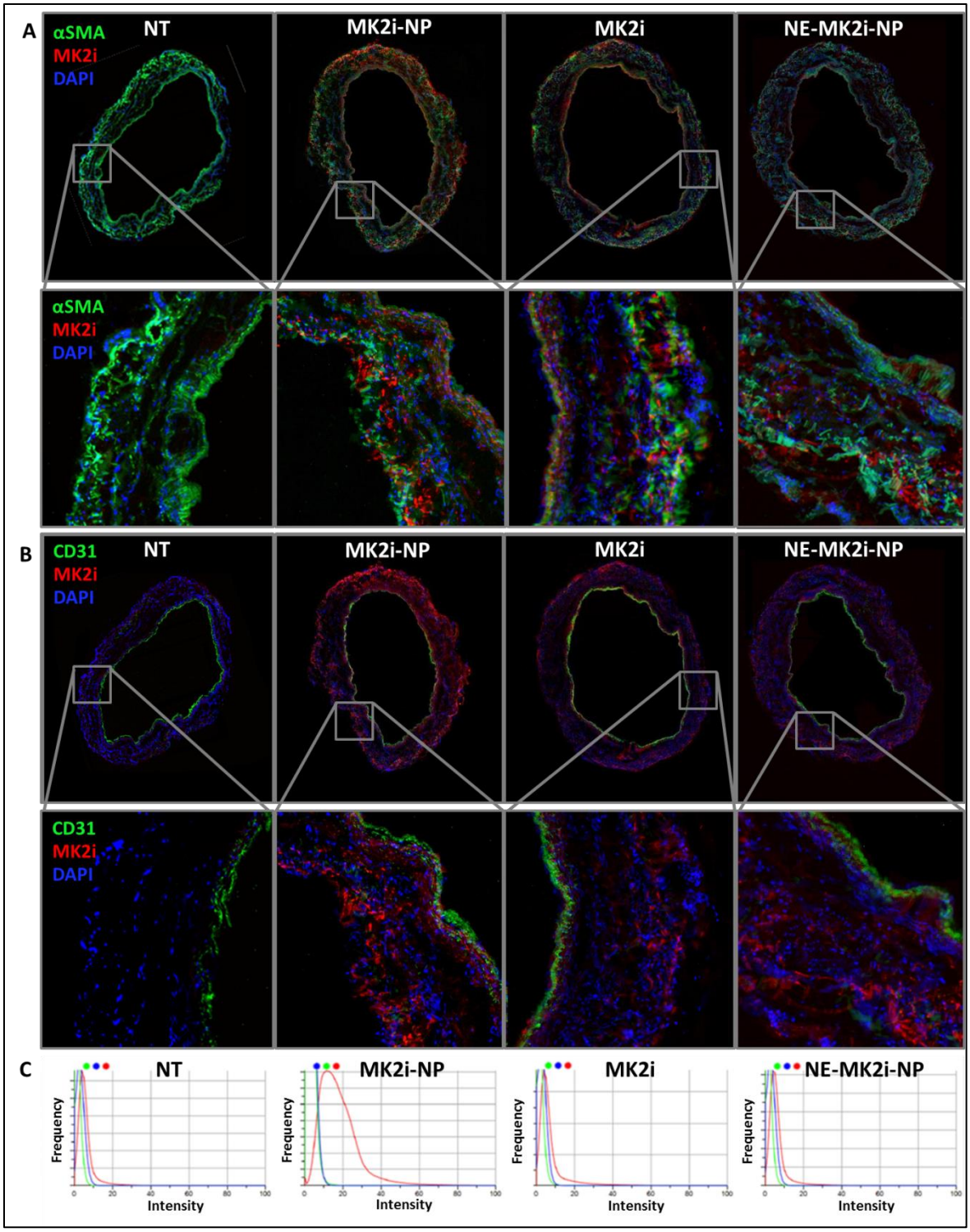

Figure 4.2 - MK2i-NP formulation increases peptide delivery to human vein. (A) Immunofluorescence microscopy images and zoomed insets of human saphenous vein cross sections treated with Alexa-568 labeled MK2i, MK2i-NPs, or NE-MK2i-NPs (red) and stained for the vascular smooth muscle cell marker α-smooth muscle actin (green) and the nuclear marker DAPI (blue). (**B)** Immunofluorescence microscopy images and zoomed insets of human saphenous vein cross sections treated with Alexa-568 labeled MK2i, MK2i-NPs, or NE-MK2i-NPs (red) and stained for the endothelial marker CD31 (green) and the nuclear marker DAPI (blue). **(C)** Pixel intensity distribution derived from the red fluorescent channel of entire (un-zoomed) cross sectional images in **A** and **B**. From [1], reprinted with permission from AAAS.

Delivery of MK2i-NPs to intact HSV *ex vivo* modulated phosphorylation of several MK2 substrates relevant to graft IH (**fig. 1.2**). The post-transcriptional gene regulator hnRNP A0 is among these relevant downstream MK2 effectors and effectively stabilizes the mRNA of inflammatory cytokines thereby increasing their translation [35, 104, 105]. MK2i-NP treatment significantly reduced phosphorylation of hnRNP A0 in HSV at all concentrations whereas the free MK2i peptide only produced significant effects at 100 µM (**fig. 4.3**). These results indicate that NP formulation enhances MK2i mediated inhibition of hnRNP A0 in human vein and agrees with *in vitro* data demonstrating equivalent MK2i-NP bioactivity at an order of magnitude lower dose than the free peptide.

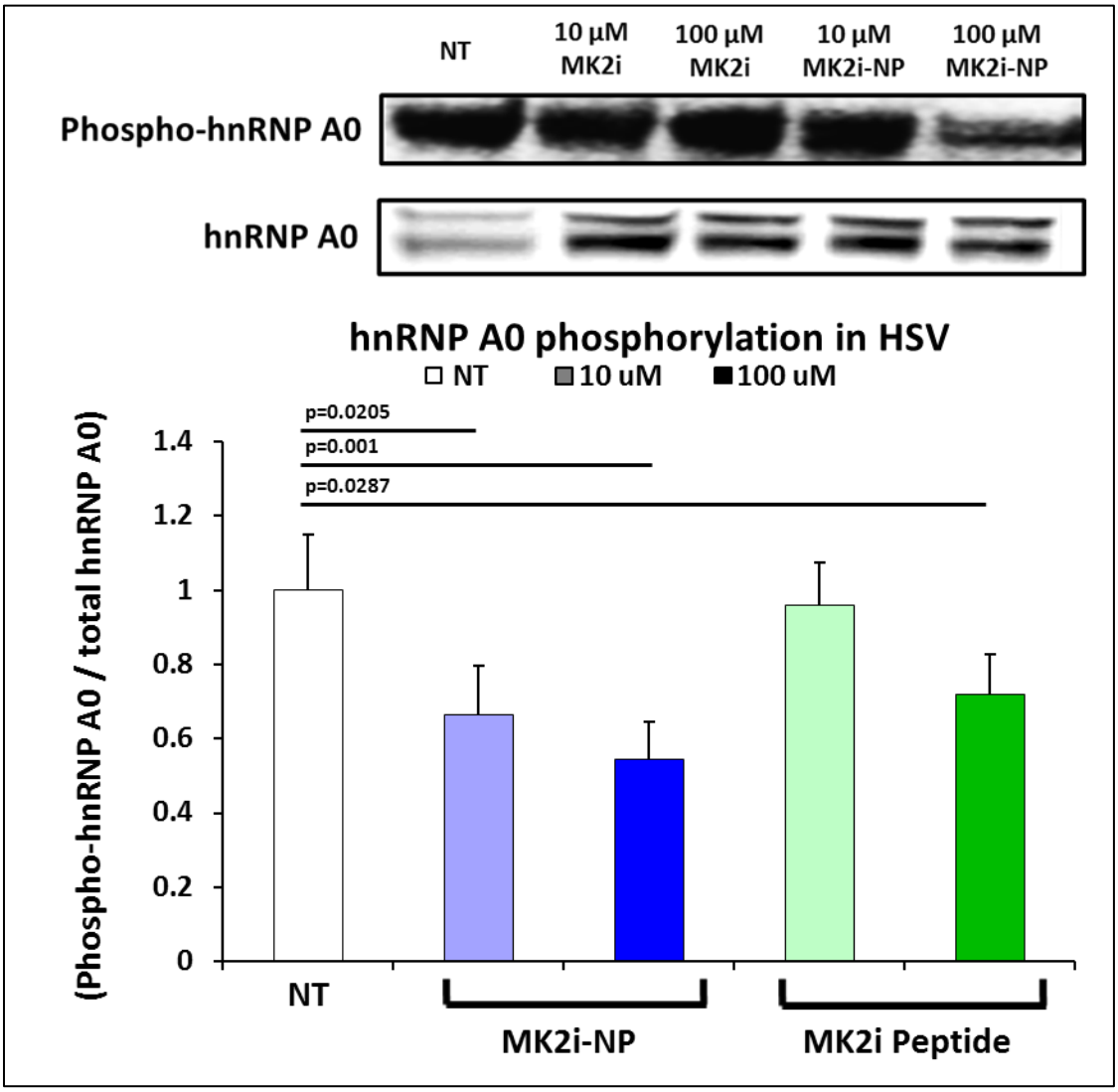

Figure 4.3 – Western blot analysis of hnRNP A0 phosphorylation in treated HSV. Representative western blots and quantification of western blot analysis showing the phosphorylation of MK2 substrate hnRNP A0 with and without treatment. Data are mean ± SEM (n ≥ 3 separate biological replicates from 3 separate donors). *P* values determined via one way ANOVA. From [1], reprinted with permission from AAAS.

In addition to hnRNP A0, activated MK2 phosphorylates the transcription factor CREB which binds to cAMP-responsive elements to promote expression of genes that induce smooth muscle cell migration [106, 107], proliferation [39, 108], and production of the inflammatory cytokines such as IL-6 [8]. Similar to hnRNP A0 phosphorylation results, MK2i-NPs were found to significantly enhance Mk2i-mediated inhibition of CREB phosphorylation (**fig. 4.4**). Moreover, a 10 µM dose of MK2i-NPs were significantly more effective than an equivalent dose of free peptide, again demonstrating equivalent bioactivity at a 10-fold lower dose of peptide (i.e., 10 µM MK2i-NP vs. 100 µM MK2i).

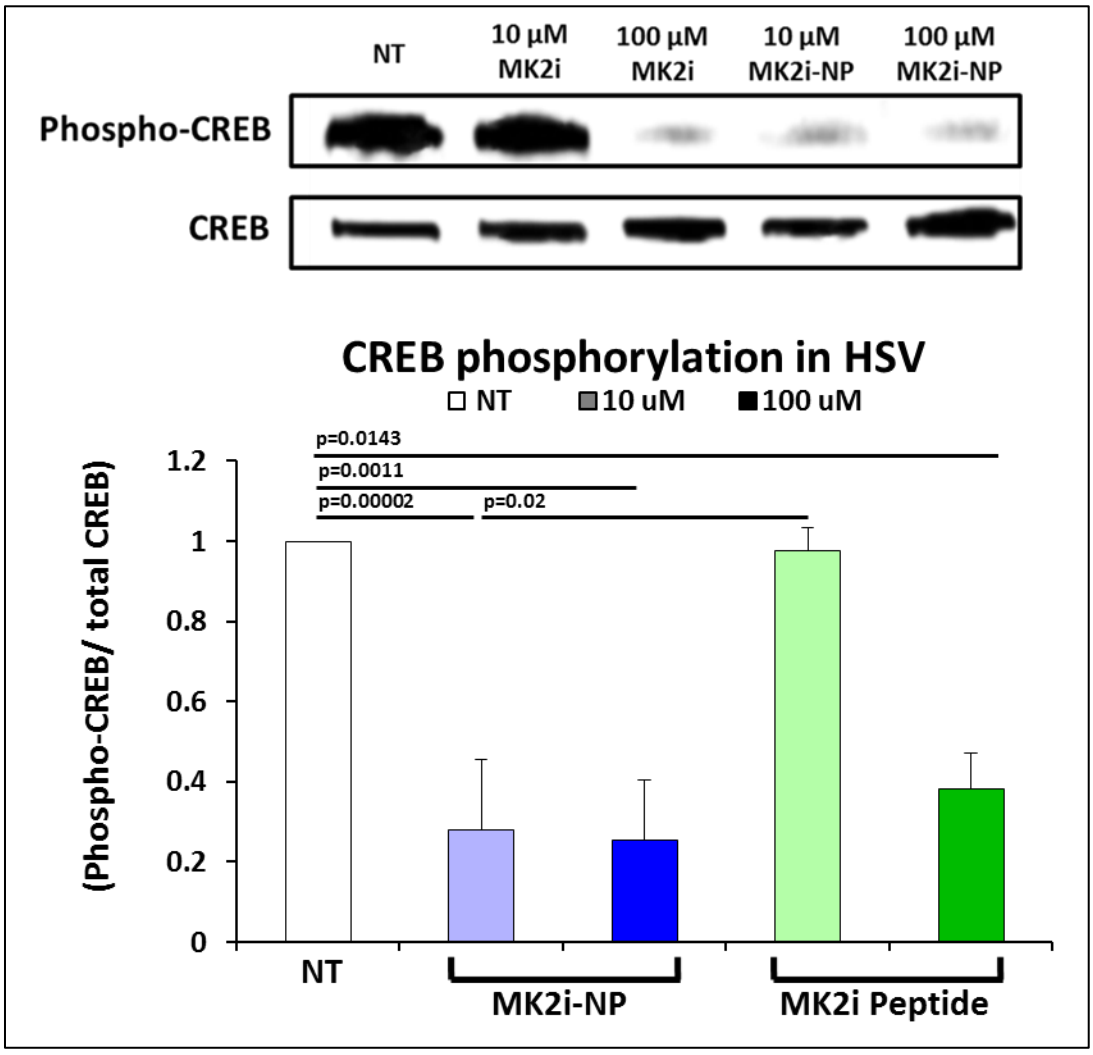

Figure 4.4 – Western blot analysis of CREB phosphorylation in treated HSV. Representative western blots and quantification of western blot analysis showing the phosphorylation of MK2 substrate CREB with and without treatment. Data are mean ± SEM (n ≥ 3 separate biological replicates from 3 separate donors). *P* values determined via one way ANOVA. From [1], reprinted with permission from AAAS.

It was also confirmed that MK2i-NPs, as well as MK2i, significantly decreased phosphorylation of the MK2 substrate HSP-27 (**fig. 4.5**), which along with CREB, is believed to promote pathological vascular smooth muscle cell migration characteristic of IH [38, 42, 109].

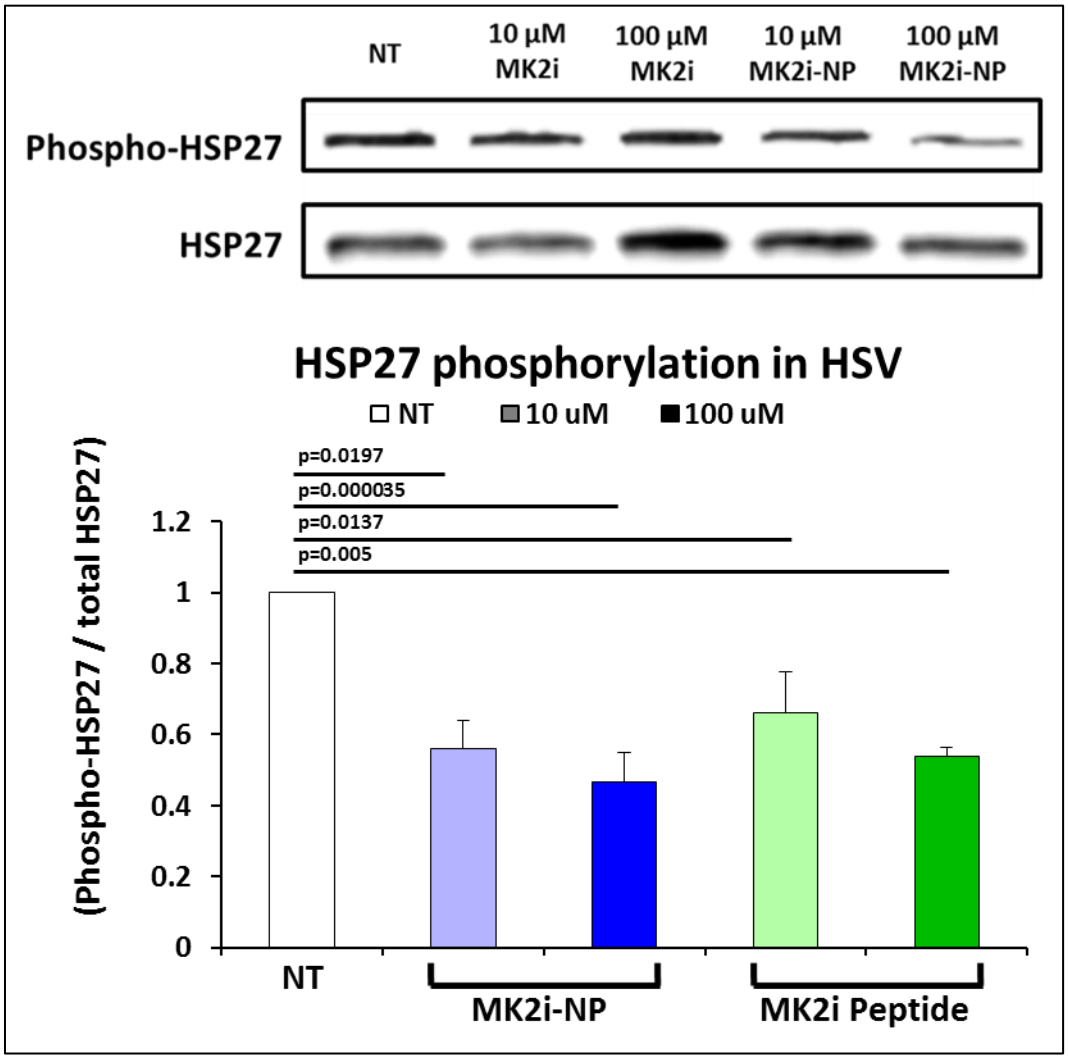

Figure 4.5 – Western blot analysis of HSP27 phosphorylation in treated HSV. Representative western blots and quantification of western blot analysis showing the phosphorylation of MK2 substrate HSP27 with and without treatment. Data are mean ± SEM (n ≥ 3 separate biological replicates from 3 separate donors). *P* values determined via one way ANOVA. From [1], reprinted with permission from AAAS.

To investigate if the inhibited activity of these MK2 substrates would translate into a multipronged therapeutic approach to prevent vein graft failure, an *ex vivo* organ culture model of IH was carried out in HSV over a two week period. This study revealed that MK2i-NPs significantly inhibited neointima formation in a dose-dependent fashion and at an order of magnitude lower peptide dose than free MK2i (**fig. 4.6**). Furthermore, MK2i-NP therapy at 100 µM MK2i was the only treatment that fully abrogated IH, yielding intimal thickness statistically equivalent to control tissues prepared for histology immediately after harvest (p=0.49).

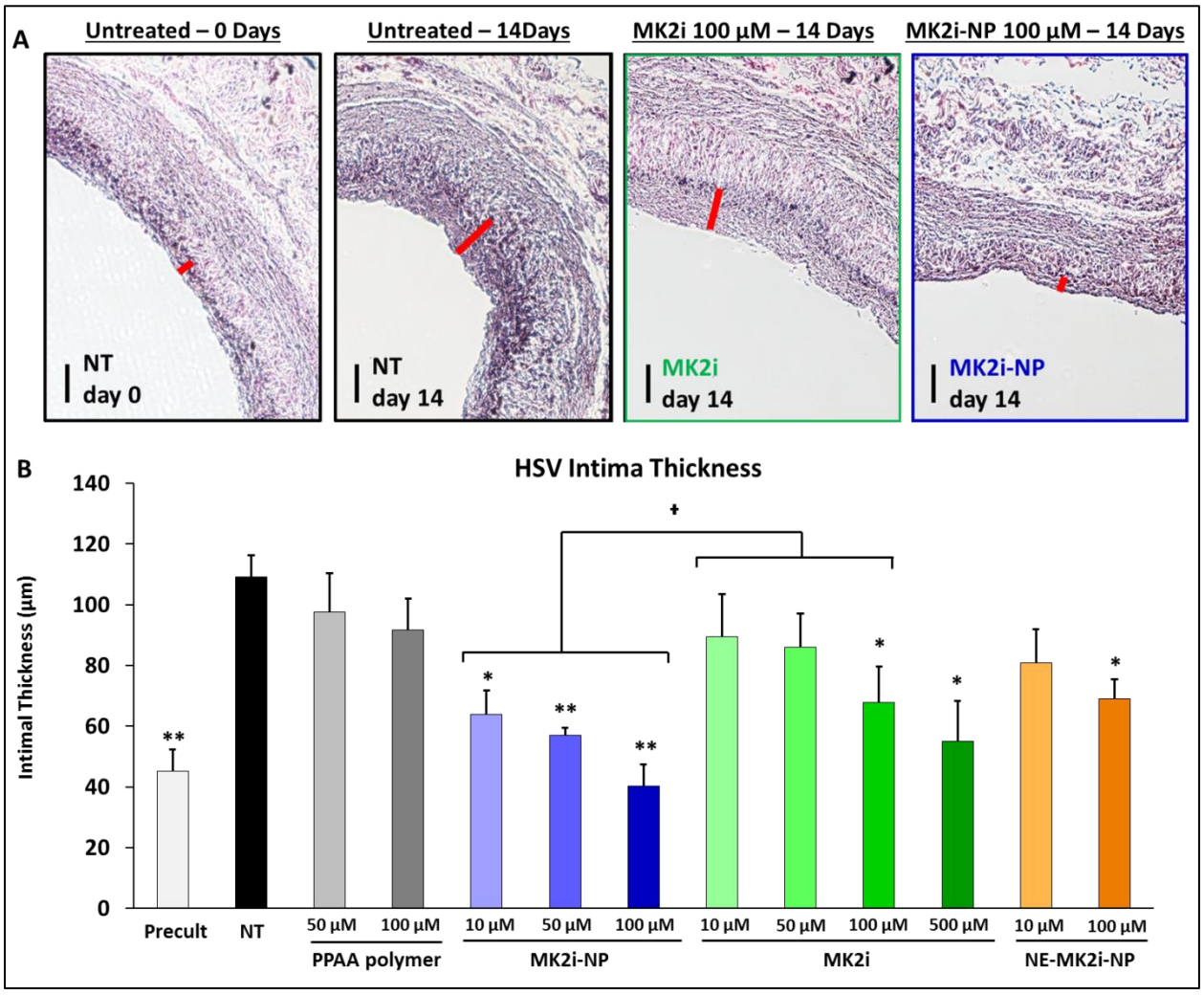

Figure 4.6 - *Ex vivo* treatment with MK2-NPs reduces neointima formation in human saphenous vein. (A) Neointima were visualized using Verhoeff Van Gieson staining of human saphenous vein samples that were treated for 2 hours and maintained in organ culture for 14 days. Red bars demarcate intimal thickness (scale bars, 100 µm). **(B)** Intimal thickness in human saphenous vein samples quantified after 14 days in organ culture. Data are mean ± SEM (n ≥ 3 separate biological replicates from 3 separate donors). *p ≤ 0.01 compared to no treatment control(NT), **p ≤ 0.001 compared to NT, ǂ p ≤ 0.05. *P* values determined via one way ANOVA. From [1], reprinted with permission from AAAS.

To ensure that treatments did not inhibit neointima formation due to tissue toxicity, an MTT assay was performed on HSV rings at 1 and 14 days post-treatment revealing that none of the treatments had any significant effect on HSV viability (**fig. 4.7**).

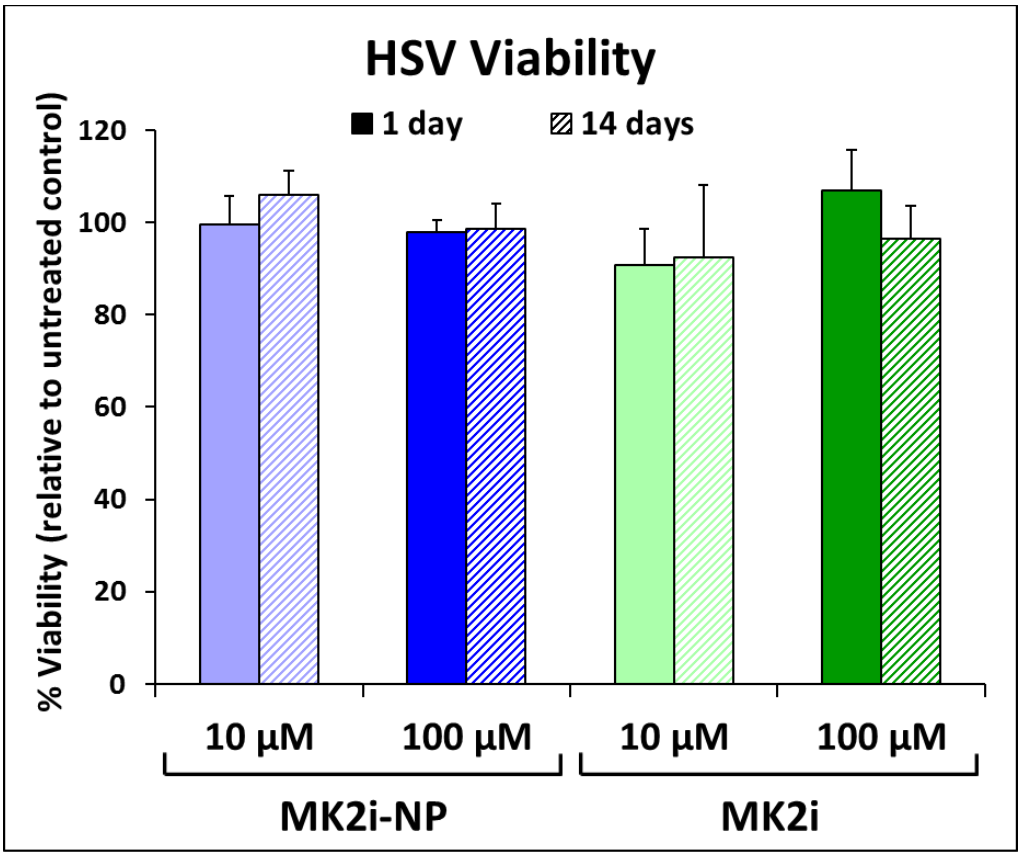

Figure 4.7 - Human saphenous vein viability. Quantification of tissue viability in human saphenous vein rings treated for 2 hours and subsequently maintained in organ culture for 1 or 14 days as assessed through an MTT assay. Data are mean ± SEM, *n* = 3 biological replicates from 3 separate donors. No statistically significant differences were observed. *P* values determined via one way ANOVA.

To assess *ex vivo* cell-based mechanisms underlying MK2i-NP mediated inhibition of neointima formation in human saphenous vein, ki67 stained histological sections of treated HSV were used to analyze intimal/medial cellular proliferation. Ki67 is a nuclear protein that is associated with cellular proliferation and ribosomal RNA transcription and, thus, is a protein marker of proliferating cells. Analaysis of stained sections revealed that cellular proliferation markedly increased in untreated HSV over the 14 day organ culture period (**fig. 4.8**). However, treatment with MK2i-NPs as well as the free MK2i peptide was found to reduce cellular proliferation to baseline levels evinced by HSV samples prior to organ culture (i.e., preculture).

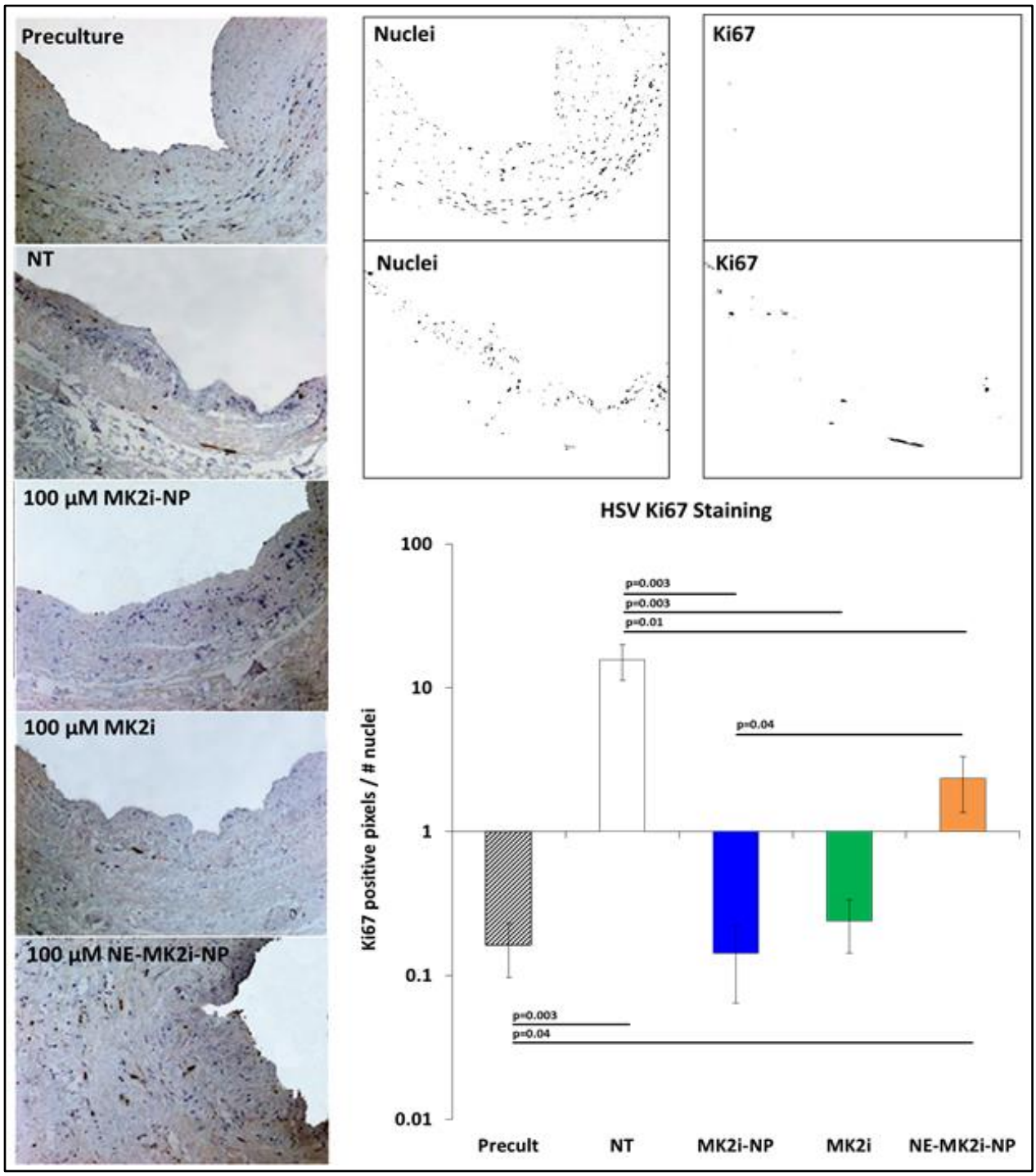

Figure 4.8 - *Ex vivo* treatment with MK2i-NPs reduces cellular proliferation in human saphenous vein. Representative images of ki67 stained histological sections of treated HSV. Ki67 positive staining was quantified by normalizing positive pixel staining to the number of nuclei as shown at the top of the figure. Data are represented as mean ± SEM (n = 8 separate histological images). *P* values determined by one way ANOVA.

In addition to assessing cellular proliferation, Caspase 3 stained histological sections of treated HSV were used to analyze apoptosis of intimal cells. Caspase 3 is a protein that interacts with other caspase proteins, where sequential activation of caspases plays a key role in effecting cellular apoptosis. Cellular apoptosis was significantly increased in all treated HSV samples relative to preculture samples (**fig. 4.9**). In agreement with *ex vivo* intimal thickening results, MK2i-NP treated HSV evinced significantly more intimal apoptosis than MK2i or NE-MK2i-NP treated HSV.

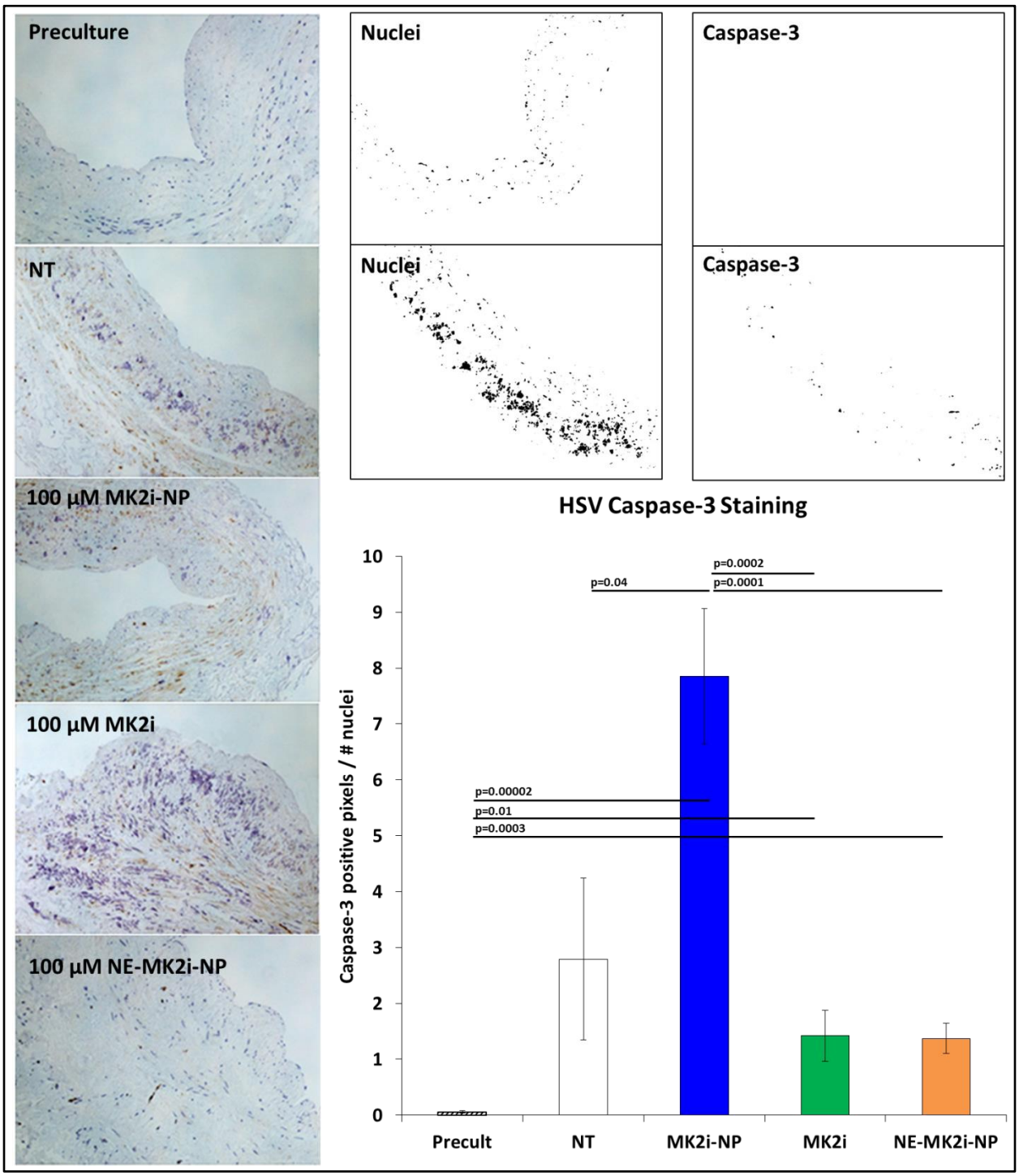

Figure 4.9 - *Ex vivo* treatment with MK2i-NPs increases intimal apoptosis in human saphenous vein. Representative images of Caspase 3 stained histological sections of treated HSV. Caspase 3 positive staining was quantified by normalizing positive pixel staining in the intima to the number of nuclei as shown at the top of the figure. Data are represented as mean ± SEM (n = 8 separate histological images). *P* values determined by one way ANOVA.

In order to evaluate MK2i-NP effects on vascular smooth muscle cell phenotype, α-smooth muscle actin (**α-SMA**) stained histological sections of treated HSV were analyzed. α-SMA is a multifunctional protein that forms microfilaments that vascular smooth muscle cells utilize to generate contractile force, and expression of α-SMA is correlated with a healthy, contractile vascular smooth muscle cell phenotype [106, 110]. As expected, intimal expression of α-SMA significantly decreased during two weeks of organ culture indicating vascular smooth muscle cell transdifferentiation into a pathological, synthetic phenotype (**fig. 4.10**). Analysis of treated samples revealed that treatment with MK2i-NPs maintained significantly more α-SMA expression compared to untreated samples, whereas the free MK2i peptide did not.

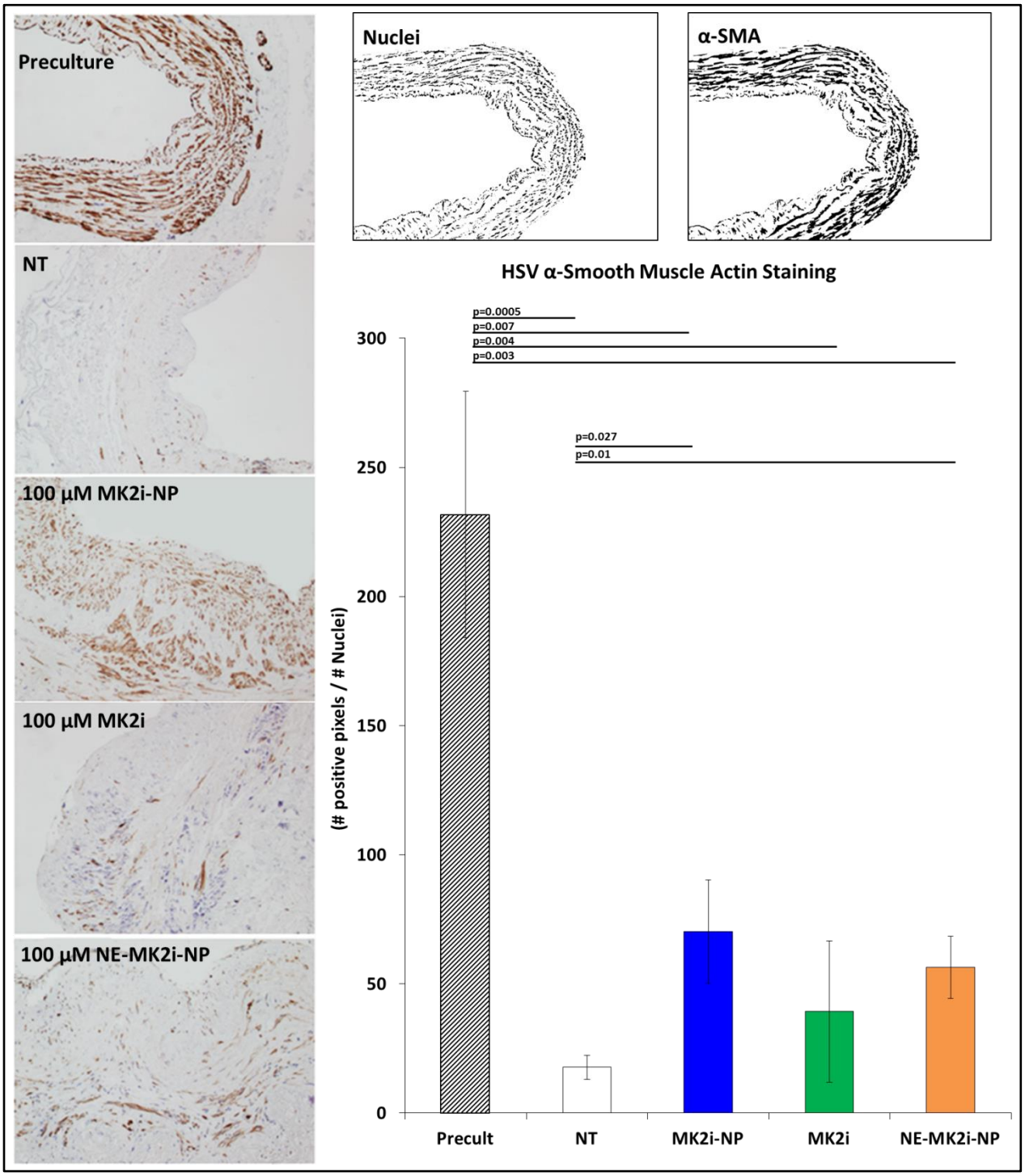

Figure 4.10 - *Ex vivo* treatment with MK2i-NPs maintains a contractile vascular smooth muscle cell phenotype in human saphenous vein. Representative images of α-SMA stained histological sections of treated HSV. α-SMA positive staining was quantified by normalizing positive pixel staining I the intima to the number of nuclei as shown at the top of the figure. Data are represented as mean ± SEM (n = 8 separate histological images). *P* values determined by one way ANOVA.

In contrast to assessing vascular smooth muscle cell expression of contractile phenotypic markers, vimentin stained histological sections of treated HSV were prepared to analyze the intimal presence of synthetic vascular smooth muscle cell phenotypic markers. Vimentin is a type II intermediate filament protein that is expressed in mesenchymal cells and is one of the most common markers of a synthetic smooth muscle cell phenotype [110]. Considering that organ culture resulted in a loss of expression of the contractile marker α-SMA, it is hypothesized that a concomitant gain in synthetic phenotypic marker expression would occur. Indeed, untreated HSV subjected to two weeks in high serum organ culture demonstrated a significant increase in intimal vimentin expression (**fig. 4.11**). Treatment with MK2i-NPs, NE-MK2i-NPs, and free MK2i were all found to significantly reduce vimentin expression to levels less than or equal to preculture samples. Moreover, treatment with MK2i-NPs was not only found to significantly decrease vimentin expression compared to HSV treated with NE-MK2i-NPs or free MK2i, but also compared to preculture samples.

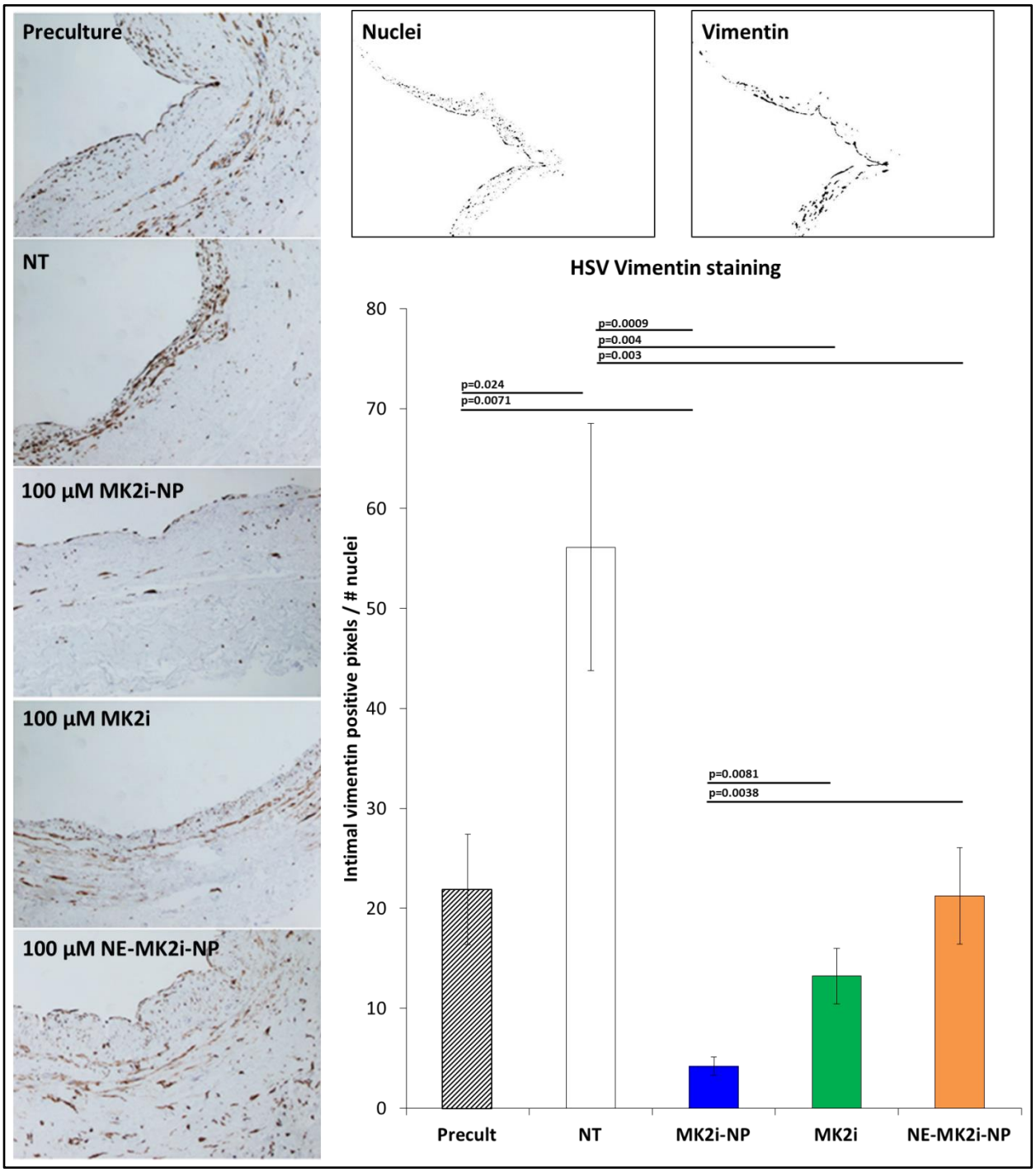

Figure 4.11 - *Ex vivo* treatment with MK2i-NPs inhibits vascular smooth muscle cell transdifferentiation into a synthetic phenotype in human saphenous vein. Representative images of vimentin stained histological sections of treated HSV. Vimentin positive staining was quantified by normalizing positive pixel staining I the intima to the number of nuclei as shown at the top of the figure. Data are represented as mean ± SEM (n = 8 separate histological images). *P* values determined by one way ANOVA.

The therapeutic benefit of MK2i-NPs *in vivo* was assessed in a rabbit bilateral jugular vein graft interpositional transplant model that employs a polymeric cuff method to induce turbulent blood flow and accelerate graft IH [111]. In this model, jugular vein grafts were treated or given vehicle control for 30 minutes *ex vivo* prior to transplant. Grafts were harvested 28 days post-operatively, and Verhoeff Van-Gieson (**VVG**) stained histological sections were used to quantify intimal thickness (**fig. 4.12 A**). Treatment with 30 µM MK2i-NPs significantly inhibited neointima formation compared to both untreated controls and the free MK2i peptide, which did not produce any significant change in neointima formation relative to vehicle controls at the 30 □M dose tested (**fig. 4.12 B**).

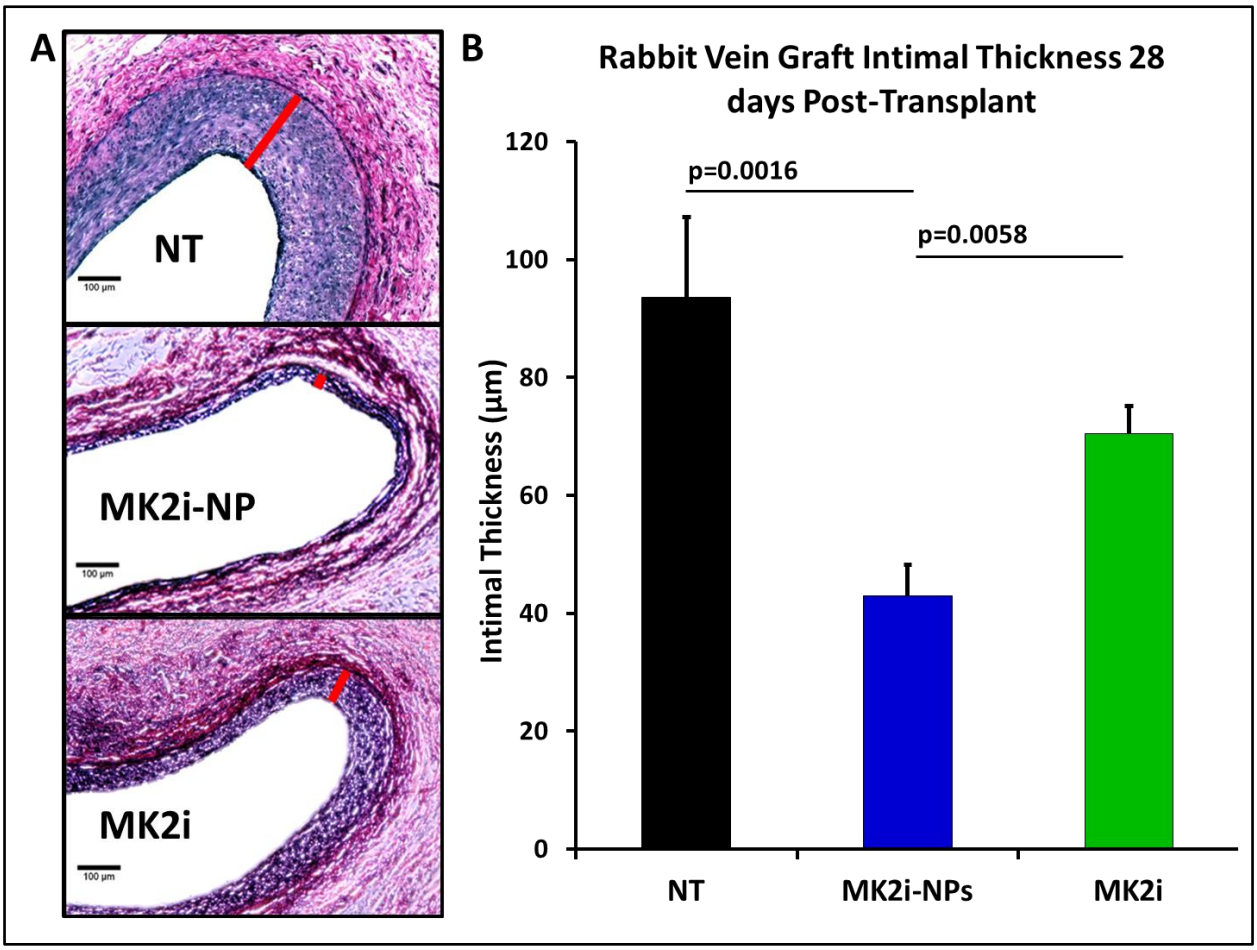

Figure 4.12 - Intraoperative treatment with MK2i-NPs reduces neointima formation *in vivo* in transplanted rabbit vein grafts. Rabbits vein graft transplants were treated for 30 minutes with MK2i or MK2i-NP (30 µM) in Heparin Plasma-Lyte. No treatment grafts were incubated in Heparin Plasma-Lyte alone. Tissue sections were evaluated 28 days later. **(A)** Neointima were visualized using Verhoeff Van Gieson staining of vein grafts. Red bars demarcate intimal thickness (scale bars, 100 µm). **(B)** Intimal thickness in perfusion fixed jugular vein interposition grafts was quantified 28 days post-treatement. Data are represented as mean ± SEM (n ≥ 7 grafts per treatment group). *P* values determined by one way ANOVA. From [1], reprinted with permission from AAAS.

To assess *in vivo* cell-based mechanisms underlying MK2i-NP mediated inhibition of neointimal thickening, proliferating cell nuclear antigen (**PCNA**), α-smooth muscle actin (**α-SMA**), and vimentin stained histological sections were used to analyze cellular proliferation and vascular smooth muscle cell phenotype. Intimal PCNA staining was significantly decreased by ~17-fold in grafts treated with MK2i-NPs, whereas treatment with the free MK2i were similar to untreated grafts (**fig. 4.13**).

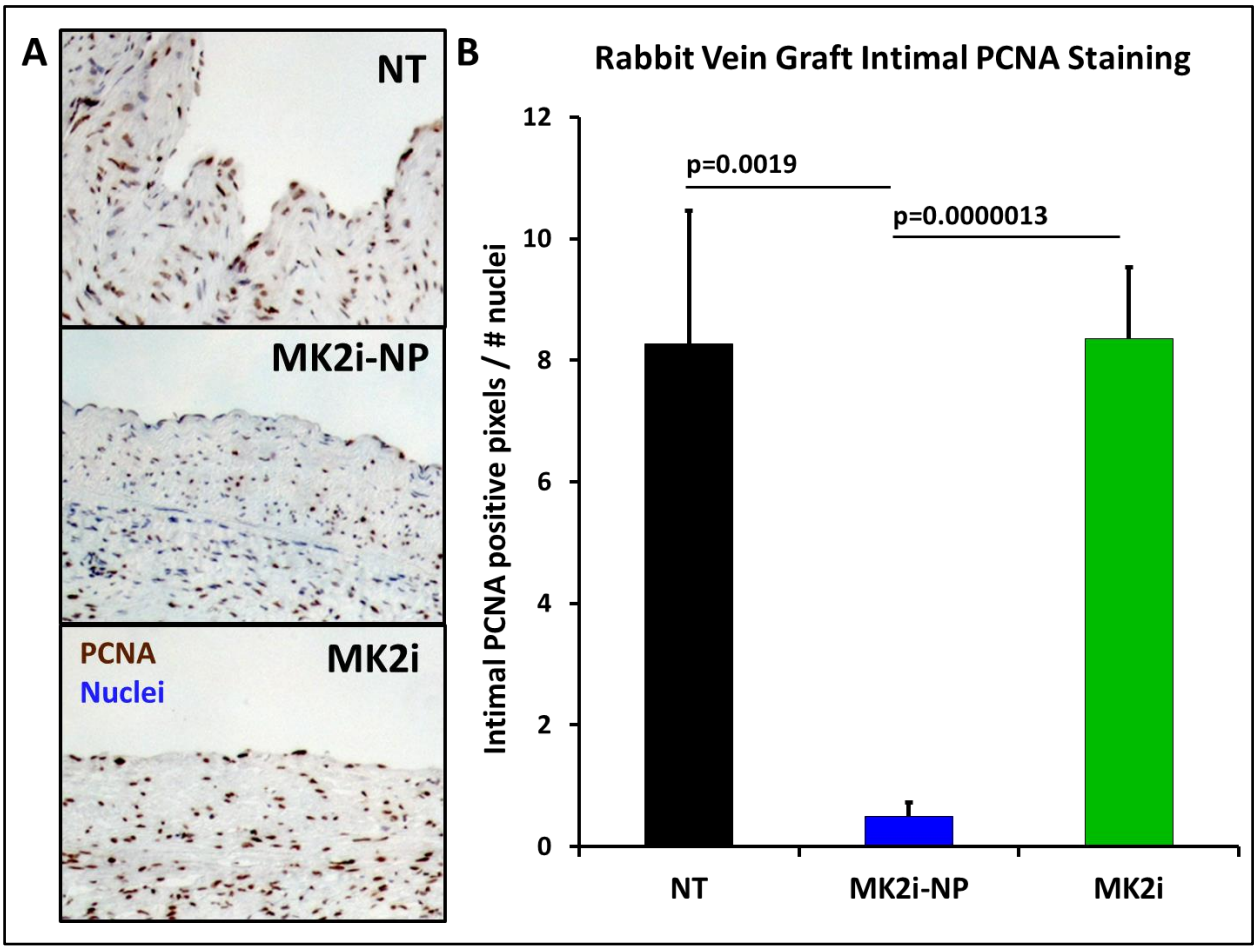

Figure 4.13 - Intraoperative treatment with MK2i-NPs reduces cellular proliferation of intimal cells *in vivo* in transplanted rabbit vein grafts. **(A)** Proliferation of intimal cells as shown using PCNA immunohistochemistry. **(B)** Quantification of PCNA positive nuclear staining in jugular vein graft sections normalized to intimal nuclei number. Data are represented as mean ± SEM (n ≥ 7 grafts per treatment group). *P* values determined by one way ANOVA. From [1], reprinted with permission from AAAS.

MK2i-NP treated grafts also demonstrated increased staining intensity for α-SMA, which is a marker for contractile SMC phenotype[112], relative to untreated grafts or grafts treated with free MK2i (**fig. 4.14 B**). Images of α-SMA immunostained sections revealed that untreated and free MK2i treatment groups showed sparse intimal staining (**fig. 4.14 A**), indicating loss of the contractile VSMC phenotype and/or excess production of extracellular matrix proteins, both of which are implicated in vein graft IH.

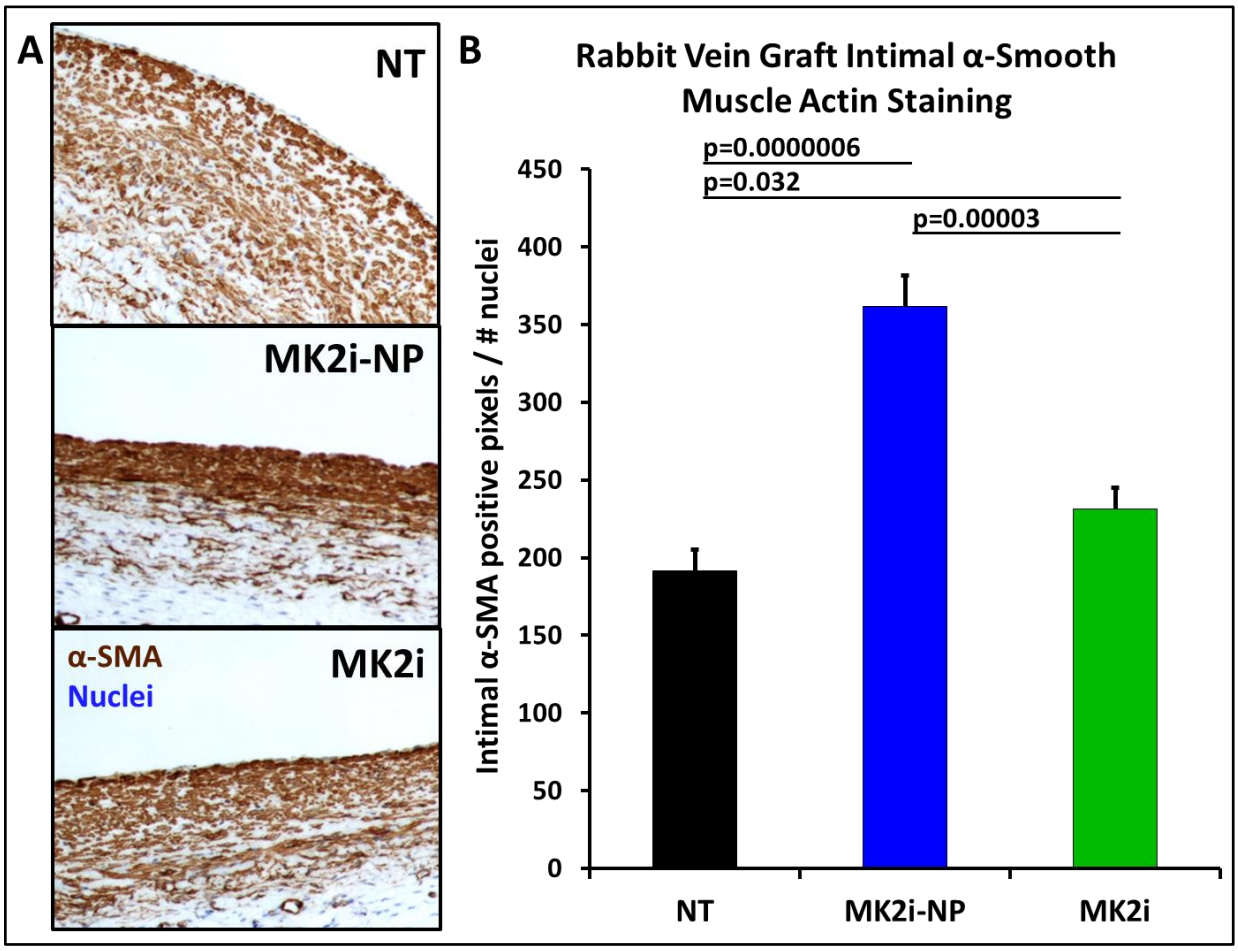

Figure 4.14 - Intraoperative treatment with MK2i-NPs promotes a contractile smooth muscle cell phenotype *in vivo* in transplanted rabbit vein grafts. **(A)** Intimal expression of the contractile marker α-smooth muscle actin (SMA). **(B)** Quantification of α-SMA–positive staining in jugular vein graft sections were normalized to intimal nuclei number. Data are represented as mean ± SEM (n ≥ 7 grafts per treatment group). *P* values determined by one way ANOVA. From [1], reprinted with permission from AAAS.

In agreement with and conversely to increased contractile marker expression, intimal expression of the synthetic VSMC marker vimentin was also decreased in MK2i-NP treated grafts but not in grafts treated with free MK2i peptide (**fig. 4.15**).

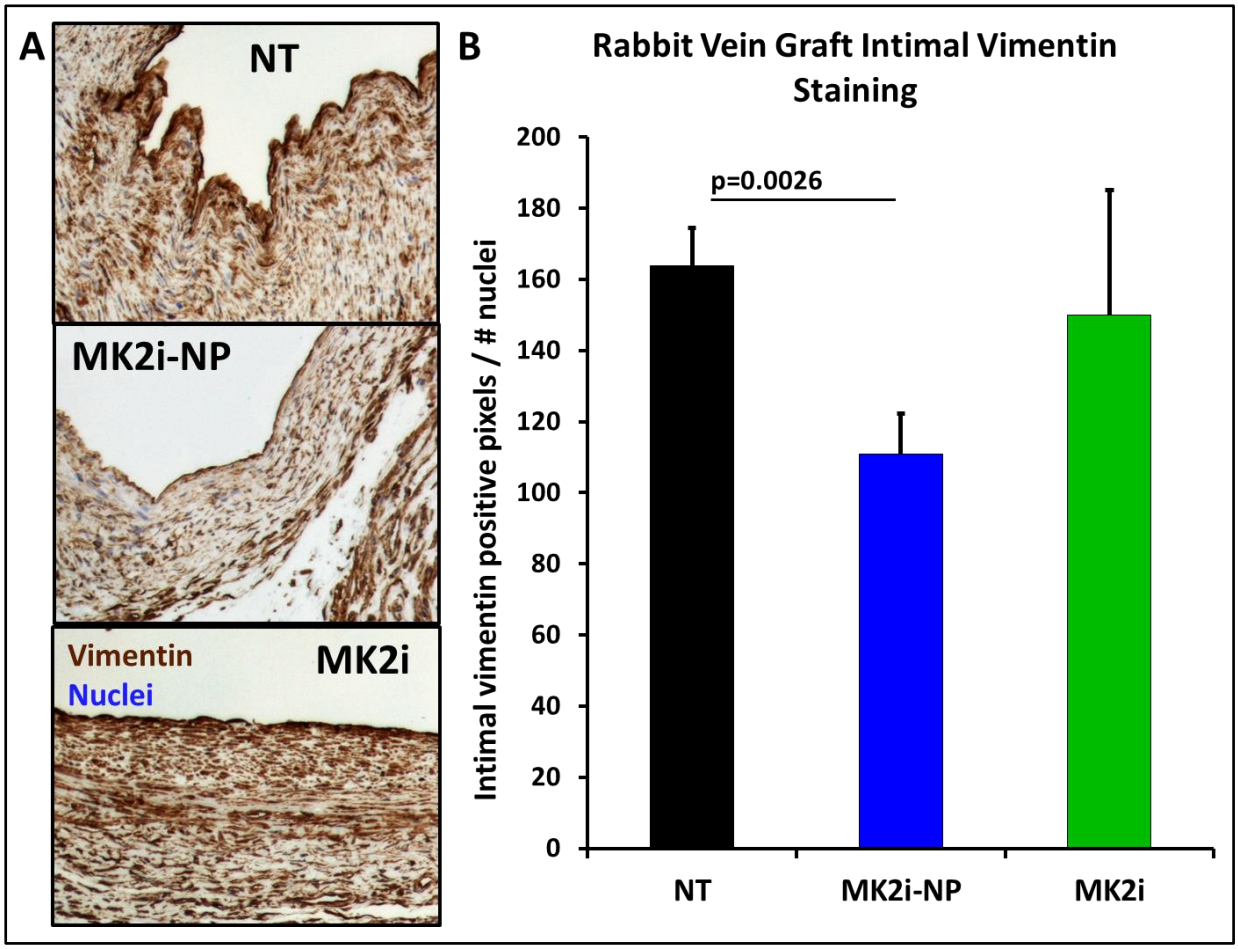

Figure 4.15 - Intraoperative treatment with MK2i-NPs inhibits vascular smooth muscle cell transdifferentiation to a syntehtic phenotype *in vivo* in transplanted rabbit vein grafts. **(A)** Intimal expression of the synthetic vascular smooth muscle phenotypic marker vimentin. **(B)** Quantification of intimal vimentin-positive staining in jugular vein graft sections were normalized to intimal nuclei number. Data are represented as mean ± SEM (n ≥ 7 grafts per treatment group). *P* values determined by one way ANOVA. From [1], reprinted with permission from AAAS.

The number of residual macrophages present in the intima of the vein grafts was also assessed in tissue sections using a rabbit macrophage specific antibody, RAM-11 (**fig. 4.16 A and B**). Fewer intimal macrophages were detected in MK2i-NP treated grafts, suggesting that MK2i-NPs blunted local macrophage recruitment and/or persistence (**fig. 4.16 C**). This mechanism is potentially mediated through decreased secretion of macrophage inflammatory protein 2 (**MIP-2**, also known as CXCL2) and/or MCP-1 [56], both of which attract inflammatory cells and are upregulated either directly or indirectly through hnRNP A0 [35, 113, 114]. This mechanism is supported by our *in vitro* study results showing that MK2i-NPs inhibited MCP-1 production in both smooth muscle and endothelial cells. Though the inflammatory response was predominately resolved in all samples at 28-days, macrophage persistence in untreated

samples agrees with previous observations that MCP-1 can be elevated even at 8 weeks after vein grafting, resulting in local recruitment of monocytes and pathogenesis of IH [92].

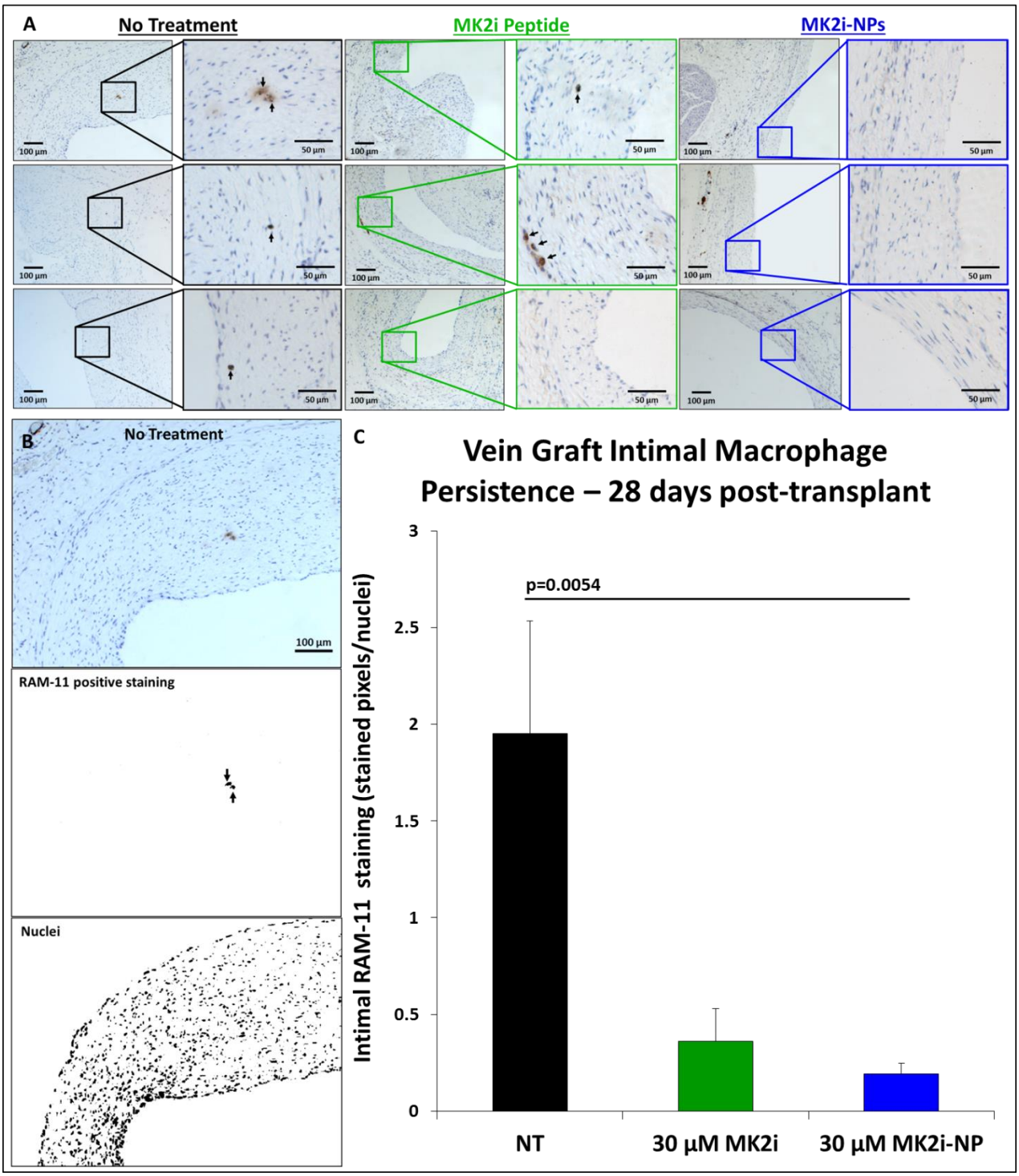

Figure 4.16 - Intraoperative treatment with MK2i-NPs reduces macrophage persistence *in vivo* in transplanted rabbit vein grafts. **(A)** Representative RAM-11 staining of rabbit jugular vein graft explant histological sections for each treatment group. Arrows demarcate positively stained cells. Left column scale bar = 100 µm, right column zoomed view scale bar = 50 µm. **(B)** Example images from the color deconvolution method utilized to quantify positive RAM-11 staining in the intima of rabbit jugular vein explants. **(C)** Quantification of RAM-11 positive macrophage staining in jugular vein graft sections normalized to intimal nuclei number. Data are represented as mean ± SEM (n ≥ 7 grafts per treatment group). *P* values determined by one way ANOVA. From [1], reprinted with permission from AAAS.

Discussion

Previous studies have characterized the time course of IH pathogenesis in rabbit and canine models. The investigators detected an initial burst in cellular proliferation during the first week, followed by continued graft adaptation that reaches steady state by week 12 [91, 115]. Here, it was hypothesized that enhanced endosomal escape would extend intracellular peptide half-life and that this would improve long-term graft patency following a single intraoperative treatment by more potently inhibiting IH-relevant signaling pathways and accelerating resolution of inflammation and the time required to reach steady-state conditions. Indeed, avoiding endosomal entrapment was associated with increased longevity of intracellular peptide retention ($\mathbf{T_{1/2}}$ was increased 14-fold by incorporation into MK2i-NPs: MK2i-NP $T_{1/2}$ = 57.8 days vs. MK2i $T_{1/2}$ = 4.1 days) and prolonged bioactivity *in vitro*. The latter was demonstrated by the sustained inhibition of migration and sustained inhibition of inflammatory cytokine production 5 days post-treatment in both vascular smooth muscle and endothelial cells. A sustained effect was also seen in intact HSV, and treatment with 100 μM MK2i-NPs completely abrogated neointimal growth over 2 weeks in an *ex-vivo* organ culture model of IH; in this study, the shorter-lived, free MK2i peptide delivered at equivalent dose had an intermediate effect. Furthermore, there was also a long-term (28-day) therapeutic effect in treated grafts that were transplanted *in vivo*.

At the cellular level, the long-term therapeutic benefit of MK2i-NP treatment in the rabbit vein graft model was associated with significantly decreased intimal cell proliferation, neointimal thickening, and number of macrophages. MK2i-NP treatment was also found to modulate vascular smooth muscle cell phenotype *in vivo*. It is well established that intimal hyperplasia is characterized by vascular smooth muscle cell transdifferentiation from a contractile phenotype to a 'synthetic' phenotype. A normal, contractile vascular smooth muscle cell phenotype is defined by high expression of contractile proteins such as α-SMA, low rough endoplasmic reticulum content, a low proliferative index, and fusiform, spindle-shaped morphology. In contrast, a pathological, synthetic vascular smooth muscle cell phenotype is defined by low expression of contractile proteins, extensive extracellular matrix synthesis, high rough endoplasmic reticulum content, a high proliferative index, and a less elongated cobblestone morphology that is commonly referred to as epitheloid or rhomboid [110, 112]. In the context of modulating these phenotypic characteristics, MK2i-NP treatment increased neointimal expression of the contractile

phenotypic marker α-SMA and decreased expression of the synthetic phenotypic marker vimentin both *ex vivo* in human vein and *in vivo* in rabbit jugular vein grafts. In contrast, cell proliferation and expression of contractile vs. synthetic smooth muscle cell phenotypic markers were similar between *in vivo* grafts treated with the free MK2i peptide versus untreated control grafts. These data suggest that any cell-level therapeutic benefit from free MK2i treatment had been exhausted prior to the 28 day terminal time point. Although the mechanism through which MK2 modulates vascular smooth muscle cell phenotype is unclear, these results are the first to our knowledge that suggest that MK2 is a key factor in VSMC phenotypic modulation in vein graft remodeling. Phosphorylation of the CREB transcription factor contributes to cellular proliferation and the pathological, synthetic VSMC phenotype characteristic of IH [108, 116] which is a potential link since MK2i-NPs were found to reduce CREB phosphorylation in HSV. These combined data suggest that MK2i-NP graft treatment may have a unique capability to decrease the level of acute inflammation and/or accelerate the resolution of inflammation, block VSMC phenotypic modulation, and decrease the time post-transplant that it takes the graft to reach a steady state. These possibilities motivate future studies to better understand the role of MK2 in VSMC phenotype and to elucidate the *in vivo* pharmacokinetics and pharmacodynamics of MK2i-NPs in transplanted grafts in a larger animal model and over a broader timescale.

The current studies validate the broad anti-inflammatory and anti-migratory mechanism of action of MK2i-NPs and confirm the utility of targeting the p38-MK2 pathway to inhibit multiple factors underlying IH pathogenesis. MK2i-NPs were shown to modulate pro-inflammatory mediators activated downstream of MK2 such as hnRNP A0 [35, 104, 105] and CREB[8]. MK2i-NP decreased hnRNP A0 phosphorylation in human tissue, which correlated to a decrease in production of the pro-inflammatory cytokines TNF-α, IL-6, and MCP-1 *in vitro* and reduced inflammatory cell recruitment/persistence *in vivo* at 28 days post-transplant. MK2i-NPs were also shown to modulate migration-related pathways in human tissue, as demonstrated by reduced phosphorylation of HSP27, which triggers VSMC transition to a migratory and fibrotic myofibroblast phenotype [34, 38] and causes vein graft vasoconstriction [34, 35, 117]. The effects of HSP27 are mediated through regulation of cytoskeleton dynamics, which impacts migration towards pathologically relevant stimuli such as angiotensin II and PDGF [37, 38, 53, 118]. MK2i-NPs also decreased phosphorylation of the CREB transcription factor, which is also known to contribute to VSMC

migration [8, 106, 107]. Inhibition of both HSP27 and CREB activation correlated to reduced VSMC migration *in vitro*. To my knowledge, these results are the first to establish the relationship between MK2 and the downstream pro-inflammatory and pro-migratory factors hnRNP A0, CREB, and HSP27 in intact, human vascular tissue. However, one major shortcoming of performing protein expression analysis in the whole organ setting is that the contribution of distinct cell populations (i.e. medial vascular smooth muscle cells vs. endothelial cells vs, adventitial cells) remains unclear. To this end, novel techniques such as laser capture microdissection (**LCM**) have been developed that allow for selective isolation of endothelial and smooth muscle cells from vein graft tissue [108]. The advent of this type of technology not only motivates more in-depth studies focused on the contribution of specific vascular cell populations to vein graft IH but also on the influence that these cell populations have on each other through juxtacrine and paracrine signaling.

Conclusion

A simple, translational approach was developed for formulation of nanoparticles that enhance cellular uptake and retention of a highly specific therapeutic peptide inhibitor of MK2. NP formulation enhanced the potency and longevity of action of the MK2i peptide, and the clinical translatability of this delivery technology was demonstrated in human tissue *ex vivo* and in a pre-clinical *in vivo* model. These results also validate and provide mechanistic insight into the key role of MK2 in VSMC behavior/phenotype and vascular graft IH.

The collective anti-inflammatory, anti-migratory, and phenotype-modulating actions of MK2i-NPs emphasize the utility of this therapy against a multifactorial process like IH, which involves a complex interplay of cell proliferation, migration, inflammation, and matrix synthesis. Because this translationally-relevant MK2i-NP formulation (formed by simple mixing; no complex syntheses, conjugations, or purifications required) comprehensively targets multiple factors involved in IH, it has potential to overcome the shortfalls of prior therapeutic candidates with more narrow mechanisms of action. This work further elucidates the molecular mechanisms underlying the initiation and progression of intimal hyperplasia and highlight key therapeutic targets to improve vein graft patency. MK2i-NPs showed significant clinical potential as an IH prophylactic therapy to be applied during vascular graft transplantation, and these

findings firmly establish the potential use of nanotechnology to enhance cell and tissue delivery, bioactivity, and intracellular pharmacokinetics of therapeutic peptides such as MK2i.

CHAPTER V

NANO-POLYPLEXES AS A PLATFORM TECHNOLOGY

Introduction

Preliminary data demonstrates that formulation of the cationic MK2i peptide into an optimized NP formulation significantly increases cellular uptake and retention and facilitates endosomal escape. These attributes resulted in a significant enhancement in bioactivity *in vitro*, *ex vivo*, and *in vivo*. A multitude of cationic, cell penetrating peptide modified therapeutics have been developed that show potential for treatment of human disease [5, 13, 52, 54, 119-126]. Considering the potential of these cell penetrating peptide containing therapeutics in the context of the therapeutic enhancement seen with MK2i-NPs begs the question of whether or not this nano-polyplex approach can serve as a platform technology.

In order to test if the nano-polyplex approach can be generalized to other therapeutic cell penetrating peptides, 2 different vasoactive peptides will be used in the formulation of NP libraries for characterization and optimization for further biological studies *in vitro* and *ex vivo* (**Table 3**).

Peptide	Sequence	MW	Function
MK2i (MMI-0100)	YARAAARQARAKALARQLGVAA	2283.67	MAPKAP Kinase II inhibitor
p-HSP20 (AZX-100)	YARAAARQARAWLRRAsAPLPGLK	2690.06	HSP20 mimetic

Table 5.1. Nano-polyplex peptide library. The vasoactive peptides MK2i and p-HSP20 that will be further studied *in vitro* and *ex vivo.* Red amino acid abbreviations indicate the presence of polar amino groups in the amino acid side chain that potentiate electrostatic interaction with PPAA: R (arginine), K (lysine) - primary amines (strong base); N (asparagine), Q (glutamine) - amides (weak bases).

Peptides will be made through solid phase peptide synthesis with standard Fmoc chemistry. To determine an optimal nanoparticle formulation, a library of nano-polyplexes (**NPs**) will be prepared at a range of charge ratios (**CR** = $([NH_3^+]_{MK2i}/[COO^-]_{PPAA}$) from 10:1 to 1:10 for each peptide and characterized. Following filtration through 0.45 μm, MK2iNP size and surface charge based on ζ-potential will be analyzed through dynamic light scattering (**DLS**) analysis. Optimized MK2i--NP, p-HSP20-NP, RN22-NP and BH3-NP formulations size and morphology will be further characterized through TEM analysis of

uranyl-acetate counterstained samples. The MK2i and p-HSP20 peptides will be fluorescently labeled with an amine-reactive Alexa-488 or Alexa-568 succinimidyl ester for the formulation of fluorescent NPs for *in vitro* uptake, retention, and endosomal escape studies. Biocompatibility of MK2i-NPs and p-HSP20-NPs will be assessed through an LDH cytotoxicity assay performed 24 hours after treatment.

As discussed in chapter 1, a significant unmet clinical need exists for more specific therapeutic interventions for pathological vasoconstriction especially in the context of symptomatic vasospasm following subarachnoid hemorrhage. The mortality associated with subarachnoid hemorrhages is high (40%), largely due to delayed cerebral ischemia secondary to vasospasm. The cost to society of SAH is greater than that of ischemic stroke due to the younger average age of those affected. Current rescue therapies, nimodipine and endovascular coiling of the aneurysm are only marginally effective. Thus, neuroischemic events due to SAH which result in permanent neurological, cognitive, or functional deficits represent a large unmet need. Both the MK2i and p-HSP20 peptides have shown promise to selectively target vasospastic vessels: both peptides inhibit vasoconstriction without having systemic vasodilatory effects by modulating actin dynamics in vascular smooth muscle cells as shown in **figure 1.3.** However, sequestration and accumulation of these vasoactive peptides in the endolysosomal trafficking pathway remains a key barrier to achieving optimal bioactivity on the actin regulatory machinery in the cytoplasm of vascular smooth muscle cells. Thus, the ability of optimized, fluorescently labeled MK2i-NP and p-HSP20-NP formulations to facilitate cytoplasmic peptide delivery will be assessed through a modified subcellular fractionation procedure that enables effective separation of cytosolic and endosomal cellular content through selective semi-permeabilization of the outer membrane of vascular smooth muscle cells. This procedure will be optimized by monitoring release of the cytoplasmic enzyme lactate dehydrogenase under a range of semi-permeabilization conditions. Fluorescent MK2i- and p-HSP20-NP formulations will also be utilized to assess MK2i and p-HSP20 uptake and retention in vascular smooth muscle cells. Since each peptide is hypothesized to modulated actin dynamics, an actin stress fiber assay will be performed in angiotensin II stimulated vascular smooth muscle cells to assess peptide mediated inhibition of F-actin (i.e., filamentous actin) stress fiber formation.

To further assess MK2i- and p-HSP20-NP mediated vasorelaxation of smooth muscle, human saphenous vein (**HSV**) explants will be obtained from consenting patients, sectioned into 1mm rings, and

suspended in a muscle bath outfitted with a force transducer. After verifying HSV viability through KCL contractions, rings will be treated with NPs or free peptide and subsequently contracted with phenylephrine (10^{-6} - 10^{-7} M) to determine % inhibition of contraction and relaxed with cumulative log doses of sodium nitroprusside to determine % relaxation vs. pretreatment. Underlying mechanisms for results obtained through physiology studies will be assessed qualitatively through the visualization of F-actin stress fiber formation in treated HSV explants that have been stimulated with angiotensin II.

Methods

*MAPKAP Kinase II inhibitor (**MK2i**) peptide and phosphorylated heat shock protein 20 (**p-HSP20**) mimetic peptide syntheses.*

A cell permeant MK2 inhibitory peptide (MK2i) with the sequence YARAAARQARA-KALARQLGVAA and a cell permeant phosphorylated heat shock protein 20 mimetic peptide (p-HSP20) with the sequence YARAAARQARA-WLRRAsAPLPGLK (where s denotes a phosphorylated serine residue corresponding to serine 16 in HSP20 that is activated by cyclic nucleotide signaling) were synthesized on a PS3 peptide synthesizer (Protein Technologies, Inc. Tucson, AZ) utilizing standard Fmoc Chemistry. N-methylpyrrolidone (NMP, Fischer Scientific) was utilized as a solvent in all peptide syntheses. HCTU was used as an activator (Chempep, Wellington, FL) in the presence of N-methylmorpholine. All amino acids were double coupled in order to maximize yield and purity. Peptides were cleaved/deprotected in TFA/Phenol/H_2O/triisopropylsilane (88/5/5/2). The peptide was then further purified by reverse phase HPLC on a Waters 1525 binary HPLC pump outfitted with an extended flow kit, a Waters 2489 UV/Visible detector, and a phenomenex Luna C18(2) AXIA packed column (100A, 250 x 21.2 mm, 5 micron). **A)** HPLC grade water with 0.05% formic acid and **B)** HPLC grade acetonitrile were used as the mobile phase, and the peptide was purified utilizing a 90% A to 90% B gradient over 25 mins (16 mL/min). Acetonitrile was removed from purified fractions with a rotary evaporator, and the purified fractions were then lyophilized. Peptide purity was verified through electrospray ionization mass spectrometry (**ESI-MS**) on a Waters Synapt ESI-MS.

Monomer and polymer synthesis

All reagents were purchased from Sigma and were of analytical grade unless otherwise stated. 2-propylacrylic acid was synthesized according to the procedure outlined by Ferrito et al.[127] utilizing diethyl propylmalonate (Alfa Aesar) as a precursor. The 4-cyano-4-(ethylsulfanylthiocarbonyl) sulfanylvpentanoic acid (ECT) chain transfer agent (CTA) was synthesized as previously described[128]. RAFT polymerization of the poly(propylacrylic acid) (**PPAA**) was carried out in bulk under a nitrogen atmosphere at 70°C for 48 hours using 2,2'-azo-bis-isobutyrylnitrile (**AIBN**) as the free radical initiator. The reaction mix was put through three freeze-vacuum-thaw cycles and purged with nitrogen for thirty minutes prior to polymerization. The molar ratio of CTA to AIBN was 1 to 1, and the monomer to CTA ratio was set so that a degree of polymerization of 190 would be achieved at 100% conversion. Following polymerization, the resultant polymer was dissolved in DMF and precipitated into ether 5 times before drying overnight *in vacuo*. Gel permeation chromatography (GPC, Agilent) was used to determine molecular weight and polydispersity (M_w/M_n, PDI) of the PPAA homopolymer using HPLC-grade DMF containing 0.1% LiBr at 60°C as the mobile phase. Molecular weight calculations were performed with ASTRA V software (Wyatt Technology) and were based on experimentally-determined dn/dc values determined through offline injections of serial dilutions of the polymer through a refractive index detector (calculated PPAA dn/dc = 0.087 mL/g). Polymer purity and molecular weight were then verified through NMR spectroscopy. Samples were dissolved in D_6MSO and analyzed using a Bruker 400 MHz NMR spectrometer equipped with a 9.4 Tesla Oxford magnet controlled by a Bruker VA-400 console. NMR spectra were subsequently analyzed using Bruker Topspin 3.0 software.

*MK2i nano-polyplex (**MK2i-NP**), phospho-HSP20 nano-polyplex (**p-HSP20-NP**) library syntheses and characterization*

PPAA was dissolved in 1 M NaOH and diluted into a phosphate buffer (pH 8) to obtain a stock solution. Purified MK2i peptide or p-HSP20 peptide was dissolved in phosphate buffer (pH 8). The MK2i or p-HSP20 peptide were then mixed with the PPAA polymer at a range of CRs from $[NH_3^+]$:$[COO^-]$ = 10:1 to 1:10 to form MK2i-NPs or p-HSP20-NPs, respectively. The resulting nano-polyplexes were syringe filtered through a 0.45 μm PTFE filter, and the hydrodynamic diameter and ζ-potential were characterized

on a Malvern Zetasizer Nano-ZS with a reusable dip cell kit (Malvern Instruments Ltd., Worcestershire, U.K.).

A CR of 1:3 was chosen as the lead MK2i-NP formulation whereas a charge ratio of 3:1 was chosen as the lead p-HSP20-NP formulation. The optimized MK2i-NP and p-HSP20-NP formulations were used in subsequent *in* vitro and *ex vivo* experiments. In order to verify the sizes indicated by DLS analysis, NP formulations were visualized through transmission electron microscopy (TEM) imaging. TEM samples were prepared by inverting carbon film-backed copper grids (Ted Pella) onto a 20 µL droplet of aqueous polyplex suspensions (1 mg/mL) and blotted dry. All samples were then inverted onto a 20 µL droplet of 3% Uranyl Acetate and stained for 30 seconds. Samples were then desiccated *in vacuo* for 2 h prior to imaging on a FEI Tecnai Osiris system.

Cell culture

Primary human coronary artery vascular smooth muscle cells (**HCAVSMCs**) were obtained from Lonza; HCAVSMCs were cultured in complete growth medium [vascular cell basal medium (ATCC) supplemented with 5% FBS, human basic fibroblast growth factor (bFGF, 5 ng/mL), human insulin (5µg/mL), ascorbic acid (50 µg/mL), L-glutamine (10 mM), human epidermal growth factor (EGF, 5 ng/mL), 1% penicillin-streptomycin and 50 ug/mL plasmocin (Invivogen)] in a sterile incubator maintained at 37°C with a humidified, 5% CO_2 atmosphere.

All cultures were maintained in 75cm^2 polystyrene tissue culture flasks (BD Falcon) in a 37°C and 5% CO_2 environment with cell culture media refreshed every other day. Cells were grown to 80-90% confluence prior to being harvested and passaged. All cells were seeded at a density of 20,000-30,000 cells/cm^2, as required for each specific experiment. Only cells from early passages (numbers 3-8) were used in experiments.

Cytotoxicity assay

200 µL of cell suspension (at 10,000 cells/well) were seeded onto 96-well plates to yield an approximate 70% confluence per well. Cells were allowed to adhere to the plate overnight. Cells were then treated with 10, 50, 100, and 500 µM doses of MK2i-NPs, p-HSP20-NPs, MK2i peptide, p-HSP20

peptide, or PBS as a control treatment for 2 hours in Opti-MEM medium supplemented with 1% penicillin-streptomycin. Treatments were subsequently removed and the cells were cultured in fresh complete growth medium for 24 hours. Cells were then washed 2x with PBS +/+ and cell viability was then determined by a CytoTox-ONE Homogenous Membrane Integrity assay (Promega) according to the manufacturer's protocol. Briefly, 100 µL of Ambion KDalert Lysis Buffer was added to each well, and then 100 µL of freshly prepared CytoTox-ONE reagent was added to each well. After 10 minutes of incubation, 50 µL of stop solution was added, and the fluorescence of each well (λ_{ex} = 560 nm, λ_{em} = 590 nm) was determined with a TECAN Infinite M1000 Pro plate reader.

Flow cytometric quantification of peptide uptake and retention in HCAVSMCs

An amine-reactive Alexa-488 succinimidyl ester (Life Technologies) was dissolved in DMSO and mixed at a 1 to 3 molar ratio with the MK2i or p-HSP20 peptide in 100 mM sodium bicarbonate buffer (pH = 8.3) and allowed to react for 3 hours. Unreacted fluorophore and organic solvent were removed using a PD-10 miditrap G-10 desalting column, and the fluorescently labeled MK2i and p-HSP20 peptides were lyophilized. PPAA polymer was mixed with fluorescently labeled MK2i peptide at a CR of $[NH_3^+]/[COO^-]$ = 1:3 and syringe filtered through a 0.45 µm PTFE filter to form fluorescent MK2i-NPs. Similarly, PPAA was mixed with fluorescently labeled p-HSP20 at a CR of $[NH_3^+]/[COO^-]$ = 1:3 and syringe filtered through a 0.45 µm PTFE filter to form fluorescent HSP20-NPs. HCAVSMCs were grown to 80-90% confluence, harvested, and seeded at 20,000 cells/well in a 24 well plate and allowed to adhere overnight. HCAVSMCs were treated with fluorescent MK2i peptide, MK2i-NPs, p-HSP20 peptide, p-HSP20-NPs, or PBS as a control at a concentration of 10 µM peptide in Opti-MEM medium supplemented with 1% penicillin-streptomycin for 30 minutes. Following treatment, cells were washed 2x in PBS, and either immediately harvested or incubated in complete growth media for an additional 72 hours. Cells were harvested with 0.05% trypsin-EDTA, centrifuged, and suspended in 0.1% Trypan blue in PBS (-/-) for analysis on a FACSCalibur flow cytometer (Becton Dickinson) with BD CellQuest™ Pro software (V 5.2). Data was exported and analyzed with FlowJo software (V 7.6.4). All samples were run in triplicate.

F-Actin stress fiber assay

HCAVSMCs were seeded in Lab-Tek II 8-well chambered coverglass (Thermo Scientific Nunc) at 15,000 cells/well and allowed to adhere overnight. Cells were then treated in low serum media (Optimem, 1% FBS, and 1% P/S) with MK2i-NPs, p-HSP20-NPs, MK2i peptide, p-HSP20 peptide, or at concentrations of 10, 25, and 50 μM (PBS -/- as a control) for 1 hour. Following treatment, cells were washed 2x with PBS -/- and subsequently treated with 1 μM Angiotensin II (Sigma Aldrich) or PBS -/- (negative control) for 2 hours. After ANG-II stimulation cells were washed 2x with PBS, fixed in 4% paraformaldehyde for 5 minutes, permeabilized with 0.4% Triton-X 100 for 10 minutes, and blocked with 1% BSA in PBS -/- for 15 minutes. Cells were then stained with Hoechst solution (1/5000 dilution in PBS -/-) for 10 minutes followed by staining with Alexa-488-Phallodin (Life Technologies) for 30 minutes according to the manufacturer's instructions. Stained coverslips were then inverted onto glass cover slides with ProLong Gold Antifade mounting medium (Invitrogen). Slides were allowed to dry for 24 hours prior to sealing and imaging. Treated cells were imaged using a Nikon Eclipse Ti inverted fluorescence microscope (Nikon Instruments Inc, Melville, NY) with NIS Elements imaging software. Gain settings and exposure times were kept constant for all images taken. The number of stress fibers per cell was quantified as previously described[129]. Briefly, in the NIS elements software, 3 separate intensity profiles were generated across the axis of stained cells perpendicular to the cell's polarity. Prior to image analysis, the background noise from each image was removed using a rolling ball background subtraction filter with a radius of 70 pixels. A fluorescence level of 2000 RFU was set as the threshold for positive F-actin fiber staining as the background fluorescence outside of the stained cells was never greater than this value. The stress fibers per cell were then quantified from the average of 3 intensity profiles from $n \geq 6$ cells from 2 separate experiments for each treatment group. Relative quantification of cellular F-actin content was further quantified using imageJ software to free hand select individual cells and to calculate the relative fluorescence intensity of $n \geq 6$ cells from 2 separate experiments for each treatment group.

Quantification of cytosolic vs. organelle bound peptide through semi-permeabilization

In order to quantify the cytosolic bioavailability of the MK2i and HSP20 peptides a method to separate cytosolic and organelle bound (i.e. endosomal, lysosomal, golgi, etc.) peptide was adapted from

the methods developed by Liu et al [130]. The procedure was optimized for this experiment based upon LDH release from HCAVSMCs treated with varying concentrations of digitonin (Calbiochem) in buffer (150 mM NaCl, 0.2 mM EDTA, 20 mM HEPES-NaOH (pH 7.4), 2 mM DTT and 2 mM $MgCL_2$) on ice for 10 mins on a rotary shaker operating at 100 RPM. A concentration of 25 µg/mL was then chosen as the optimal digitonin concentration for selective semi-permeabilization of the HCAVSMC membrane and subsequently used for the analysis of intracellular peptide distribution.

To quantify intracellular distribution of the MK2i and p-HSP20 peptides, HCAVSMCs were seeded into a 96 well plate at a density of 20,000 cells/cm^2 and allowed to adhere overnight in complete growth medium. Cells were then treated with Alexa-488 labeled MK2i peptide, MK2i-NPs, p-HSP20 peptide, p-HSP20-NPs at a concentration of 10 µM peptide (or PBS -/- as a control) in Opti-MEM medium supplemented with 1% penicillin-streptomycin for 30 minutes. Treatments were removed and cells were incubated in fresh medium for 6 hours. Each well was then washed 1x with ice cold PBS +/+ and then subsequently incubated with 20 uL of 25 µg/mL digitonin solution at 0°C (on ice) on a rotary shaker operating at 100 RPM for 10 minutes. The supernatant from each well was then transferred to a new 96 well plate, and each well was washed with 80 µL ice cold PBS +/+ which was then transferred to the 96 well plate containing the digitonin (cytosolic) fractions. 100 uL of 1% triton X-100 in PBS -/- was then added to each well to obtain a 96 well plate containing all non-cytosolic (i.e. organelle bound) cellular components, and the fluorescence of each well (λ_{ex} = 495 nm, λ_{em} = 519 nm) was determined with a TECAN Infinite M1000 Pro plate reader. Readings were normalized to cell number and cytosolic content as determined by a CytoTox-ONE Homogenous Membrane Integrity assay (Promega) according to the manufacturer's protocol (section 4.5).

Western blot verification of cytosolic separation from intracellular organelles

To further verify separation of the cytosol from intracellular organelles such as endosomes and lysosomes, western blot analysis of the cytosolic and organelle fractions from the digitonin semi-permeabilization procedure was performed. Briefly, cytosolic and organelle fractions were concentrated on a centrifuge using Vivacon 500 DNA concentrators (2000 MWCO). Equal amounts of protein (20 µg per lane) were loaded on 4–20% SDS–PAGE gels; proteins were electrophoretically separated and then

transferred to Immobilon membranes. The membranes were then probed overnight at 4°C with primary antibodies for the cytosolic proteins mitogen-activated protein kinase kinase 1/2 (**MEK1/2**) and glyceraldehyde 3-phosphate dehydrogenase (**GAPDH**) and the endo-lysosomal markers early endosomal antigen 1 (**EEA1**) and lysosomal-assocaited protein 1 (**LAMP1**). All antibodies were obtained from Cell Signaling Technologies. After washing, the membranes were incubated with appropriate secondary antibodies (Li-Cor) for 1 hour at room temperature. The secondary antibody was imaged using the Odyssey direct infrared fluorescence imaging system and densitometrically quantified with LiCor Odyssey software v2.1 at 800 and 680 nm wavelengths.

Human saphenous vein

Upon approval by Vanderbilt Medical Center's Institutional Review Board, de-identified, discarded segments of human saphenous vein (**HSV**) were collected from consented patients undergoing coronary or peripheral vascular bypass surgeries. Following surgical resection, HSV segments were stored in buffered salt solution until the end of the surgical procedure, at which time they were placed in cold transplant harvest buffer (100 mM potassium lactobionate, 25 mM KH_2PO_4, 5 mM $MgSO_4$, 30 mM raffinose, 5 mM adenosine, 3 mM glutathione, 1 mM allopurinol, 50 g/L hydroxyethyl starch, pH 7.4). All HSV segments were used within 24 hours of harvest. Utilizing sterile technique in a sterile culture hood, HSV segments were transferred to a 60 mm Petri dish. The end of each segment (0.5 mm) was removed with a blade, and excess adventitial and adipose tissue was removed with minimal manipulation. HSV segments were cut into consecutive rings with an approximate width of 1.0 mm.

Prior to experiments, HSV viability was confirmed. HSV rings were weighed and their lengths recorded. HSV rings were then suspended in a muscle bath containing a bicarbonate buffer (120mM NaCl, 4.7 mM KCl, 1.0 mM $MgSO_4$, 1.0 mM NaH_2PO_4, 10 mM glucose, 1.5 mM $CaCl_2$, and 25 mM Na_2HCO_3, pH 7.4) equilibrated with 95% O2 and 5% CO2 at 37 °C. The rings were stretched and the length progressively adjusted until maximal tension was obtained[131]. Normalized reactivity was obtained by determining the passive length–tension relationship for each vessel segment. Rings were maintained at a resting tension of 1 g, which produces maximal responses to contractile agonists, as previously determined, and equilibrated for 2 h in buffer. Force measurements were obtained using a

Radnoti Glass Technology (Monrovia, CA) force transducer (159901A) interfaced with a Powerlab data acquisition system and LabChart software (AD Instruments, Colorado Springs, CO).

HSV rings were initially isometrically contracted with 110 mM KCl (with equimolar replacement of NaCl in bicarbonate buffer), and the generated force was measured. 110 mM KCl causes membrane depolarization, leading to contraction of vessels containing functionally viable smooth muscle. After vessel viability was verified with multiple KCl challenges, additional rings were cut to be utilized in smooth muscle physiology experiments and for F-actin staining.

HSV Smooth Muscle Physiology Studies

Inhibition of HSV Contraction

Viable HSV rings were washed, allowed to equilibrate in bicarbonate solution for 30 min, and then contracted with phenylephrine (PE, 1 μM). All rings were washed and equilibrated in fresh buffer and allowed to relax until baseline contraction was achieved. Rings were then incubated with either MK2i peptide, MK2i-NPs, p-HSP20 peptide, p-HSP20-NPs, or buffer alone for 2 h. Treated HSV rings were then contracted with the same doses of PE, and the forces generated were again recorded (see **fig. 7A**). Measured force was normalized for ring weight and length and percent inhibition of contraction was calculated by dividing the post-treatment contractile force with the pre-treatment contractile force; pre-treatment force generated with 1 μM PE was set as 100% contraction. Data was obtained in HSV from n ≥ 3 separate patients.

Enhanced HSV vasorelaxation

Viable HSV rings were washed and allowed to equilibrate in bicarbonate solution for 30 min, and then contracted with phenylephrine (PE, 1 μM). Rings were relaxed with a cumulative log dose of sodium nitroprusside (SNP, 0.1-10 μM), a nitric oxide donor, and the resulting decrease in contractile force was recorded over time (see **fig. 7D**). All rings were again washed and equilibrated in buffer for 15 min. Rings were then incubated with either MK2i peptide, MK2i-NPs, p-HSP20, p-HSP20-NPs, or buffer alone for 2 h, followed by treatment with the same doses of PE and SNP. The forces generated were again recorded, and measured force was normalized for ring weight and length and percent relaxation was calculated;

force generated with 100 μM PE was set as 0% relaxation. Data was obtained in HSV from n ≥ 3 separate patients.

Actin staining of Angiotensin II stimulated HSV

Viable HSV rings were placed in a 24 well plate in RPMI medium supplemented with 10% FBS and 1% penicillin-streptomycin and allowed to equilibrate in an incubator at 37°C and 5% CO_2 for several hours. HSV rings were then treated with 100 μM MK2i peptide, 100 μM MK2i-NPs, 500 μM p-HSP20, or 500 μM p-HSP20-NPs or PBS -/- as a negative control for 30 minutes in Opti-MEM medium supplemented with 1% penicillin-streptomycin and then washed 2x in PBS -/-. Subsequently, treated HSV rings were stimulated with 10 μM angiotensin II for 2 hours and then washed 2x in PBS -/-. HSV rings were then immediately fixed in 4% paraformaldehyde for 4 hours at 37°C. HSV rings were then incubated overnight in 30% sucrose in 1x PBS -/-. HSV rings were washed 2x in PBS -/-, embedded in OCT and frozen. 10 micron cryosections were cut from the midportion of each HSV rings and placed onto SuperFrost Plus microscope slides (Fisher Scientific). The slides were then stained and imaged according to the procedure stated in the F-actin stress fiber assay section above. Full HSV sections were compiled through the image stitching capability in the NIS Elements software.

Statistics

Statistical analysis was performed with one-way ANOVA followed by Tukey's post-hoc test to compare experimental groups. Analyses were done with OriginPro 8 software (Originlab, Northampton, MA) or Minitab 16 software (State College, PA). Statistical significance was accepted within a 95% confidence limit. Results are presented as arithmetic mean ± SEM graphically and p-values are included within figures or in the figure legends.

Results

The MK2i peptide with the sequence YARAAARQARA-KALARQLGVAA and the p-HSP20 peptide with the sequence YARAAARQARA-WLRRAsAPLPGLK were synthesized via solid phase synthesis, and purity was verified through electrospray-ionization mass spectrometry (**fig. 5.1**).

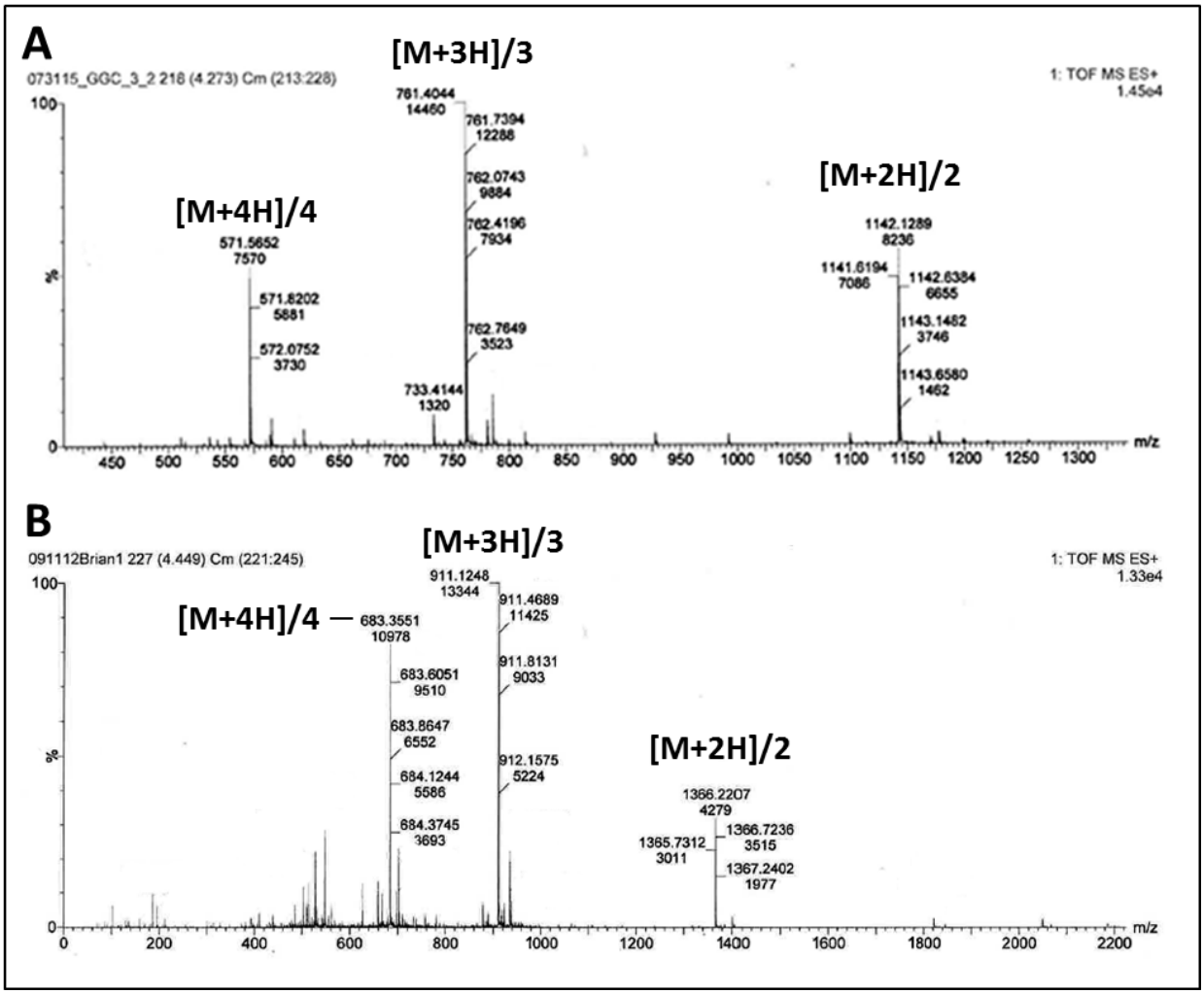

Figure 5.1 – MK2i and p-HSP20 peptide characterization. Electrospray-ionization mass spectrometry (ESI-MS) mass spectra for the HPLC-purified **A)** MK2i peptide (sequence: YARAAARQARA-KALARQLGVAA, MW = 2283.67 g/mol) and **B)** p-HSP20 peptide (sequence: YARAAARQARA-WLRRAsAPLPGLK, MW = 2731 g/mol). The mass spectra show three major peaks each corresponding to the fragmentation of the full peptide sequence. Reprinted with permission from [1]. Copyright 2015 American Chemical Society.

Reversible addition fragmentation chain transfer (**RAFT**) polymerization was utilized to synthesize poly(propylacrylic acid) (**PPAA**) [DP = 193 (GPC), DP = 190 (H^1 NMR), PDI = 1.47 (GPC)]. NPs were formed by simple mixing of the PPAA homopolymer with the MK2i or p-HSP20 peptides in PBS at pH 8.0, which is between the pKa values of the primary amines present on the peptides (pKa~9-12 depending on the amino acid residue) and the carboxylic acid moieties in the PPAA polymer (pKa~6.7); this ensures optimal solubility and net charge on both molecules to facilitate electrostatic complexation.

To determine optimal nanoparticle formulation conditions, a series of MK2i-NPs and p-HSP20-NPs were prepared at a range of charge ratios [i.e. **CR** = ($[NH_3^+]_{MK2i\ /\ p\text{-}HSP20}$:$[COO^-]_{PPAA}$)], and the size distribution and particle surface charge were characterized through dynamic light scattering (DLS) and ζ-potential analysis, respectively. As expected, MK2i-NP and p-HSP20-NP ζ-potential was directly proportional to the CR (**figs. 5.2 A and 5.3 A**). The CR also significantly affected NP size, with a narrow range of CRs yielding a unimodal size distribution (i.e. CR = 1:2 and 1:3 for MK2i-NPs, **table 5.2**, and CR = 3:1 for p-HSP20-NPs, **table 5.3**). A CR of 1:3 was utilized in subsequent studies for the MK2i-NP formulation, and a CR of 3:1 was utilized for the p-HSP20-NP formulation; these charge ratios consistently yielded a unimodal size distribution with minimal particle size and polydispersity (MK2i-NP d_h=119 ± 28 nm, ζ = -11.9 ± 3.2 mV, **fig. 5.2 B**; p-HSP20-NP d_h=141 ± 6 nm, ζ = -7.5 ± 2.8 mV, **fig. 5.3 B**). MK2i-NPs and p-HSP20-NPs prepared at optimal CRs were also characterized through TEM imaging (**figs. 5.2 C and 5.3 C**), which confirmed the presence of nano-structures with size distributions in accordance with DLS results. For subsequent *in vitro* and *ex vivo* studies, optimized NP formulations (**figs. 5.2 D and 5.3 D**) were compared to the corresponding free peptide. These optimized NP formulations are intentionally designed to respond to the decreased pH encountered in the endo-lysosomal trafficking pathway to facilitate cytosolic peptide delivery, as the PPAA polymer has well-defined pH-dependent endosomolytic activity[21, 77] and has previously demonstrated biocompatibility in animal models[78].

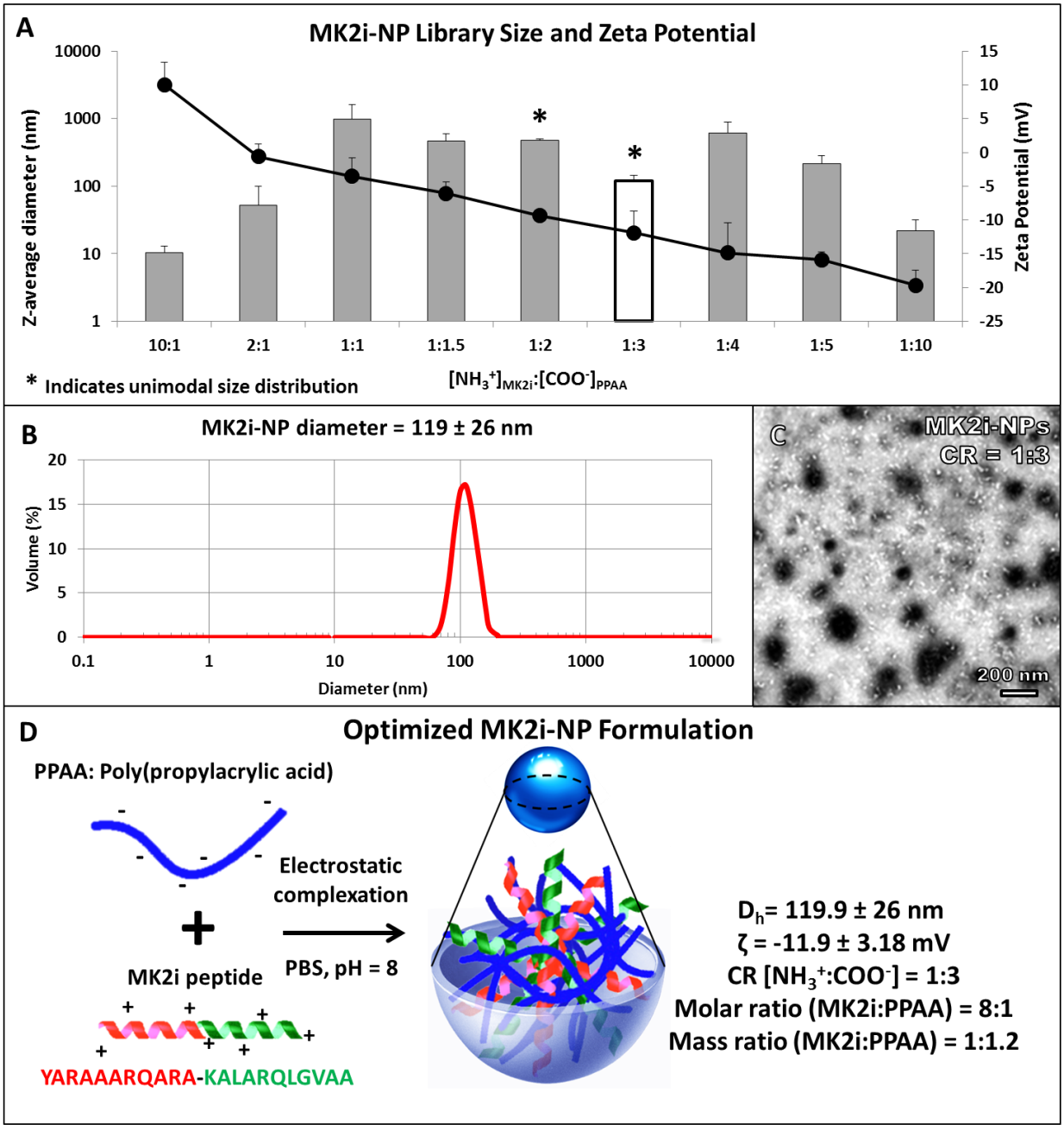

Figure 5.2 - MK2i-NP formulation. A) Z-average diameter (bars) and zeta potential (circles) of MK2i-NPs prepared at a different charge ratios (CR = $[NH_3^+]_{MK2i}$: $[COO^-]_{PPAA}$). Asterisks (*) denote a unimodal size distribution and the white bar represents the optimal MK2i-NP formulation that yielded a unimodal size distribution with minimal size and polydispersity. **B)** Representative DLS trace of optimal MK2i-NP formulation (CR = 1:3). **C)** Representative TEM image of uranyl acetate stained MK2i-NPs, scale bar = 200 nm. **D)** Synthesis and characterization summary for optimal MK2i-NP formulation. CR = charge ratio, D_h= hydrodynamic diameter, ζ = zeta potential. Reprinted with permission from [1]. Copyright 2015 American Chemical Society.

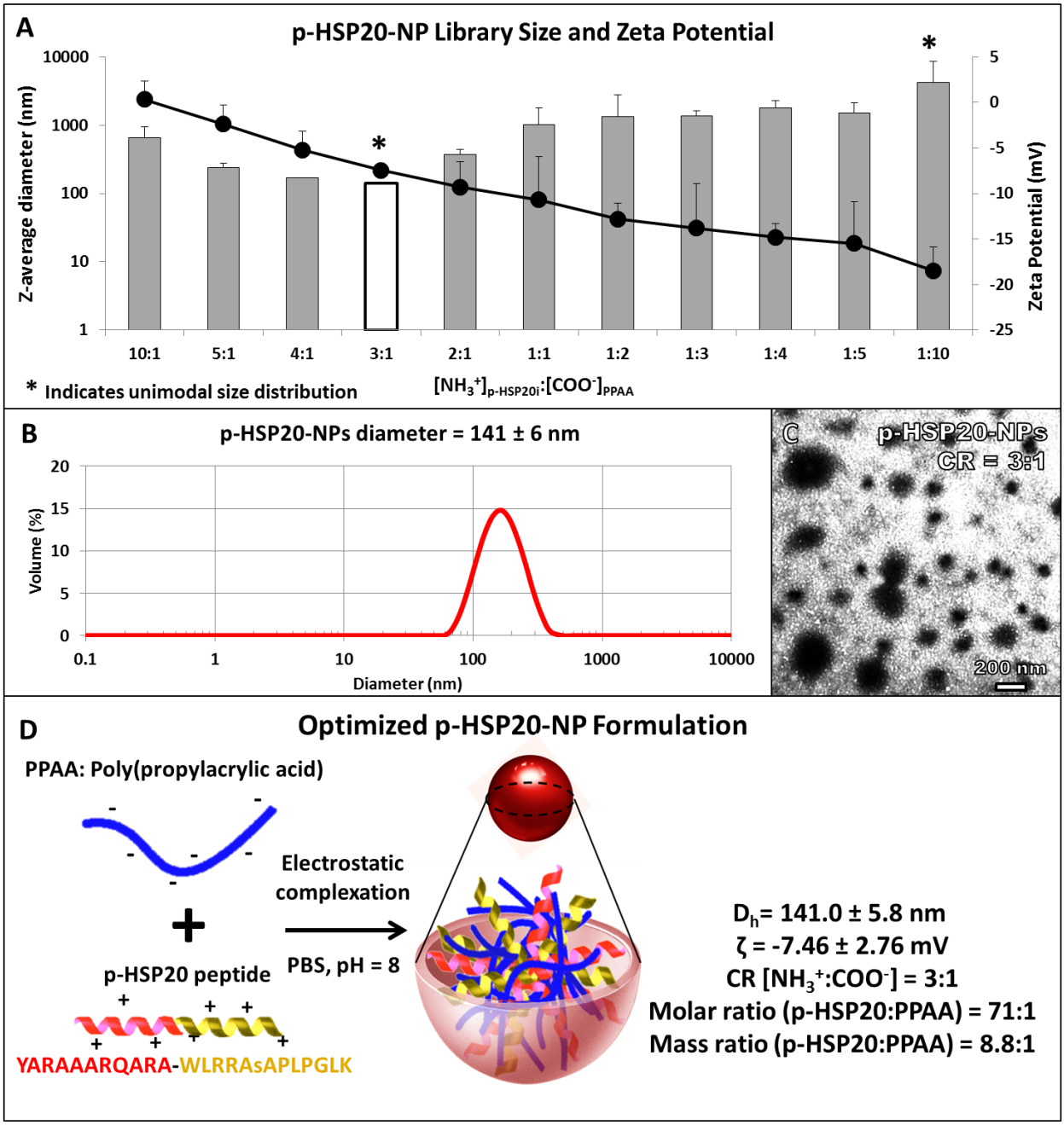

Figure 5.3 - p-HSP20-NP formulation. A) Z-average diameter (bars) and zeta potential (circles) of p-HSP20-NPs prepared at a different charge ratios (CR = $[NH_3^+]_{p\text{-}HSP20}$: $[COO^-]_{PPAA}$). Asterisks (*) denote a unimodal size distribution, and the white bar represents the p-HSP20-NP formulation that yielded a unimodal size distribution with minimal size and polydispersity. **B)** Representative DLS trace of optimal p-HSP20-NP formulation (CR = 3:1). **C)** Representative TEM image of uranyl acetate stained p-HSP20-NPs, scale bar = 200 nm. **D)** Synthesis and characterization summary for optimal p-HSP20-NP formulation. CR = charge ratio, D_h= hydrodynamic diameter, ζ = zeta potential. Reprinted with permission from [1]. Copyright 2015 American Chemical Society.

NH_3^+:COO^-	Z-ave diameter (nm)	PDI
10:1	10.32 ± 2.63*	0.314
2:1	52.1 ± 46.86*	0.297
1:1	970.6 ± 662.4*	0.41
1:1.5	465.1 ± 138.4*	0.5465
1:2	474.2 ± 32.59	0.239
1:3	118.8 ± 26.76	0.271
1:4	607.4 ± 285.2*	0.662
1:5	213.0 ± 67.95*	0.407
1:10	21.57 ± 9.89*	0.355

Table 5.2 - MK2i nano-polyplex library characterization. Size summary of MK2i-NPs prepared at different charge ratios ($[NH_3^+]/[COO^-]$) as determined by DLS analysis. Asterisks (*) indicate multimodal size distributions (multiple peaks present). A CR of 1:3 was chosen as the optimal MK2i-NP formulation (red). Reprinted with permission from [1]. Copyright 2015 American Chemical Society.

NH_3^+:COO^-	Z-ave diameter (nm)	PDI
10:1	659.4 ± 293.7*	0.594
5:1	238.3 ± 38.13*	0.574
4:1	169.1 ± 2.501*	0.591
3:1	141.0 ± 5.783	0.207
2:1	369.3 ± 69.83*	0.554
1:1	1018 ± 786.6*	0.903
1:2	1321 ± 1430*	0.662
1:3	1369 ± 255.9*	0.750
1:4	1772 ± 513*	0.470
1:5	1496 ± 602.9*	0.429
1:10	4246 ± 4428	0.741

Table 5.3 - p-HSP20 nano-polyplex library characterization. Size summary of p-HSP20-NPs prepared at different charge ratios ($[NH_3^+]/[COO^-]$) as determined by DLS analysis. Asterisks (*) indicate multimodal size distributions (multiple peaks present). A CR of 3:1 was chosen as the optimal p-HSP20-NP formulation (red). Reprinted with permission from [1]. Copyright 2015 American Chemical Society.

The biocompatibility of the lead candidate MK2i-NP and HSP20-NP formulations was compared to the corresponding free peptide at range of doses (10 – 500 μM peptide) in human coronary artery vascular smooth muscle cells (**HCAVSMCs**) *in vitro*. HCAVSMCs were treated for 2 hours and then incubated in fresh medium for 24 hours prior to running the cytotoxicity assay. No significant cytotoxicity was evident for MK2i-NPs at all concentrations tested, whereas the free MK2i peptide demonstrated mild toxicity at the highest dose tested (76% cell viability at 500 μM, **fig. 5.4**). HSP20-NPs and the HSP20 peptide were found to be biocompatible with the exception of mild cytotoxicity detected at 500 μM (60% and 77% viability for p-HSP20-NPs and the free p-HSP20 peptide, respectively).

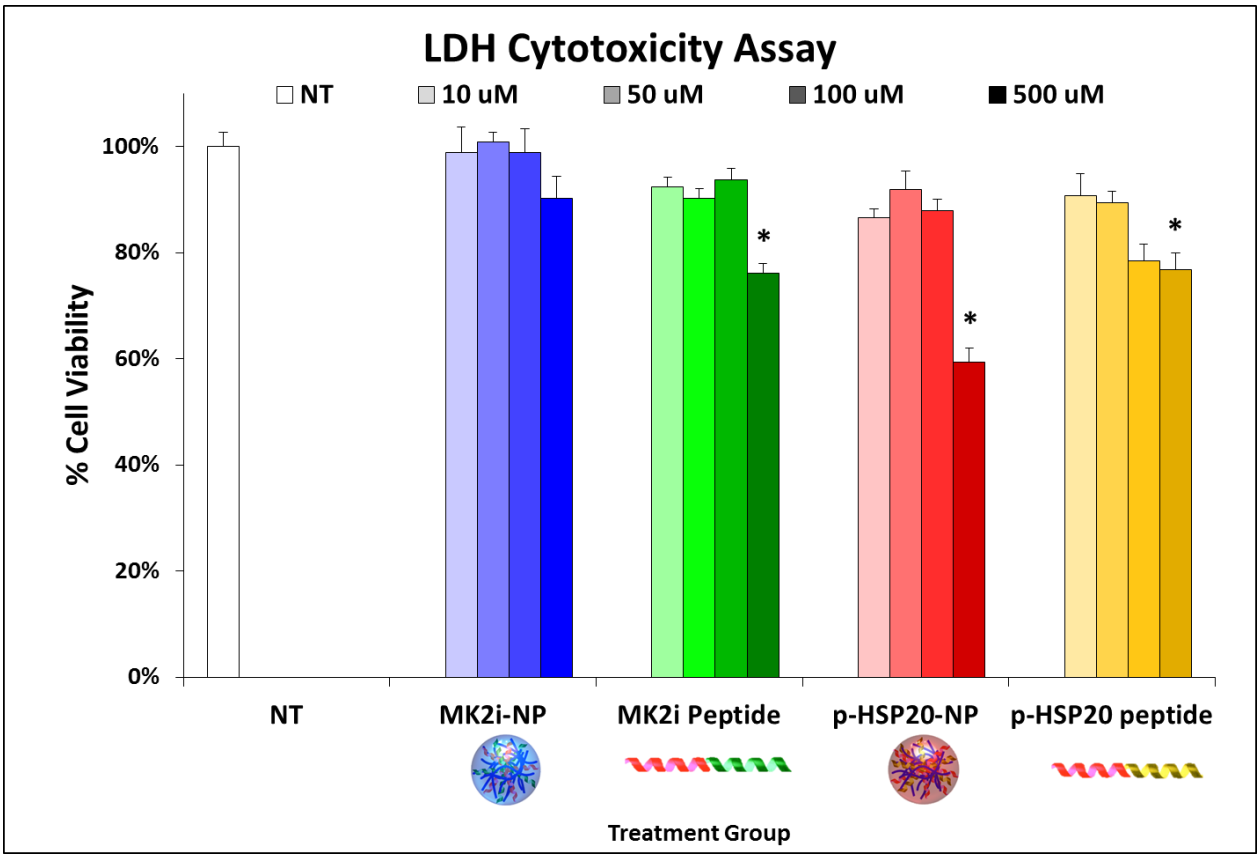

Figure 5.4. - NP cytocompatibility. The cytotoxicity of MK2i-NPs and p-HSP20-NPs was compared to the corresponding dose of free peptide in HCAVSMCs. Cells were treated for 2 hours and then allowed to incubate in fresh medium for 24 hours prior to running the cytotoxicity assay. *p<0.05 vs. NT, n=4 mean ± SEM. Reprinted with permission from [1]. Copyright 2015 American Chemical Society.

Quantity of MK2i-NP and p-HSP20-NP uptake and intracellular retention over time were assessed through flow cytometric analysis of HCAVSMCs treated for 30 minutes, washed, and maintained in fresh medium for 0 or 3 days. More than an order of magnitude increase in uptake (~70-fold

increase in MK2i uptake and ~35-fold increase in p-HSP20 uptake) was detected for both peptides when incorporated into NPs (**fig. 5.5**). Furthermore, HCAVSMCs treated with MK2i-NPs or p-HSP20-NPs demonstrated increased intracellular peptide retention 3 days after treatment removal compared to the free MK2i or p-HSP20 peptide (82% vs. 54% of initial uptake remaining for MK2i-NPs vs. free MK2i, **fig. 5.5 A and E**; 70% vs. 35% retention of p-HSP20-NPs vs. free p-HSP20, **fig. 5.5 B and F**). Intracellular retention can be improved by reducing exocytosis of the intact peptide and/or degradation of the peptide in the endo-lysosomal pathway [87]. Considering that endo-lysosomes are preferentially exycotosed in nonsecretory smooth muscle cells[132], escape from endo-lysosomal trafficking would result in a decreased rate of exocytosis suggesting that peptide formulation in NPs facilitates endo-lysosomal escape.

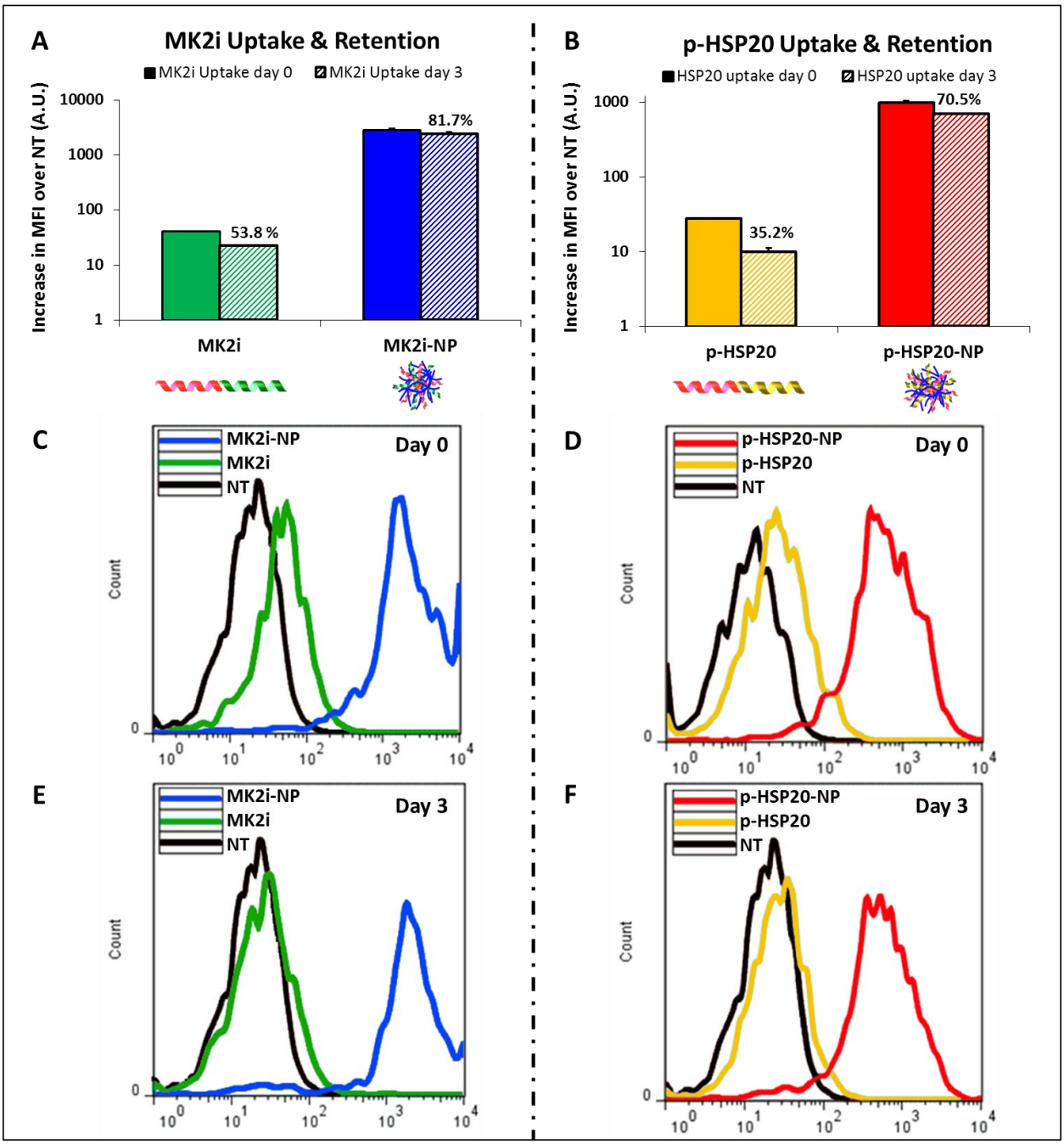

Figure 5.5 - NP uptake and retention. Flow cytometric quantification of peptide uptake and retention of **A)** MK2i-NPs vs. MK2i and **B)** p-HSP20-NPs vs. HSP20 at a 10 μM dose of peptide after 30 minutes of treatment. MK2i-NPs achieved ~70 fold increase in peptide uptake at the same concentration whereas p-HSP20-NPs achieved a ~35 fold increase in uptake. **C,D)** Representative flow histograms of HCAVSMCs immediately after treatment and **E,F)** representative flow histograms demonstrating that formulation into NPs increased peptide cellular retention after 3 days of culture in fresh medium post-treatment. The percentages overwritten on **A-B** represent the % retention at 3 days relative to 0-days post-treatment. Reprinted with permission from [1]. Copyright 2015 American Chemical Society.

To investigate this potential connection between increased peptide intracellular retention and endosomal escape of peptides delivered via the NP formulation, a digitonin-based, semi-permeabilization technique[130] was adapted and optimized for measuring the relative quantity of cytosolic and vesicle-bound peptide for NP and free peptide treated HCAVSMCs (**fig. 5.6 A**). Digitonin is a non-ionic detergent that under optimized conditions results in the selective semi-permeabilization of the cell membrane while leaving intracellular organelles (e.g., endosomes and lysosomes) intact. An optimized semi-permeabilization procedure was determined by measuring the LDH (which is known to be localized to the cytosol) quantity in the "cytosolic" and "organelle" fractions from HCAVSMCs incubated with a range of concentrations of digitonin for 10 minutes on ice. (**fig. 5.7**). Western blot analysis of the cytosolic and organelle fractions collected using the optimized semi-permeabilization protocol verified effective separation of the cytosolic proteins mitogen-activated protein kinase kinase 1/2 (**MEK1/2**) and glyceraldehyde 3-phosphate dehydrogenase (**GAPDH**) from the endo-lysosomal markers early endosomal antigen 1 (**EEA1**) and lysosomal-assocaited protein 1 (**LAMP1**, **fig. 5.6 B**). Utilizing fluorescently labeled MK2i and p-HSP20 peptides allowed for quantification of the intracellular distribution of both peptides following delivery in their free form versus via NP formulations. This analysis revealed that formulation into NPs not only increased peptide uptake but also significantly increased the fraction of internalized peptide in the cytosol; the net effect was an approximately 8-fold increase in cytosolic MK2i delivery and ~29-fold increase in p-HSP20 delivery (**fig. 5.6 C and D**). These data suggest that the known pH-dependent membrane disruptive activity of PPAA enables the peptide-NP formulations to escape endo-lysosomal vesicles.

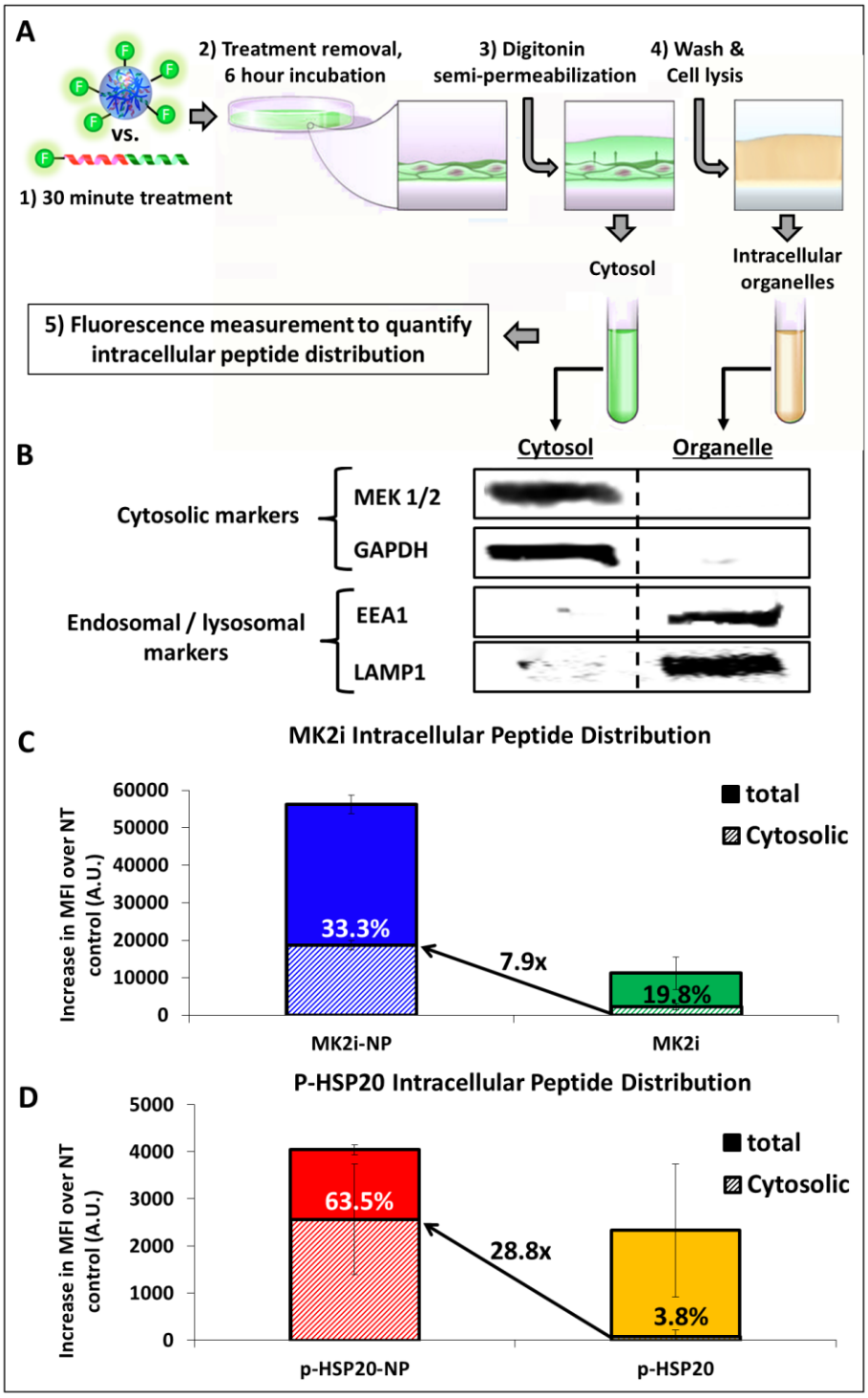

Figure 5.6 - NP Endosomal Escape and Cytosolic Peptide Delivery. A) Experimental design for separation of treated vascular smooth muscle cell cytosol and intracellular organelles using digitonin semi-permeabilization. Conditions for semi-permeabilization were optimized as shown in supplementary figure 3. **B)** Western blot validation of the optimized digitonin semi-permeabilization procedure confirmed separation of the cytosolic proteins mitogen-activated protein kinase kinase 1/2 (**MEK1/2**) and glyceraldehyde 3-phosphate dehydrogenase (**GAPDH**) from the endo-lysosomal markers early endosomal antigen 1 (**EEA1**) and lysosomal-associated protein 1 (**LAMP1**). Comparison of the intracellular distribution of **C)** MK2i and **D)** p-HSP20 peptides when delivered alone or formulated into NPs demonstrates that increased cytosolic delivery is achieved with the NP formulations. Reprinted with permission from [1]. Copyright 2015 American Chemical Society.

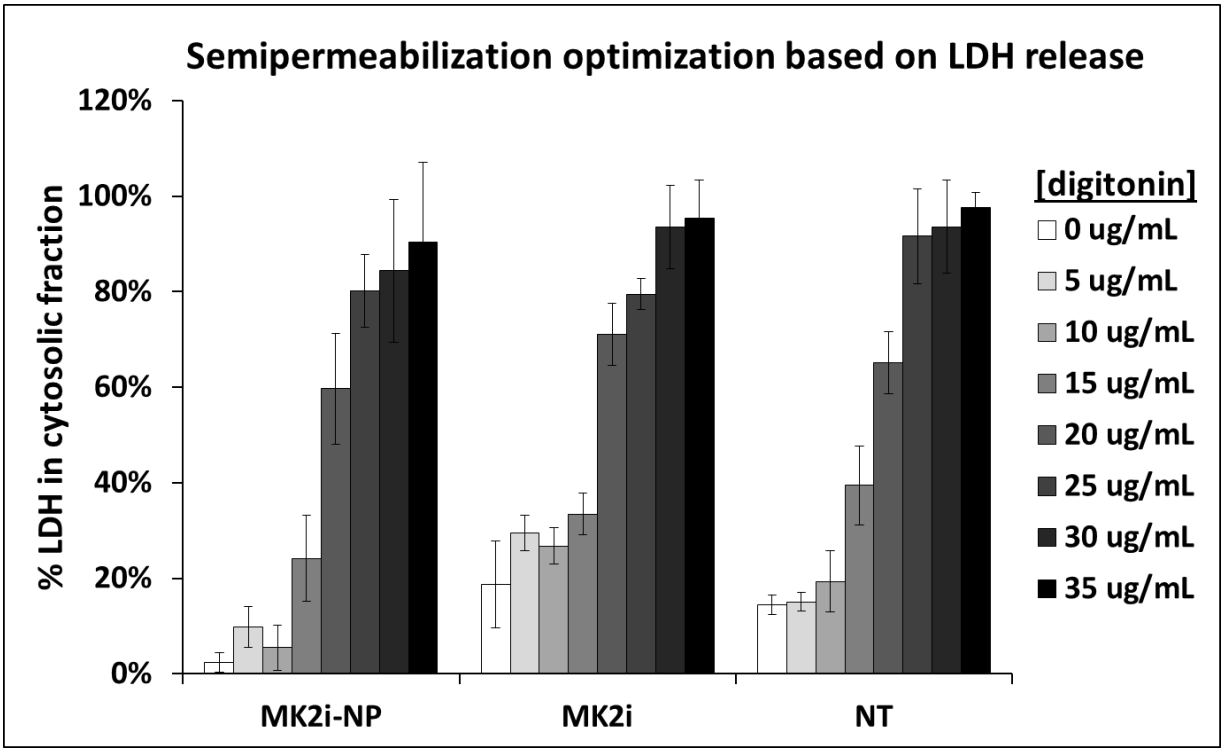

Figure 5.7 - Digitonin semi-permeabilization optimization. The conditions for the digitonin semi-permeabilization procedure to separate cytosolic components from intracellular organelles (i.e., endo-lysosomal compartments) were optimized based upon LDH release following 10 minutes of incubation with various concentrations of digitonin at 0°C on rotary shaker operating at 100 RPM. 25 ug/mL digitonin was chosen as the optimal condition as no significant increase in release of cytosolic LDH was seen at higher concentrations. Reprinted with permission from [1]. Copyright 2015 American Chemical Society.

Subsequently, the efficacy of MK2i-NP and p-HSP20-NP mediated inhibition of F-actin stress fiber formation was quantified in Angiotensin-II (**ANG II**) stimulated HCAVSMCs. Both NP formulations enhanced peptide functional bioactivity as measured by a significant decrease in the average number of stress fibers per cell (**fig. 5.8 A**). Qualitatively, HCAVSMCs treated with the NP formulations yielded cell morphology and staining consistent with unstimulated control cells whereas HCAVSMCs treated with the free peptide still demonstrated stress fiber formation similar to stimulated control cells (**fig. 5.8 B**).

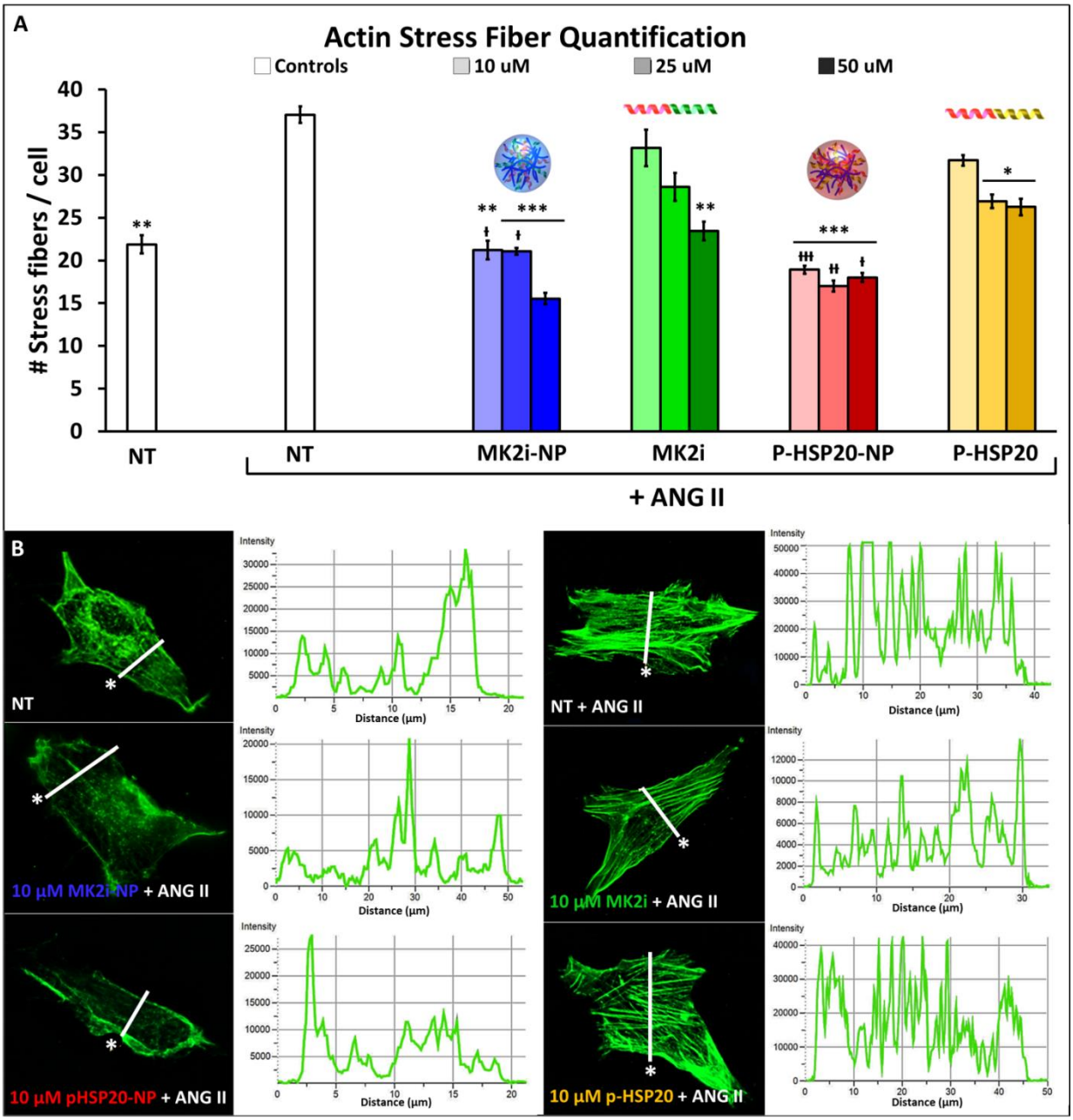

Figure 5.8 - Inhibition of F-actin stress fiber formation in vascular smooth muscle cells. A) F-actin stress fiber quantification in HCAVSMCs pre-treated with p-HSP20-NPs, free p-HSP20 peptide, MK2i-NPs or free MK2i for 1 hour and then stimulated with ANG II for 2 hours. The number of stress fibers per cell was calculated from three intensity profiles taken from the axis transverse to the cellular polarity from at least 6 different cells for each treatment group, *p<0.05, **p<0.01 , ***p<0.001 vs. NT + ANG II; ŧp<0.1, ǂp<0.01, ǂǂp<0.001 vs. the free peptide at the same concentration. **B)** Representative fluorescence microscopy images of F-actin stress fiber formation in ANG II-stimulated HCAVSMCs and the corresponding intensity profile derived from the line shown in the image. The asterisk denotes the left side of the intensity profile shown. Gain settings were kept constant for all images obtained. Reprinted with permission from [1]. Copyright 2015 American Chemical Society.

The total amount of F-actin per cell was also quantified using Alexa-488 phalloidin, a stain that selectively binds to filamentous but not globular, actin (**figs. 5.9 and 5.10**). This analysis revealed a dose dependent inhibition of F-actin stress fiber formation by both peptide-NP formulations. Consistent with the average number of stress fibers per cell, the NP formulations of both peptides also demonstrated significantly enhanced inhibitory activity compared to the corresponding free peptide. Furthermore, a 50 μM dose of MK2i-NPs or p-HSP20-NPs yielded actin staining similar to unstimulated control cells; in comparison, cells treated with 50 μM of each free peptide demonstrated robust stress fiber formation upon stimulation with ANG II.

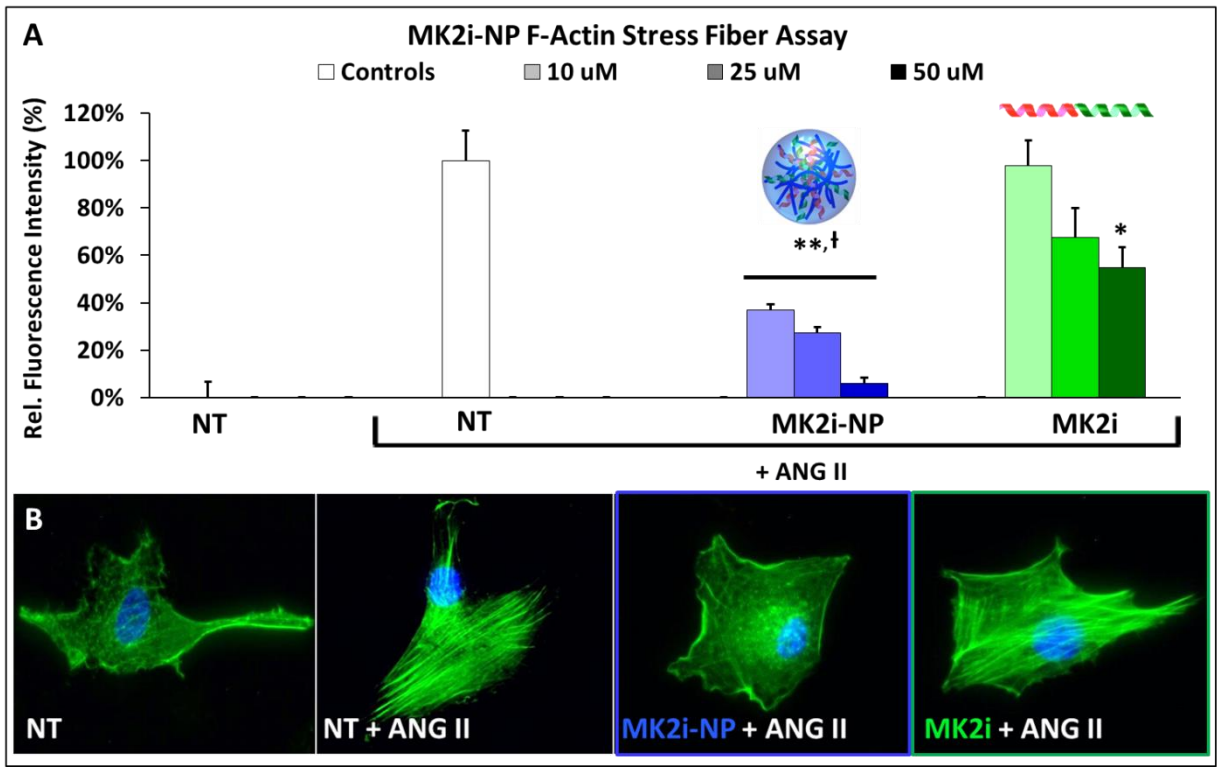

Figure 5.9 - Inhibition of F-actin stress fiber formation by MK2i-NPs.. **A)** F-actin stress fiber quantification in HCAVSMCs pre-treated with MK2i-NPs or free MK2i for 1 hour and then stimulated with ANG II for 2 hours. Data represents n ≥ 6 cells from 2 separate experiments: *p<0.05 vs. NT + ANG II **p<0.001 vs. NT + ANG II, łp<0.05 vs. MK2i at same concentration. **B)** Representative fluorescence microscopy images of F-actin stress fiber formation in ANG II-stimulated HCAVSMCs after 1 hour treatment with free MK2i or MK2i-NPs. Reprinted with permission from [1]. Copyright 2015 American Chemical Society.

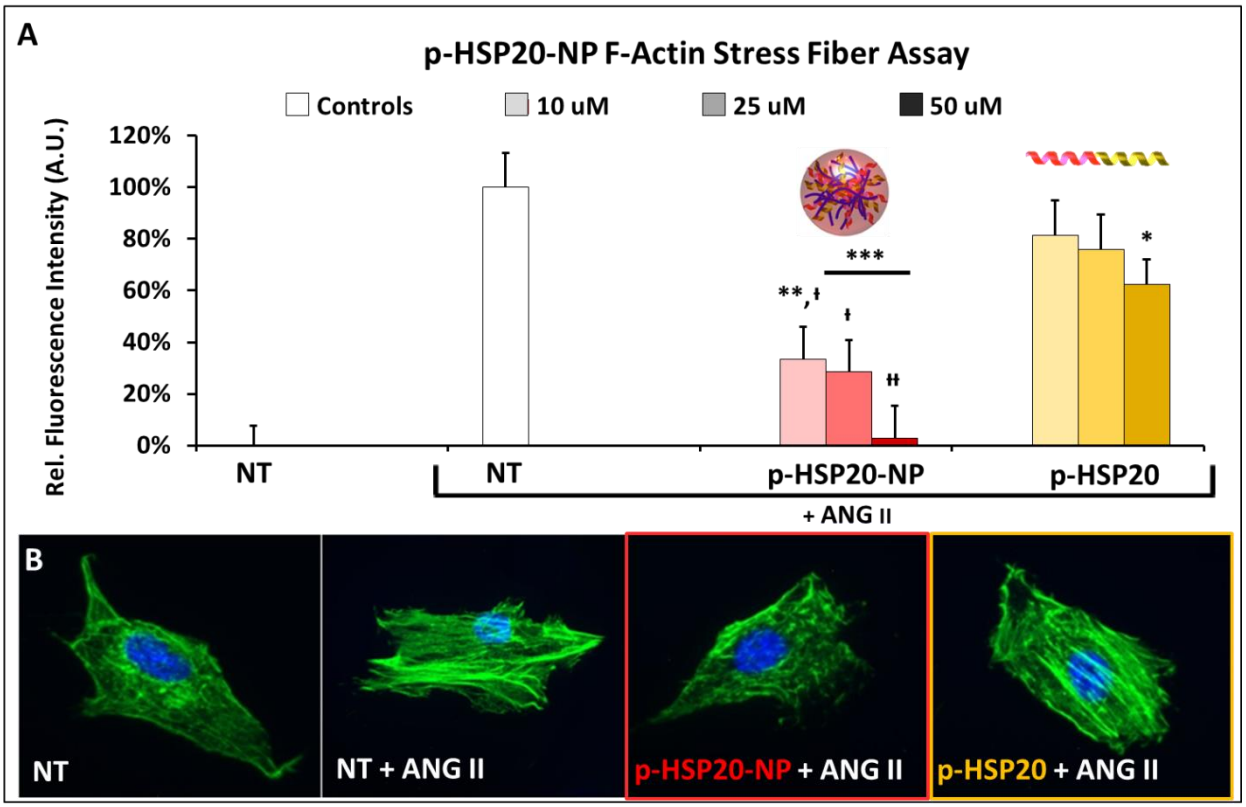

Figure 5.10 - Inhibition of F-actin stress fiber formation by p-HSP20-NPs. A) F-actin stress fiber quantification in HCAVSMCs pre-treated with p-HSP20-NPs or free p-HSP20 for 1 hour and then stimulated with ANG II for 2 hours. Data represents n ≥ 6 cells from 2 separate experiments: *p<0.05, **p<0.01, ***p<0.001 vs. NT + ANG II, łp<0.05, łłp<0.001 vs p-HSP20 at same concentration**. B)** Representative fluorescence microscopy images of F-actin stress fiber formation in ANG II-stimulated HCAVSMCs after 1 hour treatment with free p-HSP20 or p-HSP-20-NPs. Reprinted with permission from [1]. Copyright 2015 American Chemical Society.

The effect of the MK2i-NP and p-HSP20-NP formulations on smooth muscle physiology in human vascular tissue was assessed in order to evaluate them as potential treatments for vasospasm. For these studies, human saphenous vein (**HSV**) was collected from consented patients undergoing bypass grafting surgery and sectioned into rings. After verifying viability through KCL challenge in a muscle bath, the ability of each NP formulation to inhibit phenylephrine (**PE**) induced vasoconstriction was measured in HSV rings using an organ bath system outfitted with a force transducer with an experimental design where vessels were contracted, relaxed, treated, and then contracted again (**fig. 5.11**).

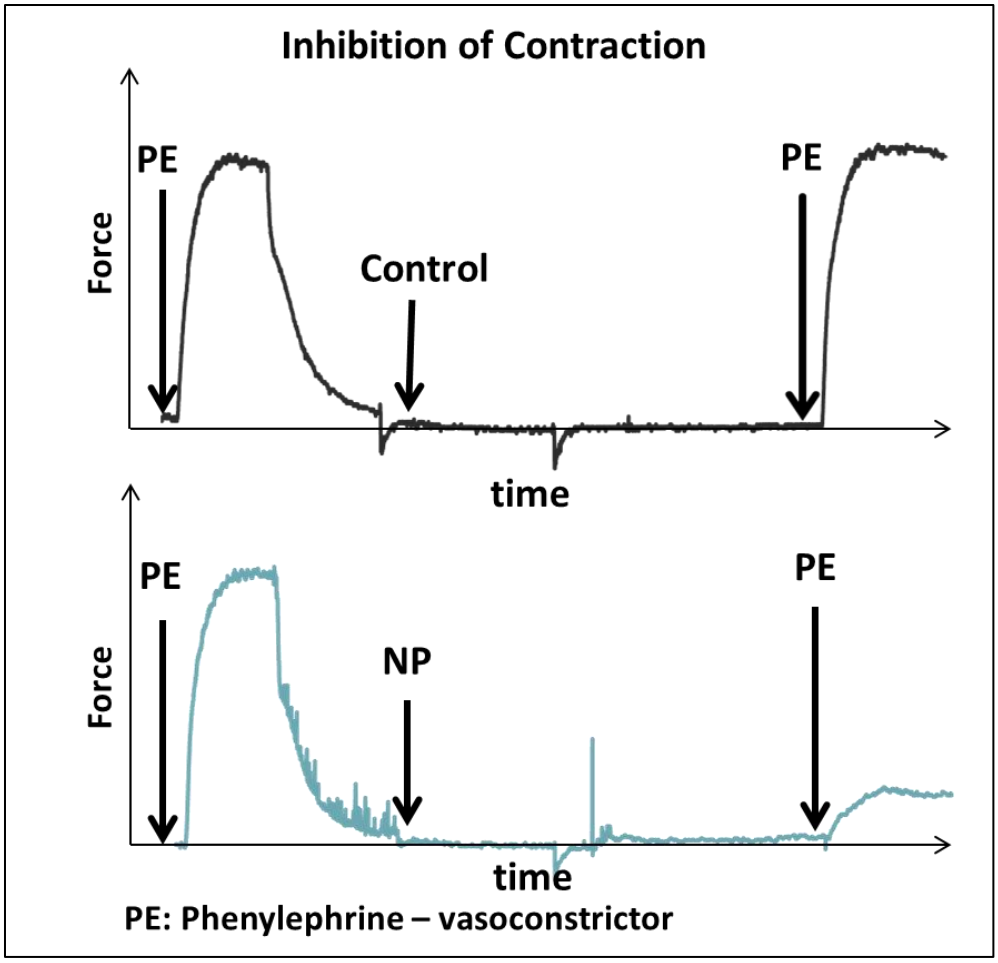

Figure 5.11 – Experimental design for inhibition of contraction studies. HSV rings are initially contracted with PE and then relaxed. After 2 hours of treatment with NPs, free peptide, or control, post treatment contraction is measured. Reprinted with permission from [1]. Copyright 2015 American Chemical Society.

Untreated control HSV rings displayed no changes in the second round of PE induced contraction relative to the initial contraction. However, intermediate treatment with the MK2i or p-HSP20 peptides significantly inhibited the second PE-induced HSV contraction (**figs. 5.12 and 5.13**). Consistent with *in vitro* F-actin stress fiber results, equivalent doses of peptide delivered via NP formulations demonstrated significantly enhanced peptide-mediated inhibition of contraction compared to the free peptide. Notably, treatment with a dose of free PPAA polymer equivalent to the highest NP dose administered showed negligible effects on PE-induced HSV contraction (**fig. 5.12**) indicating that the enhanced inhibitory activity is mediated through enhanced peptide bioactivity and is not a non-specific effect of the endosomolytic polymer. This enhanced ability to inhibit vasoconstriction demonstrates the translational

potential of these NP formulations as a prophylactic approach to prevent vasospasm in applications such as coronary or peripheral bypass grafting.

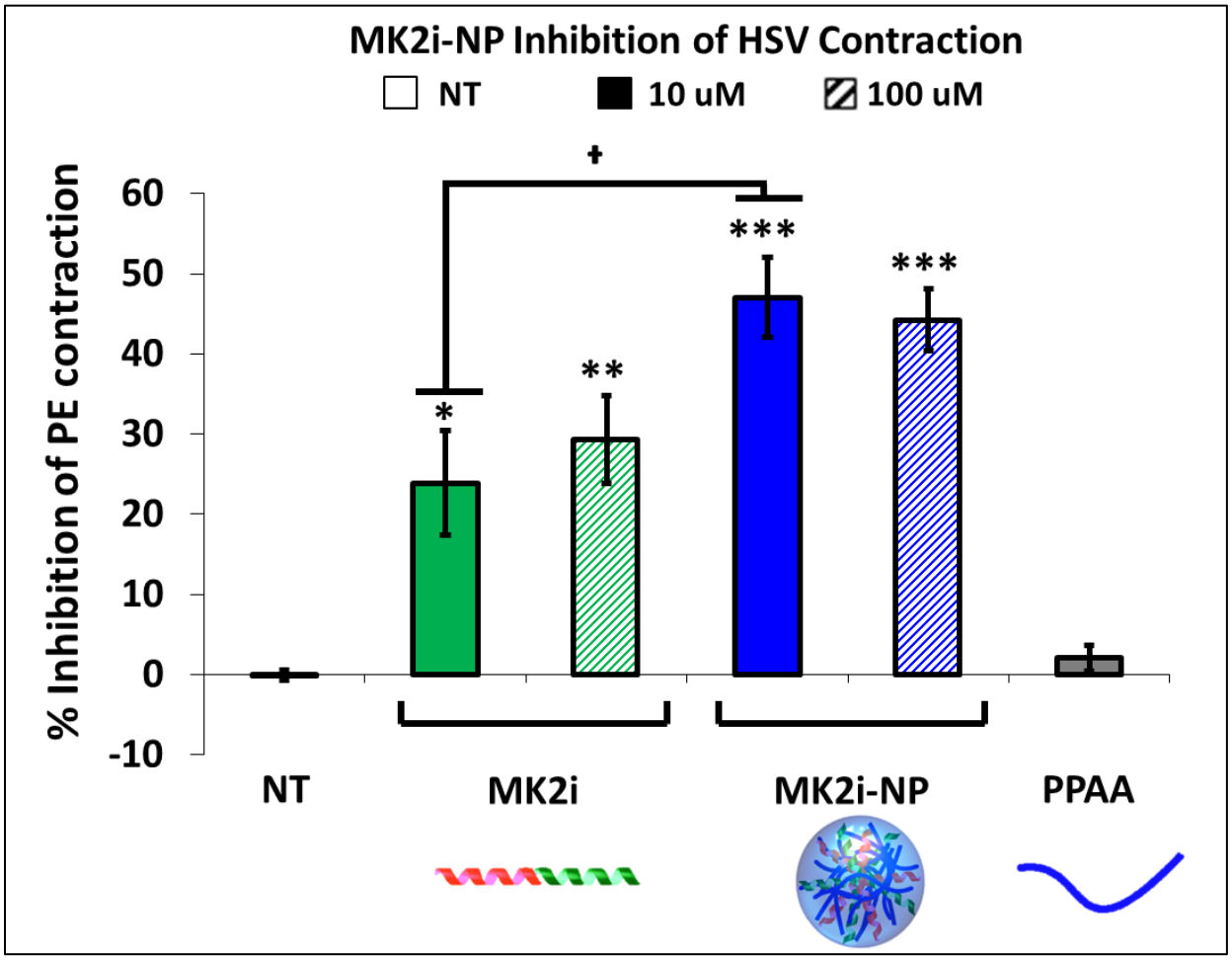

Figure 5.12 - MK2i-NP treatment inhibits vasoconstriction in human saphenous vein. Quantification of MK2i and MK2i-NP mediated inhibition of contraction. PPAA polymer equivalent to the highest dose of MK2i-NPs was included as a vehicle control. ł$p < 0.05$; *$p < 0.05$, **$p<0.01$, ***$p<0.01$ vs. NT, $n \geq 3$ separate donors. Reprinted with permission from [1]. Copyright 2015 American Chemical Society.

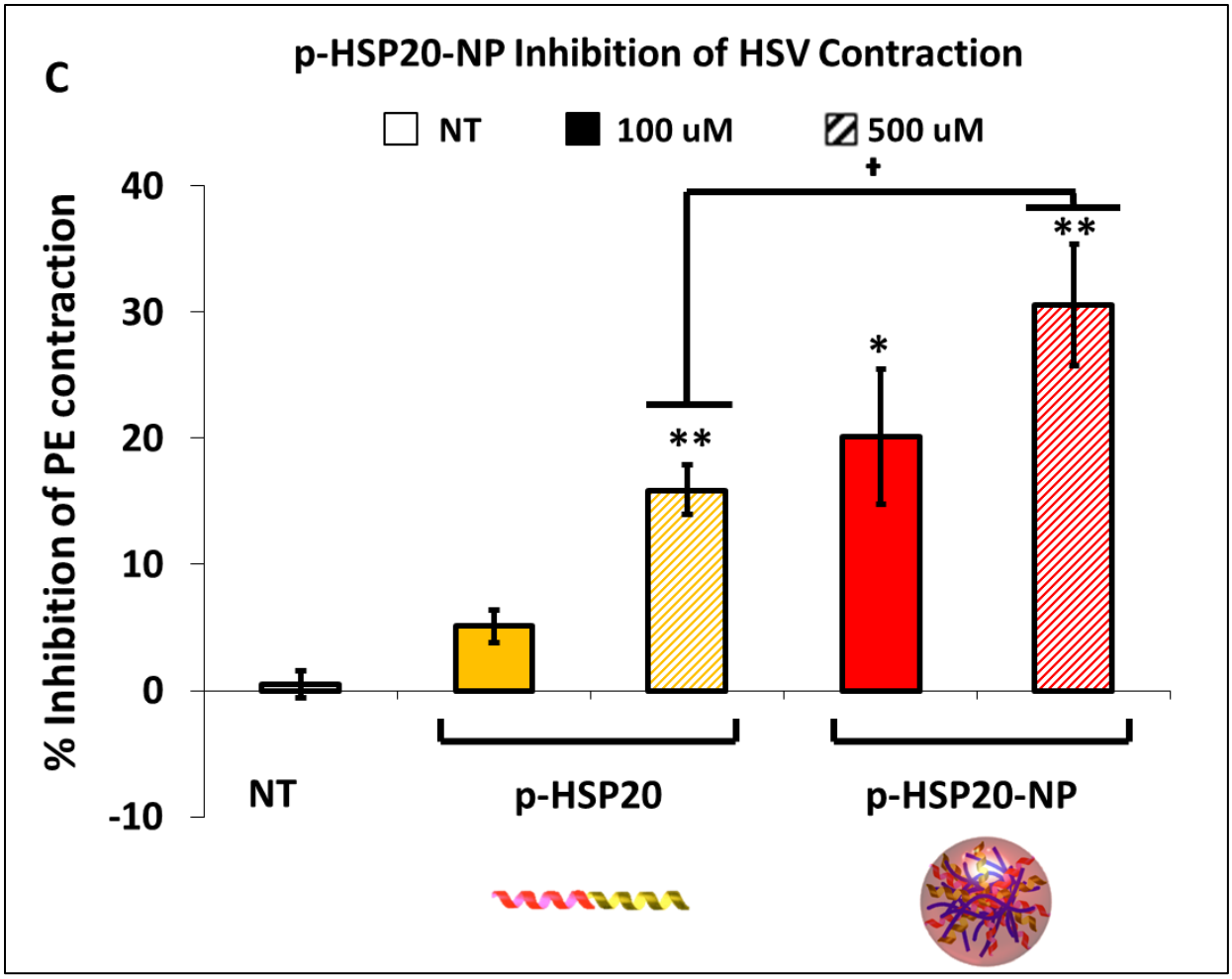

Figure 5.13 - p-HSP20-NP treatment inhibits vasoconstriction in human saphenous vein. Quantification of p-HSP20 and p-HSP20-NP mediated inhibition of contraction. ŧp < 0.05; *p < 0.05, **p<0.01, ***p<0.01 vs. NT, n ≥ 3 separate donors. Reprinted with permission from [1]. Copyright 2015 American Chemical Society.

In addition to testing the efficacy of these NP formulations as a prophylactic therapy, the ability of the MK2i- and p-HSP20-NPs to enhance sodium nitroprusside (**SNP**) induced vasorelaxation was evaluated as a potential salutary therapeutic intervention (e.g., to treat SAH induced vasospasm) in viable HSV explants (**fig. 5.14**).

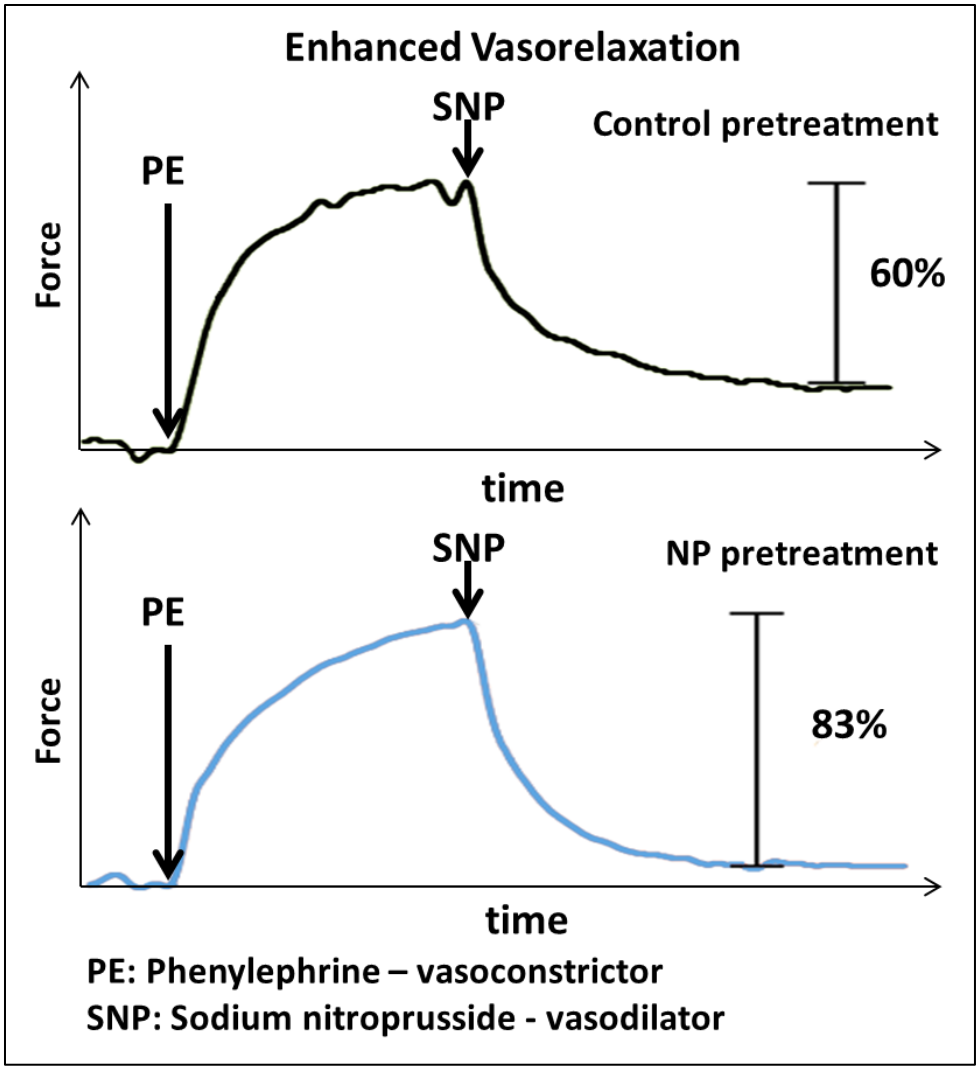

Figure 5.14 – Experimental design for inhibition of contraction studies. Experimental design for enhanced vasorelaxation studies: HSV rings are initially contracted with PE and subsequently relaxed with SNP. HSV rings are then treated for two hours with NPs, free peptide, or control and then contracted and relaxed under the same conditions to compare post-treatment to pre-treatment relaxation. Reprinted with permission from [1]. Copyright 2015 American Chemical Society.

Again, both NP formulations demonstrated an enhanced ability to promote SNP-induced vasorelaxation at all concentrations tested (**figs. 5.15 and 5.16**) whereas untreated HSV or HSV treated with the PPAA polymer alone showed negligible differences in vasorelaxation (**fig. 5.15**). This enhanced ability to enhance vasorelaxation demonstrates the translational potential of these NP formulations as a salutary intervention to treat vasospasm in applications such as symptomatic vasospasm following subarachnoid hemorrhage.

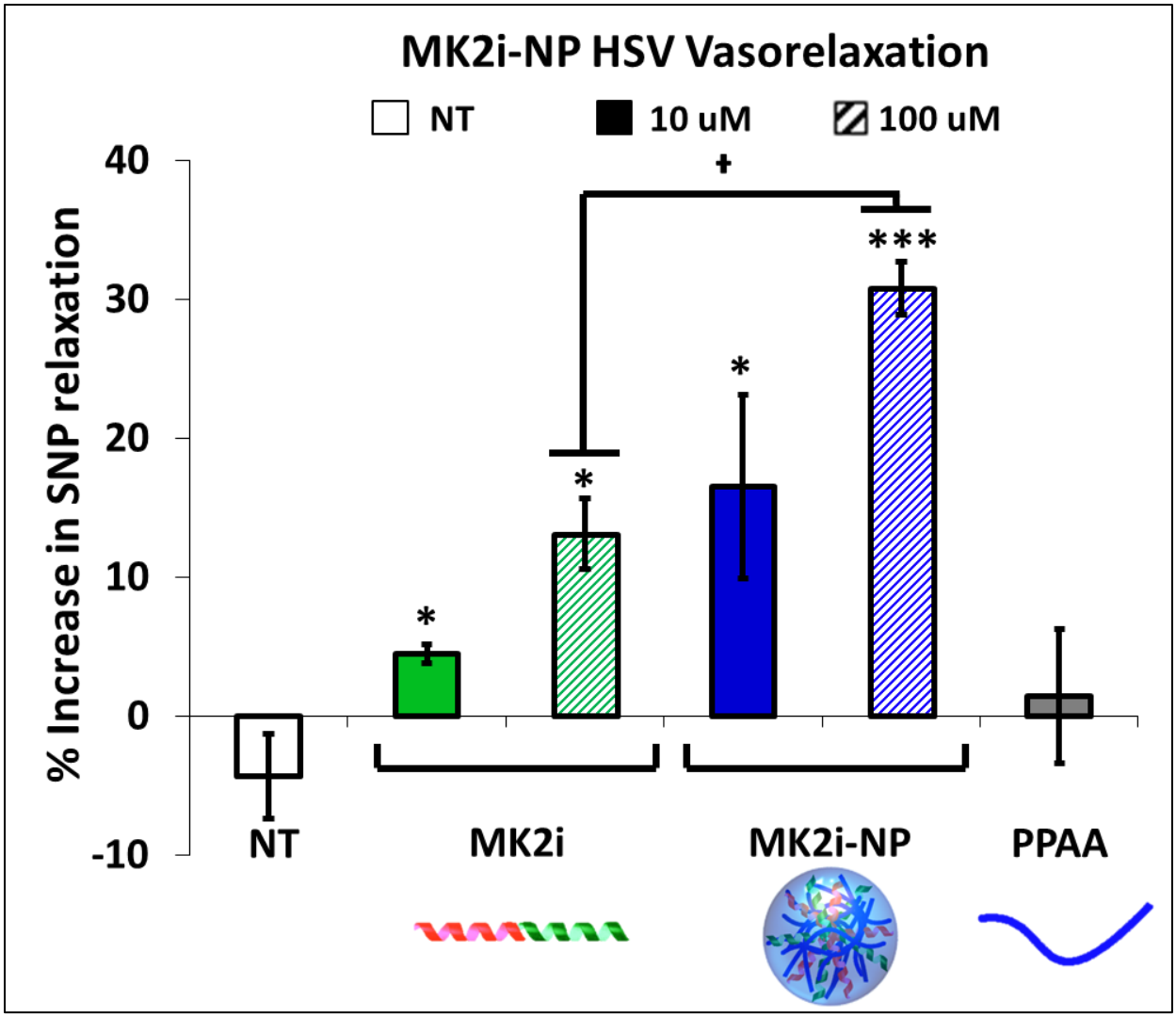

Figure 5.15 - MK2i-NP treatment enhances vasorelaxation in human saphenous vein. Quantification of MK2i and MK2i-NP enhanced vasorelaxation. PPAA polymer equivalent to the highest dose of MK2i-NPs was included as a vehicle control. ł$p < 0.05$; *$p < 0.05$, **$p<0.01$, ***$p<0.01$ vs. NT, $n \geq 3$ separate donors. Reprinted with permission from [1]. Copyright 2015 American Chemical Society.

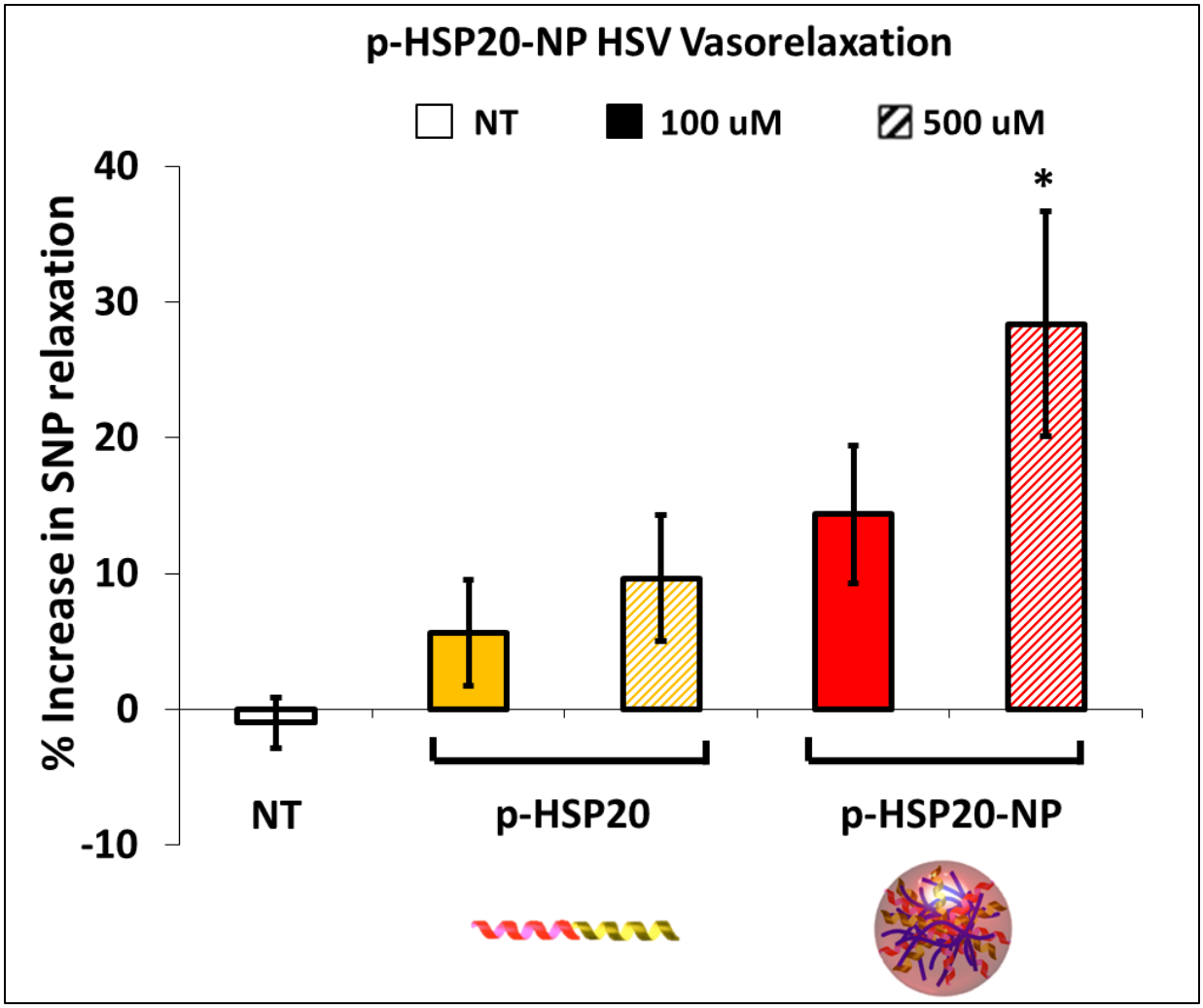

Figure 5.16 – p-HSP20-NP treatment enhances vasorelaxation in human saphenous vein. Quantification of p-HSP20 and p-HSP20-NP enhanced vasorelaxation. łp < 0.05; *p < 0.05, **p<0.01, ***p<0.01 vs. NT, n ≥ 3 separate donors. Reprinted with permission from [1]. Copyright 2015 American Chemical Society.

In order to qualitatively assess the correlation of F-actin stress fiber formation with the smooth muscle physiology results in human tissue, HSV rings were pretreated with free peptide or the NP formulations and then subsequently stimulated with ANG II prior to F-actin staining with Alexa-488 phalloidin (**fig. 5.17**). In concordance with the smooth muscle physiology results, HSV rings treated with NP formulations showed diminished phalloidin staining compared to HSV treated with the free peptide. Altogether, these results indicate that MK2i- and p-HSP20-NPs significantly enhance the ability of the MK2i and p-HSP20 peptide to inhibit vasoconstriction and promote vasorelaxation by modulating actin dynamics in human smooth muscle tissue.

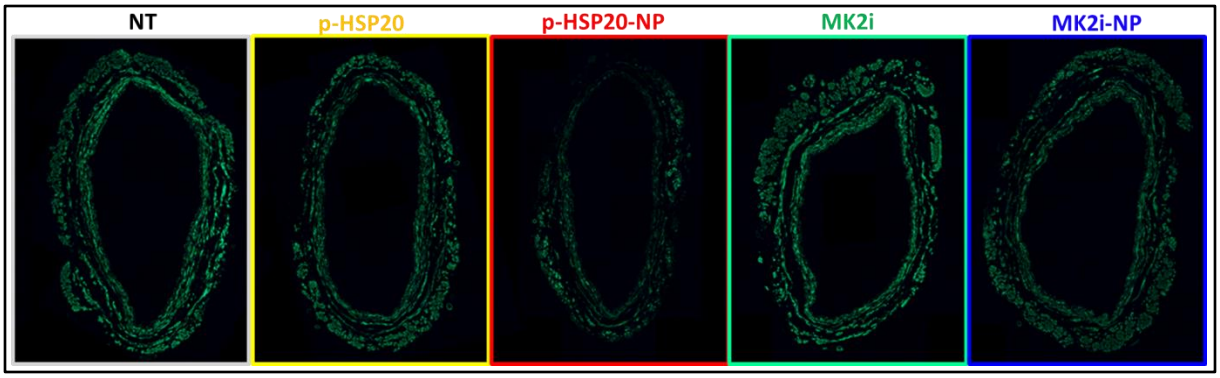

Figure 5.17 - MK2i-NP & p-HSP20-NP treatment inhibit stress fiber formation in human saphenous vein. F-actin visualization in Alexa-488 phalloidin stained cryosections of human saphenous vein explants pretreated and subsequently stimulated with ANG-II demonstrating decreased F-actin in samples treated with the NP formulations. Reprinted with permission from [1]. Copyright 2015 American Chemical Society.

Discussion

Biomacromolecular therapeutics, specifically therapeutic CPPs, show great promise for improving upon the lack of specificity, potency, and biocompatibility that characterize small molecule drugs. However, a number of delivery barriers exist that undermine the feasibility of their clinically translation. Thus, a significant unmet need exists to address the delivery barriers that therapeutic CPPs face. There are a large number of intracellular targets that can be effectively modulated with biomacromolecular therapeutics such as peptides, yet the barriers of uptake and endosomal entrapment have essentially rendered these targets 'undruggable.' As a result, this simple approach to increasing peptide uptake and facilitating endosomal escape opens a previously unexplored therapeutic space that harbors significant potential to improve treatment options for a broad spectrum of pathologies. Furthermore, the global pharmaceutical industry has faced prohibitive costs in the development new molecular entities; thus, the nano-polyplex technology presented herein befits the major transition that is occurring to shift focus onto the development of drug delivery systems that can improve extant therapeutics [133].

In addition to establishing a modular platform for cytosolic delivery of biomacromolecular therapeutics, these studies provide key insight into the role that MK2 and HSP20 play in regulating vascular tone by modulating cytoskeletal dynamics. The data presented herein verify the feasibility of this method and demonstrate a novel approach to the treatment, both prophylactic and salutary, of vasospasm. These results motivate further studies in animal models of vasospasm, for instance in an established rat model of subarachnoid hemorrhage induced symptomatic vasospasm [134] in which

MK2i-NPs or p-HSP20-NPs are used as preventative or interventional treatments with real time monitoring of cerebral perfusion using quantitative imaging methods. However, the use of this technology in intravascular applications raises the question of whether or not these NPs are hemocompatible and amenable to intravenous (**IV**) administration, as recent studies have shown that analogous polyplexes are not compatible with IV dosing due to aggregation and poor biodistribution [135]. Thus, future studies evaluating NP hemocompatibility and the investigation of alternative approaches to impart hemocompatibility to the NP formulations are required to expand the applicability of this platform technology to systemic delivery applications. Furthermore, considering that the MK2i and p-HSP20 peptides were modified with the same CPP sequence (i.e., YARAAARQARA) which begs the question of whether this approach is equally effective with other commonly used CPPs such as TAT, penetratin, oligoarginines, etc. Similarly, are other biomacromolecules such as nucleic acid based or protein/enzyme based therapeutics that are modified with cationic CPP sequences also amenable to this NP approach in addition to peptide based therapeutics? These questions motivate additional investigation of this approach to define the limitations of this platform technology in its current form and to guide future technology development and optimization.

Conclusion

A platform technology was developed for formulation of electrostatically-complexed nanoparticles that facilitate intracellular delivery and concomitantly increase the bioactivity of therapeutic peptides. Specifically, this platform was applied to deliver vasoactive peptides that modulate vascular tone by affecting actin dynamics in vascular smooth muscle cells. NP formulation enhanced the potency of both a MK2 inhibitory peptide and a phosphorylated HSP20 mimetic peptide, and the translatability of this delivery technology was demonstrated in human vascular tissue *ex vivo*. These results also validate and provide mechanistic insight into the role of actin dynamics in vascular smooth muscle physiology and highlight promising therapeutic targets for prevention of pathological vasoconstriction and enhancement of salutary vasorelaxation.

CHAPTER VI

CONCLUSION & FUTURE DIRECTIONS

Summation of presented work

The therapeutic potential of peptides has continually increased as a result of an ever expanding interest in biologically derived medical interventions: a simple search for literature relevant to the phrase 'therapeutic peptide' in the PubMed biomedical literature archive at the beginning of 2015 yields over 29,000 results. Peptides are especially attractive due to their increased specificity, biocompatibility, and solubility in contrast to small molecule drugs that dominate the current pharmaceutical market. Despite these advantages, there is a lack of effective delivery technologies that can circumvent the numerous anatomical and metabolic barriers present *in vivo* that limit intracellular delivery of peptides; peptides generally have short half-lives, suffer from proteolytic degradation, lack the ability to translocate the cell membrane, and have poor intracellular bioavailability due to entrapment within the degradative/recycling vesicles of the endo-lysosomal trafficking pathways [5-8]. Approaches previously explored to overcome these barriers have included altering peptide chemistry to improve proteolytic resistance and in vivo half-life [9-11] and use of electroporation or cell-penetrant/fusogenic peptides to increase cellular internalization [12-14]. The development of colloidal drug carriers such as liposomes, micelles, and nanoparticles for delivery of biomacromolecular therapeutics has also increased dramatically in the past decade [15-17]. Despite these advances, there are no examples of nanocarrier formulations for intracellular peptide delivery that have been simple, robust, and scalable enough to justify translation for clinical use. Thus, the goal of this work was to develop a simple, generalizable peptide drug delivery nano-formulation to enhance the cellular uptake, endosomal escape, intracellular retention, and bioactivity of therapeutic peptides.

The nano-polyplex platform technology that was developed for this purpose met all of these criteria and the translatability of this approach was demonstrated through the ability of an NP formulation containing an MK2 inhibitory peptide to inhibit the multifactorial pathogenesis of intimal hyperplasia in human tissue *ex vivo* and *in vivo* in a rabbit vein graft model. Furthermore, the modular

nature of this platform was demonstrated by the enhanced cytosolic delivery and therapeutic efficacy of two vasoactive peptides that were incorporated into optimized NP formulations targeted towards vasospasm. These results establish the feasibility and promise of this NP approach, but they also raise a plethora of questions that motivate further research:

- What is the specific interaction responsible for increased uptake of NP formulations? How does NP formulation alter intracellular trafficking following internalization?
- How does MK2 inhibition, specifically mediated through NP formulation of an MK2 inhibitory peptide, modulate vascular smooth muscle cell phenotype? What are the underlying molecular mechanisms and signaling pathways involved, and what are the temporal dynamics underlying these changes in the context of vein graft remodeling? How does MK2i formulation into NPs affect the entire transcriptome of VSMCs and are there off target effects?
- How does MK2 inhibition and MK2i delivery in an NP formulation affect endothelial function in vein graft remodeling? How is intercellular signaling between distinct vascular populations affected in the context of MK2 inhibition?
- How can treatment penetration into the vessel wall be improved when topically administering MK2i-NPs *ex vivo*?
- What are the pharmacokinetics and pharmacodynamics of MK2i-NPs *in vivo*?
- Are other CPP sequences and biomacromolecular drug such as DNA, siRNA, miRNA, proteins, and enzymes that are modified with cationic CPPs equally amenable to NP formulation and do they result in increases in uptake, retention, and bioactivity consistent with the data presented here?
- Are NPs hemocompatible (i.e., IV administerable) and, if not, can we alter their structure and/or composition to impart hemocompatibility?
- Can we further improve the biocompatibility of NPs by altering their structure and/or composition?
- Can MK2i-NPs and/or p-HSP-20 NPs effective prevent/treat SAH induced symptomatic vasospasm *in vivo*?
- Can we improve the synthesis of NPs and is their synthesis scalable? Can we alter their production to increase reproducibility, homogeneity, and yield?

Future Directions

Elucidation of MK2i-NP uptake mechanisms and subsequent intracellular trafficking

It is well established that facilitating endosomal escape of biomacromolecular therapeutics with intracellular targets enhances bioactivity by increasing cytoplasmic bioavailability and circumventing lysosomal degradation and/or exocytosis out of the cell [7, 58, 94, 136]. However, formulation of a CPP based therapeutic peptide into a nanoparticle can significantly alter cellular uptake kinetics and can alter the underlying mechanisms of uptake [84, 137-139]. The MK2i CPP chosen for this study is cationic in nature, whereas formulation into a NP results in a negative surface charge as shown by DLS results ($\zeta \sim$ -12 mV for MK2i-NPs at a CR = 1:3). A number of studies have demonstrated that the surface charge significantly affects the uptake and trafficking of therapeutic nanoparticles [140, 141], and, as a result, formulation of cationic CPP-based peptides, such as MK2i, into an anionic nanoparticle formulation is anticipated to have a significant effect on cellular uptake and trafficking. A number of approaches can be utilized to investigate uptake mechanisms, including uptake inhibition studies (**table 6.1**) and ultrastructural analysis of cellular organelles during uptake through electron microscopy.

Tools to Investigate Cellular Internalization		
Name	**Use**	**Mechanism**
Amiloride	Inhibits macropinocytotsis	Inhibits Na^+/H^+ ion transport [8]
Chondroitin Sulfate A/B (CSA/CSB)	Competitive binding to chondroitin sulfate	Competitvely inhibitis binding to chondrotin sulfate on the cell surface[8]
Colchicine	Inhibit microtubule polymerization / destabilize microtubules	Plant metabolite that binds to tubilin, preventing microtubule polymerization[8]
Cytochalasin D	Inhibit macro pinicytosis/phagocytosis	Inhibits actin polymerization; clathrin- and caveolae-mediated pathways have recently been shown to require actin for formation and invagination of both coated pits and caveosomes[142]
Dynasore	Inhibit clathrin-mediated endocytosis	Inhibits dynamin-GTPase [142]
Genistein	Inhibit caveolae-mediated endocytosis	Inhibits natural isoflavone tyrosine kinase [142]
Heparin	Competitive binding to Heparin sulfate	Competitvely inhibitis binding to Heparin sulfate on the cell surface[143]
Ionomycin	Macropinocytotic regurgitation	Calcium ionophore that raises intracellular calcium levels[8]
Methyl-beta-cyclodextrin (MβCD)	May inhibit both clathrin- and caveolae-mediated pathway	Cyclic heptasaccharide that sequesters and alters cholesterol-rich domains within the plasma membrane[144]
Dextran sulfate	competes with modified LDL for scavenger receptor mediated uptake	The negative charge associated with dextran sulfate causes uptake through scavenger receptors responsible for LDL internalization[145]
polyinosine/polyinosinic acid	Competitively binds to SR-A	Immunostimulant known to interact with toll like receptor 3[146]
low density lipoprotein (LDL)	Competitvely binds to SR-B and CD36 scavenger receptors	Lipoprotein known to be internalized by various scavenger receptors[147]

Table 6.1 - Summary of various cellular uptake inhibitors and their function.

To this end, preliminary uptake inhibition studies were performed in HCAVSMCs inhibited with either 50 μM amiloride (macropinocytosis inhibitor), 50 μM Dynasore (clathrin-mediated endocytosis inhibitor), or 5 mM methyl-β cyclodextrin (inhibitor of lipid raft mediated endocytosis, both clathrin- and caveolae-mediated). Every treatment group demonstrated inhibition of uptake for all inhibitors tested, indicating that multiple endocytic routes are involved in cellular uptake (**fig. 6.1**). However, only MK2i-NPs were significantly inhibited by pre-treatment with amiloride, indicating that macropincytosis plays a significant role in MK2i-NP uptake but not in NE-MK2i-NP or MK2i uptake. Both Dynasore and MβCD also significantly inhibited MK2i-NP uptake, and it has been shown that Dynasore can also inhibit macropinocytosis under certain circumstances [148].

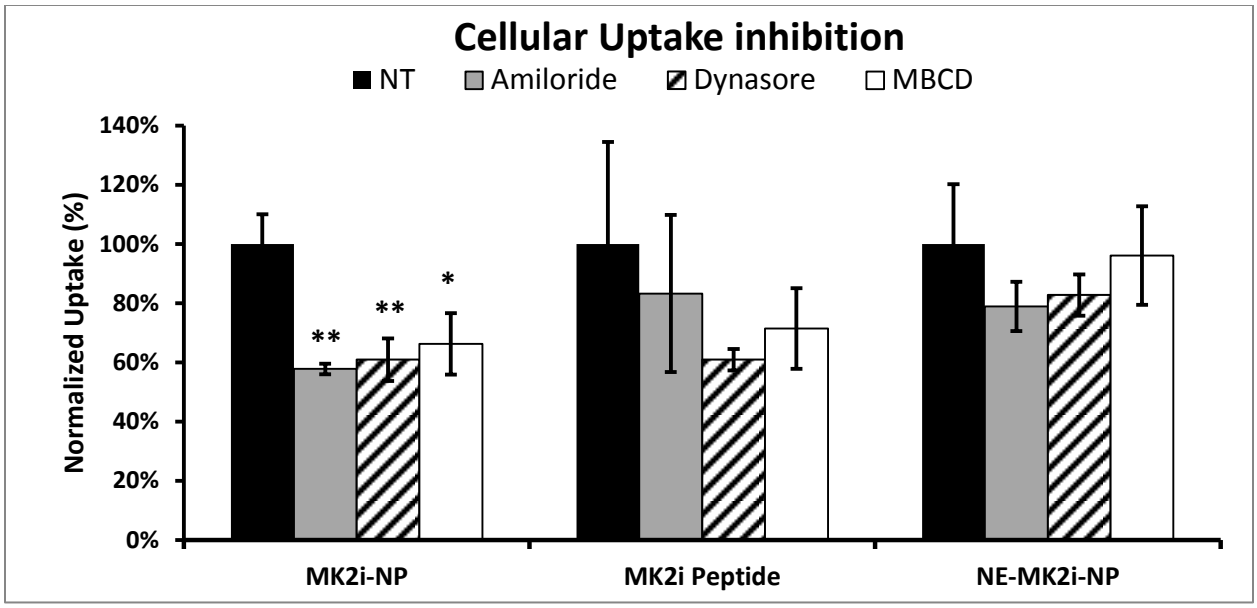

Figure 6.1 – MK2i-NP uptake inhibition. HCAVSMCs were either pre-treated for 30 minutes with either 50 µM Amiloride, 50 µM Dynasore, or 5 mM MβCD and subsequently treated with MK2i-NPs, NE-MK2i-NPs, or MK2i peptide. *P<0.05, **p<0.01 vs. NT in the same treatment group.

Furthermore, preliminary TEM analysis of HCAVSMCs treated for 10 minutes with MK2i-NPs or free MK2i peptide demonstrated vesicular morphologies consistent with those seen in fluorescence microscopy and in agreement with results from uptake inhibition studies, with MK2i-NP treated cells demonstrating large invaginations indicative of macropinocytosis (vesicles 250 nm- 1µm in diameter, **fig. 6.2 A-D**), whereas HCAVSMCs treated with free peptide showed much smaller vesicles indicative of endocytosis (25-100 nm, **fig. 6.2 D**).

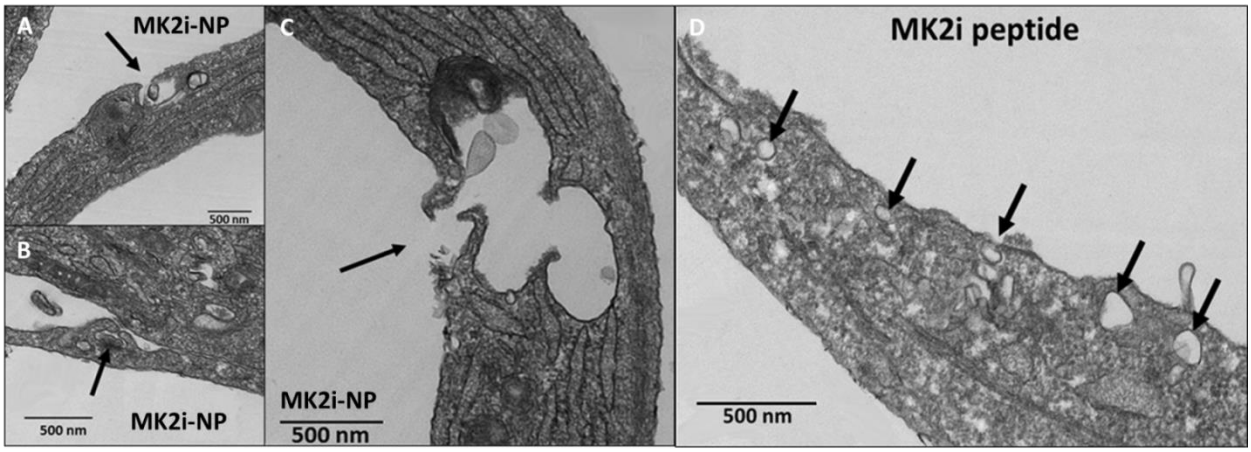

Figure 6.2 – TEM analysis of MK2i-NP uptake. Representative TEM images of A-C) MK2i-NP and D) MK2i peptide uptake in HCAVSMCs.

Future studies looking at a wider range of uptake inhibitors and the utilization of MK2i-labeling (e.g., with gold or some other contrast agent for electron microscopy) for electron microscopy mediated visualization of MK2i localization in cellular organelles will provide further insight into the mechanism of MK2i-NP uptake. Furthermore, microscopic analysis of fluorescently labeled MK2i-NP uptake in conjunction with cells transfected with plasmids coding for protein markers of various trafficking pathways (e.g., markers of early endosomes, late endosomes, lysosomes, golgi, etc.) will further elucidate the changes in MK2i intracellular trafficking following internalization.

Investigation of MK2i-NP mediated modulation of vascular smooth muscle cell phenotype

MK2 is activated downstream of p38 MAPK and is implicated as a key effector of the pro-inflammatory, migratory VSMC phenotype that characterizes IH. Phosphorylated MK2 translocates from the nucleus to the cytosol [37] where it activates a number of downstream effector and regulatory proteins that induce an inflammatory response, vasoconstriction, and pathological VSMC proliferation, migration, and excess ECM production [56, 124]. Vasoconstriction and migration are primarily mediated through MK2 phosphorylation of LIM-K and HSP 27: LIM-K phosphorylates and inactives members of the ADF/cofilin family of actin filament severing proteins resulting in stabilization of F-actin stress fibers [76, 79], whereas phosphorylation of HSP27 results in relocalization from the tip of actin filaments to the cell surface, allowing for actin polymerization. Pro-inflammatory effects of MK2 are primarily a result of downstream phosphorylation of the post-transcriptional gene regulators heterogeneous nuclear ribonucleoprotein A0 (**hnRNP A0**) and tristetraprolin (**TTP**), which modulates their interactions with AU-rich regions of mRNA, leads to stabilization and enhanced expression of inflammatory cytokine mRNAs such as MIP-2, TNF-α and IL-6 [149-151].As a result, inhibition of MK2 activation should significantly curtail the transition of VSMC to a pathological phenotype. In order to further understand how inhibition of MK2 modulates vascular smooth muscle cell phenotype, future studies looking at changes in expression levels of phenotypic markers in treated human vascular tissue over time, either through immunohistochemical or western blot analysis, will provide further insight into the temporal dynamics of phenotypic changes. Furthermore, investigation of the underlying signaling responsible for these changes

through analysis of the vascular smooth muscle cell transcriptome will further elucidate the molecular level regulation of vascular smooth muscle cell phenotype.

Further investigation of MK2i-NPs as a prophylactic treatment to prevent vein graft failure

In vivo data from a rabbit vein graft model demonstrate that MK2i-NP treatment significantly inhibits intimal hyperplasia. However, *ex vivo* uptake studies in viable human vascular tissue demonstrated uptake that was predominantly concentrated on the luminal and adventitial surfaces of the vessel indicating that endothelial cells also internalize a significant amount of MK2i-NPs. This heterogeneous uptake raises several issues: 1) What are the effects of MK2 inhibition on endothelial function during vein graft remodeling? 2) How does intercellular juxtacrine signaling between endothelial and vascular smooth muscle cells affect vein graft remodeling? 3) How can we increase penetration of the treatment into the vessel wall to provide a more homogenous treatment distribution through the target tissue? As mentioned in the conclusion of chapter 4, techniques such as laser capture microdissection could potentially be utilized to more specifically investigate the effects of MK2 inhibition on endothelial cells during vein graft remodeling. Furthermore, techniques such as pressure seeding the MK2i-NP treatment into the vessel wall using a multi-stage balloon catheter (e.g., using the Occlusion Perfusion Catheter developed by Advanced Catheter Therapeutics) could potentially increase treatment penetration into the vessel wall and further improve vascular graft patency.

MK2i-NP treatment appeared to significantly extend the duration of therapeutic efficacy of the MK2i peptide which motivates further investigation of the *in vivo* pharmacokinetics and pharmacodynamics of MK2i-NP treatment. Studies utilizing radiolabeled MK2i can be utilized to elucidate *in vivo* pharmacokinetics and gene expression analysis of treated tissue over time can be used to further elucidate *in vivo* pharmacodynamics. These studies would provide valuable insight into the ability of NP formulation to extend the therapeutic half-life of peptide based therapeutics and would further bolster the feasibility and translatability of MK2i-NPs as a prophylactic treatment to prevent adverse vein graft remodeling and improve vein graft patency.

Applicability of NP formulation to other cell penetrating peptides and biomacromolecular therapeutics

Considering that the studies using the MK2i- and p-HSP20-NP formulations utilized that peptides were modified with the same CPP sequence (i.e., YARAAARQARA) motivates investigation of the feasibility of this approach to other CPP sequences that are commonly conjugated to peptides and other biologic drugs to increase uptake. To this end, preliminary proof of concept studies using two proapoptotic peptides with potential for antineoplastic applications were undertaken (**table 6.2**)

Peptide	Sequence	MW	Function
R3-RN22	RRRKFVRSRRPRTASCALAFVN	2648.17	p19ARF tumor suppressor mimetic
Penetratin-Bak-BH3	RQIKIWFQNRRMKWKKMG QVGRQLAIIGDDINRRY	4404.28	Bak-derived Bcl-2 homology 3 domain

Table 6.2 - Pro-apoptotic peptides for NP formulation. The pro-apoptotic peptides R3-RN22 and Penetratin-Bak-BH3 for proofs of concept for the nanopolyplex platform. Red amino acid abbreviations indicate the presence of polar amino groups in the amino acid side chain that potentiate electrostatic interaction with PPAA: R (arginine), K (lysine) - primary amines (strong base); N (asparagine), Q (glutamine) - amides (weak bases).

The Penetratin- (i.e., antennapedia) Bak-BH3 fusion peptide was purchased from Anaspec (As-62262) and the p19 ARF tumor suppressor mimetic peptide was kindly gifted by Dr. Stephen R. Hann's cell and developmental biology laboratory at Vanderbilt University. Both oligoargnines and penetratin (which is derived from the homeodomain of the *Drosophila* transcription factor antennapedia) are commonly used CPP sequences to increase the uptake of biologics and nanoparticles. DLS analysis and TEM imaging studies were used to assess the size and zeta potential of RN22 nano-polyplexes (**RN22-NPs, fig. 6.3**) and Penetratin-Bak-BH3 nano-polyplexes (**BH3-NPs, fig. 6.4**). An optimal CR of 1:3 was chosen for each NP formulation and zeta potential was found to be directly proportional to CR in all cases. Interestingly, this charge ratio was identical to the optimal CR for the MK2i-NP formulation, possibly indicating that a CR of 1:3 may be an optimal CR for a wide array of NP formulations regardless of peptide and CPP identity. These results indicate that this NP approach is applicable to other CPP sequences and further supports that this modular technology can serve as a platform for intracellular peptide delivery. However, it has yet to be demonstrated whether these proapoptotic NP formulations increase peptide uptake, retention, and bioactivity which motivates further *in vitro* investigation of other NPs formulated with peptides for various applications. In addition, it has yet to be demonstrated that non peptide-based

biomacromolecular therapeutics such as nucleic acids and proteins or enzymes that are modified with cationic CPPs are also amenable to this NP approach. Future studies looking at NP formulations utilizing CPP modified DNA, RNA, PNA, proteins, and/or enzymes will provide further insight into the broad applicability and potential limitations of nano-polyplex formulation of biomacromolecular therapeutics.

A

NH2:COOH	Z-ave diameter (nm)	PDI
10 to 1	27180 ± 25330 nm	1
5 to 1	1335 ± 94.78 nm	0.483
4 to 1	730.8 ± 821.2 nm*	0.656
3 to 1	11750 ± 6316 nm	1
2 to 1	3604 ± 1559 nm	0.567
1 to 1	10990 ± 3748 nm	1
1 to 2	660.5 ± 54.13 nm	0.242
1 to 3	155.4 ± 14.65 nm	0.251
1 to 4	193.0 ± 46.75 nm*	0.313
1 to 5	392.5 ± 91.81 nm*	0.458
1 to 10	261.8 ± 35.51 nm*	0.583

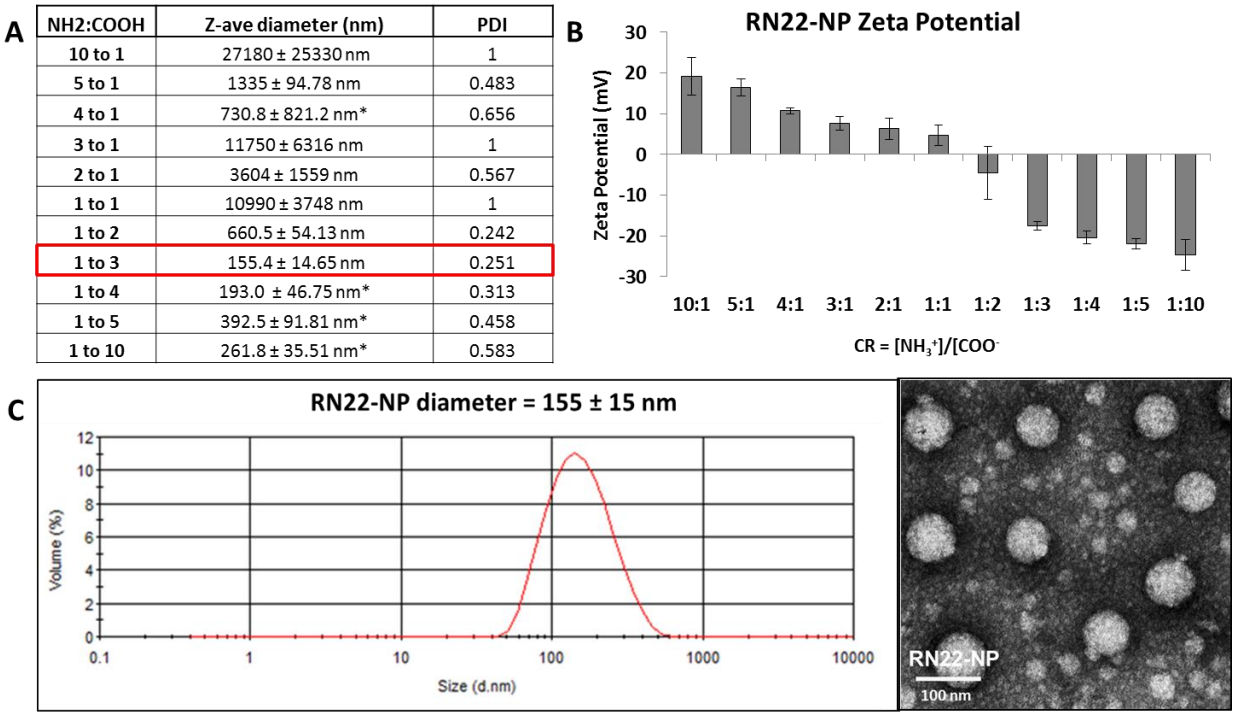

Figure 6.3 – RN22-NP formulation. A) Size summary of RN22-NP library. Asterisks (*) indicate multimodal size distributions (multiple peaks present). The red box indicates the optimized formulation chosen for further study. **B)** Zeta potential of RN22-NP formulations. **C)** Representative size distributions and TEM image of RN22-NPs.

A

NH2:COOH	Z-ave diameter (nm)	PDI
10 to 1	3255 ± 1413	0.761
5 to 1	7809 ± 4860*	0.753
4 to 1	4554 ± 1662	0.958
3 to 1	5024 ± 2651	0.794
2 to 1	3888 ± 200*	0.803
1 to 1	1955 ± 929.7	0.452
1 to 2	230.8 ± 35.82	0.432
1 to 3	159.8 ± 9.405	0.298
1 to 4	197.6 ± 12.99*	0.465
1 to 5	202.9 ± 47.63*	0.784
1 to 10	1352 ± 798.5*	0.647

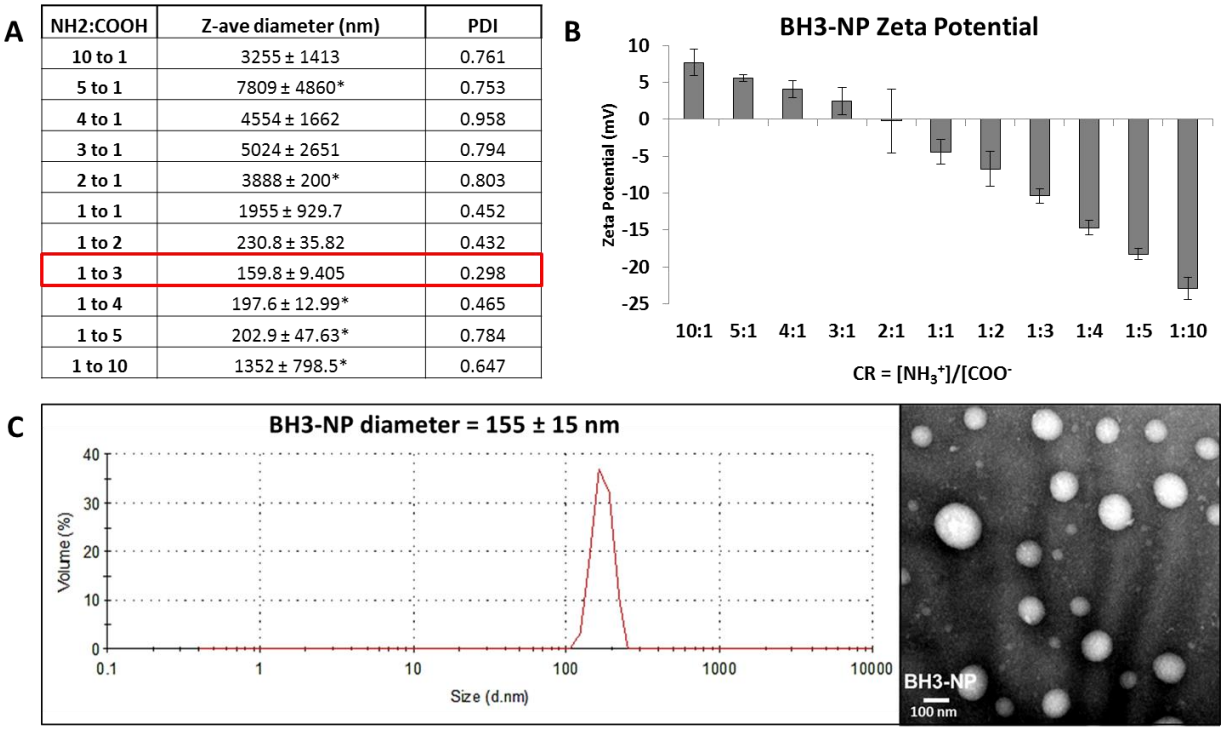

Figure 6.4 – BH3-NP formulation. A) Size summary of BH3-NP library. Asterisks (*) indicate multimodal size distributions (multiple peaks present). The red box indicates the optimized formulation chosen for further study. **B)** Zeta potential of BH3-NP formulations. **C)** Representative size distributions and TEM image of BH3-NPs.

Development of NPs for treatment of vasospasm

Preliminary results indicate that NP formulation incorporating the vasoactive peptides MK2i and p-HSP20 can effectively inhibit vasoconstriction and enhance NO-mediated vasorelaxation indicating that these formulations are a promising approach to treat vasospasm. Preliminary studies utilizing this approach in an established noncraniotomy *in vivo* rat model of subarachnoid hemorrhage induced vasospasm [134] are currently underway. This model utilizes a suture to perforate the bifurcation of the internal and ascending carotid artery to induce a brain hemorrhage, and the resulting changes in blood flow can be visualized

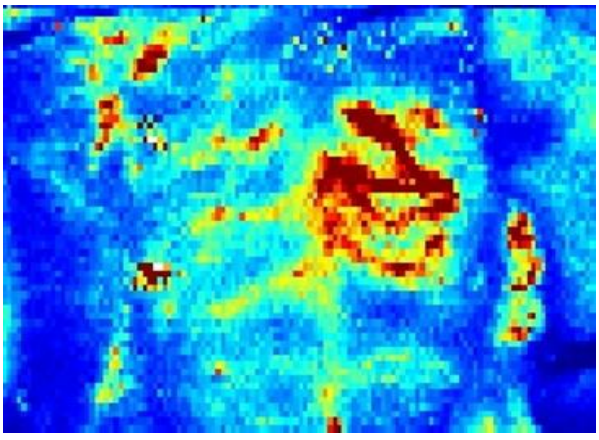

Figure 6.4 – LDPI image of cerebral perfusion in a rat. The bring portion on the right of the image corresponds to the section of the skull that was shaved down to facilitate vascular imaging.

through the use of laser doppler perfusion imaging (**LDPI**) applied to a shaved down section of the rat skull (**fig. 6.4**). Utilizing NP treatment in conjunction with this quantitative imaging technique will further elucidate the ability of MK2i- and p-HSP20-NP formulations to prevent and treat symptomatic vasospasm following subarachnoid hemorrhage.

Approaches to improving NP hemocompatibility and biocompatibility

Considering that NP treatment for vasospasm applications would likely require intravascular administration, the hemocompatibility of these NP formulations becomes a key issue. Recent studies have shown that analogous polyplexes are not compatible with IV dosing due to aggregation and poor biodistribution [135]. Thus, approaches to alter NP structure and composition must be considered to improve hemocompatibility. One promising approach is altering the NP structure to be composed of polymeric nanogels (i.e., crosslinked nanoparticles). In contrast to electrostatically complexed linear polymers, this approach would significantly increase the colloidal stability of the NPs. Furthermore, by altering the composition to incorporate hydrophilic 'stealth' polymers that are resistant to opsonization, such as poly(ethylene glycol) or poly(hydroxypropyl methacrylate) the hemocompatibility and biocompatibility of the NP formulations can be further increased. However, altering the composition and structure of the NPs may have deleterious effects on uptake and bioactivity, so extensive *in vitro* characterization of these alternative NPs would be required to verify that they retain their desired functionality.

Development of improved and scalable NP synthesis methods

Although mixing of a polymer and peptide for NP formulation provides a simple approach to NP formulation, improving upon the reproducibility and increasing the scale of NP synthesis would be required in order to translate this NP approach into clinical use. In the past decade the use of microfluidic mixing devices, or micro-mixers, has substantially increased a promising approach to improve nanoparticle synthesis [152-157]. To this end, a tangential spin micromixer that utilizing impinging vortex mixing streams has been developed to yield a reproducible method for the synthesis of monodisperse NPs through flash nano-complexation (**fig. 6.5**).

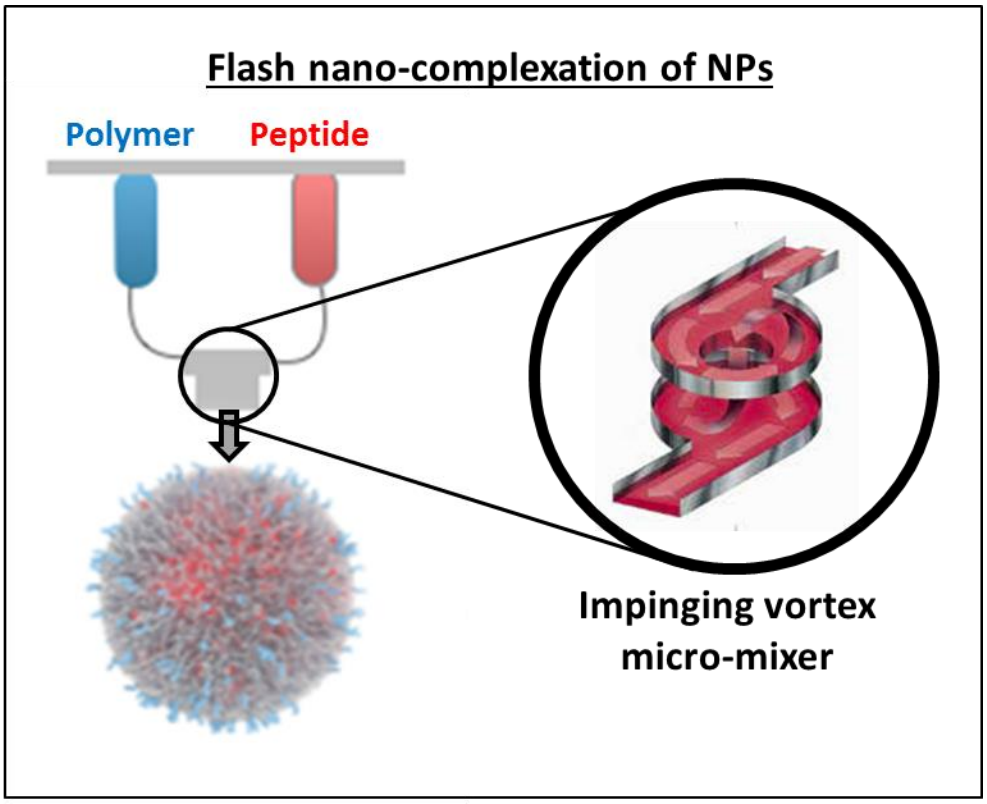

Figure 6.5 – Tangential spin micro-mixer for flash nano-complexation of nano-polyplexes. The micromixer is designed so that individual solutions of the polymer and peptide are injected through a microfluidic mixing reactor that results in the mixing of impinging vortices of each solution rotating in opposite directions, thereby decreasing mixing time and improving nano-polyplex synthesis.

By modulating the flow rates of each solution being injected via syringe pump the resulting Reynolds number and mixing conditions can be fine-tuned to modulate the size and polydispersity of the resulting nano-polyplexes. In fact, preliminary data indicates that we can reduce NP size and increase the reproducibility of NP synthesis utilizing this method (**fig. 6.6**). Thus, the use of a micromixer system to facilitate flash nano-complexation represents a promising approach to improving the reproducibility and scalability of NP synthesis for clinical translation. Investigation of whether this method of NP synthesis can be adapted to a hand-held dual-syringe device with a mixing nozzle will further bolster the translatability of this platform technology to improve therapeutic biomacromolecular delivery. Moreover, the use of a spray dryer to formulated inhalable NP formulations would further broaden the applicability of this approach to include therapies targeted for pulmonary delivery, motivating investigation of NP synthesis methods in addition to flash nanocomplexation.

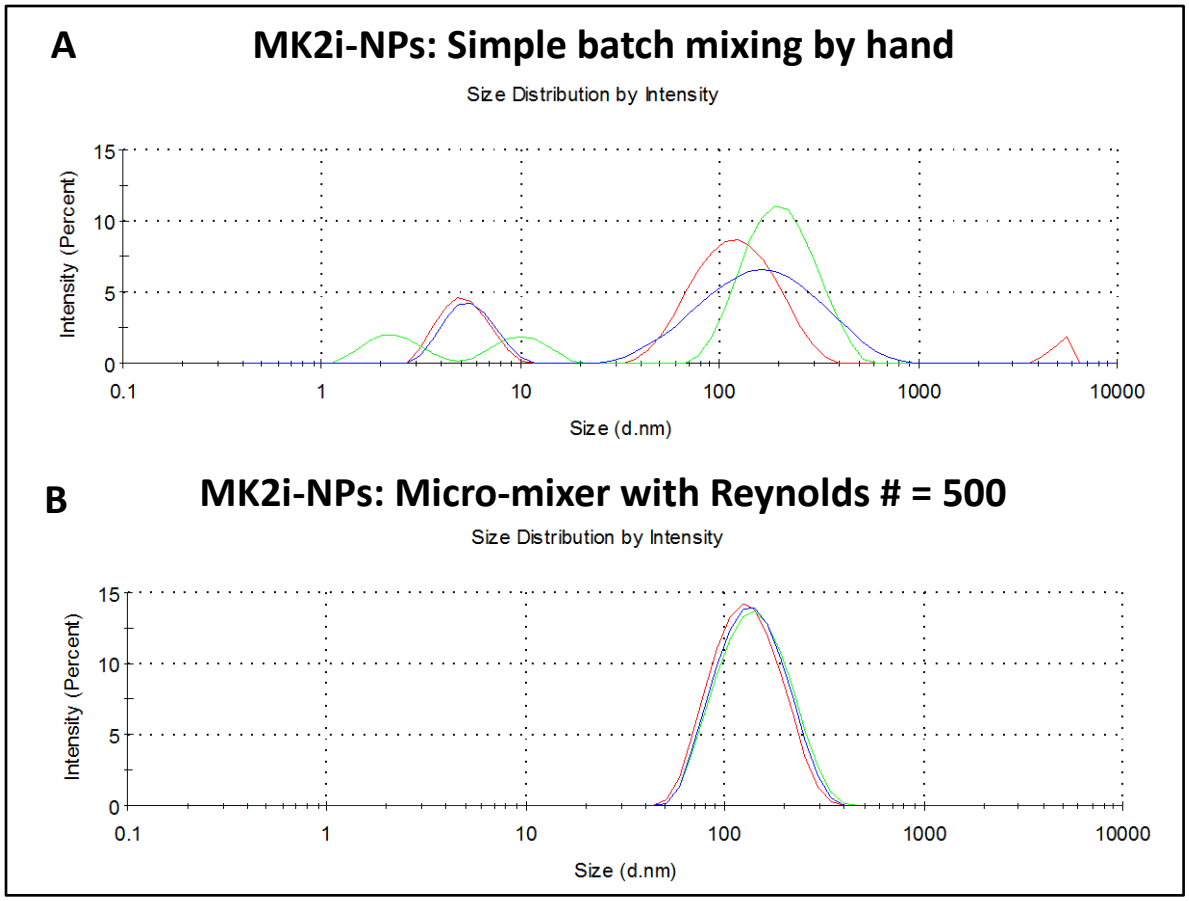

Figure 6.6 – Comparison of NP synthesis methods. (A) DLS size analysis of three separate batches of MK2i-NPs prepared by simple batch mixing with a benchtop pipette demonstrating inconsistent NP formation. **(B)** DLS size analysis of three separate batches of MK2i-NPs prepared by a tangential spin micromixer operating at a Reynolds number of 500 demonstrating improved reproducibility and decreased polydispersity.

Appendix A: List of publications

1. Li H, Nelson CE, **Evans BC**, Duvall CL. *Delivery of intracellular-acting biologics in pro-apoptotic therapies.* Curr Pharm Des. 2011; 17(3): 293-319. Review. http://www.ncbi.nlm.nih.gov/pubmed/21348831
2. **Evans, B.C**, Nelson, C.E, Yu, S.S., Kim, A.J, Li, H., Nelson, H.M, Giorgio, T.D, Duvall, C.L *Ex Vivo Red Blood Cell Hemolysis Assay For The Evaluation Of PH-responsive Endosomolytic Agents For Cytosolic Delivery Of Biomacromolecular Drugs*. J. Vis. Exp. 2013 Mar 9;(73):e50166. doi: 10.3791/50166. http://www.ncbi.nlm.nih.gov/pubmed/23524982
3. Wikswo JP, Curtis EL, Eagleton ZE, **Evans BC**, Kole A, Hofmeister LH, Matloff WJ. *Scaling and Systems Biology for Integrating Multiple Organs-on-a-Chip.* Lab on a Chip. 2013 Sep 21;13(18):3496-511. doi: 10.1039/c3lc50243k. http://www.ncbi.nlm.nih.gov/pubmed/23828456
4. **Evans BC**, Hocking KM, Osgood MJ, Voskresensky I, Dmowska J, Kilchrist KV, Brophy CM, Duvall CL. *Nano-polyplex MK2 inhibitory peptide delivery Inhibits Vascular Graft Intimal Hyperplasia.* Science Translational Medicine. Accepted with minor revisions.
5. **Evans BC**, Hocking KM, Kilchrist KV, Wise ES, Brophy CM, Duvall CL**.** *An Endosomolytic Nano-polyplex Platform Technology for Cytosolic Peptide Delivery Applied to Pathological Vasoconstriction.* ACS Nano. Accepted with minor revisions.
6. **Evans BC**, Page JM, Guelcher SA, Duvall CL. *Hydrophobic Drug Loading and Release from Micelles based on Hydrolytically Degradable, pH-Responsive Monomers.* MS in preparation.

Appendix B: Delivery of Intracellular-Acting Biologics in Pro-apoptotic Therapies

Published in final edited form as:
Curr Pharm Des. 2011 ; 17(3): 293–319.

Delivery of Intracellular-acting Biologics in Pro-Apoptotic Therapies

Hongmei Li[*,1], Chris E. Nelson[*,1], Brian C. Evans[*,1], and Craig L. Duvall[#,1]
[1]Department of Biomedical Engineering, Vanderbilt University, 2201 West End Ave. Nashville, TN 37235; USA

Abstract

The recent elucidation of molecular regulators of apoptosis and their roles in cellular oncogenesis has motivated the development of biomacromolecular anticancer therapeutics that can activate intracellular apoptotic signaling pathways. Pharmaceutical scientists have employed a variety of classes of biologics toward this goal, including antisense oligodeoxynucleotides, small interfering RNA, proteins, antibodies, and peptides. However, stability in the in vivo environment, tumor-specific biodistribution, cell internalization, and localization to the intracellular microenvironment where the targeted molecule is localized pose significant challenges that limit the ability to directly apply intracellular-acting, pro-apoptotic biologics for therapeutic use. Thus, approaches to improve the pharmaceutical properties of therapeutic biomacromolecules are of great significance and have included chemically modifying the bioactive molecule itself or formulation with auxiliary compounds. Recently, promising advances in delivery of pro-apoptotic biomacromolecular agents have been made using tools such as peptide "stapling", cell penetrating peptides, fusogenic peptides, liposomes, nanoparticles, smart polymers, and synergistic combinations of these components. This review will discuss the molecular mediators of cellular apoptosis, the respective mechanisms by which these mediators are dysregulated in cellular oncogenesis, the history and development of both nucleic-acid and amino-acid based drugs, and techniques to achieve intracellular delivery of these biologics. Finally, recent applications where pro-apoptotic functionality has been achieved through delivery of intracellular-acting biomacromolecular drugs will be highlighted.

Keywords

biomacromolecular drug; apoptosis; intracellular delivery; RNA interference; siRNA; peptide drug; endosome escape; delivery barriers

1. Introduction

Traditionally, cancer treatments have utilized relatively crude techniques such as surgical resection, chemotherapy, and radiation. These approaches can suffer from multiple shortcomings including incomplete eradication of the cancer, emergence of treatment-resistant cell phenotypes, and undesirable side-effects on healthy tissues. One of the basic paradigms of tumorigenesis is that cells that become defective or damaged are able to survive and grow in an abnormal, uncontrolled manner rather than succumbing to built-in programmed death pathways. An improved understanding of the signaling pathways

[#]**Author to whom all correspondence should be addressed:** PMB 351631, 2301 Vanderbilt Place, Nashville, TN 37235-1631, craig.duvall@vanderbilt.edu, office phone: (615)322-3598, fax: (615)343-7919.
[*]equally contributing co-authors

responsible for tumor cell evasion of apoptosis combined with recent technological advances in the engineering of molecularly-targeted drugs will potentially revolutionize cancer therapies by enabling the rational design of specialized therapeutics that target cancer-specific phenomena. These advances could lead to cancer-specific, if not patient-specific, therapeutics tailored to directly combat the aberrant, tumorigenic molecules responsible for diverse neoplastic phenotypes.

The ability to more rationally design pro-apoptotic therapeutics for cancer is strongly dependent upon robust knockdown or inhibition of targeted molecules with great affinity and specificity. Synthetic small molecule drugs are the traditional approach for pharmacological inhibition, but synthesis and screening of prospective compounds is a long and tedious process and often yields products with suboptimal target specificity and/or pharmacokinetic profiles. In the normal, healthy cell, numerous levels of negative feedback exist for regulating molecular activities, including contributors at both post-transcriptional and post-translational levels. It may be ideal to utilize or mimic these “natural” mechanisms in the cell through delivery of therapeutics made from the same biologic building blocks (nucleic and amino acids) as the regulatory molecules endogenously present. For example, if exogenous doublestranded RNA with an antisense strand complementary to a target mRNA is delivered, it can commandeer the evolutionarily-conserved intracellular machinery in the cell to achieve sequence-specific gene silencing [1]. Alternatively, naturally-occurring protein antagonists or abbreviated peptide fragments containing their active sequences can be exogenously delivered to bolster the bioactive, intracellular pool of the antagonist, which may be functionally depleted (i.e., not present or mutated) in certain cancers.

Biomimetic, nucleic acid- or amino acid-based drugs clearly have the potential to be therapeutically applied to alter intracellular apoptotic signaling pathways. However, delivery can be a challenge, especially for intracellularacting macromolecules, because they are generally not able to cross cellular membranes. This delivery barrier can have negative effects both on cellular internalization and on escape from intracellular vesicles (i.e., endosomes) that inhibit access to the microenvironment (i.e., cytosol or mitochondria) where the molecular target is localized. For this reason, extracellular-acting molecules represent the largest sector of biologics currently used in the pharmaceutical industry. For example, biotechnological development of monoclonal antibody drugs is a strong and rapidly expanding field. Recent reviews indicate that there are at least 22 FDA-approved therapeutic monoclonal antibodies and hundreds more in the pipeline, with anticancer agents like Herceptin (trastuzumab), Rituxan (rituximab), and Avastin (bevacizumab) leading the way [2, 3]. This recent surge in biological drug development can be used as a precedent to indicate that establishing the basic infrastructure necessary for the manufacture of biologic drugs is feasible. Pro-apoptotic, RNA-based antisense drugs have also been extensively tested in clinical trials for multiple cancer types including melanomas, leukemias, lymphomas, gastroesophogeal carcinoma, and prostate cancer [4–9]. Although a distinct therapeutic advantage for use of antisense drugs has not been unequivocally proven at this point, the volume of trials in this area provide added optimism that intracellular-acting biologics can be feasibly developed for clinical use.

Overall, the accrual of new knowledge by cancer biologists to elucidate the molecular underpinnings of cancers has outpaced the rate at which pharmaceutical scientists and engineers have developed technologies that capitalize on this information clinically. Broadly-applicable platform technologies that confer the ability to efficiently deliver protein and RNA-based drugs intracellularly may be the key link to opening up a fertile new world of druggable targets that enable better clinical translation of new findings in cancer biology. Herein, the current molecular understanding of both the intrinsic (mitochondrial) and extrinsic (death receptor) apoptosis pathways is reviewed. Subsequently, delivery barriers of

intracellular-acting biomacromolecular apoptotic agents and a survey of the current pharmaceutical and biomaterial technologies that can be employed to overcome these barriers is discussed. Finally, a survey of recent pro-apoptotic therapeutic applications employing intracellular-acting biologic drugs, including the delivery techniques used and the molecular targets pursued, is presented.

2. Apoptosis

Apoptosis is a normal physiological process that occurs both in the homeostatic maintenance of adult tissues and during embryonic development. Apoptotic cells undergo a characteristic set of prominent morphological changes including alteration in cellular shape, nuclear and cytoplasmic condensation, and cellular fragmentation [10]. Eventually, apoptotic fragments of these cells are removed by phagocytes, and cytoplasmic leakage (i.e., necrosis) is avoided. Apoptosis can be triggered through both extrinsic and intrinsic pathways, where the extrinsic pathway is mediated by transmembrane death receptors, and the intrinsic pathway is triggered by a variety of factors [11] including environmental stress (e.g. hypoxia and reactive oxygen species), growth factor withdrawal [12], chemotherapy [13], and radiation [14]. These pathways converge at the level of activation of caspases, which are intracellular proteases that serve as the "executioners" of apoptosis [15, 16]. Under normal circumstances, caspase activation is primarily controlled by the B cell lymphoma 2 (Bcl-2) family of proteins, which provides upstream regulation of mitochondrial membrane potential [17, 18]. Importantly, mutations that lead to cancerous apoptotic resistance typically leave the intrinsic machinery intact, allowing it to be harnessed therapeutically [19].

2.1 Extrinsic Apoptosis Pathway

The extrinsic apoptotic pathway is regulated by members of the tumor necrosis factor (TNF) receptor superfamily known as death receptors (see Fig. 1). This group of transmembrane death receptors includes Fas (CD95/Apo-1) and the TNF-related apoptosis inducing ligand (TRAIL) receptors TRAIL-R1 (DR4) and TRAIL-R2 (DR5) [20]. The Fas and TRAIL receptors are activated by the Fas ligand (FasL) and TRAIL, respectively, and these events result in the clustering of death receptors and the recruitment of the Fas-associated death domain (FADD) molecule [21]. In the case of TRAIL receptor activation, the recruited FADD molecule contains an effector region that catalyzes the caspase cascade by binding and activating caspase-8 and caspase-10 (known as the death-inducing signaling complex, or DISC). The activated Fas death receptor, on the other hand, recruits the death-associated protein (Daxx), which promotes apoptosis through activation of the apoptosis signal-regulating kinase-1 (ASK-1) and c-Jun N-terminal kinase (JNK) pathway [22]. Extracellular Inhibitors of the extrinsic pathway include membrane-bound decoy receptors 1–3 (DcR1, DcR2, DcR3), soluble Fas receptors (sFas), and soluble osteoprotegerin (OPG). Downstream from TRAIL receptor ligation, activation of caspase-8 is inhibited intracellularly by phosphoprotein enriched in astrocytes 15 (PEA-15) and cellular FLICE inhibitory protein (c-FLIP) [23–25]. Examples of potential therapeutic targets within the extrinsic pathway include activation of Fas and TRAIL death receptors as well as decreasing the expression of inhibitory molecules such as c-FLIP [26–28].

2.2 Intrinsic Apoptosis Pathway

A variety of cellular stresses activate the transcription factor p53, which is known as the tumor suppressor gene. p53 inhibits tumorigenesis by triggering apoptosis in stressed or damaged cells and operates through several proposed mechanisms including the transactivation of pro-apoptotic factors [29]. One of the important functions of p53 is its role in the Bcl-2 pathway. The members of the Bcl-2 family of proteins are key regulators of caspase activation and are considered to constitute the cell's intrinsic "apoptotic switch" [17,

30]. There are two subsets of pro-apoptotic proteins in the Bcl-2 family and one subset of anti-apoptotic proteins, all of which contain one to four of the Bcl-2 homology (BH) domains. The first pro-apoptotic subset includes Bcl-2-associated X protein (Bax) and Bcl-2-antagonist/killer protein (Bak), both of which contain BH domains 1–3. Bax is normally free within the cytoplasm and translocates to the mitochondrial membrane following an apoptotic stimulus, whereas Bak permanently resides on the mitochondrial membrane [31]. Bak and Bax are generally considered to be redundant in function, and once activated, they each homo-oligomerize into multimers that insert into the mitochondrial membrane. These multimeric structures create "pores" that release cytochrome C, ATP, Smac, and Omi from the mitochondria to trigger a signaling cascade that results in caspase activation and apoptosis (see Fig. 1) [31, 32].

The other two subsets of Bcl-2 family members (Bcl-2-like and BH3-only proteins) are upstream mediators of apoptosis, and their interplay controls the activation of Bak and Bax. The Bcl-2-like subset includes members such as Bcl-2, Bcl-xL, and Mcl-1, and this group is anti-apoptotic in function. In general, these proteins contain all four BH domains, and the highly conserved BH1, BH2, and BH3 domains of Bcl-2-like proteins are thought to form a hydrophobic pocket that engages the BH3 domain of Bak/Bax [33, 34]. This interaction is the means by which the Bcl-2-like proteins neutralize the pro-apoptotic function of Bak/Bax. The ability of Bcl-2-like proteins to antagonize Bak/Bax and functionally inhibit apoptosis is believed to be determined by their relative activity compared to the third subset of the Bcl-2 family, the BH3-only proteins.

The members of the BH3-only subset, as the name implies, contain only the BH3 domain, and this group is represented by proteins such as Bim, Bid, Bad, Noxa, Puma, and several more. The BH3-only group promotes apoptosis by engaging the Bcl-2-like proteins in the same binding cleft that the Bcl-like proteins utilize to antagonistically bind to the BH3 domain of Bak and Bax [11]. Essentially, the BH3-only proteins compete with the BH3 domains of Bak/Bax for this binding pocket on the Bcl-2-like proteins, and by occupying this site, the BH3-only proteins inhibit Bcl-2-like inhibition of Bak/Bax and indirectly activate apoptosis [35, 36]. It is by this set of competing interactions that the relative balance of pro-apoptotic BH-3-only and pro-survival Bcl-2-like proteins is believed to control the apoptotic switch.

The discussed model for apoptotic control is known as the indirect activation model (i.e., BH3-only proteins indirectly activate Bak/Bax). It is important to note that a direct activatioBak and are inhibiten model has also been proposed where BH3-only proteins Bid and Bim directly activate Bax and d by anti-apoptotic Bcl-2, Bcl-X_L, Mcl-1, Bcl-w, and Bfl/A1. Bad, Bik, Noxa, Hrk, Bmf, and Puma are considered to be sensitizers that compete for the binding site of anti-apoptotic molecules in this model [37]. However, more recent studies have shown compelling evidence in favor of the indirect activation model, and the discussion herein will assume its accuracy [38, 39]. It is also important to note that the descriptions of the models provided in this review are somewhat simplified in that all members within each of the three Bcl-2 family subclasses are not identical in function. For example, cytosolic Bad binds to Bcl-2 and Bcl-X_L, which can indirectly activate Bak/Bax, enabling oligomerization, mitochondrial disruption, and apoptosis [40]. However, Bad interacts weakly with Mcl-1, and as a result, if Mcl-1 is predominantly present in the cell, apoptosis may still be resisted even in the presence of Bad [41]. In contrast, Noxa is known to bind only to Mcl-1 and A1 [38]. Although a discussion of the differences in the specific interactions mediated by each of the proteins within each of the Bcl-2 subsets is outside the scope of this review, these are important points to consider in drug design. For example, pro-apoptotic therapies that target specific Bcl-2 family members may not be effective if the

cells upregulate alternate Bcl-2-like members that are able to circumvent the drug activity and maintain pro-survival signaling.

There is also a family known as inhibitors of apoptosis proteins (IAPs) that operates downstream of Bak/Bax and activation of initiator caspases to prevent activation of the executioner caspases (caspase-3,-7, and -9) [42]. The IAP family has eight members including cellular-IAP1 (cIAP1), cIAP2, X-linked IAP (XIAP), Survivin, Bruce, and Livin, all of which contain the baculovirus IAP repeat (BIR) domain [43]. Negative regulators of the IAP family members also exist and examples include the pro-apoptotic molecules Smac and Omi, which are released upon depolarization of the mitochondrial membrane by Bak and Bax [44]. A diversity of tumors overexpress IAPs, with survivin in neuroblastoma and c-IAP1/2 in epithelial malignancies being notable examples, and this dysregulation contributes to their apoptotic resistance [45]. Current therapeutic targets within the IAP family include XIAP and Survivin inhibition or delivery of Smac or Omi to enhance chemotherapeutic effects [11, 46].

2.3 Oncogenes

"Oncogene" is a broad term for genes that are normally responsible for general cell maintenance and proliferation that have been mutated, resulting in tumorigenic phenotypes. Oncogenes can be derived from genes that normally encode a variety of proteins such as growth factors, growth factor receptors, transcription factors, and kinases. There are many examples of oncogenes, and this topic has been reviewed extensively elsewhere [47]. An important example of a cell survival pathway whose mutation is associated with oncogenesis is the epidermal growth factor receptor (EGFR) family of protein tyrosine kinases (PTKs). In humans, the EGFR family consists of the human epidermal receptors (HERs) and includes HER1, HER2, HER3, and HER4 [48, 49]. Activation of these protein tyrosine kinases results in downstream activation of pro-survival pathways such as the phosphatidylinositol 3-kinase/Akt (PI3K/Akt) and signal transducers and activators of transcription (STAT) pathways [50]. Akt can inhibit pro-apoptotic Bad, activate the pro-survival nuclear factor-κB (NF-κB), and also inhibit the pro-apoptotic transcription factor Forkhead [51]. NF-κβ activation induces the transcription of the key anti-apoptotic genes c-FLIP, Bcl-2, and Bcl-X_L, whereas Forkhead induces the transcription of the pro-apoptotic genes FasL and Bim [52, 53]. PTKs can also activate STAT-3 and STAT-5, which results in their translocation to the nucleus and transactivation of the anti-apoptotic genes Bcl-X_L, Mcl-1, and Survivin [54–56]. Cancer cells can become reliant on oncogenes for their sustained survival and growth, making oncongene inhibition an excellent target for induction of apoptosis. Current therapeutic strategies targeting the described oncogenic pro-survival pathway include using antibodies (e.g. cetuximab and panitumumab) or small molecule drugs (e.g. gefitinib and erlotinib) to inhibit EGFR binding [11], NF-κB activation (e.g. the proteasome inhibitor bortezomib) [57], or progression of the PI3K/Akt pathway [58]. The transcription factor c-myc represents another oncogene that is often dyregulated in cancerous cells [59], and therapeutic applications for the inhibition of this oncogene will also be discuess in more detail herein.

3. Biomacromolecular Drugs with Potential as Pro-apoptotic Therapeutics

3.1 RNA Interference

Controlled manipulation of gene expression using RNA interference (RNAi) has been rigorously pursued for almost two decades now, and thorough elucidation of this mechanism combined with recent breakthroughs in RNA delivery technologies have RNAi poised to make a tremendous impact on pro-apoptotic therapies. RNAi is an especially promising therapeutic approach for inhibition of anti-apoptotic Bcl-2-like proteins, oncogenes, or other

relevant targets because it allows for optimal therapeutic specificity and breadth (i.e., in theory, any desired gene target can be efficiently silenced). The initial discovery of RNAi came in 1990 when Napoli et al. observed an unexpected reduction in expression when delivering RNA in an attempt to overexpress chalcone synthase in Petunias [60]. Others elucidated and applied this finding by delivering antisense oligodeoxynucleotides (ODN), complementary sequences of DNA, which yielded modest reduction in gene expression in C. elegans [61]. In 1998, Fire et al. showed that intracellular-acting double stranded RNA (dsRNA) was more effective than either the sense or anti-sense strand alone [1]. In fact, dsRNA has been shown to be 100 to 1000 times more effective than ODNs due to a longer half-life and greater potency [62]. Over the next few years, researchers proved that endogenous RNAi, known as microRNA (miRNA), exist and that it serves as a natural, post-transcriptional controller of gene expression where cellular machinery selectively degrades complementary mRNA in an enzymatic manner [63]. The elucidation of similar machinery for RNAi in mammalian cells further heightened the interest in therapeutically harnessing these pathways [64].

Since these early findings, the mechanisms of ODN and that of miRNA, dsRNA, siRNA, and short hairpin RNA (shRNA) have been more clearly elucidated (see Fig. 2). Single-stranded antisense ODN are thought to function by multiple mechanisms including translational arrest due to steric blockage of ribosomes by ODN-mRNA Watson-Crick base pairing and also through RNase-H-mediated cleavage of both the ODN and mRNA strands [65]. Endogenous RNAi molecules in the form of microRNA (miRNA) enter the cytoplasm after transcription, or alternatively, functionally-similar dsRNA can be exogenously delivered. shRNA that more closely mimic the structure of endogenous miRNA have also been exogenously delivered [66]. In each of these cases, the RNase III family enzyme Dicer cleaves the miRNA/dsRNA/shRNA to produce guide RNA, more commonly known as small interfering RNA (siRNA). siRNA are double-stranded RNA 19–21 base pairs in length with 3’ nucleotide overhangs [67], these molecules can assemble into the RNA induced silencing complex (RISC), a nuclease complex that degrades complementary mRNA in a sequence specific, enzymatic manner [63]. RNAi efficiency has been further improved by delivering siRNA that directly enters the RISC rather than upstream dsRNA/shRNA that must be processed first by Dicer [68]. Because of the tremendous promise of siRNA to be used therapeutically (i.e., for silencing anti-apoptotic genes in cancer cells), most of the RNAi applications in this review will be focused on delivery of siRNA. However, to be used clinically, a number of significant delivery barriers must be overcome between initial application of the siRNA (i.e. intravenously or intratumorally) and its association with the RISC machinery in the cytoplasm of target cells.

3.2 Peptide-based Pro-apoptotic Strategies

The relative abundance of Bcl-2-like proteins and the BH3-only proteins is a major determinant in Bak/Bax activity and therefore, cellular homeostasis [69]. The disruption of this homeostasis caused by abnormal, excessive Bcl-2-like protein activity is thought to be a primary cause of both tumorigenesis and the ability of established tumors to resist conventional cancer therapies [70–73]. For example, dysregulation of apoptosis was first linked to neoplasia by Vaux et. al upon the elucidation of the function of Bcl-2 as a potential oncogene [74]. Since that initial report, Bcl-2 overexpression has been found to be a common hallmark of many cancers, especially lymphomas, and it is linked to decreased likelihood of cancer patient survival [71–73, 75–77]. As a result of the remarkable efforts of scientists to elucidate the apoptosis signaling pathway and to define the molecular causes for cellular oncogenesis, pharmaceutical scientists have been able to rationally design pro-apoptotic peptides and other amino acid-based drugs that target tumorigenesis at its molecular foundations. One promising strategy is application of peptides derived from the

BH3 domains of Bcl-2 family members. For example, minimal 16 amino acid sequences contained in the BH3 domains of pro-apoptotic Bcl2 family members are capable of mimicking the activity of full-length BH3-only proteins by occupying the binding site of Bcl2-like proteins and blocking their ability to repress Bak/Bax [78]. Therefore, synthesis and delivery of these peptides presents a logical approach for negating overexpression of Bcl-2-like proteins and triggering apoptosis in cancer cells (see Fig. 3). However, like RNA drugs, peptide drugs face a robust set of delivery challenges related to maintenance of stability, biodistribution to the tumor, and intracellular delivery to the microenvironment containing the pertinent molecular target.

4. Biomacromolecular Drug Delivery Barriers

Advances in the understanding of the molecular etiology of cellular oncogenesis have made it apparent that nucleic acids, peptides, and other biologics have great potential for specific manipulation of aberrant intracellular apoptosis signaling pathways to trigger death or chemosensitivity of cancer cells. However, the desired bioactivity of intracellular-acting pro-apoptotic biomacromolecular therapeutics can be limited by numerous delivery barriers including: proteolytic/nuclease degradation in the in vivo environment, opsonization leading to systemic clearance, inability to achieve specific targeting to the desired tissues/cells, non-specific binding and/or side-effects, inability to translocate the cellular membrane, inability to escape from the endo-lysosomal and exocytosis pathways, and lack of therapeutically-relevant concentrations of drug achieved within the intracellular microenvironment where the molecular target is located (Fig. 4) [79–82]. Stability of biologics is a primary concern considering the harsh environment encountered in vivo. The inherent intermediacy of RNA during gene expression predisposes it to having a relatively short half-life. For example, naked siRNA is degraded in minutes to one hour [83], and absorbance of serum proteins to drug carriers can opsonize them for removal from the body through the macrophages of the reticuloendothelial system (i.e., in the liver) [84, 85]. Furthermore, delivery to nontargeted, healthy tissues can lead to significant, non-specific cytotoxicity and negative side effects. Therefore, targeted delivery is often pursued to augment the effect of the drug and potentially avoid undesirable cell/tissue damage. The biologics discussed herein have therapeutic action in the cytoplasm, so cell membrane translocation is also essential. However, RNA- and amino acid-based drugs have relatively large molecular weight and hydrophilicity relative to small molecule drugs that can diffuse through lipid bilayer membranes. As a result, these drugs are internalized by endocytosis, which creates the added barrier of escaping from endo-lysosomal vesicles. Herein, currently available delivery technologies and recent pro-apoptotic applications are surveyed for both RNA- and amino acid-based therapeutics.

5. Overcoming Barriers to Delivery of Amino Acid- and Nucleic Acid-Based Therapeutics

Advances in pharmaceutical technology and an increased understanding of the pharmacokinetics of biomacromolecular drugs have led to the development of a variety of tools to address systemic and intracellular delivery barriers. Pharmaceutical techniques for efficient intracellular delivery of peptide/protein therapeutics and siRNA include electroporation, fusion with cell-penetrating peptides (CPPs) and/or fusogenic peptides, chemical modifications that convey pharmaceutical properties onto the bioactive molecule itself (i.e. peptide “stapling”), formulation into liposomes/nanoparticles, and conjugation to “smart” polymers, among others. The specific approach utilized is typically selected based upon the pathological application and class of drug being delivered. For example, while neither peptide nor siRNA therapeutics can traverse cell membranes by simple diffusion, there are additional RNA-specific properties that pose unique delivery challenges. One

distinguishing characteristic of RNA is that it is a polyanionic material due to the negative charges from the phosphate groups in the RNA backbone. Since anionic macromolecules are not very efficiently internalized by cells, approaches for shielding the neagative charges on nucleic acids (i.e. by loading into liposomes or formulation into cationic polyplexes) is an important consideration that is typically less relevant for peptide delivery.

5.1 Electroporation, Iontophoresis, and Sonophoresis

There are a variety of relatively simplistic techniques useful for in vitro transfection or for in vivo application to superficial pathologies where the primary goal is getting past the skin barrier. For example, electroporation is a technique where high voltage pulses are applied to the target tissue (usually skin) triggering a voltage drop across the cell membrane of locally affected cells. This stimulus disrupts the lipid structure and forms aqueous pathways in the membrane that allow biomacromolecules to diffuse across [86]. Despite the lack of a clear mechanistic understanding of the permeabilization process, it is widely accepted that electric fields above 200 mV form nanopores in the cell membrane [87–89]. Electroporation has been used to deliver siRNA, proteins, and antibodies to various cell types. For example, optimized electroporation of deoxycytidine kinase (dCK) siRNA into acute T-cell lymphoblastic CEM cells resulted in 70–80% suppression of dCK mRNA and its enzyme activity [90]. Similarly, novel electroporation microchips have been shown to achieve transfection of the GFP plasmid into HEK-293 cells with transfection efficiency as high as 90% [91]. There are also numerous protein delivery applications that have been pursued. Electroporation of the enzyme β-galactosidase into murine melanoma cells has been achieved at efficiencies of 20% [87], and electroporation has also been used to deliver exogenous antigens into the cytoplasm of T-hybridoma cells in order to preferentially activate class I MHC processing [92]. In addition, it was found that electroporation delivered detectable levels of monoclonal antibodies against G1-specific cyclin D1into 80% of CV1 and MCF7 cells, and intracellular delivery of the antibody successfully inhibited mitosis in these cells [93]. Although electroporation can potentially affect cell viability, optimized electroporation protocols have resulted in techniques that sufficiently permeabilize cell membranes (i.e. >90% of cells) for therapeutic translocation while maintaining 80–90% cell viability [94, 95].

Another technique similar to electroporation is iontophoresis, which involves application of a constant current to move charged proteins or siRNA (i.e., through the epidermis) [96, 97]. Due to the ion-driven nature of this approach, delivery efficiency correlates to the charge of the drug utilized, and example applications of this technique include transdermal delivery of the insulin protein [97–99] and siRNA delivery for ocular gene therapy [100]. Application of ultrasound has also been explored as a means of peptide delivery (i.e. low-frequency sonophoresis) [101]. Sonophoresis is thought to disrupt lipid structure in various tissues, and tissue-specificity is achievable by varying the frequency of ultrasound waves applied. This approach has primarily been studied for applications involving transdermal drug delivery. Although iontophoresis and sonophoresis can be used to effectively translate through the skin's stratum corneum, they do not necessarily enable cellular internalization. Thus, electroporation is the most promising technique within this category based on potential for intracellular delivery. However, loss of cell viability and the inability to pursue in vivo applications where less superficial tissues are targeted represent key limitations of electroporation.

5.2 Photochemical Internalization and Laser Irradiation

Other techniques explored for biomacromolecular drug delivery include photochemical internalization and tissue permeation using laser irradiation. Photochemical internalization is a technique that relies on the localization of amphiphilic photosensitizing agents into the

endosomal membrane. Upon exposure to a light source, these agents generate highly-reactive singlet oxygen species that damage and permeabilize the endosome [102]. The use of photochemical internalization as a tool for intracellular delivery was originally proposed by Berg et. al. who utilized lysosomes as photochemical targets [103]. Subsequently, Berg and authors used photochemical internalization for the cytosolic delivery of the protein toxin gelonin, as well as for the site-specific, photochemically enhanced delivery of the anti-neoplastic glycopeptide bleomycin [104, 105]. Photochemical internalization has also been utilized for prolonging siRNA-mediated gene silencing [106]. Despite the intracellular biomacromolecular drug delivery potential of photochemical internalization, current applications are limited by the lack of supporting technologies (i.e., fiber-optic probes) that can be employed to activate photochemical agents in deeper tissues in vivo.

Another technique with applicability for the delivery of pro-apoptotic peptides and siRNA is laser-irradiation induced tissue permeation, specifically with an erbium:YAG laser [107–109]. Use of laser irradiation has been found to increase antigen-induced antibody production following skin vaccination and enhanced transdermal delivery of a number of other therapeutic agents including vitamin C, 5-fluoruracil, and 5-aminolevulinic acid [107–109]. Additionally, skin pre-treatment with a low-fluence erbium:YAG laser has been shown to increase transdermal siRNA delivery up to 10-fold compared to untreated groups [110]. The mechanism underlying the laser irradiation delivery method is thought to involve the disruption of intercellular connections (i.e. gap junctions) allowing for enhanced drug permeation through the skin barrier [107]. However, like electroporation and iontophoresis, laser irradiation is used to enhance the transdermal transport of drugs, and it is limited by the inability to overcome intracellular delivery barriers.

5.3 Cell-Penetrating Peptides

CPPs, also known as protein transduction domains (PTDs), were originally developed to mimic viruses that are able to translocate their own genetic material across cell and endosomal membranes. The 1988 discovery that the transactivating transcriptional factor (TAT) of HIV-1 can penetrate cell membranes [111, 112], followed by the discovery of antennapedia (a.k.a. penetratin) which is derived from Drosophila [113], rapidly stimulated the use of CPPs for intracellular biomacromolecular drug delivery. The finding that the antennapedia peptide was rich in positively charged arginine residues subsequently motivated the development of synthetic, arginine-rich CPPs (AR_CPPs, or oligoarginines) [114]. A multitude of other CPPs have since been discovered from naturally occurring sequences or synthetically designed, including transportan, VE-cadherin derived peptide (pVEC), the herpes simplex virus type I derived CPP VP22, diatos peptide vectors (Vectocell®), various oligoarginines, and many other novel sequences [88, 114–120]. A representative list of some of the most widely studied CPPs is given in Table 1.

The mechanism of cellular internalization of CPPs is thought to vary depending on the peptide sequence, the architecture of the drug formulation, and the cargo being delivered [121]. Cell entry mechanisms are hypothesized to include membrane fusion via binding of CPPs to cell surface proteoglycans, the endocytosis pathway (caveolindependent, clathrin-dependent, or caveolin- and clathrin-dependent), and macropinocytosis [121–124]. If the CPP and its cargo are taken up through endocytosis or macropinocytosis and a mechanism to escape these intracellular vesicles (inherent or through modification) is not present, the drug may be either degraded in the lysosome, remain sequestered in the early or late endosome, or undergo trafficking for exocytosis [121, 125]. Thus, a combinatorial therapeutic approach is commonly employed where the cell-penetrating properties of a CPP are coupled with the endosomolytic properties of fusogenic proteins/peptides or pH–responsive “smart” polymers [125–129]. Additional consideration must also be given to ensure that the CPP does not result in non-specific side effects. For example, Ward and co-

authors reported unexpected effects of CPPs on kinase inhibition [130]. Furthermore, some CPPs have also been shown to have cytotoxic effects depending on the synthetic route and CPP formulation used (e.g. some retroinverso cell penetrating peptides have been shown to result in severe cytotoxicity mediated through nonspecific side effects) [131]. Other potential disadvantages of CPPs include poor serum and protease stability and their indiscriminate cell entry, which could be problematic for systemic delivery applications where specific cells (i.e., in a tumor) are targeted. Herein, CPP delivery of pro-apoptotic biomacromolecules will be the focus. However, CPP conjugation to small molecule chemotherapeutics (i.e., doxorubicin and camptothecin) has also been assessed and found to either meet or exceed current standards achievable through delivery of the "free" drug [132–134].

5.4 Fusogenic Peptides

In order to avoid sequestration or degradation within the endo-lysosomal pathway, peptides with membrane fusogenic activity can be employed. These peptides are generally amphipathic in structure and transition into a more lipophilic state at slightly acidic pH (i.e., in the microenvironment of endo-lysosomes), allowing them to partition into and disrupt lipid bilayer membranes [135]. Initially, the understanding of the structure and function of fusogenic peptides depended upon studies on the viral and cellular fusion proteins found in nature. These fusion proteins are generally either glycoproteins contained in viral envelopes or proteins involved with fusion protein attachment receptors (i.e., soluble N-ethylmaleimide-sensitive fusion protein attachment protein receptor (SNARE)) [136]. In the case of the viral envelop, this interaction involves insertion of an α-helical peptide domain into the cell membrane catalyzing fusion of the viral envelope with the cellular or endosomal membrane. One of the most widely utilized fusogenic peptides is the N-terminal sequence of the Influenza hemagglutinin subunit HA-2 and its derivatives [137–140]. A multitude of other fusogenic proteins have also been discovered or created, including synthetic hemagglutinin derivatives, model amphipathic peptides (MAPs), β-amyloid trans-membrane protein derivatives, membrane-disruptive peptides found in various toxins and venoms, and a family of fusion-associated small transmembrane (FAST) proteins (i.e. the p10 avian reovirus, the p14 reptilian reovirus, and the p15 baboon reovirus) [121, 135–148]. A representative list of fusogenic peptides is given in Table 2. Note that penetratin, transportan, and TAT are classified as both fusogenic peptides as well as CPPs due to their fusion based mechanism of cell entry at physiological pH. In contrast, other fusogenic peptides listed typically rely on a stimulus, such as lowered pH, in order to catalyze membrane fusion, and, therefore, they are best used toward endo-lysosomal escape as opposed to cellular uptake.

5.5 Liposomes / Nanoparticles

Colloidal systems, including liposomes, micelles, and nanoparticles, are widely used for drug delivery because they can carry large drug quantities, physically shield drug cargo from enzymatic activity, and provide simple routes for modification with other molecules that can be used to finely tune the pharmaceutical properties [149]. For example, multiple functional components can be incorporated through loading (i.e., drug) into the interior of the nanoparticle or surface modification with moieties such as cell-targeting molecules, CPPs, fusogenic peptides, pHresponsive polymers for endosomal escape, and hydrophilic polymers (i.e. PEGylation for increased stealth within the systemic environment). Modification with the CPP TAT has been one of the more widely utilized approaches, while other colloidal drug carrier modifications include alternate CPPs such as R8 and IRQ, fusogenic peptides such as GALA and penetratin, and a variety of molecules including nuclear localization signals (NLS) and extracellular receptor-targeting ligands such as folic acid [121, 126, 128, 149–154]. Mitochondria-targeted vehicles are one especially promising, recent development

in colloidal drug carriers pertinent to the delivery of pro-apoptotic peptides. Since mitochondria are central to controlling cellular apoptosis, targeted drug delivery to these organelles may enable development of more potent pro-apoptotic therapies. One successful liposome-based approach to mitochondrial drug delivery incorporated the mitochondriotropic lipid triphenylphosphonium (TPP), mitochondrial targeting signal (MTS) peptides, CPPs, or synergistic combinations of these components [155]. However, significant challenges to mitochondrial drug delivery still exist, especially for applications that require control of intra mitochondrial trafficking. This combinatorial approach, however, provides a good example of the complex optimization possible through modulation of the composition and stoichiometric ratios of the different components of multifunctional particulate carriers.

One of the most common methods for nucleic acid transfection is formulation with lipids [156–158]. Lipid agents can form vesicles with a lipid bilayer membrane surrounding an aqueous interior where hydrophilic drugs can be encapsulated, or cationic lipids can be used to form lipoplexes with anionic nucleic acids. Lipids can either fuse to the cell membrane or enter the cell by endocytosis, eventually releasing their cargo into the cytoplasm [159, 160]. Information on liposome preparation, physicochemical properties, and applications can be found in more detail in a review of liposomal drug delivery systems by Samad et al. [160]. Lipids are commonly combined with other components to incorporate added functionality. For example, Morrissey et al used a cationic and fusogenic lipid (SNALP) delivery vesicle coated with a PEG-lipid layer to provide a neutral, hydrophilic exterior [161]. As a result of the multi-functional potential of liposomes and nanoparticles, they have also become promising candidates for the treatment of drug resistant cancers. For example, Huang and authors have developed multifunctional liposomes with a removable PEG shield that are capable of highly efficient tumor biodistribution and intracellular co-delivery of siRNA and doxorubicin to combat tumor cells with multi-drug resistant (MDR) phenotypes [162, 163]. In another analogous design, a guanidinium-containing liposome incorporated multiple components including a P-glycoprotein drug efflux pump inhibitor to combat drug resistance, anisamide for cancer cell targeting, and doxorubicin as a chemotherapeutic agent. The guanidinium compounds have been shown to generate reactive oxygen species (ROS) such as hydroxyl free radicals (•OH) [164], and these ROS radicals are hypothesized to act as second messengers that reduce MDR phenotype through activation of c-Jun N-terminal kinase (JNK) and c-Jun [165, 166].

A variety of inorganic nanoparticles and polyplex- or micelle-forming polymers have also been pursued as biomacromolecular delivery vehicles. In some applications, especially with inorganic nanoparticles, technological advances have been pursued that combine both image contrast and therapeutic functionalities. For example, siRNA-loaded Au nanoparticles (AuNPs) coated with cationic polymers have been reported to increase RNA half-life 6-fold when compared to naked RNA in vitro [167]. Quantum dot nanoparticles, renowned for their optical properties, have also been functionalized to successfully deliver siRNA and have tremendous potential to serve as “theranostic” platforms [168, 169]. Several natural organic polymers have also been used to make polyplex nanoparticles for siRNA delivery including sugar containing polymers such as atelocollagen [170, 171] and chitosan [172]. One important consideration in fabrication of nanoparticles is control of particle size and polydispersity. For example, control of nanoparticle size and aggregation for polyplexes is typically controlled by adjusting the nitrogen to phosphate charge ratio (N/P ratio). Kong et al. showed that the hydrodynamic diameter of nanoparticles consisting of poly[2-(dimethylamino) ethyl methacrylate] PDMAEMA/siRNA binary polyplexes could be varied from 102 nm to 58 nm simply by increasing the N/P ratio from 1 to 3 [173]. However, for polyplexes, further consideration must be given to the possibility that siRNA bioactivity could be hindered by stable (nonreversible) complexation with a polycationic carrier. One

method to address this issue is to utilize bioreducible disulfide linkages to connect siRNA to their carriers rather than using electrostatic complexation, a technique that has demonstrated significant improvements in transfection efficiency with no apparent cytotoxic effects [174, 175].

5.6 "Smart" pH-responsive Polymers

The ability to escape endo-lysosomal pathways in order to avoid degradation or exocytotic recycling out of the cell represents one of the most important carrier functionalities for biomacromolecular drug cytosolic delivery. "Smart", pH-responsive synthetic polymers with membrane-disruptive behavior that mimics the functionality of fusogenic peptides have been intensely studied for this purpose. This class of delivery systems can take the form of soluble polymer-drug conjugates, polyplexes, and micelles, and, thus, it overlaps partially with the more general "nanoparticle" category. These polymer therapeutics are typically designed to be activated by the decreasing pH gradient experienced during trafficking from the extracellular environment (i.e. pH ~7.4) into the intracellular endolysosomal pathway (i.e., $6.8 > pH > 5$). "Smart" polymers can be finely-tuned to respond in this physiologicallyrelevant pH range to trigger endo-lysosomal vesicle disruption, and this functionality can be harnessed to deliver therapeutic biomacromolecules to the cytosol.

Two primary subclasses of synthetic, pH-responsive polymers exist (anionic and cationic), and they produce endo-lysosomal escape through very different mechanisms (see Fig. 5 for structures of representative anionic and cationic pH-responsive polymers). The anionic polymers, for example, become more hydrophobic in acidic environments, triggering adoption of a less solvated, compact globule conformation that partitions into and disrupts lipid bilayers [176–179]. Some of the most thoroughly studied pH-responsive polymers are poly(alkylacrylic acids), a family of anionic polymers that was primarily pioneered by the Tirrell laboratory's work on poly(ethylacrylic acid) (PEAA) [176, 178]. Examples of other anionic, pH-sensitive polymers that have since been applied for intracellular delivery include poly(styrene-alt-maleic anhydride) (PSMA), poly(propylacrylic acid) (PPAA), and various copolymers containing PPAA and PSMA [127, 129, 180–183]. Murthy et. al. developed a related class of "encrypted" polymers that also have lipophilic activity that disrupts endo-lysosomal membranes. In the encrypted delivery system, PEG polymers attached via acid-labile acetal linkages "shield" a hydrophobic, endosomolytic polymer backbone until being shed upon exposure to acidic pH [183, 184]. We and others have successfully applied members of the anionic smart polymer subclass toward intracellular delivery of polymer-peptide and polymerprotein soluble conjugates as well as for siRNA delivery using particulate polyplex- and micelle-based formulations [125, 127, 185, 186].

A variety of cationic endosomolytic polymers have also been developed, and this alternate subclass of "smart" polymers employs a colloid osmotic mechanism described by Behr et. al. as the "proton sponge" effect [129, 176, 177, 180, 187]. Following internalization of extracellular cargo, early endosomal compartments are normally acidified by the action of an ATPase-driven proton pump in their membrane. The proton sponge effect is triggered by weakly basic cationic polymers that "absorb" the protons pumped into these vesicles, which buffers against the acidification of the endosomal microenvironment. This buffering triggers continued, abnormal import of protons and their counter-ions, establishing an osmotic imbalance that triggers water influx, vesicle swelling, and endosomal disruption [75]. Examples from this class of pH-responsive polymers include poly(L-lysine), linear and branched poly(ethylenimine) (PEI), poly(amidoamine) (PAMAM) dendrimers, poly(β-amino esters) (PBAE), and histidine and/or imidazole containing copolymers [188–194]. Due to the inherent electrostatic interaction between positive and negative macromolecules, it is logical to utilize cationic polymers to condense nucleic-acid based drugs. The electrostatic packaging approach also protects the nucleic acids by providing resistance to

nucleases present in vivo. However, the cationic nature of these polymers also predisposes them to indiscrimate cellular uptake, instability due to competing interactions with charged serum or extracellular matrix proteins, and cytotoxicity. All of these are significant barriers to clinical use of polycations, and as a result, recent developments have been aimed at overcoming these shortcomings. For example, for the "gold standard" polycation PEI, cytotoxicity and serum instability can both be improved simply by using lower molecular weight PEIs (5–48 kDa) [195–197]. Alternatively, partial modification of PEI amines with other molecules, such as poly(ethylene glycol), imidazole, peptides, or receptor-targeting moieties has also been shown to reduce nonspecific cellular uptake and cytotoxicity [198–202]. Polymer biodegradability can also be a significant advantage as exemplified by PBAE carriers, which decompose into cytocompatible, low molecular weight degradation products and are significantly less toxic than PEI and poly(L-lysine) [203, 204]. A representative list of cationic polymer-mediated siRNA delivery applications is given in Table 3.

5.7 PEGylation

Drugs designed for intravenous delivery must be equipped to navigate a complex variety of potential interactions with erythrocytes, serum proteins in the blood, and extracellular matrix proteins in the target tissue prior to cell uptake. For example, opsonization with serum proteins can "mark" drug carriers for removal from the body through the reticuloendothelial system, and anionic matrix proteins such as glycosaminoglycans can destroy the integrity of electrostatic polyplexes [84, 85, 205]. PEGylation is the primary method used to increase longevity in the circulation and make drugs more inert in order to minimize nonspecific cell uptake, drug aggregation, immunogenicity, and toxicity [206–211]. PEGylation is well-accepted to increase in vivo blood circulation half-life [212], but it can also reduce therapeutic efficacy by interfering with cellular uptake and endosomal escape [209]. For example, Hatakeyama and coworkers found gene silencing achievable using a lipid-based nano-device carrying interfering RNA to vary from 70% to 5%, with level of knockdown activity being inversely proportional to amount of PEGylation [213]. This observation suggests that the degree of PEGylation and PEG chain lengths should be optimized to balance inhibition of undesirable drug interactions with maintenance of bioactivity. For example, Gao et al. tested a series of liposomes with varied degrees of PEGylation for siRNA delivery, and liposomes containing 2.5% PEG showed the best HER1 gene silencing activity [214]. Other studies have indicated that a degree of substitution in the range of 10 to 30 using a PEG chain length of 2000 Da to be the most effective approach to stealth liposome formulation [202]. Wang and authors demonstrated PEGylated nanoparticles to reduce cytotoxicity relative to traditional formulations with PEI or cationic liposomes, although this was at the expense of significantly reduced cellular uptake. However, the loss of uptake could be compensated for by inclusion of the targeting peptide Bombesin, and this also enabled better cell-type specificity by limiting internalization of the carrier to receptormediated uptake [211]. In another study, Huang et al. recently found that the "shedability" of PEG from the surface of liposomes played an important role in improving tumor biodistribution and activity. In these studies, an unprecedented 70–80% of the injected drug dose accumulated within xenograft tumors, and effective silencing of oncogenes was achieved at impressively low (i.e., <1mg/kg) siRNA doses [208, 215, 216]. Finally, another means to minimize negative effects of PEGylation is to incorporate cleavable peptide linkages between the base carrier and the PEG chains such that the PEG layer is cleaved off by enzyme (i.e., matrix metalloproteinase (MMP)) activity present in the target tissue [213]. Ultimately, PEGylation provides a method to increase systemic half-life and avoid non-specific interactions with blood components, but targeting molecules enabling receptor-mediated uptake or removal of the PEG chains may be necessary for optimal therapeutic activity.

5.8 Drug Targeting

Ligands or antibodies specific to internalized extracellular receptors that are expressed specifically on targeted cell types can be used to achieve drug selectivity in the body. For example, the peptide (EPPT), which targets the tumor-specific, underglycosylated MUC-1 (uMUC-1) antigen, has been used to deliver siRNA to HBV cells [161]. Other examples include anisamide, a ligand of sigma receptor that is overexpressed in many human malignant tumor cells [162] and folic acid (FA), a ligand whose receptor is highly expressed in many epithelial cancers [217–219]. Another common cancer cell target is the transferrin receptor (TrfR), a glycoprotein involved in iron homeostasis and cell growth that is overexpressed on numerous tumor cells [220]. In fact, the amount of transferrin receptors on malignant cells has been shown to be as much as 100-fold greater than on normal cells [221, 222]. As a result, transferrin [223–225] and TrfR antibodies [226–228] have been used in a number of targeted drug delivery applications. These examples provide a sampling of the receptor-mediated targeting used to enhance drug uptake by cancer cells.

5.9 Chemical Modifications of Biomacromolecular Drugs

5.9.a. siRNA Design and Modification—Many of the characteristics of idealized siRNA sequences were initially identified by Elbashir and authors. For example they discovered that duplexes made of 21 base pairs with 3' overhangs 2 nucleotides in length are optimal, and they also determined that mismatches between the antisense siRNA and mRNA in the middle of the siRNA can abolish activity, while the 3' nucleotide has little effect on gene silencing [64, 68, 229]. Reynolds and co-authors more recently completed a systematic, mass screening of siRNA sequences for 2 genes and identified low Guanine/Cytidine content, a low internal stability at the 3' end of the sense strand, and lack of inverted repeats as desirable siRNA characteristics in addition to uncovering sense strand base preferences at specific sites in the sequence [230]. Since the primary focus here is on the carriers utilized for siRNA delivery, the reader is referred to reviews by Aigner for a more thorough discussion on siRNA sequence optimization [231, 232]. One common approach to silencing a new gene is to acquire several siRNA sequences that satisfy these design criteria and that target different loci on the mRNA. The sequences can be either pooled together or screened individually to identify an optimal sequence for further study. Off-target gene silencing and nonspecific immune responses mediated through toll-like receptors can also be triggered by suboptimal siRNA sequences, and instances have occurred where nonspecific effects have been misinterpreted as siRNA-driven phenotype modification resulting from silencing of a target gene [233]. However, siRNA therapeutic potential remains strong as chemical modifications and new rules for sequence identification are progressing in-step with the iterative improvements in delivery approaches. In preclinical studies, testing for immune activation and verifying phenotypes independently using different siRNA sequences against the gene of interest are desirable standards of practice [234].

5.9.b. Peptide Stapling—Generally, peptides have poor in vivo stability, cellular uptake, and overall pharmacokinetics, but recent synthetic advances have led to the development of peptidic therapeutics endowed with these properties. With this approach, peptide intracellular delivery barriers can be overcome through the physicochemical properties of the peptide therapeutic itself as opposed to gaining these functionalities through conjugation to a peptide/polymer or loading into a liposome or nanoparticle. The modification of peptide therapeutics to improve stability and potency was initiated by the advent of retroinverso peptides, or peptides in which each naturally occurring L-amino acid is replaced with the D-enantiomer and the peptide bonds are reversed [235]. In addition to retroinverso peptides, chemical cross-linking has also been used to stabilize secondary structure of peptides, and this method of stabilizing peptides containing α-helices increases stability of the secondary

structure and peptide potency [236]. The crosslinking chemistry as well as the chemoselectivity of the reaction can significantly affect the pharmacological and structural properties of the peptide and continue to be optimized for various therapeutics [237]. Classical approaches to stabilization of α-helices make use of covalent bonding between the i and i+4 or i and i+7 side chain groups and are comprised of lactam, disulfide, or metal-mediated linkages [237–240].

Early peptide cross-linking approaches have since evolved into the development of stapled peptides, or peptides in which non-natural, olefin-conjugated amino acids are used to incorporate controllable cross-links. The link between olefin groups consists of an all hydrocarbon 'staple' between successive turns (i.e., i and i+4) of the α-helical structure and is formed through a ring-closing ruthenium-catalyzed olefin metathesis reaction [241–243]. Blackwell and Grubbs first described stapled peptides [244], and later, the Verdine laboratory further optimized the metathesis reaction and the overall stapled peptide design [243]. Use of an all hydrocarbon 'staple' can improve structural stability, potency, protease resistance, and even cell permeability [241]. The ability of stapled peptides to achieve cellular entry is hypothesized to be a consequence of their stabilized structure and has been shown to involve an energy-dependent endocytotic uptake mechanism [245]. Stapled peptides are evolving into an indispensable tool for the intracellular delivery of pro-apoptotic sequences, and significant clinical promise has been shown for the stapled peptides known as stabilized α-helix of BCL-2 domains, or SAHBs [241].

6. Pro-apoptotic RNAi Therapeutic Applications

Cancer biologists have provided a relatively thorough understanding of the aberrantly expressed genes that grant cancerous cells their hallmark ability to evade apoptosis, possess self-sufficiency in growth signals, display high proliferative potential, promote angiogenesis, and metastatically invade other tissues [246]. RNAi has been pursued for a diversity of gene targets responsible for these traits, both those where silencing directly induces apoptosis and those that sensitize cells to secondary therapeutics. Initial RNAi applications in cancer therapy were primarily ODN approaches, and 21 example gene targets that have been pursued with antisense directed at inducing apoptosis in breast cancer were reviewed in a 2002 report [247]. However, due to the subsequent elucidation of the enzymatic mechanism and higher potency of double-stranded siRNA, the field has predominantly shifted from ODN toward siRNA approaches for cancer therapies [65]. The more recent approaches have utilized siRNA to manipulate targets in the Bcl-2 family and IAPs, in addition to other targets related to cell signaling, viral oncogenes, cell cycle, metabolism, and nutrient transport [248]. Robustly testing for therapeutic effects mediated by siRNA is contingent upon successful siRNA intracellular delivery and target gene silencing. Supplementary Materials Table 1 surveys a sampling of published siRNA delivery approaches and the relative level of gene knockdown that has been achieved using different transfection techniques. Herein, we specifically highlight siRNA applications in pro-apoptotic therapies, and because clinical utilization of siRNA is the ultimate goal, we attempt to differentiate between reports where apoptosis-related targets where tested in vitro (Table 4) versus the more translational studies done in vivo (Table 5).

6.1 Bcl-2 Family Proteins

The most direct and aggressively pursued pro-apoptotic RNAi method has been silencing of Bcl-2-like proteins Bcl-2 and Bcl-xl [249]. Knockdown of these Bcl-2-like subfamily members allows the indirect activation and homo-oligomerization of Bax/Bak, the critical pro-apoptotic triggers of the mitochondrial apoptosis pathway (see Fig. 1). RNAi of Bcl-2 has been proven to increase apoptosis and arrest growth of HeLa and several other cancer cell lines, and the apoptotic effect can be amplified with co-delivery of chemotherapeutics

[250, 251]. Poeck et al. introduced 5'-triphosphate modifications onto Bcl-2 siRNA, with the triphosphate chemistry being incorporated to activate Retinoic acid-inducible gene 1 (RIG-1) in innate immune cells. This triggered interferon expression, creating an immune response that acted synergistically with Bcl-2 silencing, and the combined effects produced 50% apoptosis of melanoma cells and a reduction in tumor size in mice [252]. Silencing of intracellular Bcl-2 has also been utilized to increase sensitivity to activators of the extrinsic apoptosis pathway (i.e., TRAIL) in melanomas, but Bcl-2 knockdown was found to be a less effective sensitizer relative to knockdown of the IAPs Survivin and XIAP [253].

6.2 IAPs

Apoptotic resistance in various cancers can, in part, be attributed to the overexpression of specific IAPs. For example, Survivin and Livin are overexpressed in neuroblastoma, and c-IAP1 and c-IAP2 are overexpressed in epithelial malignancies [45, 254]. As a result, silencing of IAPs has also been pursued as a route to reduce cancer cell resistance to apoptosis [255]. Survivin is released from the mitochondria during apoptotic signaling to negatively regulate caspase activation [256], and its silencing in HeLa cells has been shown to induce apoptosis [257]. However, in other cell lines like human sarcoma, the apoptotic effect was limited to only 10% of the cells when no secondary treatment was applied [258]. In a more recent in vivo study, Survivin siRNA (4 mg/dose) complexed with DharmaFECT was injected intratumorally into mice twice per week over a 3 week period. This approach resulted in a 40% reduction in human lung adenocarcinoma tumor weights, and co-delivery of Survivin siRNA with cisplatin produced a stronger antitumor response than either drug alone [259]. Livin is a newly discovered IAP that inhibits caspases 3, 7, 9, and cytochrome c, making it a logical choice for pro-apoptotic RNAi therapy. Knockdown of Livin created an apoptotic effect in HeLa cells [257] but only limited response in other cell types. XIAP is another IAP that inhibits caspases 3, 7, and 9, and thus, it is also a viable target for RNAi-mediated apoptosis. Dan and co-authors found that approximately 80% apoptosis was induced when XIAP was inhibited in ovarian cancer cells [260]. Furthermore, in vivo transfection of XIAP siRNA using intratumoral injection and electrotransfection pulsing decreased tumor cell proliferation by 75% relative to control groups in a 50-day tumor study on MCF-7 breast cancer xenografts [261].

6.3 Oncogenes

Normal cells regulate the transcription factor c-myc tightly, but in cancerous cells, mutations in c-myc deregulate its expression, triggering uncontrolled cellular proliferation [59]. In fact, mutation of c-myc is a hallmark of some cancers (i.e., Burkitt's lymphoma), and in some cases it is essential for cancer cell survival, making it a promising potential drug target [262]. For example, in vitro silencing of c-myc (80% knockdown) in MCF-7 cells has been found to reduce their growth rate both in vitro and in vivo (in cells transfected prior to their inoculation into the mouse), and a 40% induction of apoptosis was measured upon serum withdrawal in c-myc deficient cells versus only 6% in controls [263]. Systemic delivery of siRNA through electrostatic condensation onto protamine-functionalized targeting antibodies has been used for delivery of pooled siRNA sequences against c-myc, MDM2, and VEGF, which was shown to reduce the size of subcutaneous B16 melanoma tumors by more than 50% relative to control groups at a 9-day endpoint [264]. Huang and co-authors have thoroughly assessed c-myc knockdown in mouse models using lipid-based carriers, and they have found that c-myc silencing effectively induces apoptosis and reduces tumor growth [262, 265, 266].

Although c-myc has been a primary oncogene drug target, inhibition of other onconges has also been pursued therapeutically. HER2 is an example of an oncogene that is often dysregulated in many types of cancers and causes excessive cell growth. This oncogene is

particularly relevant in breast cancer, and siRNA targeting HER2 has been shown to arrest growth and trigger apoptosis in vitro in several cell types, including HER2-expressing MCF-7 breast cancer cells [267]. Polo-like kinase 1 (PLK-1) is another gene involved in regulation of cell cycle progression. Many cancer cells overexpress PLK-1, and it is hypothesized that this aberrant expression can cause excessive cell growth and inhibition of p53-induced activation of apoptosis [268]. PLK-1 overexpression promotes chromosome instability and overrides mitotic checkpoints leading to immature cell division [269]. Silencing the expression of PLK-1 in nasopharyngeal carcinoma (C666-1) cells with systemic delivery of siRNA has been found to result in significant apoptosis and decreased tumor growth [270]. In addition to nasopharyngeal carcinoma, dramatically increased apoptosis has been shown to result from PLK-1 siRNA silencing in breast cancer cells, HeLa cells, colon cancer cells, and lung cancer cells, with as high as 50% apoptotic induction reported in some cell lines [271]. Furthermore Benoit, Henry, and authors showed that an approximately 50% reduction of PLK-1 gene expression in NCI/ADR-RES and OVCAR8 ovarian cancer cells lines sensitized these cells to doxorubicin cytotoxicity [272]. This study, among others discussed below, achieved powerful, synergistic effects by co-delivering siRNA and small molecule chemotherapeutic drugs.

6.4 Gene Targets for Sensitization to Radiation and Chemotherapy

Most of the studies discussed up to this point demonstrate the potential of siRNA to directly induce apoptosis through silencing of Bcl-2 proteins, IAPs, and oncogenes. However, many of these studies have indicated that application of siRNA alone is often not enough to create a robust pro-apoptotic effect, and, thus, multi-component approaches may be optimal. One common approach is to simultaneously deliver chemotherapeutics and RNAi agents designed to silence genes known to cause cancer chemoresistance [273]. This approach is especially relevant for cancer patients whose previously treated, residual tumors develop multidrug resistance (MDR). MDR is a genetic or acquired trait of cancer cells that exhibit resistance against multiple, structurally or mechanistically unrelated anticancer drugs. MDR cancer cells are characterized by poor uptake, increased excretion, and elevated metabolism of drugs (see Fig. 6). Drugs that are influenced by reduced uptake are mostly water soluble drugs that are internalized by routes similar to nutrients, and these include antifolate methotrexate, nucleotide analogues (5-fluorouracil and 8-azaguanine), and cisplatin [274, 275]. Drug resistance caused by increased drug efflux from the cell affects drugs that are ejected through cell membrane transporters, and these drugs include anthracyclines (doxorubicin (Dox) and daunorubicin), vinca alkaloids (vinblastine and vincristine), RNA transcription inhibitor actinomycin-D, and the microtubule-stabilizing drug paclitaxel [276]. In many cases, MDR cells simultaneously acquire mechanisms that impede intracellular drug accumulation and also undergo oncogenic alterations that diminish their susceptibility to the drugs.

The "classical" MDR phenotype results from decreased intracellular drug accumulation due to the drug efflux activity of the adenosine triphosphate binding cassette (ABC)-transporter MDR1/P-glycoprotein (MDR1/P-gp, ABCB1) encoded by the human MDR1 gene. Overexpression of P-gp frequently contributes to MDR phenotype because it transports a broad spectrum of drugs including Dox, vinblastine, and paclitaxel out of the cell. Development of P-gp inhibitors selectively targeting MDR cancer cells to decrease drug efflux may sensitize these cells to chemotherapy and improve patient outcomes [277]. To this end, more than a 10-fold decrease in the LC_{50} of amrubicinol was recently observed in an amrubicinol-resistant small-cell lung cancer cell line (PC-6/AMR-OH) treated with P-gp siRNA (~70% knockdown achieved) relative to controls with basal P-gp levels [278]. Another recent study tested P-gp silencing as an adjunct to Bortezomib, which is a selective inhibitor of the proteasomal pathway. Despite its potency in chemoresistant myeloma

patients, some patients become refractory to prolonged treatment [279, 280]. Rumpold et al. demonstrated that sensitivity to Bortezomib could be restored by knockdown of P-gp with siRNA [281]. In this study, siRNA silencing of P-gp was found to improve the EC_{50} of Bortezomib from 25 mg/mL to 4.5 mg/mL and the EC_{50} of MLN273 (another proteasomal inhibitor) from 253 ng/mL to 9.8 ng/mL in MDR myeloma cells. Minimizing the active dose, in addition to cell-specific targeting (if achievable), are of paramount importance in P-gp silencing approaches because P-gp serves as a vital cellular transport mechanism in normal cells, and its nonspecific inhibition can lead to negative side effects.

Ral-interacting protein (RLIP76) is another multifunctional membrane transporter, involved in stress-defense and apoptosis resistance. RLIP76 transports glutathione-conjugate (GS-E) compounds, thus controlling the intracellular concentration of pro-apoptotic, oxidized lipid byproducts and also chemotherapeutic agents. Depletion or suppression of RLIP76 with antibodies or siRNA confers increased chemosensitivity (e.g., to 2–3 fold higher cell death from 4-hydroxynonenal in small cell lung cancer) [282–284]. Furthermore, recent studies have shown that inhibition or depletion of RLIP76 by antibodies, siRNA, or antisense can lead to drastic and sustained regression of lung, kidney, melanoma, colon, and prostate cancer xenografts with no observed recurrence of tumors and no evident toxicity [282, 285–289].

The oncogene c-Myc has also been proposed to contribute to MDR efflux pump expression [290, 291], and for this reason inhibition of c-Myc has been hypothesized to enhance tumor sensitivity to chemotherapeutics. Dox is known to be especially susceptible to MDR efflux pump activity [292], and Huang and authors have attempted to address this problem through co-delivery of Dox with siRNA against c-Myc. In this study, it was demonstrated that delivery of c-Myc siRNA to mice with MDR ovarian cancer xenografts down-regulated efflux pump expression and promoted nearly 2 times greater tumor uptake of Dox relative to controls not receiving c-Myc siRNA [162]. However, other evidence suggests that c-Myc knockdown and chemotherapy treatments may be more effective if done sequentially rather than simultaneously. For example, silencing of c-Myc in medulloblastoma cells was found to slow cell growth. However, c-Myc knockdown also decreased cell sensitivity to cisplatin, etoposide, and ionizing radiation and reduced apoptosis by 24–56%, presumably due to the key role c-Myc plays in apoptotic signaling in these cells [293].

Cyclin D1 proto-oncogene is another potentially relevant anticancer gene target because it is an important regulator of G1 to S-phase transition during cell division, and it also serves as a cofactor for several transcription factors. Cyclin D1 is overexpressed in many human pancreatic cancers, a cancer type with an especially poor patient prognosis due to shortcomings in early detection and the fact that pancreatic tumors are commonly resistant to chemotherapeutic agents [294, 295]. Thus, improvement of pancreatic cancer therapies is an area of significant clinical need, and siRNA knockdown of Cyclin D1 may have promise in this area. For example, siRNA silencing of Cyclin D1 in pancreatic tumor cells has been shown to enhance cisplatin- and fluoropyrimidine-mediated growth inhibition. In these studies, cisplatin- and fluoropyrimidine-mediated apoptosis was enhanced by approximately 3-fold in Cyclin D1-overexpressing pancreatic tumor cells delivered Cyclin D1 siRNA relative to cells treated with a control siRNA [294]. Several studies have also demonstrated that the anti-apoptotic, tumorigenic activity of D-type cyclins (D1, D2, and D3) may be dependent on cooperative interaction with other growth promoting genes such as c-Myc and Ras [296, 297]. For example, co-expression of c-Myc and cyclin D3 promotes lymphoid cell resistance to dexamethasone-induced apoptosis, and overexpression of cyclin D1 inhibits drug-induced apoptosis in rat embryo fibroblasts ectopically expressing c-myc [298]. Furthermore, cyclin D1 positively correlates with high basal and cisplatin-induced activity of NF-κB, which contributes to chemoresistance and cell survival through inducing

expression of anti-apoptotic Bcl-2 family of proteins [299, 300]. Finally, a recent investigation by Biliran et al. revealed a relationship between c-Myc and cyclin D1 that affects cell apoptosis and drug sensitivity [301] (see Fig. 7). This exemplifies the complex interrelationships that occur between oncogenes during tumorigenesis and provides a number of viable gene targets whose silencing may act synergistically with other cancer therapies.

In addition to serving as an adjunct to small molecule drugs, gene silencing has also been utilized to sensitize cancer cells to radiation therapy. For example, DNA-dependent protein kinase (DNA-PK) is hypothesized to make cells resistant to radiation therapy, and An and co-authors tested the effect of DNA-PK silencing in HeLa cells. The authors demonstrated a 7-fold decrease in cancer cell number 6 days after a 2 Gy dose of irradiation in HeLa cells delivered siRNA targeting the catalytic motif of DNA-PK relative to control cells receiving irradiation only. Interestingly, the hypothesized mechanism for this effect was a concomitant repression (~80% decrease) of c-Myc expression in cells where DNA-PK was silenced [302]. Thus, the DNA-PK gene could be an attractive anticancer gene target for sensitization of cancer cells to radiation therapy whose inhibition may lead to co-repression of other harmful oncogenes.

7. Pro-apoptotic Peptide Therapeutic Applications

The intracellular delivery of peptides that mimic BH3-only protein activity is one of the most extensively studied amino acid-based pro-apoptotic strategies [125, 241, 242, 245, 303–306]. Peptide therapeutics occupy a small but promising niche among other classes of pro-apoptotic anticancer drugs such as therapeutic antibodies and small molecule Bcl-2 antagonists [307–309]. Among the pro-apoptotic peptide sequences derived from BH3 domains, stapled BH3 peptides (SAHBs) may have the most ideal pharmacological properties because of their improved stability of the α-helical structure, protease resistance, cell permeability, and increased affinity to the multi-domain, BH3 binding “pockets” on Bcl-2-like proteins [245]. However, BH3 peptide mimics continue to be developed and screened in new formulations in an effort to optimize their therapeutic potential. The utilization of BH3 peptides has also stimulated the discovery of small molecule drugs, including ABT-737 and ABT-263, which have similar functionality to BH3-only peptides [303, 306, 310]. Peptide mimics of BH3-only proteins have been derived from several of the BH3-only proteins (i.e. Bim, Bid, Bad, Noxa, Puma, etc.) and also from the BH3 domains of Bak and Bax. Peptides derived from BH3 domains of different parent proteins have different specificities, and, clinically, this may be important for the design of cancer- or patient-specific therapeutic regimes. For example, Shangary and co-authors demonstrated that agents based on the Bax BH3 domain may be best aimed at cancers overexpressing Bcl-2, while peptides derived from the BH3 domain of Bad may be more useful for tumors overexpressing Bcl-xL [311]. Generally, BH3 peptides have shown promise as pro-apoptotic agents, and herein we will survey the results of tests where they have been delivered using electroporation, CPPs, stapled peptides, liposomes/nanoparticles, and pH-responsive smart polymers.

Pro-apoptotic peptides derived from the BH3 domains of Bak and Bax have been tested with electroporation, and it was found that at 48 hours after peptide delivery, cell viability was reduced by 40% in prostate tumor cells [312]. BH3 peptides have also been conjugated with CPPs to improve intracellular delivery. For example, peptides derived from the Bak BH3 domain have been fused with the CPP penetratin, and this approach resulted in ~80% decrease in HeLa cell viability relative to the unmodified BH3 peptide control [304]. Likewise, a truncated Bax-derived BH3 peptide fused with TAT (i.e. pTAT-p3Bax) chemosensitized NRP-154 prostate epithelial cells and enhanced induction of apoptosis by

thapsigargin (a non-competitive inhibitor of sarco-endoplasmic reticulum Ca^{2+} ATPase) [313].

In addition to the use of CPPs to enhance intracellular delivery of pro-apoptotic therapeutics, cell-specific targeting peptides/ligands can be utilized to achieve tumor selectivity. For example, Minko and authors delivered apoptotic BH3 peptide drugs targeted with the Luteinizing-hormone-releasing hormone (LHRH) peptide, a molecule whose receptor is overexpressed on numerous cancer cell types. In this study, the LHRH-BH3 peptide produced a significant loss in cell viability (peptide IC_{50} 3.97 ± 0.33 ng/mL) in A2780 human ovarian carcinoma cells, while no significant toxicity was caused by the BH3 peptide without the LHRH sequence [314]. CPP-conjugates have also been created that incorporate mechanisms for tissue-targeted delivery. In one example of this approach, the antineoplastic agent chlorambucil was conjugated to a chimeric peptide containing the cyclic, breast-tumor targeting peptide cCPGPEGAGC (PEGA) the CPP pVEC. In breast cancer MCF-7 cells, the IC_{50} for chlorambucil was 128 μM, while chlorambucil conjugated to the PEGA-pVEC had an approximately 4-fold lower IC_{50} of 30 μM [133]. In a prostate cancer application, Li et al. developed a novel fusion peptide (BSD352) that consisted of the CPP TAT, a sequence from the BH3-only protein Puma (TAT-$BH3_{Puma}$), an anti-vascular endothelial growth factor peptide (SP5.2), and an anti-basic fibroblast growth factor peptide (DG2). It was found that the components of the fusion peptide acted synergistically to inhibit the growth of androgen-sensitive human prostate adenocarcinoma (LNCaP) xenograft tumors in a mouse model, and tumor volume was decreased from ~1500 mm^3 to ~300 mm^3 in treated mice relative to PBS controls. Mechanistically, the fusion peptide was found to elevate levels of Bax, enhance cytochrome c release, and induce caspase-9 cleavage to induce tumor cell apoptosis while simultaneously inhibiting angiogenesis and endothelial cell proliferation [315]. However, despite observing a dose-dependent, synergistic apoptotic effect in LNCaP cells, minimal levels of apoptosis were observed in PC3 and RWPE-1 cell lines. Finally, tissue specific delivery has also been sought using photochemical internalization. In this realm, Shamay et al. have tested a light-activated, caged CPP fused with a pro-apoptotic peptide (D)$(KLAKLAK)_2$, a peptide that was designed by Ellerby and coworkers [316]. It was found that upon 10 minutes of light exposure, 80% of the therapeutic was internalized, producing a 90% loss of viability in PC3 prostate cancer cells [317].

Stapled peptides have also been used in several pro-apoptotic peptide delivery applications and have shown potential as potent in vivo therapeutics. Walensky et al. tested a BH3 stapled peptide, or SAHB, derived from the BH3 domain of the BID protein in a murine RS4;11 leukemia xenograft model. Their results demonstrated that daily treatment with the stapled peptide significantly prolonged survival and, by day 5, regression of leukemia cells from the spleen and kidney was detectable, while leukemic expansion was apparent at these sites in the control group [245]. In another leukemia model, Moellering and authors used a stapled peptide termed SAHM1 to inhibit the NOTCH transcription factor in a murine model of T-cell acute lymphoblastic leukemia (T-ALL). It was found that daily treatment with the SAHM1 therapeutic resulted in dose-dependent tumor regression and a 5-fold increase in caspase 3/7 activities in treated cells [318]. Other preliminary studies that have not yet reached in vivo testing are exploring new SAHBs, and in one recent application, Stewart and authors reported promising in vitro results from a Mcl-1-derived SAHB Mcl-1 inhibitor [319].

Liposomes have also been employed as pro-apoptotic delivery vehicles with promising results in animal tumor models. Ko et al. reported that cationic liposomes loaded with pro-apoptotic peptide (D)$(KLAKLAK)_2$ and Bcl-2 antisense oligodeoxynucleotide G3139 inhibited B16(F10) melanoma tumor growth in a mouse model by over 50% (reduction in tumor size from ~1000 mm^3 to <500 mm^3) and that the inhibitory effects correlated with

increased caspase activity [154]. Additionally, Xu and authors studied the therapeutic efficacy of a liposomal carrier loaded with caspase-6 and anti-human epidermal growth factor receptor (HER2) antibody in both HER2 positive (i.e. SK-BR-3 human breast cancer and SKOV-3 human ovarian cancer) and HER2 negative (i.e HeLa human utero-cervical carcinoma and BT325 human glioma) cancer cell lines [307, 308]. Time-dependent cell death was observed in HER2 positive cells, whereas no significant effect was observed in HER2 negative cells. In a murine SK-BR-3 tumor xenograft model, liposomes loaded with the anti-HER2 antibody resulted in a >50% decrease in tumor growth and prolonged survival when compared to the liposome alone. In a parallel study, Wang and authors utilized the same antibody-loaded liposome approach to prolong survival and significantly inhibit tumor metastasis in a murine model of human osteosarcoma [308].

"Smart" pH-responsive polymers have also been investigated for the intracellular delivery of pro-apoptotic amino acid-based biologic drugs. For example, we have developed a multifunctional, endosomolytic polymer that enhanced delivery and pro-apoptotic effects of a CPP-BH3 peptide [79]. This delivery system is based on poly(N-(2-hydroxypropylmethacrylamide))-b-poly(propylacrylic acid-co-butyl methacrylate-co-dimethylaminoethyl methacrylate) (pHPMA-b-p(PAA-co-BMA-co-DMAEMA) containing a pyridyl disulfide polymer chain end functionality incorporated through a reversible addition fragmentation chain transfer (RAFT)-based synthetic procedure. This reversible pyridyl disulfide conjugation site was utilized so that the peptide could be released from its carrier in the reducing environment of the cytoplasm. The pHPMA block was designed to confer long circulation times, and the propylacrylic acid-containing pH-responsive terpolymer block was incorporated to mediate pH-activated endosomal escape. Peptide conjugates with pHPMA-b-p(PAA-co-BMA-co-DMAEMA increased HeLa cervical carcinoma cell apoptotic activity over free peptide and resulted in 50% tumor cell death in cultures after 6 h of treatment [79]. More recently, we have also utilized pH-responsive homopolymers of propylacrylic acid to deliver protein antigens for anticancer vaccines. In these studies, ovalbumin was incorporated as a model protein antigen to test the ability of these polymer-based vaccines to stimulate class I MHC presentation and antigen-specific cytotoxic T-cell activation. These activities require cytosolic delivery and processing of the antigen, which was augmented in this case using the endosomolytic polymer carrier. In an in vivo study using the EG.7-OVA mouse tumor protection model, PPAA ovalbumin conjugates produced a functionally significant prophylactic effect. PPAA-based protein vaccine delivery facilitated an 8-fold increase in antigen-specific CTL production and an approximately 3.5-fold increase in the length of tumor-free survival relative to mice delivered vehicle controls [185].

8. Conclusions

The discovery of new pro-apoptotic drug targets, the development of new delivery techniques for intracellularacting biologics, and the identification of novel cell-targeting strategies are providing researchers with the tools needed to produce more effective anti-cancer therapies. As demonstrated through numerous in vivo preclinical tests, delivery of pro-apoptotic siRNA, proteins, peptides, and antibodies is being optimized through continually evolving approaches to overcome delivery barriers. Among these approaches, stapled peptides and stealth liposomes have great potential, especially with respect to the improved stability and specificity of stapled peptides and the capability of recent liposome formulations to deliver as much as 80% of systemically injected payloads into a tumor. These promising technologies enable scientists to unlock a new universe of intracellular targets that are druggable by biomacromolecules. The optimal targets for these drugs tend to be dependent on the type of cancer, and future treatments may be tailored to patient-specific cancer phenotypes. While these approaches will potentially be utilized to develop new

stand-alone therapeutics, the most promise to this point has been demonstrated through synergistic combinations of biomacromolecular drugs and currently available chemotherapeutics. Thus, future trends may include further development and optimization of technologies that can successfully navigate the array of both extra- and intracellular barriers to achieve co-delivery of biologic and small molecule drugs. Rapid progress in both the fundamental understanding of apoptosis and in the engineering of improved delivery systems suggests that clinical successes utilizing intracellular-acting pro-apoptotic biomacromolecular drugs are forthcoming.

Supplementary Material

Refer to Web version on PubMed Central for supplementary material.

Acknowledgments

C.L.D. would like to acknowledge NIH F32CA134152 for funding support and Patrick Stayton, Allan Hoffman, Oliver Press, Anthony Convertine, Danielle Benoit, and Corinna Palanca-Wessels for constructive conversations on this research area.

ABBREVIATIONS

STAT	Signal tranducers and activators of transcription
RNAi	RNA interference
shRNA	Short-hairpin RNA
siRNA	Small interfering RNA
uMUC-1	Underglycosylated MUC-1
FA	Folic acid
TrfR	Transferrin receptor
CPP	Cell penetrating peptides
MAP	Mitogen-activated protein
MAPK14	p38 MAP kinase
PCD	Cystamine bisacrylamide-diaminohexane
PCM	Primary cardiomyocyte
MEND	Multifunctional envelope type nano device comprised of lipid/protein transduction domain peptide
TUNEL	TdT dUTP nick end labeling
Dox	Doxorubicin
CDP	Cyclodextrin-containing polycations
AuNPs	Au nanoparticles
PAMAM	Poly(amidoamine)
EHCO	N-(1-aminoethyl)iminobis[N-(oleicyl-cysteinyl-Histinyl-1-aminoethyl)propionamide
PBAE	Poly(B-amino esters)
RGD	Arg-Gly-Asp

MDR	Multi drug resistance
ROS	Reactive oxygen species
JNK	c-Jun N-terminal kinase
BN	Bombesin
StA	Stearic acid
RIG-1	Retinoic acid-inducible gene 1
plk-1	Polo-like kinase 1
RRM2	Ribonucletodide reductase
ABC	ATP-binding cassette
DNA-PK	DNA-dependent protein kinase
RLIP76	RaI-interacting protein
GS-E	Glutathione-conjugate
P-gp	P-glycoprotein
AMR	Amrubicinol
FDA	Food and Drug Administration
PTDs	Protein transduction domains
TAT	Trans-activating transcriptional factor
pVEC	VE-cadherin derived peptide
FAST	Fusion-associated small transmembrane
MAPs	Model amphipathic peptides
NLS	Nuclear localization signal
TPP	Triphenylphosphonium
MTS	Mitochondrial targeting signal
PSMA	Poly(styrene-alt-maleic anhydride
PPAA	Poly(propylacryic acid)
PEI	Polyethylenimine
PAMAM	Poly(amidoamine
SAHBs	Stabilized α-helix of BCL-2 domains
Bim	Bcl-2-interacting mediator of cell death
Bid	BH3-interacting-domain death agonist
Bad	Bcl-2-associated death promoter
Bmf	Bcl-2-modifying factor
Puma	P53-upregulated modulator of apoptosis
Bik	Bcl-2-interacting killer
Hrk	Harakiri
LHRH	Leutinizing-hormone-releasing hormone

REFERENCES

1. Fire A, Xu SQ, Montgomery MK, Kostas SA, Driver SE, Mello CC. Potent and specific genetic interference by double-stranded RNA in Caenorhabditis elegans. Nature. 1998; 391:806–811. [PubMed: 9486653]
2. Reichert JM, Valge-Archer VE. Development trends for monoclonal antibody cancer therapeutics. Nat Rev Drug Discov. 2007; 6:349–356. [PubMed: 17431406]
3. Dimitrov DS, Marks JD. Therapeutic Antibodies: Current State and Future Trends – Is a Paradigm Change Coming Soon? Methods Mol Biol. 2009; 525:1–27. [PubMed: 19252861]
4. Sternberg CN, Dumez H, Van Poppel H, et al. Docetaxel plus oblimersen sodium (Bcl-2 antisense oligonucleotide): an EORTC multicenter, randomized phase II study in patients with castration-resistant prostate cancer. Annals of Oncology. 2009; 20:1264–1269. [PubMed: 19297314]
5. Waters JS, Webb A, Cunningham D, et al. Phase I clinical and pharmacokinetic study of bcl-2 antisense oligonucleotide therapy in patients with non-Hodgkin's lymphoma. J Clin Oncol. 2000; 18:1812–1823. [PubMed: 10784621]
6. Pro B, Leber B, Smith M, et al. Phase II multicenter study of oblimersen sodium, a Bcl-2 antisense oligonucleotide, in combination with rituximab in patients with recurrent B-cell non-Hodgkin lymphoma. Br J Haematol. 2008; 143:355–360. [PubMed: 18764869]
7. Bedikian AY, Millward M, Pehamberger H, et al. Bcl-2 antisense (oblimersen sodium) plus dacarbazine in patients with advanced melanoma: the Oblimersen Melanoma Study Group. J Clin Oncol. 2006; 24:4738–4745. [PubMed: 16966688]
8. O'Brien S, Moore JO, Boyd TE, et al. Randomized phase III trial of fludarabine plus cyclophosphamide with or without oblimersen sodium (Bcl-2 antisense) in patients with relapsed or refractory chronic lymphocytic leukemia. J Clin Oncol. 2007; 25:1114–1120. [PubMed: 17296974]
9. Raab R, Sparano JA, Ocean AJ, et al. A Phase I Trial of Oblimersen Sodium in Combination With Cisplatin and 5-Fluorouracil in Patients With Advanced Esophageal, Gastroesophageal Junction, and Gastric Carcinoma. American Journal of Clinical Oncology. 33:61–65. [PubMed: 19738454]
10. Kerr JF, Wyllie AH, Currie AR. Apoptosis: A Basic Biological Phenomenon with Wideranging Implications in Tissue Kinetics. Br J Cancer. 1972; 26:239–257. [PubMed: 4561027]
11. Wilson TR, Johnston PG, Longley DB. Anti-apoptotic mechanisms of drug resistance in cancer. Curr Cancer Drug Targets. 2009; 9:307–319. [PubMed: 19442051]
12. Kolesnick RN, Kronke M. Regulation of ceramide production and apoptosis. Annu Rev Physiol. 1998; 60:643–665. [PubMed: 9558480]
13. Asakura T, Sawai T, Hashidume Y, Ohkawa Y, Yokoyama S, Ohkawa K. Caspase-3 activation during apoptosis caused by glutathione-doxorubicin conjugate. Br J Cancer. 1999; 80:711–715. [PubMed: 10360648]
14. Mesner PW Jr, Budihardjo II, Kaufmann SH. Chemotherapy-induced apoptosis. Adv Pharmacol. 1997; 41:461–499. [PubMed: 9204156]
15. Thornberry NA, Lazebnik Y. Caspases: enemies within. Science. 1998; 281:1312–1316. [PubMed: 9721091]
16. Cohen GM. Caspases: the executioners of apoptosis. Biochem. J. 1997; 326:1–16. [PubMed: 9337844]
17. Adams JM, Cory S. The Bcl-2 protein family: arbiters of cell survival. Science. 1998; 281:1322–1326. [PubMed: 9735050]
18. Adams JM, Cory S. The Bcl-2 apoptotic switch in cancer development and therapy. Oncogene. 2007; 26:1324–1337. [PubMed: 17322918]
19. Lowe SW, Cepero E, Evan G. Intrinsic tumour suppression. Nature. 2004; 432:307–315. [PubMed: 15549092]
20. Ashkenazi A, Dixit VM. Death receptors: signaling and modulation. Science. 1998; 281:1305–1308. [PubMed: 9721089]
21. Chinnaiyan AM, O'Rourke K, Tewari M, Dixit VM. FADD, a novel death domain-containing protein, interacts with the death domain of Fas and initiates apoptosis. Cell. 1995; 81:505–512. [PubMed: 7538907]

22. Chang HY, Nishitoh H, Yang X, Ichijo H, Baltimore D. Activation of apoptosis signal-regulating kinase 1 (ASK1) by the adapter protein Daxx. Science. 1998; 281:1860–1863. [PubMed: 9743501]
23. Walczak H, Krammer PH. The CD95 (APO-1/Fas) and the TRAIL (APO-2L) apoptosis systems. Exp Cell Res. 2000; 256:58–66. [PubMed: 10739652]
24. Krueger A, Baumann S, Krammer PH, Kirchhoff S. FLICE-inhibitory proteins: regulators of death receptor-mediated apoptosis. Mol Cell Biol. 2001; 21:8247–8254. [PubMed: 11713262]
25. Araujo H, Danziger N, Cordier J, Glowinski J, Chneiweiss H. Characterization of PEA-15, a major substrate for protein kinase C in astrocytes. Journal of Biological Chemistry. 1993; 268:5911–5920. [PubMed: 8449955]
26. McDermott U, Longley DB, Galligan L, Allen W, Wilson T, Johnston PG. Effect of p53 status and STAT1 on chemotherapy-induced, Fas-mediated apoptosis in colorectal cancer. Cancer Res. 2005; 65:8951–8960. [PubMed: 16204068]
27. Ashkenazi A, Pai RC, Fong S, et al. Safety and antitumor activity of recombinant soluble Apo2 ligand. J Clin Invest. 1999; 104:155–162. [PubMed: 10411544]
28. Longley DB, Wilson TR, McEwan M, et al. c-FLIP inhibits chemotherapy-induced colorectal cancer cell death. Oncogene. 2006; 25:838–848. [PubMed: 16247474]
29. Green DR, Kroemer G. Cytoplasmic functions of the tumour suppressor p53. Nature. 2009; 458:1127–1130. [PubMed: 19407794]
30. Cory S, Adams JM. The Bcl2 family: regulators of the cellular life-or-death switch. Nat Rev Cancer. 2002; 2:647–656. [PubMed: 12209154]
31. Wei MC, Zong WX, Cheng EH, et al. Proapoptotic BAX and BAK: a requisite gateway to mitochondrial dysfunction and death. Science. 2001; 292:727–730. [PubMed: 11326099]
32. Lindsten T, Ross AJ, King A, et al. The combined functions of proapoptotic Bcl-2 family members bak and bax are essential for normal development of multiple tissues. Mol Cell. 2000; 6:1389–1399. [PubMed: 11163212]
33. Muchmore SW, Sattler M, Liang H, et al. X-ray and NMR structure of human Bcl-xL, an inhibitor of programmed cell death. Nature. 1996; 381:335–341. [PubMed: 8692274]
34. Sattler M, Liang H, Nettesheim D, et al. Structure of Bcl-xL-Bak peptide complex: recognition between regulators of apoptosis. Science. 1997; 275:983–986. [PubMed: 9020082]
35. Chou JJ, Li H, Salvesen GS, Yuan J, Wagner G. Solution structure of BID, an intracellular amplifier of apoptotic signaling. Cell. 1999; 96:615–624. [PubMed: 10089877]
36. McDonnell JM, Fushman D, Milliman CL, Korsmeyer SJ, Cowburn D. Solution structure of the proapoptotic molecule BID: a structural basis for apoptotic agonists and antagonists. Cell. 1999; 96:625–634. [PubMed: 10089878]
37. Richardson A, Kaye SB. Pharmacological inhibition of the Bcl-2 family of apoptosis regulators as cancer therapy. Curr Mol Pharmacol. 2008; 1:244–254. [PubMed: 20021437]
38. Chen L, Willis SN, Wei A, et al. Differential targeting of prosurvival Bcl-2 proteins by their BH3-only ligands allows complementary apoptotic function. Mol Cell. 2005; 17:393–403. [PubMed: 15694340]
39. Willis SN, Fletcher JI, Kaufmann T, et al. Apoptosis initiated when BH3 ligands engage multiple Bcl-2 homologs, not Bax or Bak. Science. 2007; 315:856–859. [PubMed: 17289999]
40. Franke TF, Cantley LC. Apoptosis. A Bad kinase makes good. Nature. 1997; 390:116–117. [PubMed: 9367147]
41. Certo M, Del Gaizo Moore V, Nishino M, et al. Mitochondria primed by death signals determine cellular addiction to antiapoptotic BCL-2 family members. Cancer Cell. 2006; 9:351–365. [PubMed: 16697956]
42. Deveraux QL, Reed JC. IAP family proteins-suppressors of apoptosis. Genes & Development. 1999; 13:239–252. [PubMed: 9990849]
43. Liston P, Fong WG, Korneluk RG. The inhibitors of apoptosis: there is more to life than Bcl2. Oncogene. 2003; 22:8568–8580. [PubMed: 14634619]
44. Srinivasula SM, Gupta S, Datta P, et al. Inhibitor of apoptosis proteins are substrates for the mitochondrial serine protease Omi/HtrA2. Journal of Biological Chemistry. 2003; 278:31469–31472. [PubMed: 12835328]

45. Altieri DC. Survivin and IAP proteins in cell-death mechanisms. Biochem J. 2010; 430:199–205. [PubMed: 20704571]
46. Yang L, Mashima T, Sato S, et al. Predominant suppression of apoptosome by inhibitor of apoptosis protein in non-small cell lung cancer H460 cells: therapeutic effect of a novel polyarginine-conjugated Smac peptide. Cancer Res. 2003; 63:831–837. [PubMed: 12591734]
47. Croce CM. Oncogenes and cancer. N Engl J Med. 2008; 358:502–511. [PubMed: 18234754]
48. Blume-Jensen P, Hunter T. Oncogenic kinase signalling. Nature. 2001; 411:355–365. [PubMed: 11357143]
49. Jorissen RN, Walker F, Pouliot N, Garrett TP, Ward CW, Burgess AW. Epidermal growth factor receptor: mechanisms of activation and signalling. Exp Cell Res. 2003; 284:31–53. [PubMed: 12648464]
50. Olayioye MA, Neve RM, Lane HA, Hynes NE. The ErbB signaling network: receptor heterodimerization in development and cancer. EMBO J. 2000; 19:3159–3167. [PubMed: 10880430]
51. Fresno Vara JA, Casado E, de Castro J, Cejas P, Belda-Iniesta C, Gonzalez-Baron M. PI3K/Akt signalling pathway and cancer. Cancer Treat Rev. 2004; 30:193–204. [PubMed: 15023437]
52. Lin A, Karin M. NF-kappaB in cancer: a marked target. Semin Cancer Biol. 2003; 13:107–114. [PubMed: 12654254]
53. Burgering BM, Medema RH. Decisions on life and death: FOXO Forkhead transcription factors are in command when PKB/Akt is off duty. J Leukoc Biol. 2003; 73:689–701. [PubMed: 12773501]
54. Grandis JR, Drenning SD, Zeng Q, et al. Constitutive activation of Stat3 signaling abrogates apoptosis in squamous cell carcinogenesis in vivo. Proc Natl Acad Sci U S A. 2000; 97:4227–4232. [PubMed: 10760290]
55. Aoki Y, Feldman GM, Tosato G. Inhibition of STAT3 signaling induces apoptosis and decreases survivin expression in primary effusion lymphoma. Blood. 2003; 101:1535–1542. [PubMed: 12393476]
56. Yu H, Jove R. The STATs of cancer--new molecular targets come of age. Nat Rev Cancer. 2004; 4:97–105. [PubMed: 14964307]
57. Berenson JR, Ma HM, Vescio R. The role of nuclear factor-kappaB in the biology and treatment of multiple myeloma. Semin Oncol. 2001; 28:626–633. [PubMed: 11740821]
58. Mitsiades CS, Mitsiades N, Koutsilieris M. The Akt pathway: molecular targets for anti-cancer drug development. Curr Cancer Drug Targets. 2004; 4:235–256. [PubMed: 15134532]
59. Ponzielli R, Katz S, Barsyte-Lovejoy D, Penn LZ. Cancer therapeutics: Targeting the dark side of Myc. European Journal of Cancer. 2005; 41:2485–2501. [PubMed: 16243519]
60. Napoli C, Lemieux C, Jorgensen R. Introduction of a Chimeric Chalcone Synthase Gene into Petunia Results in Reversible Co-Suppression of Homologous Genes in trans. Plant Cell. 1990; 2:279–289. [PubMed: 12354959]
61. Guo S, Kemphues KJ. Par-1, a Gene Required for Establishing Polarity in C-Elegans Embryos, Encodes a Putative Ser/Thr Kinase That Is Asymmetrically Distributed. Cell. 1995; 81:611–620. [PubMed: 7758115]
62. Bertrand JR, Pottier M, Vekris A, Opolon P, Maksimenko A, Malvy C. Comparison of antisense oligonucleotides and siRNAs in cell culture and in vivo. Biochemical and Biophysical Research Communications. 2002; 296:1000–1004. [PubMed: 12200148]
63. Hammond SM, Bernstein E, Beach D, Hannon GJ. An RNA-directed nuclease mediates post-transcriptional gene silencing in Drosophila cells. Nature. 2000; 404:293–296. [PubMed: 10749213]
64. Elbashir SM, Harborth J, Lendeckel W, Yalcin A, Weber K, Tuschl T. Duplexes of 21-nucleotide RNAs mediate RNA interference in cultured mammalian cells. Nature. 2001; 411:494–498. [PubMed: 11373684]
65. Vogl, DT.; Gewirtz, AM. Nucleic Acid Therapies for Cancer Treatment. Totowa, N.J: Humana; 2008.

66. Paddison PJ, Caudy AA, Bernstein E, Hannon GJ, Conklin DS. Short hairpin RNAs (shRNAs) induce sequence-specific silencing in mammalian cells. Genes Dev. 2002; 16:948–958. [PubMed: 11959843]
67. Bernstein E, Caudy AA, Hammond SM, Hannon GJ. Role for a bidentate ribonuclease in the initiation step of RNA interference. Nature. 2001; 409:363–366. [PubMed: 11201747]
68. Elbashir SM, Lendeckel W, Tuschl T. RNA interference is mediated by 21-and 22-nucleotide RNAs. Genes & Development. 2001; 15:188–200. [PubMed: 11157775]
69. Bouillet P, Cory S, Zhang LC, Strasser A, Adams JM. Degenerative disorders caused by Bcl-2 deficiency prevented by loss of its BH3-only antagonist Bim. Dev Cell. 2001; 1:645–653. [PubMed: 11709185]
70. Bold RJ, Chandra J, McConkey DJ. Gemcitabine-induced programmed cell death (apoptosis) of human pancreatic carcinoma is determined by Bcl-2 content. Ann Surg Oncol. 1999; 6:279–285. [PubMed: 10340887]
71. Strasser A, Harris AW, Bath ML, Cory S. Novel primitive lymphoid tumours induced in transgenic mice by cooperation between myc and bcl-2. Nature. 1990; 348:331–333. [PubMed: 2250704]
72. Amundson SA, Myers TG, Scudiero D, Kitada S, Reed JC, Fornace AJ Jr. An informatics approach identifying markers of chemosensitivity in human cancer cell lines. Cancer Res. 2000; 60:6101–6110. [PubMed: 11085534]
73. Kirkin V, Joos S, Zornig M. The role of Bcl-2 family members in tumorigenesis. Biochim Biophys Acta. 2004; 1644:229–249. [PubMed: 14996506]
74. Vaux DL, Cory S, Adams JM. Bcl-2 gene promotes haemopoietic cell survival and cooperates with c-myc to immortalize pre-B cells. Nature. 1988; 335:440–442. [PubMed: 3262202]
75. Tracey L, Perez-Rosado A, Artiga MJ, et al. Expression of the NF-kappaB targets BCL2 and BIRC5/Survivin characterizes small B-cell and aggressive B-cell lymphomas, respectively. J Pathol. 2005; 206:123–134. [PubMed: 15880597]
76. Reed JC, Kitada S, Takayama S, Miyashita T. Regulation of chemoresistance by the bcl-2 oncoprotein in non-Hodgkin's lymphoma and lymphocytic leukemia cell lines. Ann Oncol. 1994; 5(Suppl 1):61–65. [PubMed: 8172820]
77. Gascoyne RD, Adomat SA, Krajewski S, et al. Prognostic significance of Bcl-2 protein expression and Bcl-2 gene rearrangement in diffuse aggressive non-Hodgkin's lymphoma. Blood. 1997; 90:244–251. [PubMed: 9207459]
78. Cosulich SC, Worrall V, Hedge PJ, Green S, Clarke PR. Regulation of apoptosis by BH3 domains in a cell-free system. Curr Biol. 1997; 7:913–920. [PubMed: 9382837]
79. Duvall CL, Convertine AJ, Benoit DSW, Hoffman AS, Stayton PS. Intracellular Delivery of a Proapoptotic Peptide via Conjugation to a RAFT Synthesized Endosomolytic Polymer. Molecular Pharmaceutics. 2010; 7:468–476. [PubMed: 19968323]
80. Al-Taei S, Penning NA, Simpson JC, et al. Intracellular traffic and fate of protein transduction domains HIV-1 TAT peptide and octaarginine. Implications for their utilization as drug delivery vectors. Bioconjug Chem. 2006; 17:90–100. [PubMed: 16417256]
81. Belting M, Sandgren S, Wittrup A. Nuclear delivery of macromolecules: barriers and carriers. Adv Drug Deliv Rev. 2005; 57:505–527. [PubMed: 15722161]
82. Flynn CR, Cheung-Flynn J, Smoke CC, et al. Internalization and intracellular trafficking of a PTD-conjugated anti-fibrotic peptide, AZX100, in human dermal keloid fibroblasts. J Pharm Sci. 2010; 99:3100–3121. [PubMed: 20140957]
83. Tokatlian T, Segura T. siRNA applications in nanomedicine. Wiley Interdiscip Rev Nanomed Nanobiotechnol. 2010; 2:305–315. [PubMed: 20135697]
84. Opanasopit P, Nishikawa M, Hashida M. Factors affecting drug and gene delivery: effects of interaction with blood components. Crit Rev Ther Drug Carrier Syst. 2002; 19:191–233. [PubMed: 12627613]
85. Owens III DE, Peppas NA. Opsonization, biodistribution, and pharmacokinetics of polymeric nanoparticles. International Journal of Pharmaceutics. 2006; 307:93–102. [PubMed: 16303268]
86. Pliquett UF, Gusbeth CA. Perturbation of human skin due to application of high voltage. Bioelectrochem. 2000; 51:41–51.

87. Rols MP, Delteil C, Golzio M, Dumond P, Cros S, Teissie J. In vivo electrically mediated protein and gene transfer in murine melanoma. Nature Biotechnology. 1998; 16:168–171.

88. Cahill K. Cell-penetrating peptides, electroporation and drug delivery. Iet Systems Biology. 2010; 4:367–378. [PubMed: 21073236]

89. Banga AK, Prausnitz MR. Assessing the potential of skin electroporation for the delivery of protein- and gene-based drugs. Trends in Biotechnology. 1998; 16:408–412. [PubMed: 9807837]

90. Fyrberg A, Lotfi K. Optimization and evaluation of electroporation delivery of siRNA in the human leukemic CEM cell line. Cytotechnology. 2010; 62:497–507. [PubMed: 20957432]

91. Huang HA, Wei ZW, Huang YY, et al. An efficient and high-throughput electroporation microchip applicable for siRNA delivery. Lab on a Chip. 2011; 11:163–172. [PubMed: 20957267]

92. Harding CV. Electroporation of Exogenous Antigen into the Cytosol for Antigen Processing and Class-I Major Histocompatibility Complex (Mhc) Presentation - Weak Base Amines and Hypothermia (18-Degrees-C) Inhibit the Class-I Mhc Processing Pathway. European Journal of Immunology. 1992; 22:1865–1869. [PubMed: 1623927]

93. Lukas J, Bartek J, Strauss M. Efficient Transfer of Antibodies into Mammalian-Cells by Electroporation. Journal of Immunological Methods. 1994; 170:255–259. [PubMed: 8158003]

94. Potter H. Electroporation in Biology - Methods, Applications, and Instrumentation. Analytical Biochemistry. 1988; 174:361–373. [PubMed: 3071177]

95. Chakrabarti R, Wylie DE, Schuster SM. Transfer of Monoclonal-Antibodies into Mammalian-Cells by Electroporation. Journal of Biological Chemistry. 1989; 264:15494–15500. [PubMed: 2768274]

96. Kigasawa K, Kajimoto K, Hama S, Saito A, Kanamura K, Kogure K. Noninvasive delivery of siRNA into the epidermis by iontophoresis using an atopic dermatitis-like model rat. International Journal of Pharmaceutics. 2010; 383:157–160. [PubMed: 19732811]

97. Langkjaer L, Brange J, Grodsky GM, Guy RH. Iontophoresis of monomeric insulin analogues in vitro: effects of insulin charge and skin pretreatment. Journal of Controlled Release. 1998; 51:47–56. [PubMed: 9685903]

98. Degim IT, Celebi N. Controlled delivery of peptides and proteins. Current Pharmaceutical Design. 2007; 13:99–117. [PubMed: 17266590]

99. Kari B. Control of Blood-Glucose Levels in Alloxan-Diabetic Rabbits by Iontophoresis of Insulin. Diabetes. 1986; 35:217–221. [PubMed: 3510926]

100. Hao JS, Li SK, Liu CY, Kao WWY. Electrically assisted delivery of macromolecules into the corneal epithelium. Experimental Eye Research. 2009; 89:934–941. [PubMed: 19682448]

101. Mitragotri S, Kost J. Low frequency sonophoresis: A noninvasive method of drug delivery and diagnostics. Biotechnology Progress. 2000; 16:488–492. [PubMed: 10835253]

102. Fretz MM, Hogset A, Koning GA, Jiskoot W, Storm G. Cytosolic delivery of liposomally targeted proteins induced by photochemical internalization. Pharmaceutical Research. 2007; 24:2040–2047. [PubMed: 17541733]

103. Berg K, Moan J. Lysosomes as photochemical targets. Int J Cancer. 1994; 59:814–822. [PubMed: 7989124]

104. Berg K, Dietze A, Kaalhus O, Hogset A. Site-specific drug delivery by photochemical internalization enhances the antitumor effect of bleomycin. Clin Cancer Res. 2005; 11:8476–8485. [PubMed: 16322311]

105. Selbo PK, Sandvig K, Kirveliene V, Berg K. Release of gelonin from endosomes and lysosomes to cytosol by photochemical internalization. Biochim Biophys Acta. 2000; 1475:307–313. [PubMed: 10913830]

106. Raemdonck K, Naeye B, Hogset A, Demeester J, De Smedt SC. Prolonged gene silencing by combining siRNA nanogels and photochemical internalization. Journal of Controlled Release. 2010; 145:281–288. [PubMed: 20403396]

107. Lee WR, Pan TL, Wang PW, Zhuo RZ, Huang CM, Fang JY. Erbium:YAG laser enhances transdermal peptide delivery and skin vaccination. Journal of Controlled Release. 2008; 128:200–208. [PubMed: 18471920]

108. Lee WR, Shen SC, Lai HH, Hu CH, Fang JY. Transdermal drug delivery enhanced and controlled by erbium:YAG laser: a comparative study of lipophilic and hydrophilic drugs. Journal of Controlled Release. 2001; 75:155–166. [PubMed: 11451505]
109. Fang JY, Lee WR, Shen SC, Fang YP, Hu CH. Enhancement of topical 5-aminolaevulinic acid delivery by erbium:YAG laser and microdermabrasion: a comparison with iontophoresis and electroporation. Br J Dermatol. 2004; 151:132–140. [PubMed: 15270882]
110. Lee WR, Shen SC, Zhuo RZ, Wang KC, Fang JY. Enhancement of Topical Small Interfering RNA Delivery and Expression by Low-Fluence Erbium: YAG Laser Pretreatment of Skin. Human Gene Therapy. 2009; 20:580–588. [PubMed: 19239381]
111. Green M, Loewenstein PM. Autonomous Functional Domains of Chemically Synthesized Human Immunodeficiency Virus Tat Trans-Activator Protein. Cell. 1988; 55:1179–1188. [PubMed: 2849509]
112. Frankel AD, Pabo CO. Cellular Uptake of the Tat Protein from Human Immunodeficiency Virus. Cell. 1988; 55:1189–1193. [PubMed: 2849510]
113. Derossi D, Joliot AH, Chassaing G, Prochiantz A. The 3rd Helix of the Antennapedia Homeodomain Translocates through Biological-Membranes. Journal of Biological Chemistry. 1994; 269:10444–10450. [PubMed: 8144628]
114. El-Sayed A, Futaki S, Harashima H. Delivery of Macromolecules Using Arginine-Rich Cell-Penetrating Peptides: Ways to Overcome Endosomal Entrapment. Aaps Journal. 2009; 11:13–22. [PubMed: 19125334]
115. Lopes LB, Flynn C, Komalavilas P, Panitch A, Brophy CM, Seal BL. Inhibition of HSP27 phosphorylation by a cell-permeant MAPKAP Kinase 2 inhibitor. Biochemical and Biophysical Research Communications. 2009; 382:535–539. [PubMed: 19289101]
116. Nishikawa M, Otsuki T, Ota A, et al. Induction of Tumor-specific Immune Response by Gene Transfer of Hsp70-cell-penetrating Peptide Fusion Protein to Tumors in Mice. Molecular Therapy. 2010; 18:421–428. [PubMed: 19724264]
117. De Coupade C, Fittipaldi A, Chagnas V, et al. Novel human-derived cell-penetrating peptides for specific subcellular delivery of therapeutic biomolecules. Biochemical Journal. 2005; 390:407–418. [PubMed: 15859953]
118. Saalik P, Elmquist A, Hansen M, et al. Protein cargo delivery properties of cell-penetrating peptides. A comparative study. Bioconjugate Chemistry. 2004; 15:1246–1253. [PubMed: 15546190]
119. Banoczi Z, Gorka-Kereskenyi A, Remenyi J, et al. Synthesis and in Vitro Antitumor Effect of Vinblastine Derivative-Oligoarginine Conjugates. Bioconjugate Chemistry. 2010; 21:1948–1955. [PubMed: 20973492]
120. Yu HH, Nakase I, Pujals S, et al. Expressed protein ligation for the preparation of fusion proteins with cell penetrating peptides for endotoxin removal and intracellular delivery. Biochimica Et Biophysica Acta-Biomembranes. 2010; 1798:2249–2257.
121. Heitz F, Morris MC, Divita G. Twenty years of cell-penetrating peptides: from molecular mechanisms to therapeutics. British Journal of Pharmacology. 2009; 157:195–206. [PubMed: 19309362]
122. Patel LN, Zaro JL, Shen WC. Cell penetrating peptides: Intracellular pathways and pharmaceutical perspectives. Pharmaceutical Research. 2007; 24:1977–1992. [PubMed: 17443399]
123. Fuchs SM, Raines RT. Pathway for polyarginine entry into mammalian cell. Biochemistry. 2004; 43:2438–2444. [PubMed: 14992581]
124. Raagel H, Saalik P, Pooga M. Peptide-mediated protein delivery-Which pathways are penetrable? Biochimica Et Biophysica Acta-Biomembranes. 2010; 1798:2240–2248.
125. Duvall CL, Convertine AJ, Benoit DS, Hoffman AS, Stayton PS. Intracellular delivery of a proapoptotic peptide via conjugation to a RAFT synthesized endosomolytic polymer. Mol Pharm. 2010; 7:468–476. [PubMed: 19968323]
126. Torchilin VP. Cell penetrating peptide-modified pharmaceutical nanocarriers for intracellular drug and gene delivery. Biopolymers. 2008; 90:604–610. [PubMed: 18381624]

127. Convertine AJ, Benoit DSW, Duvall CL, Hoffman AS, Stayton PS. Development of a novel endosomolytic diblock copolymer for siRNA delivery. Journal of Controlled Release. 2009; 133:221–229. [PubMed: 18973780]
128. Futaki S, Masui Y, Nakase I, et al. Unique features of a pH-sensitive fusogenic peptide that improves the transfection efficiency of cationic liposomes. Journal of Gene Medicine. 2005; 7:1450–1458. [PubMed: 16025556]
129. Kyriakides TR, Cheung CY, Murthy N, Bornstein P, Stayton PS, Hoffman AS. pH-sensitive polymers that enhance intracellular drug delivery in vivo. Journal of Controlled Release. 2002; 78:295–303. [PubMed: 11772470]
130. Ward B, Seal BL, Brophy CM, Panitch A. Design of a bioactive cell-penetrating peptide: when a transduction domain does more than transduce. Journal of Peptide Science. 2009; 15:668–674. [PubMed: 19691016]
131. Holm T, Raagel H, Andaloussi SE, et al. Retro-inversion of certain cell-penetrating peptides causes severe cellular toxicity. Biochim Biophys Acta. 2010
132. Huang S, Liu YW, Jiang Y. Cell penetrating peptides in cancer therapy. Sheng Li Ke Xue Jin Zhan. 2007; 38:301–306. [PubMed: 18232298]
133. Myrberg H, Zhang L, Mae M, Langel U. Design of a tumor-homing cell-penetrating peptide. Bioconjug Chem. 2008; 19:70–75. [PubMed: 18001077]
134. Bitler BG, Schroeder JA. Anti-cancer therapies that utilize cell penetrating peptides. Recent Pat Anticancer Drug Discov. 2010; 5:99–108. [PubMed: 19961434]
135. Li W, Nicol F, Szoka FC Jr. GALA: a designed synthetic pH-responsive amphipathic peptide with applications in drug and gene delivery. Adv Drug Deliv Rev. 2004; 56:967–985. [PubMed: 15066755]
136. Top D, de Antueno R, Salsman J, et al. Liposome reconstitution of a minimal protein-mediated membrane fusion machine. EMBO J. 2005; 24:2980–2988. [PubMed: 16079913]
137. Van Rossenberg SM, Sliedregt-Bol KM, Meeuwenoord NJ, et al. Targeted lysosome disruptive elements for improvement of parenchymal liver cell-specific gene delivery. Journal of Biological Chemistry. 2002; 277:45803–45810. [PubMed: 12237290]
138. Efremov RG, Nolde DE, Volynsky PE, Chernyavsky AA, Dubovskii PV, Arseniev AS. Factors important for fusogenic activity of peptides: molecular modeling study of analogs of fusion peptide of influenza virus hemagglutinin. Febs Letters. 1999; 462:205–210. [PubMed: 10580120]
139. Monsigny M, Roche AC, Midoux P, Mayer R. Glycoconjugates as Carriers for Specific Delivery of Therapeutic Drugs and Genes. Advanced Drug Delivery Reviews. 1994; 14:1–24.
140. Plank C, Oberhauser B, Mechtler K, Koch C, Wagner E. The Influence of Endosome-Disruptive Peptides on Gene-Transfer Using Synthetic Virus-Like Gene-Transfer Systems. Journal of Biological Chemistry. 1994; 269:12918–12924. [PubMed: 8175709]
141. Wyman TB, Nicol F, Zelphati O, Scaria PV, Plank C, Szoka FC Jr. Design, synthesis, and characterization of a cationic peptide that binds to nucleic acids and permeabilizes bilayers. Biochemistry. 1997; 36:3008–3017. [PubMed: 9062132]
142. Turk MJ, Reddy JA, Chmielewski JA, Low PS. Characterization of a novel pH-sensitive peptide that enhances drug release from folate-targeted liposomes at endosomal pHs. Biochim Biophys Acta. 2002; 1559:56–68. [PubMed: 11825588]
143. Niidome T, Takaji K, Urakawa M, et al. Chain length of cationic alpha-helical peptide sufficient for gene delivery into cells. Bioconjug Chem. 1999; 10:773–780. [PubMed: 10502342]
144. Rittner K, Benavente A, Bompard-Sorlet A, et al. New basic membrane-destabilizing peptides for plasmid-based gene delivery in vitro and in vivo. Molecular Therapy. 2002; 5:104–114. [PubMed: 11829517]
145. Kichler A, Leborgne C, Marz J, Danos O, Bechinger B. Histidine-rich amphipathic peptide antibiotics promote efficient delivery of DNA into mammalian cells. Proc Natl Acad Sci U S A. 2003; 100:1564–1568. [PubMed: 12563034]
146. Pillot T, Goethals M, Vanloo B, et al. Fusogenic properties of the C-terminal domain of the Alzheimer beta-amyloid peptide. Journal of Biological Chemistry. 1996; 271:28757–28765. [PubMed: 8910517]

147. Ogris M, Carlisle RC, Bettinger T, Seymour LW. Melittin enables efficient vesicular escape and enhanced nuclear access of nonviral gene delivery vectors. Journal of Biological Chemistry. 2001; 276:47550–47555. [PubMed: 11600500]

148. Chen CP, Kim JS, Steenblock E, Liu DJ, Rice KG. Gene transfer with poly-melittin peptides. Bioconjugate Chemistry. 2006; 17:1057–1062. [PubMed: 16848415]

149. Marty C, Meylan C, Schott H, Ballmer-Hofer K, Schwendener RA. Enhanced heparan sulfate proteoglycan-mediated uptake of cell-penetrating peptide-modified liposomes. Cellular and Molecular Life Sciences. 2004; 61:1785–1794. [PubMed: 15241554]

150. Ayame H, Morimoto N, Akiyoshi K. Self-assembled cationic nanogels for intracellular protein delivery. Bioconjugate Chemistry. 2008; 19:882–890. [PubMed: 18336000]

151. Zhao PQ, Wang HJ, Yu M, et al. Paclitaxel-Loaded, Folic-Acid-Targeted and TAT-Peptide-Conjugated Polymeric Liposomes: In Vitro and In Vivo Evaluation. Pharmaceutical Research. 2010; 27:1914–1926. [PubMed: 20582454]

152. El-Sayed A, Khalil IA, Kogure K, Futaki S, Harashima H. Octaarginine- and octalysine-modified nanoparticles have different modes of endosomal escape. Journal of Biological Chemistry. 2008; 283:23450–23461. [PubMed: 18550548]

153. Kuai R, Yuan WM, Qin Y, et al. Efficient Delivery of Payload into Tumor Cells in a Controlled Manner by TAT and Thiolytic Cleavable PEG Co-Modified Liposomes. Molecular Pharmaceutics. 2010; 7:1816–1826. [PubMed: 20701288]

154. Ko YT, Falcao C, Torchilin VP. Cationic Liposomes Loaded with Proapoptotic Peptide D-(KLAKLAK)(2) and Bcl-2 Antisense Oligodeoxynucleotide G3139 for Enhanced Anticancer Therapy. Molecular Pharmaceutics. 2009; 6:971–977. [PubMed: 19317442]

155. Yamada Y, Akita H, Kogure K, Kamiya H, Harashima H. Mitochondrial drug delivery and mitochondrial disease therapy - An approach to liposome-based delivery targeted to mitochondria. Mitochondrion. 2007; 7:63–71. [PubMed: 17296332]

156. Huang Z, King MR. An immobilized nanoparticle-based platform for efficient gene knockdown of targeted cells in the circulation. Gene Ther. 2009; 16:1271–1282. [PubMed: 19554031]

157. Peer D, Park EJ, Morishita Y, Carman CV, Shimaoka M. Systemic leukocyte-directed siRNA delivery revealing cyclin D1 as an anti-inflammatory target. Science. 2008; 319:627–630. [PubMed: 18239128]

158. Immordino ML, Dosio F, Cattel L. Stealth liposomes: review of the basic science, rationale, and clinical applications, existing and potential. Int J Nanomedicine. 2006; 1:297–315. [PubMed: 17717971]

159. Judge AD, Sood V, Shaw JR, Fang D, McClintock K, MacLachlan I. Sequence-dependent stimulation of the mammalian innate immune response by synthetic siRNA. Nat Biotechnol. 2005; 23:457–462. [PubMed: 15778705]

160. Samad A, Sultana Y, Aqil M. Liposomal drug delivery systems: an update review. Curr Drug Deliv. 2007; 4:297–305. [PubMed: 17979650]

161. Morrissey DV, Lockridge JA, Shaw L, et al. Potent and persistent in vivo anti-HBV activity of chemically modified siRNAs. Nat Biotechnol. 2005; 23:1002–1007. [PubMed: 16041363]

162. Chen Y, Bathula SR, Li J, Huang L. Multifunctional nanoparticles delivering small interfering RNA and doxorubicin overcome drug resistance in cancer. J Biol Chem. 2010; 285:22639–22650. [PubMed: 20460382]

163. Chen Y, Sen J, Bathula SR, Yang Q, Fittipaldi R, Huang L. Novel cationic lipid that delivers siRNA and enhances therapeutic effect in lung cancer cells. Mol Pharm. 2009; 6:696–705. [PubMed: 19267451]

164. Mori A. Biochemistry and neurotoxicology of guanidino compounds. History and recent advances. Pavlov J Biol Sci. 1987; 22:85–94. [PubMed: 2821470]

165. Wartenberg M, Ling FC, Schallenberg M, et al. Down-regulation of intrinsic P-glycoprotein expression in multicellular prostate tumor spheroids by reactive oxygen species. J Biol Chem. 2001; 276:17420–17428. [PubMed: 11279018]

166. Cai Y, Lu J, Miao Z, Lin L, Ding J. Reactive oxygen species contribute to cell killing and P-glycoprotein downregulation by salvicine in multidrug resistant K562/A02 cells. Cancer Biol Ther. 2007; 6:1794–1799. [PubMed: 18032928]

167. Song WJ, Du JZ, Sun TM, Zhang PZ, Wang J. Gold nanoparticles capped with polyethyleneimine for enhanced siRNA delivery. Small. 2010; 6:239–246. [PubMed: 19924738]

168. Derfus AM, Chen AA, Min D-H, Ruoslahti E, Bhatia SN. Targeted Quantum Dot Conjugates for siRNA Delivery. Bioconjugate Chemistry. 2007; 18:1391–1396. [PubMed: 17630789]

169. Yezhelyev MV, Qi L, Oâ€™Regan RM, Nie S, Gao X. Proton-Sponge Coated Quantum Dots for siRNA Delivery and Intracellular Imaging. Journal of the American Chemical Society. 2008; 130:9006–9012. [PubMed: 18570415]

170. Takeshita F, Minakuchi Y, Nagahara S, et al. Efficient delivery of small interfering RNA to bone-metastatic tumors by using atelocollagen in vivo. Proc Natl Acad Sci U S A. 2005; 102:12177–12182. [PubMed: 16091473]

171. Takeshita F, Ochiya T. Therapeutic potential of RNA interference against cancer. Cancer Sci. 2006; 97:689–696. [PubMed: 16863503]

172. Noh SM, Han SE, Shim G, et al. Tocopheryl oligochitosan-based self assembling oligomersomes for siRNA delivery. Biomaterials. 2011; 32:849–857. [PubMed: 20926129]

173. Kong WH, Sung DK, Shim YH, et al. Efficient intracellular siRNA delivery strategy through rapid and simple two steps mixing involving noncovalent post-PEGylation. Journal of Controlled Release. 2009; 138:141–147. [PubMed: 19426771]

174. Nam HY, McGinn A, Kim PH, Kim SW, Bull DA. Primary cardiomyocyte-targeted bioreducible polymer for efficient gene delivery to the myocardium. Biomaterials. 2010; 31:8081–8087. [PubMed: 20674007]

175. Christensen LV, Chang CW, Kim WJ, et al. Reducible poly(amido ethylenimine)s designed for triggered intracellular gene delivery. Bioconjug Chem. 2006; 17:1233–1240. [PubMed: 16984133]

176. Thomas JL, Barton SW, Tirrell DA. Membrane Solubilization by a Hydrophobic Polyelectrolyte - Surface-Activity and Membrane-Binding. Biophysical Journal. 1994; 67:1101–1106. [PubMed: 7811920]

177. Thomas JL, Tirrell DA. Polyelectrolyte-Sensitized Phospholipid-Vesicles. Accounts of Chemical Research. 1992; 25:336–342.

178. Borden KA, Eum KM, Langley KH, Tirrell DA. Interactions of Synthetic-Polymers with Cell-Membranes + Model Membrane Systems .13. On the Mechanism of Polyelectrolyte-Induced Structural Reorganization in Thin Molecular Films. Macromolecules. 1987; 20:454–456.

179. Lackey CA, Press OW, Hoffman AS, Stayton PS. A biomimetic pH-responsive polymer directs endosomal release and intracellular delivery of an endocytosed antibody complex. Bioconjugate Chemistry. 2002; 13:996–1001. [PubMed: 12236781]

180. Akinc A, Thomas M, Klibanov AM, Langer R. Exploring polyethylenimine-mediated DNA transfection and the proton sponge hypothesis. Journal of Gene Medicine. 2005; 7:657–663. [PubMed: 15543529]

181. Lackey CA, Murthy N, Press OW, Tirrell DA, Hoffman AS, Stayton PS. Hemolytic activity of pH-responsive polymer-streptavidin bioconjugates. Bioconjugate Chemistry. 1999; 10:401–405. [PubMed: 10346870]

182. Henry SM, El-Sayed MEH, Pirie CM, Hoffman AS, Stayton PS. pH-responsive poly(styrene-alt-maleic anhydride) alkylamide copolymers for intracellular drug delivery. Biomacromolecules. 2006; 7:2407–2414. [PubMed: 16903689]

183. Murthy N, Campbell J, Fausto N, Hoffman AS, Stayton PS. Bioinspired pH-responsive polymers for the intracellular delivery of biomolecular drugs. Bioconjug Chem. 2003; 14:412–419. [PubMed: 12643752]

184. Murthy N, Campbell J, Fausto N, Hoffman AS, Stayton PS. Design and synthesis of pH-responsive polymeric carriers that target uptake and enhance the intracellular delivery of oligonucleotides. Journal of Controlled Release. 2003; 89:365–374. [PubMed: 12737839]

185. Foster S, Duvall CL, Crownover EF, Hoffman AS, Stayton PS. Intracellular Delivery of a Protein Antigen with an Endosomal-Releasing Polymer Enhances CD8 T-Cell Production and Prophylactic Vaccine Efficacy. Bioconjug Chem.

186. Convertine AJ, Diab C, Prieve M, et al. pH-Responsive Polymeric Micelle Carriers for siRNA Drugs. Biomacromolecules. 11:2904–2911.

187. Behr JP. The proton sponge: a means to enter cells viruses never thought of. Med Sci. 1996; 12:56–58.

188. Wagner E, Ogris M, Zauner W. Polylysine-based transfection systems utilizing receptor-mediated delivery. Adv Drug Deliv Rev. 1998; 30:97–113. [PubMed: 10837605]

189. Boussif O, Zanta MA, Behr JP. Optimized galenics improve in vitro gene transfer with cationic molecules up to 1000-fold. Gene Therapy. 1996; 3:1074–1080. [PubMed: 8986433]

190. Harada Y, Iwai M, Tanaka S, et al. Highly efficient suicide gene expression in hepatocellular carcinoma cells by epstein-barr virus-based plasmid vectors combined with polyamidoamine dendrimer. Cancer Gene Ther. 2000; 7:27–36. [PubMed: 10678353]

191. Anderson DG, Akinc A, Hossain N, Langer R. Structure/property studies of polymeric gene delivery using a library of poly(beta-amino esters). Molecular Therapy. 2005; 11:426–434. [PubMed: 15727939]

192. Wang CY, Huang L. Polyhistidine Mediates an Acid-Dependent Fusion of Negatively Charged Liposomes. Biochemistry. 1984; 23:4409–4416. [PubMed: 6487609]

193. Pichon C, Goncalves C, Midoux P. Histidine-rich peptides and polymers for nucleic acids delivery. Advanced Drug Delivery Reviews. 2001; 53:75–94. [PubMed: 11733118]

194. Midoux P, Kichler A, Boutin V, Maurizot JC, Monsigny M. Membrane permeabilization and efficient gene transfer by a peptide containing several histidines. Bioconjugate Chemistry. 1998; 9:260–267. [PubMed: 9548543]

195. Fischer D, Bieber T, Li Y, Elsasser HP, Kissel T. A novel non-viral vector for DNA delivery based on low molecular weight, branched polyethylenimine: effect of molecular weight on transfection efficiency and cytotoxicity. Pharm Res. 1999; 16:1273–1279. [PubMed: 10468031]

196. Kunath K, von Harpe A, Fischer D, et al. Low-molecular-weight polyethylenimine as a non-viral vector for DNA delivery: comparison of physicochemical properties, transfection efficiency and in vivo distribution with high-molecular-weight polyethylenimine. J Control Release. 2003; 89:113–125. [PubMed: 12695067]

197. Turunen MP, Hiltunen MO, Ruponen M, et al. Efficient adventitial gene delivery to rabbit carotid artery with cationic polymer-plasmid complexes. Gene Ther. 1999; 6:6–11. [PubMed: 10341870]

198. Creusat G, Rinaldi AS, Weiss E, et al. Proton sponge trick for pH-sensitive disassembly of polyethylenimine-based siRNA delivery systems. Bioconjug Chem. 21:994–1002. [PubMed: 20481503]

199. Meyer M, Philipp A, Oskuee R, Schmidt C, Wagner E. Breathing life into polycations: Functionalization with pH-responsive endosomolytic peptides and polyethylene glycol enables siRNA delivery. Journal of the American Chemical Society. 2008; 130:3272-+. [PubMed: 18288843]

200. Pack DW, Putnam D, Langer R. Design of imidazole-containing endosomolytic biopolymers for gene delivery. Biotechnol Bioeng. 2000; 67:217–223. [PubMed: 10592519]

201. Putnam D, Gentry CA, Pack DW, Langer R. Polymer-based gene delivery with low cytotoxicity by a unique balance of side-chain termini. Proc Natl Acad Sci U S A. 2001; 98:1200–1205. [PubMed: 11158617]

202. Beyerle A, Merkel O, Stoeger T, Kissel T. PEGylation affects cytotoxicity and cell-compatibility of poly(ethylene imine) for lung application: structure-function relationships. Toxicol Appl Pharmacol. 2010; 242:146–154. [PubMed: 19822165]

203. Lynn DM, Langer R. Degradable poly(beta-amino esters): Synthesis, characterization, and self-assembly with plasmid DNA. Journal of the American Chemical Society. 2000; 122:10761–10768.

204. Vandenbroucke RE, De Geest BG, Bonne S, et al. Prolonged gene silencing in hepatoma cells and primary hepatocytes after small interfering RNA delivery with biodegradable poly(beta-amino esters). J Gene Med. 2008; 10:783–794. [PubMed: 18470950]

205. Burke RS, Pun SH. Extracellular Barriers to in Vivo PEI and PEGylated PEI Polyplex-Mediated Gene Delivery to the Liver. Bioconjugate Chemistry. 2008; 19:693–704. [PubMed: 18293906]

206. Xu L, Anchordoquy T. Drug delivery trends in clinical trials and translational medicine: Challenges and opportunities in the delivery of nucleic acid-based therapeutics. J Pharm Sci. 2011; 100:38–52. [PubMed: 20575003]

207. Yan X, Scherphof GL, Kamps JA. Liposome opsonization. J Liposome Res. 2005; 15:109–139. [PubMed: 16194930]

208. Li SD, Huang L. Nanoparticles evading the reticuloendothelial system: role of the supported bilayer. Biochim Biophys Acta. 2009; 1788:2259–2266. [PubMed: 19595666]

209. Zhang Y, Li H, Sun J, et al. DC-Chol/DOPE cationic liposomes: a comparative study of the influence factors on plasmid pDNA and siRNA gene delivery. Int J Pharm. 2010; 390:198–207. [PubMed: 20116418]

210. Naeye B, Raemdonck K, Remaut K, Sproat B, Demeester J, De Smedt SC. PEGylation of biodegradable dextran nanogels for siRNA delivery. Eur J Pharm Sci. 2010; 40:342–351. [PubMed: 20435139]

211. Wang XL, Xu R, Lu ZR. A peptide-targeted delivery system with pH-sensitive amphiphilic cell membrane disruption for efficient receptor-mediated siRNA delivery. Journal of Controlled Release. 2009; 134:207–213. [PubMed: 19135104]

212. Malek A, Merkel O, Fink L, Czubayko F, Kissel T, Aigner A. In vivo pharmacokinetics, tissue distribution and underlying mechanisms of various PEI(−PEG)/siRNA complexes. Toxicol Appl Pharmacol. 2009; 236:97–108. [PubMed: 19371615]

213. Hatakeyama H, Ito E, Akita H, et al. A pH-sensitive fusogenic peptide facilitates endosomal escape and greatly enhances the gene silencing of siRNA-containing nanoparticles in vitro and in vivo. Journal of Controlled Release. 2009; 139:127–132. [PubMed: 19540888]

214. Gao J, Sun J, Li H, et al. Lyophilized HER2-specific PEGylated immunoliposomes for active siRNA gene silencing. Biomaterials. 2010; 31:2655–2664. [PubMed: 20035999]

215. Li SD, Chen YC, Hackett MJ, Huang L. Tumor-targeted delivery of siRNA by self-assembled nanoparticles. Mol Ther. 2008; 16:163–169. [PubMed: 17923843]

216. Li SD, Huang L. Stealth nanoparticles: high density but sheddable PEG is a key for tumor targeting. Journal of Controlled Release. 2010; 145:178–181. [PubMed: 20338200]

217. Cao N, Cheng D, Zou S, Ai H, Gao J, Shuai X. The synergistic effect of hierarchical assemblies of siRNA and chemotherapeutic drugs co-delivered into hepatic cancer cells. Biomaterials. 2010

218. Lu W, Zhang G, Zhang R, et al. Tumor site-specific silencing of NF-kappaB p65 by targeted hollow gold nanosphere-mediated photothermal transfection. Cancer Research. 2010; 70:3177–3188. [PubMed: 20388791]

219. Antony AC, Kincade RS, Verma RS, Krishnan SR. Identification of high affinity folate binding proteins in human erythrocyte membranes. J Clin Invest. 1987; 80:711–723. [PubMed: 3624486]

220. Daniels TR, Delgado T, Rodriguez JA, Helguera G, Penichet ML. The transferrin receptor part I: Biology and targeting with cytotoxic antibodies for the treatment of cancer. Clin Immunol. 2006; 121:144–158. [PubMed: 16904380]

221. Gomme PT, McCann KB, Bertolini J. Transferrin: structure, function and potential therapeutic actions. Drug Discov Today. 2005; 10:267–273. [PubMed: 15708745]

222. Prost AC, Menegaux F, Langlois P, et al. Differential transferrin receptor density in human colorectal cancer: A potential probe for diagnosis and therapy. Int J Oncol. 1998; 13:871–875. [PubMed: 9735419]

223. Bartlett DW, Davis ME. Impact of tumor-specific targeting and dosing schedule on tumor growth inhibition after intravenous administration of siRNA-containing nanoparticles. Biotechnol Bioeng. 2008; 99:975–985. [PubMed: 17929316]

224. Hu-Lieskovan S, Heidel JD, Bartlett DW, Davis ME, Triche TJ. Sequence-specific knockdown of EWS-FLI1 by targeted, nonviral delivery of small interfering RNA inhibits tumor growth in a murine model of metastatic Ewing's sarcoma. Cancer Research. 2005; 65:8984–8992. [PubMed: 16204072]

225. Mendonca LS, Firmino F, Moreira JN, Pedroso de Lima MC, Simoes S. Transferrin receptor-targeted liposomes encapsulating anti-BCR-ABL siRNA or asODN for chronic myeloid leukemia treatment. Bioconjug Chem. 2010; 21:157–168. [PubMed: 20000596]

226. Felber AE, Castagner B, Elsabahy M, Deleavey GF, Damha MJ, Leroux JC. siRNA nanocarriers based on methacrylic acid copolymers. Journal of Controlled Release. 2010

227. Suzuki E, Daniels TR, Helguera G, Penichet ML, Umezawa K, Bonavida B. Inhibition of NF-kappaB and Akt pathways by an antibody-avidin fusion protein sensitizes malignant B-cells to cisplatin-induced apoptosis. Int J Oncol. 2010; 36:1299–1307. [PubMed: 20372806]
228. Pirollo KF, Zon G, Rait A, et al. Tumor-targeting nanoimmunoliposome complex for short interfering RNA delivery. Hum Gene Ther. 2006; 17:117–124. [PubMed: 16409130]
229. Elbashir SM, Harborth J, Weber K, Tuschl T. Analysis of gene function in somatic mammalian cells using small interfering RNAs. Methods. 2002; 26:199–213. [PubMed: 12054897]
230. Reynolds A, Leake D, Boese Q, Scaringe S, Marshall WS, Khvorova A. Rational siRNA design for RNA interference. Nat Biotech. 2004; 22:326–330.
231. Aigner A. Delivery systems for the direct application of siRNAs to induce RNA interference (RNAi) in vivo. J Biomed Biotechnol. 2006; 2006:71659. [PubMed: 17057369]
232. Aigner A. Gene silencing through RNA interference (RNAi) in vivo: strategies based on the direct application of siRNAs. J Biotechnol. 2006; 124:12–25. [PubMed: 16413079]
233. Kleinman ME, Yamada K, Takeda A, et al. Sequence-and target-independent angiogenesis suppression by siRNA via TLR3. Nature. 2008; 452:591–597. [PubMed: 18368052]
234. Jackson AL, Linsley PS. Recognizing and avoiding siRNA off-target effects for target identification and therapeutic application. Nat Rev Drug Discov. 9:57–67. [PubMed: 20043028]
235. Chorev M, Chaturvedi N, Shavitz R, Goodman M. Partially Modified Retro-Inverso-Peptides - Novel Modification of Biologically-Active Peptides. Federation Proceedings. 1979; 38:363–363.
236. Taylor JW. The synthesis and study of side-chain lactam-bridged peptides. Biopolymers. 2002; 66:49–75. [PubMed: 12228920]
237. Henchey LK, Jochim AL, Arora PS. Contemporary strategies for the stabilization of peptides in the alpha-helical conformation. Curr Opin Chem Biol. 2008; 12:692–697. [PubMed: 18793750]
238. Ghadiri MR, Choi C. Secondary Structure Nucleation in Peptides - Transition-Metal Ion Stabilized Alpha-Helices. Journal of the American Chemical Society. 1990; 112:1630–1632.
239. Osapay G, Taylor JW. Multicyclic Polypeptide Model Compounds .2. Synthesis and Conformational Properties of a Highly Alpha-Helical Uncosapeptide Constrained by 3 Side-Chain to Side-Chain Lactam Bridges. Journal of the American Chemical Society. 1992; 114:6966–6973.
240. Brunel FM, Dawson PE. Synthesis of constrained helical peptides by thioether ligation: application to analogs of gp41. Chemical Communications. 2005:2552–2554. [PubMed: 15900323]
241. Kritzer JA. STAPLED PEPTIDES Magic bullets in nature's arsenal. Nature Chemical Biology. 2010; 6:566–567.
242. Sheridan C. Roche backs Aileron's stapled peptides. Nature Biotechnology. 2010; 28:992–992.
243. Schafmeister CE, Po J, Verdine GL. An all-hydrocarbon cross-linking system for enhancing the helicity and metabolic stability of peptides. Journal of the American Chemical Society. 2000; 122:5891–5892.
244. Blackwell HEG, R H. Highly Efficient Synthesis of Covalently Cross-Linked Peptide Helices by Ring-Closing Metathesis. Angew. Chem. Int. Ed. 1998; 37:3281–3284.
245. Walensky LD, Kung AL, Escher I, et al. Activation of apoptosis in vivo by a hydrocarbon-stapled BH3 helix. Science. 2004; 305:1466–1470. [PubMed: 15353804]
246. Hanahan D, Weinberg RA. The hallmarks of cancer. Cell. 2000; 100:57–70. [PubMed: 10647931]
247. Yang DC, Elliott RL, Head JF. Gene targets of antisense therapies in breast cancer. Expert Opin Ther Targets. 2002; 6:375–385. [PubMed: 12223074]
248. Devi GR. siRNA-based approaches in cancer therapy. Cancer Gene Ther. 2006; 13:819–829. [PubMed: 16424918]
249. Sasi N, Hwang M, Jaboin J, Csiki I, Lu B. Regulated cell death pathways: New twists in modulation of BCL2 family function. Molecular Cancer Therapeutics. 2009; 8:1421–1429. [PubMed: 19509269]

250. Futami T, Miyagishi M, Seki M, Taira K. Induction of apoptosis in HeLa cells with siRNA expression vector targeted against bcl-2. Nucleic Acids Res Suppl. 2002:251–252. [PubMed: 12903200]

251. Yin JQ, Gao J, Shao R, Tian WN, Wang J, Wan Y. siRNA agents inhibit oncogene expression and attenuate human tumor cell growth. J Exp Ther Oncol. 2003; 3:194–204. [PubMed: 14567290]

252. Poeck H, Besch R, Maihoefer C, et al. 5 '-triphosphate-siRNA: turning gene silencing and Rig-I activation against melanoma. Nature Medicine. 2008; 14:1256–1263.

253. Chawla-Sarkar M, Bae SI, Reu FJ, Jacobs BS, Lindner DJ, Borden EC. Downregulation of Bcl-2, FLIP or IAPs (XIAP and survivin) by siRNAs sensitizes resistant melanoma cells to Apo2L/TRAIL-induced apoptosis. Cell Death Differ. 2004; 11:915–923. [PubMed: 15118763]

254. Dasgupta A, Alvarado CS, Xu Z, Findley HW. Expression and functional role of inhibitor-of-apoptosis protein livin (BIRC7) in neuroblastoma. Biochem Biophys Res Commun. 2010; 400:53–59. [PubMed: 20691667]

255. Zaffaroni N, Pennati M, Daidone MG. Survivin as a target for new anticancer interventions. Journal of Cellular and Molecular Medicine. 2005; 9:360–372. [PubMed: 15963255]

256. Dohi T, Beltrami E, Wall NR, Plescia J, Altieri DC. Mitochondrial survivin inhibits apoptosis and promotes tumorigenesis. J Clin Invest. 2004; 114:1117–1127. [PubMed: 15489959]

257. Kasof GM, Gomes BC. Livin, a novel inhibitor of apoptosis protein family member. J Biol Chem. 2001; 276:3238–3246. [PubMed: 11024045]

258. Kappler M, Bache M, Bartel F, et al. Knockdown of survivin expression by small interfering RNA reduces the clonogenic survival of human sarcoma cell lines independently of p53. Cancer Gene Ther. 2004; 11:186–193. [PubMed: 14739938]

259. Liu JL, Wang Y, Jiang J, et al. Inhibition of survivin expression and mechanisms of reversing drug-resistance of human lung adenocarcinoma cells by siRNA. Chinese Medical Journal. 2010; 123:2901–2907. [PubMed: 21034604]

260. Dan HC, Sun M, Kaneko S, et al. Akt phosphorylation and stabilization of X-linked inhibitor of apoptosis protein (XIAP). Journal of Biological Chemistry. 2004; 279:5405–5412. [PubMed: 14645242]

261. Zhang YC, Wang Y, Gao WX, et al. Transfer of siRNA against XIAP induces apoptosis and reduces tumor cells growth potential in human breast cancer in vitro and in vivo. Breast Cancer Research and Treatment. 2006; 96:267–277. [PubMed: 16341821]

262. Chen Y, Bathula SR, Yang Q, Huang L. Targeted nanoparticles deliver siRNA to melanoma. J Invest Dermatol. 2010; 130:2790–2798. [PubMed: 20686495]

263. Wang YH, Liu S, Zhang G, et al. Knockdown of c-Myc expression by RNAi inhibits MCF-7 breast tumor cells growth in vitro and in vivo. Breast Cancer Research. 2005; 7:R220–R228. [PubMed: 15743499]

264. Song E, Zhu P, Lee SK, et al. Antibody mediated in vivo delivery of small interfering RNAs via cell-surface receptors. Nat Biotechnol. 2005; 23:709–717. [PubMed: 15908939]

265. Chen Y, Zhu X, Zhang X, Liu B, Huang L. Nanoparticles modified with tumor-targeting scFv deliver siRNA and miRNA for cancer therapy. Mol Ther. 2010; 18:1650–1656. [PubMed: 20606648]

266. Chen Y, Wu JJ, Huang L. Nanoparticles targeted with NGR motif deliver c-myc siRNA and doxorubicin for anticancer therapy. Mol Ther. 2010; 18:828–834. [PubMed: 20068551]

267. Choudhury A, Charo J, Parapuram SK, et al. Small interfering RNA (siRNA) inhibits the expression of the Her2/neu gene, upregulates HLA class I and induces apoptosis of Her2/neu positive tumor cell lines. Int J Cancer. 2004; 108:71–77. [PubMed: 14618618]

268. Liu XQ, Lei M, Erikson RL. Normal cells, but not cancer cells, survive severe Plk1 depletion. Molecular and Cellular Biology. 2006; 26:2093–2108. [PubMed: 16507989]

269. Degenhardt Y, Lampkin T. Targeting Polo-like kinase in cancer therapy. Clin Cancer Res. 2010; 16:384–389. [PubMed: 20068088]

270. Shi W, Alajez NM, Bastianutto C, et al. Significance of Plk1 regulation by miR-100 in human nasopharyngeal cancer. International Journal of Cancer. 2010; 126:2036–2048.

271. Spankuch-Schmitt B, Bereiter-Hahn J, Kaufmann M, Strebhardt K. Effect of RNA silencing of polo-like kinase-1 (PLK1) on apoptosis and spindle formation in human cancer cells. J Natl Cancer Inst. 2002; 94:1863–1877. [PubMed: 12488480]

272. Benoit DSW, Henry SM, Shubin AD, Hoffman AS, Stayton PS. pH-Responsive Polymeric siRNA Carriers Sensitize Multidrug Resistant Ovarian Cancer Cells to Doxorubicin via Knockdown of Polo-like Kinase 1. Molecular Pharmaceutics. 2010; 7:442–455. [PubMed: 20073508]

273. Fojo T, Bates S. Strategies for reversing drug resistance. Oncogene. 2003; 22:7512–7523. [PubMed: 14576855]

274. Shen DW, Goldenberg S, Pastan I, Gottesman MM. Decreased accumulation of [14C]carboplatin in human cisplatin-resistant cells results from reduced energy-dependent uptake. J Cell Physiol. 2000; 183:108–116. [PubMed: 10699972]

275. Shen D, Pastan I, Gottesman MM. Cross-resistance to methotrexate and metals in human cisplatin-resistant cell lines results from a pleiotropic defect in accumulation of these compounds associated with reduced plasma membrane binding proteins. Cancer Research. 1998; 58:268–275. [PubMed: 9443404]

276. Ambudkar SV, Dey S, Hrycyna CA, Ramachandra M, Pastan I, Gottesman MM. Biochemical, cellular, and pharmacological aspects of the multidrug transporter. Annu Rev Pharmacol Toxicol. 1999; 39:361–398. [PubMed: 10331089]

277. Lehne G. P-glycoprotein as a drug target in the treatment of multidrug resistant cancer. Curr Drug Targets. 2000; 1:85–99. [PubMed: 11475537]

278. Takakuwa O, Oguri T, Ozasa H, et al. Over-expression of MDR1 in amrubicinol-resistant lung cancer cells. Cancer Chemother Pharmacol. 2010

279. Richardson PG, Barlogie B, Berenson J, et al. A phase 2 study of bortezomib in relapsed, refractory myeloma. N Engl J Med. 2003; 348:2609–2617. [PubMed: 12826635]

280. Richardson PG, Sonneveld P, Schuster MW, et al. Bortezomib or high-dose dexamethasone for relapsed multiple myeloma. N Engl J Med. 2005; 352:2487–2498. [PubMed: 15958804]

281. Rumpold H, Salvador C, Wolf AM, Tilg H, Gastl G, Wolf D. Knockdown of PgP resensitizes leukemic cells to proteasome inhibitors. Biochem Biophys Res Commun. 2007; 361:549–554. [PubMed: 17662692]

282. Singhal SS, Sehrawat A, Sahu M, et al. Rlip76 transports sunitinib and sorafenib and mediates drug resistance in kidney cancer. International Journal of Cancer. 2010; 126:1327–1338.

283. Singhal SS, Wickramarachchi D, Singhal J, Yadav S, Awasthi YC, Awasthi S. Determinants of differential doxorubicin sensitivity between SCLC and NSCLC. FEBS Lett. 2006; 580:2258–2264. [PubMed: 16579994]

284. Singhal SS, Yadav S, Singhal J, Zajac E, Awasthi YC, Awasthi S. Depletion of RLIP76 sensitizes lung cancer cells to doxorubicin. Biochem Pharmacol. 2005; 70:481–488. [PubMed: 15950949]

285. Vatsyayan R, Lelsani PC, Awasthi S, Singhal SS. RLIP76: a versatile transporter and an emerging target for cancer therapy. Biochem Pharmacol. 2010; 79:1699–1705. [PubMed: 20097178]

286. Singhal SS, Roth C, Leake K, Singhal J, Yadav S, Awasthi S. Regression of prostate cancer xenografts by RLIP76 depletion. Biochem Pharmacol. 2009; 77:1074–1083. [PubMed: 19073149]

287. Awasthi YC, Sharma R, Yadav S, Dwivedi S, Sharma A, Awasthi S. The non-ABC drug transporter RLIP76 (RALBP-1) plays a major role in the mechanisms of drug resistance. Curr Drug Metab. 2007; 8:315–323. [PubMed: 17504221]

288. Singhal SS, Awasthi YC, Awasthi S. Regression of melanoma in a murine model by RLIP76 depletion. Cancer Research. 2006; 66:2354–2360. [PubMed: 16489041]

289. Singhal SS, Singhal J, Yadav S, Sahu M, Awasthi YC, Awasthi S. RLIP76: a target for kidney cancer therapy. Cancer Research. 2009; 69:4244–4251. [PubMed: 19417134]

290. Calcabrini A, Meschini S, Stringaro A, Cianfriglia M, Arancia G, Molinari A. Detection of P-glycoprotein in the nuclear envelope of multidrug resistant cells. Histochem J. 2000; 32:599–606. [PubMed: 11202156]

291. Gervasoni JE Jr, Fields SZ, Krishna S, et al. Subcellular distribution of daunorubicin in P-glycoprotein-positive and -negative drug-resistant cell lines using laser-assisted confocal microscopy. Cancer Research. 1991; 51:4955–4963. [PubMed: 1680024]

292. Puhlmann U, Ziemann C, Ruedell G, et al. Impact of the cyclooxygenase system on doxorubicin-induced functional multidrug resistance 1 overexpression and doxorubicin sensitivity in acute myeloid leukemic HL-60 cells. J Pharmacol Exp Ther. 2005; 312:346–354. [PubMed: 15501994]

293. von Bueren AO, Shalaby T, Oehler-Janne C, et al. RNA interference-mediated c-MYC inhibition prevents cell growth and decreases sensitivity to radio- and chemotherapy in childhood medulloblastoma cells. BMC Cancer. 2009; 9:10. [PubMed: 19134217]

294. Link KH, Gansauge F, Pillasch J, Beger HG. Multimodal therapies in ductal pancreatic cancer. The future. Int J Pancreatol. 1997; 21:71–83. [PubMed: 9127177]

295. Link KH, Leder G, Pillasch J, et al. In vitro concentration response studies and in vitro phase II tests as the experimental basis for regional chemotherapeutic protocols. Semin Surg Oncol. 1998; 14:189–201. [PubMed: 9548601]

296. Warenius HM, Seabra LA, Maw P. Sensitivity to cis-diamminedichloroplatinum in human cancer cells is related to expression of cyclin D1 but not c-raf-1 protein. International Journal of Cancer. 1996; 67:224–231.

297. Rhee K, Bresnahan W, Hirai A, Hirai M, Thompson EA. c-Myc and cyclin D3 (CcnD3) genes are independent targets for glucocorticoid inhibition of lymphoid cell proliferation. Cancer Research. 1995; 55:4188–4195. [PubMed: 7664296]

298. Tan A, Bitterman P, Sonenberg N, Peterson M, Polunovsky V. Inhibition of Myc-dependent apoptosis by eukaryotic translation initiation factor 4E requires cyclin D1. Oncogene. 2000; 19:1437–1447. [PubMed: 10723135]

299. Zong WX, Edelstein LC, Chen C, Bash J, Gelinas C. The prosurvival Bcl-2 homolog Bfl-1/A1 is a direct transcriptional target of NF-kappaB that blocks TNFalpha-induced apoptosis. Genes Dev. 1999; 13:382–387. [PubMed: 10049353]

300. Wang CY, Guttridge DC, Mayo MW, Baldwin AS Jr. NF-kappaB induces expression of the Bcl-2 homologue A1/Bfl-1 to preferentially suppress chemotherapy-induced apoptosis. Mol Cell Biol. 1999; 19:5923–5929. [PubMed: 10454539]

301. Biliran H Jr, Banerjee S, Thakur A, et al. c-Myc-induced chemosensitization is mediated by suppression of cyclin D1 expression and nuclear factor-kappa B activity in pancreatic cancer cells. Clin Cancer Res. 2007; 13:2811–2821. [PubMed: 17473215]

302. An J, Xu QZ, Sui JL, Bai B, Zhou PK. Downregulation of c-myc protein by siRNA-mediated silencing of DNA-PKcs in HeLa cells. International Journal of Cancer. 2005; 117:531–537.

303. Oltersdorf T, Elmore SW, Shoemaker AR, et al. An inhibitor of Bcl-2 family proteins induces regression of solid tumours. Nature. 2005; 435:677–681. [PubMed: 15902208]

304. Holinger EP, Chittenden T, Lutz RJ. Bak BH3 peptides antagonize Bcl-xL function and induce apoptosis through cytochrome c-independent activation of caspases. Journal of Biological Chemistry. 1999; 274:13298–13304. [PubMed: 10224090]

305. Shangary S, Oliver CL, Tillman TS, Cascio M, Johnson DE. Sequence and helicity requirements for the proapoptotic activity of Bax BH3 peptides. Mol Cancer Ther. 2004; 3:1343–1354. [PubMed: 15542773]

306. van Delft MF, Wei AH, Mason KD, et al. The BH3 mimetic ABT-737 targets selective Bcl-2 proteins and efficiently induces apoptosis via Bak/Bax if Mcl-1 is neutralized. Cancer Cell. 2006; 10:389–399. [PubMed: 17097561]

307. Xu YM, Wang LF, Jia LT, et al. A caspase-6 and anti-human epidermal growth factor receptor-2 (HER2) antibody chimeric molecule suppresses the growth of HER2-overexpressing tumors. J Immunol. 2004; 173:61–67. [PubMed: 15210759]

308. Wang LF, Zhou Y, Xu YM, et al. A caspase-6 and anti-HER2 antibody chimeric tumor-targeted proapoptotic molecule decreased metastasis of human osteosarcoma. Cancer Invest. 2009; 27:774–780. [PubMed: 19488908]

309. Lessene G, Czabotar PE, Colman PM. BCL-2 family antagonists for cancer therapy. Nat Rev Drug Discov. 2008; 7:989–1000. [PubMed: 19043450]

310. Tse C, Shoemaker AR, Adickes J, et al. ABT-263: a potent and orally bioavailable Bcl-2 family inhibitor. Cancer Res. 2008; 68:3421–3428. [PubMed: 18451170]
311. Shangary S, Johnson DE. Peptides Derived from BH3 Domains of Bcl-2 Family Members:â€‰ A Comparative Analysis of Inhibition of Bcl-2, Bcl-xL and Bax Oligomerization. Induction of Cytochrome c Release, and Activation of Cell Deathâ€ Biochemistry. 2002; 41:9485–9495.
312. Finnegan NM, Curtin JF, Prevost G, Morgan B, Cotter TG. Induction of apoptosis in prostate carcinoma cells by BH3 peptides which inhibit Bak/Bcl-2 interactions. Br J Cancer. 2001; 85:115–121. [PubMed: 11437412]
313. Li N, Lin P, Cai C, Pan Z, Weisleder N, Ma J. The amino-terminal peptide of Bax perturbs intracellular Ca2+ homeostasis to enhance apoptosis in prostate cancer cells. Am J Physiol Cell Physiol. 2009; 296:C267–C272. [PubMed: 19091958]
314. Dharap SS, Minko T. Targeted proapoptotic LHRH-BH3 peptide. Pharmaceutical Research. 2003; 20:889–896. [PubMed: 12817893]
315. Li B, Zhang LJ, Zhang ZL, et al. Synergistic tumor growth-inhibitory effect of the prostate-specific antigen-activated fusion peptide BSD352 for prostate cancer therapy. Anticancer Drugs. 2010
316. Ellerby HM, Arap W, Ellerby LM, et al. Anti-cancer activity of targeted pro-apoptotic peptides. Nat Med. 1999; 5:1032–1038. [PubMed: 10470080]
317. Shamay Y, Adar L, Ashkenasy G, David A. Light induced drug delivery into cancer cells. Biomaterials. 2011; 32:1377–1386. [PubMed: 21074848]
318. Moellering RE, Cornejo M, Davis TN, et al. Direct inhibition of the NOTCH transcription factor complex. Nature. 2009; 462:182–188. [PubMed: 19907488]
319. Stewart ML, Fire E, Keating AE, Walensky LD. The MCL-1 BH3 helix is an exclusive MCL-1 inhibitor and apoptosis sensitizer. Nature Chemical Biology. 2010; 6:595–601.
320. Lopes LB, Furnish E, Komalavilas P, et al. Enhanced skin penetration of P20 phosphopeptide using protein transduction domains. European Journal of Pharmaceutics and Biopharmaceutics. 2008; 68:441–445. [PubMed: 18035527]
321. Elliott G, O'Hare P. Intercellular trafficking and protein delivery by a herpesvirus structural protein. Cell. 1997; 88:223–233. [PubMed: 9008163]
322. Kokryakov VN, Harwig SS, Panyutich EA, et al. Protegrins: leukocyte antimicrobial peptides that combine features of corticostatic defensins and tachyplesins. FEBS Lett. 1993; 327:231–236. [PubMed: 8335113]
323. Mudhakir D, Akita H, Tan E, Harashima H. A novel IRQ ligand-modified nano-carrier targeted to a unique pathway of caveolar endocytic pathway. Journal of Controlled Release. 2008; 125:164–173. [PubMed: 18054812]
324. Jans DA. Nuclear signaling pathways for polypeptide ligands and their membrane receptors? FASEB J. 1994; 8:841–847. [PubMed: 8070633]
325. Alshamsan A, Hamdy S, Samuel J, El-Kadi AO, Lavasanifar A, Uludag H. The induction of tumor apoptosis in B16 melanoma following STAT3 siRNA delivery with a lipid-substituted polyethylenimine. Biomaterials. 2010; 31:1420–1428. [PubMed: 19913908]
326. Schiffelers RM, Ansari A, Xu J, et al. Cancer siRNA therapy by tumor selective delivery with ligand-targeted sterically stabilized nanoparticle. Nucleic Acids Res. 2004; 32:e149. [PubMed: 15520458]
327. Liu XX, Rocchi P, Qu FQ, et al. PAMAM dendrimers mediate siRNA delivery to target Hsp27 and produce potent antiproliferative effects on prostate cancer cells. ChemMedChem. 2009; 4:1302–1310. [PubMed: 19533723]
328. Yadav S, van Vlerken LE, Little SR, Amiji MM. Evaluations of combination MDR-1 gene silencing and paclitaxel administration in biodegradable polymeric nanoparticle formulations to overcome multidrug resistance in cancer cells. Cancer Chemother Pharmacol. 2009; 63:711–722. [PubMed: 18618115]
329. Varkouhi AK, Lammers T, Schiffelers RM, van Steenbergen MJ, Hennink WE, Storm G. Gene silencing activity of siRNA polyplexes based on biodegradable polymers. Eur J Pharm Biopharm. 2010

330. Lee WR, Shen SC, Lai HH, Hu CH, Fang JY. Transdermal drug delivery enhanced and controlled by erbium:YAG laser: a comparative study of lipophilic and hydrophilic drugs. J Control Release. 2001; 75:155–166. [PubMed: 11451505]

331. Grzmil M, Thelen P, Hemmerlein B, et al. Bax inhibitor-1 is overexpressed in prostate cancer and its specific down-regulation by RNA interference leads to cell death in human prostate carcinoma cells. American Journal of Pathology. 2003; 163:543–552. [PubMed: 12875974]

332. Crnkovic-Mertens I, Hoppe-Seyler F, Butz K. Induction of apoptosis in tumor cells by siRNA-mediated silencing of the livin/ML-IAP/KIAP gene. Oncogene. 2003; 22:8330–8336. [PubMed: 14614456]

333. Butz K, Ristriani T, Hengstermann A, Denk C, Scheffner M, Hoppe-Seyler F. siRNA targeting of the viral E6 oncogene efficiently kills human papillomavirus-positive cancer cells. Oncogene. 2003; 22:5938–5945. [PubMed: 12955072]

334. Ptasznik A, Nakata Y, Kalota A, Emerson SG, Gewirtz AM. Short interfering RNA (siRNA) targeting the Lyn kinase induces apoptosis in primary, and drug-resistant, BCR-ABL1(+) leukemia cells. Nature Medicine. 2004; 10:1187–1189.

335. Liu X, Erikson RL. Polo-like kinase (Plk)1 depletion induces apoptosis in cancer cells. Proc Natl Acad Sci U S A. 2003; 100:5789–5794. [PubMed: 12732729]

336. Troussard AA, Mawji NM, Ong C, Mui A, St Arnaud R, Dedhar S. Conditional knock-out of integrin-linked kinase demonstrates an essential role in protein kinase B/Akt activation. Journal of Biological Chemistry. 2003; 278:22374–22378. [PubMed: 12686550]

337. Glaser KB, Li JL, Staver MJ, Wei RQ, Albert DH, Davidsen SK. Role of Class I and Class II histone deacetylases in carcinoma cells using siRNA. Biochemical and Biophysical Research Communications. 2003; 310:529–536. [PubMed: 14521942]

338. Karasarides M, Chiloeches A, Hayward R, et al. B-RAF is a therapeutic target in melanoma. Oncogene. 2004; 23:6292–6298. [PubMed: 15208680]

339. Olichon A, Baricault L, Gas N, et al. Loss of OPA1 perturbates the mitochondrial inner membrane structure and integrity, leading to cytochrome c release and apoptosis. Journal of Biological Chemistry. 2003; 278:7743–7746. [PubMed: 12509422]

340. Wilda M, Fuchs U, Wossmann W, Borkhardt A. Killing of leukemic cells with a BCR/ABL fusion gene by RNA interference (RNAi). Oncogene. 2002; 21:5716–5724. [PubMed: 12173041]

341. Lee GH, Yan C, Shin SJ, et al. BAX inhibitor-1 enhances cancer metastasis by altering glucose metabolism and activating the sodium-hydrogen exchanger: the alteration of mitochondrial function. Oncogene. 2010; 29:2130–2141. [PubMed: 20118983]

342. Amarzguioui M, Peng Q, Wiiger MT, et al. Ex vivo and in vivo delivery of anti-tissue factor short interfering RNA inhibits mouse pulmonary metastasis of B16 melanoma cells. Clin Cancer Res. 2006; 12:4055–4061. [PubMed: 16818705]

343. Villares GJ, Zigler M, Wang H, et al. Targeting melanoma growth and metastasis with systemic delivery of liposome-incorporated protease-activated receptor-1 small interfering RNA. Cancer Res. 2008; 68:9078–9086. [PubMed: 18974154]

344. Liu Y, Tao J, Li Y, et al. Targeting hypoxia-inducible factor-1alpha with Tf-PEI-shRNA complex via transferrin receptor-mediated endocytosis inhibits melanoma growth. Mol Ther. 2009; 17:269–277. [PubMed: 19066596]

345. Hua J, Chen DQ, Fu H, et al. Short hairpin RNA-mediated inhibition of S100A4 promotes apoptosis and suppresses proliferation of BGC823 gastric cancer cells in vitro and in vivo. Cancer Letters. 2010; 292:41–47. [PubMed: 19945782]

346. Zamora-Avila DE, Zapata-Benavides P, Franco-Molina MA, et al. WT1 gene silencing by aerosol delivery of PEI-RNAi complexes inhibits B16–F10 lung metastases growth. Cancer Gene Ther. 2009; 16:892–899. [PubMed: 19461674]

347. Moschos SA, Jones SW, Perry MM, et al. Lung delivery studies using siRNA conjugated to TAT(48–60) and penetratin reveal peptide induced reduction in gene expression and induction of innate immunity. Bioconjug Chem. 2007; 18:1450–1459. [PubMed: 17711319]

348. Turner JJ, Jones S, Fabani MM, Ivanova G, Arzumanov AA, Gait MJ. RNA targeting with peptide conjugates of oligonucleotides, siRNA and PNA. Blood Cells Mol Dis. 2007; 38:1–7. [PubMed: 17113327]

349. Takei Y, Kadomatsu K, Yuzawa Y, Matsuo S, Muramatsu T. A small interfering RNA targeting vascular endothelial growth factor as cancer therapeutics. Cancer Research. 2004; 64:3365–3370. [PubMed: 15150085]

350. Zhao Y, Zhao L, Zhou L, et al. Quantum dot conjugates for targeted silencing of bcr/abl gene by RNA interference in human myelogenous leukemia K562 cells. J Nanosci Nanotechnol. 2010; 10:5137–5143. [PubMed: 21125862]

351. Kumar M, Yigit M, Dai G, Moore A, Medarova Z. Image-guided breast tumor therapy using a small interfering RNA nanodrug. Cancer Research. 2010; 70:7553–7561. [PubMed: 20702603]

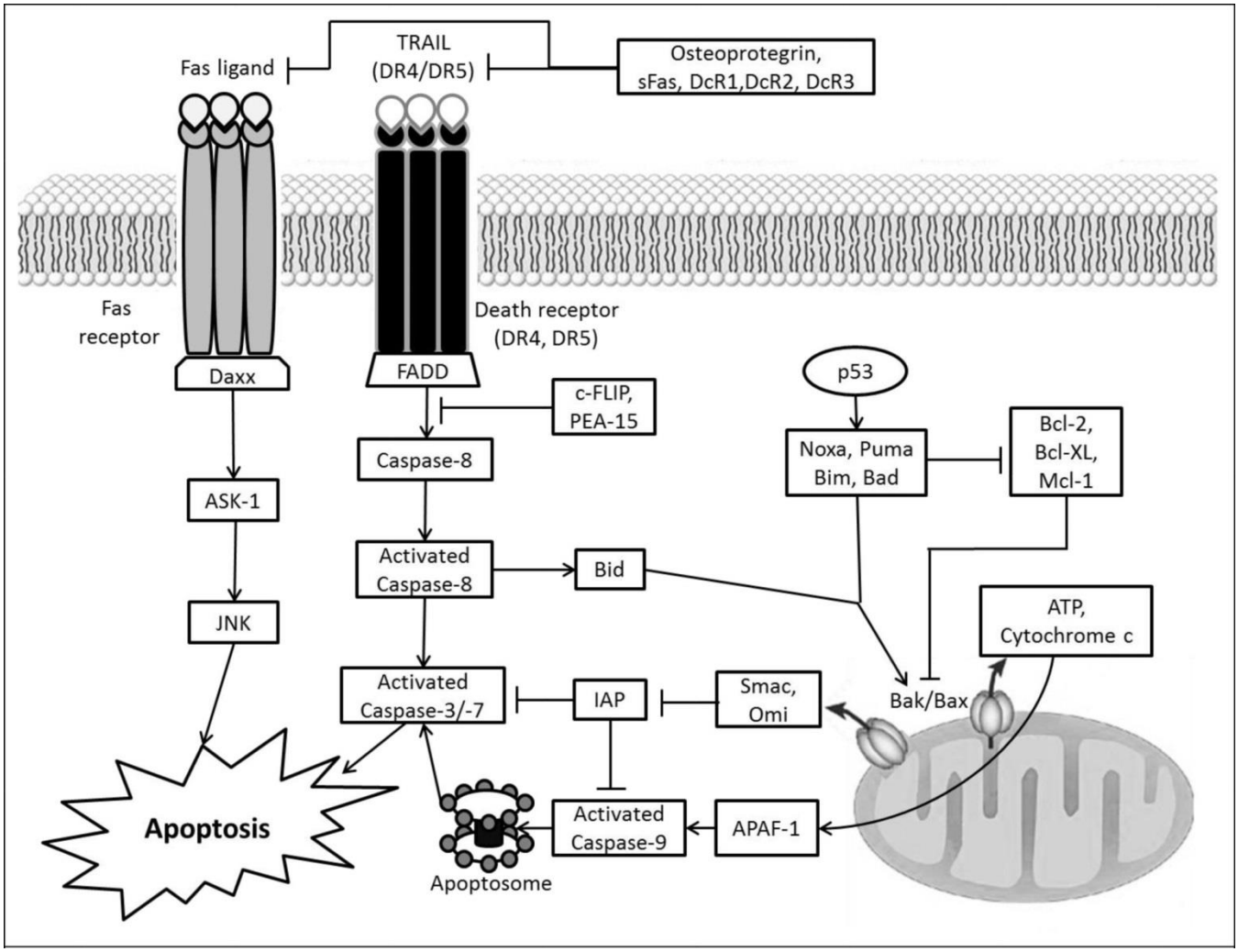

Figure 1. Schematic summarizing the cellular intrinsic and extrinsic apoptosis pathways The extrinsic pathway is activated by receptors such as Fas, DR4, and DR5 that, when bound by their ligands, associate with cytosolic adapter death domains, i.e., FADD and Daxx. The FADD complex eventually activates executioner caspases (−3 and −7) while (Fas-specific) Daxx leads to caspase-independent apoptosis mediated downstream through JNK. Osteoprotegerin, sFas, DcR1, DcR2, and DcR3 inhibit the ligation of apoptotic death receptors, and PEA-15 and c-FLIP are relevant inhibitors of caspase-8 activation via the FADD pathway. The activation of the intrinsic (or mitochondrial) pathway is predominantly controlled by the Bcl-2 family proteins. BH3 only members (i.e. Bim, Bad, Bid, Noxa, Puma) either activate Bak and Bax directly (direct activation model) or indirectly (indirect activation model) through inhibition of the anti-apoptotic Bcl-2-like proteins, i.e. Bcl-2, Bcl-X_L, and Mcl-1. Activated Bak/Bax homo-oligomerize and form mitochondrial pores that release pro-apoptotic factors such as ATP, cytochrome c, Smac, and Omi into the cytosol. Cytochrome c, ATP, APAF-1, and activated caspase-9 form the apoptosome, which can activate executioner caspases (i.e., −3, and −7). Smac and Omi further promote apoptosis by preventing IAPs, which are caspase inhibitors. Schematic modified from [11, 19].

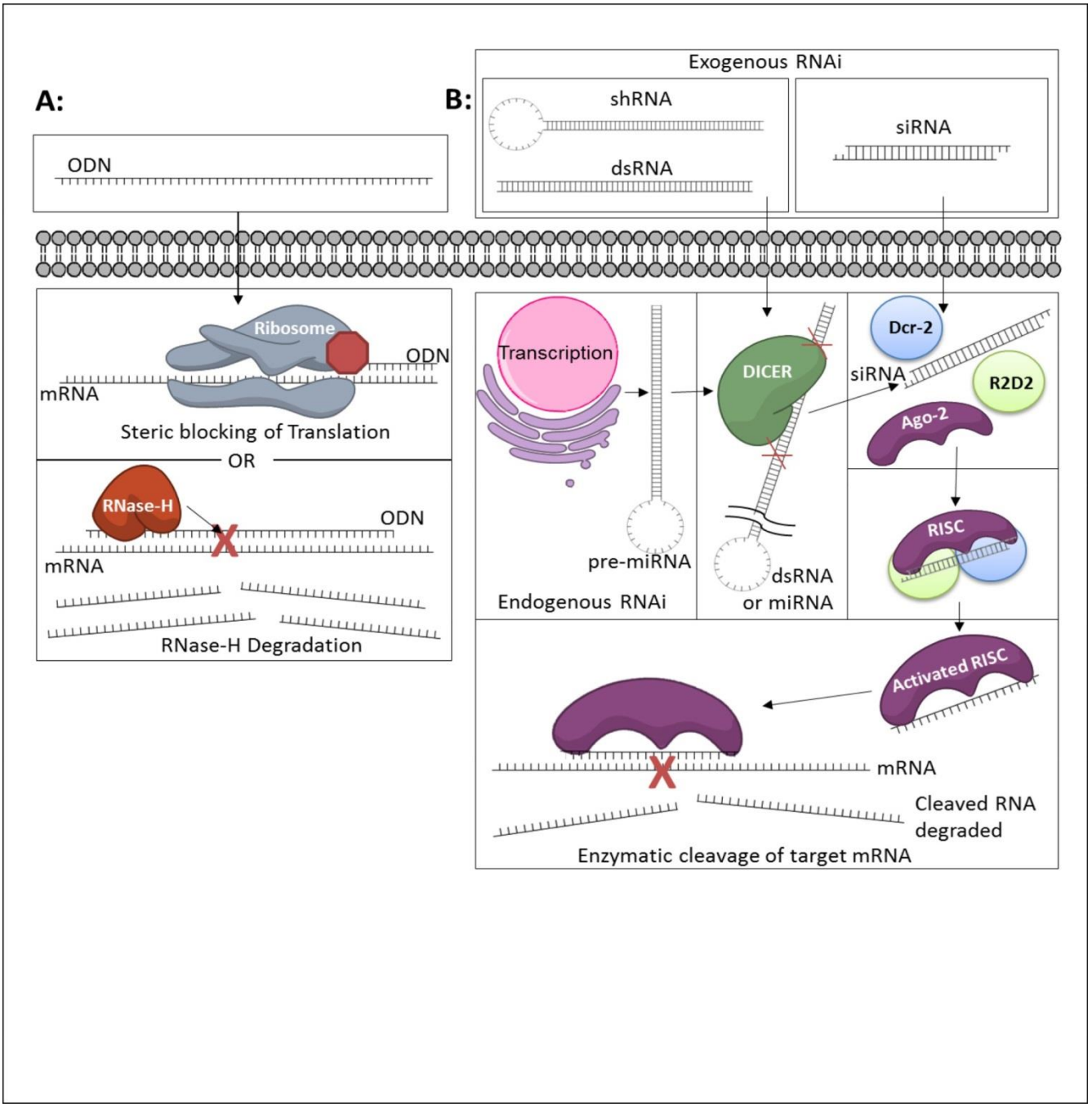

Figure 2. Mechanisms of RNA Interference

(A) ODN silencing is believed to be induced by sterically blocking translation through hybridization with mRNA and RNAse-H mediated degradation of both the ODN and mRNA (B) Proposed mechanisms for RNA interference by miRNA, shRNA, dsRNA, and siRNA. Endogenous miRNA, which is made transcriptionally, and exogenously delivered shRNA/dsRNA must all be first processed into siRNA, double stranded RNA molecules around 20 base pairs in size. Exogenous siRNA can also be delivered that circumvents the need for dicer processing. siRNA is loaded onto the RISC complex and mediates degradation of mRNA complementary to the antisense siRNA strand. For each type of therapeutic RNAi,

the exogenous RNA must reach the cytoplasm to interact with mRNA and other intracellular machinery required for gene silencing.

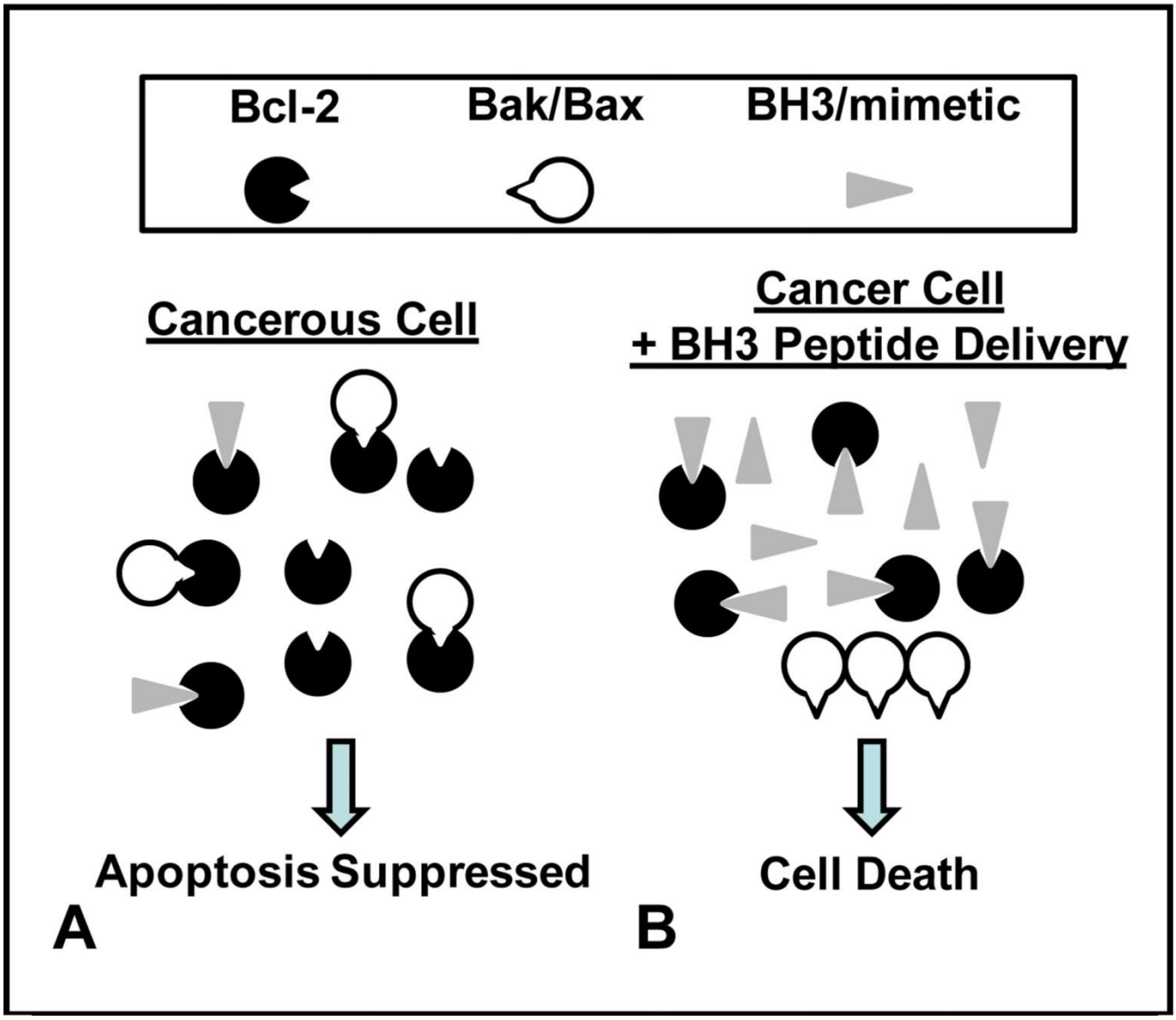

Figure 3. Model representation of BH3-only protein peptidomimetic cancer cell pro-apoptotic activity

Numerous cancers overexpress anti-apoptotic Bcl-2-like proteins, and BH3 domain-derived peptides can be utilized to antagonize Bcl-2-like protein activity to indirectly activate Bak/Bax and overcome apoptotic resistance.

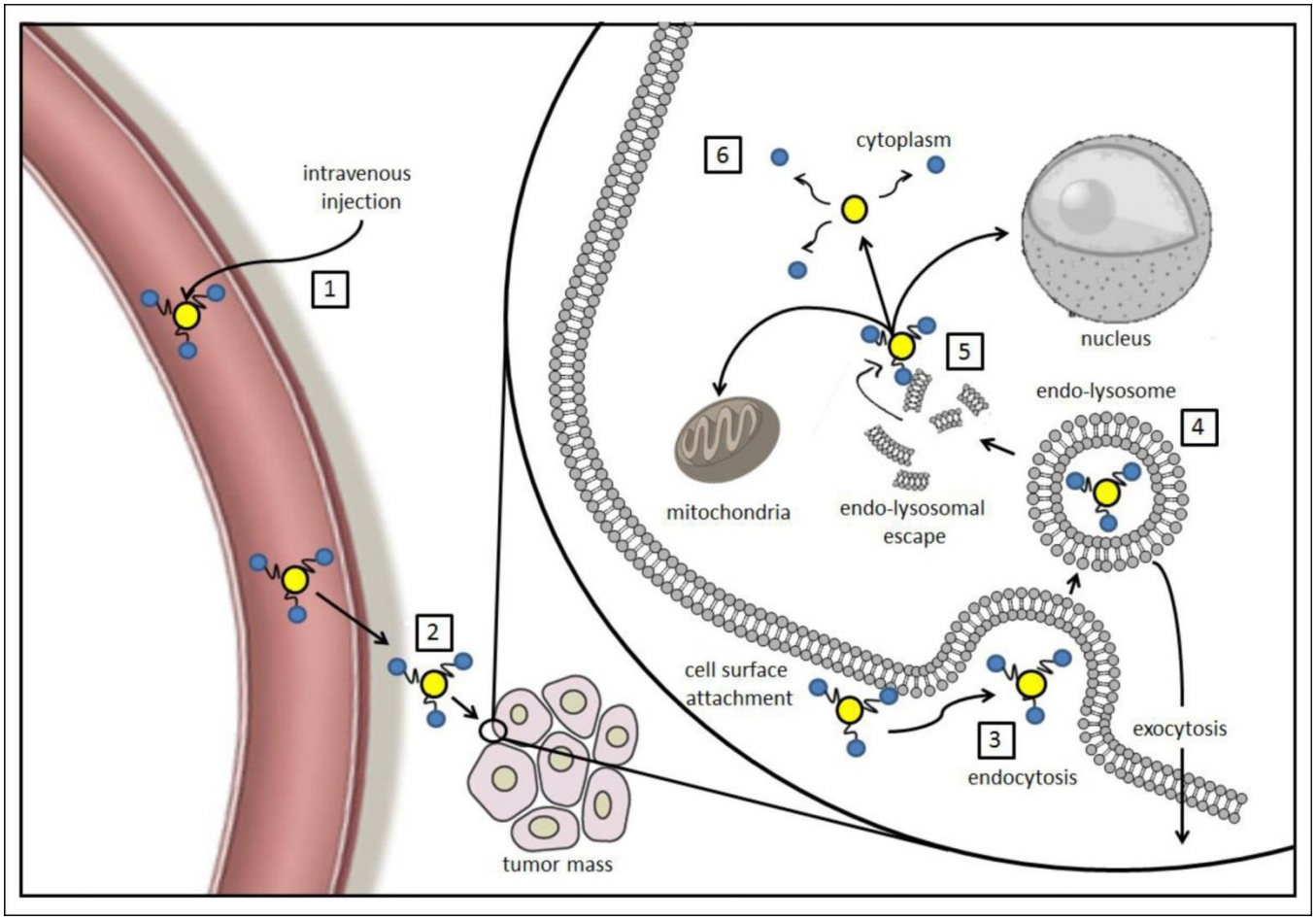

Figure 4. Intracellular delivery barriers

1) Upon entering systemic circulation, the drug formulation must protect the biomacromolecule from enzymatic degradation and serum protein destabilization and/or opsonization. 2) Drug circulation half-life needs to be long enough such that the drug persists in the vasculature until it accumulates (through specific targeting or nonspecifically thorough the enhanced permeation and retention effect) in the tumor tissue. 3) The drug must interact with the cell membrane to initiate internalization, which can result in uptake into an endosomal (or pinocytic) vesicle. 4) If no endosomal escape mechanism is present, the drug can be degraded in the lysosome, remain in the late endosome, or undergo trafficking for exocytosis. 5) If the drug is able to escape the endo-lysosomal pathway, it is released where it can diffuse to molecular targets in the cytoplasm. 6) If attached to a carrier or loaded within a nanoparticle such as a liposome, polyplex, etc., the drug may need to be released from this formulation to become bioavailable.

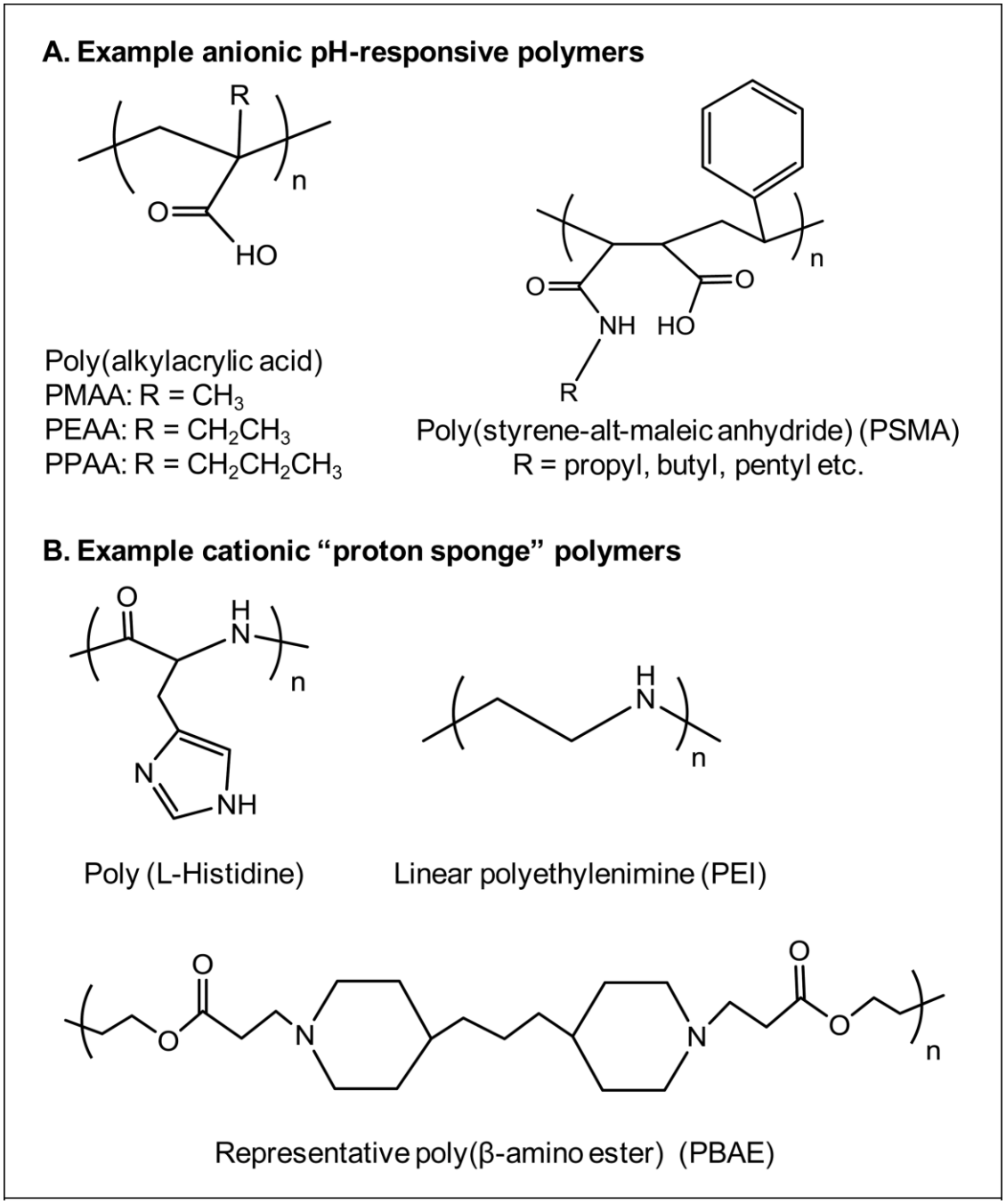

Figure 5. Chemical structures of example pH-responsive "smart" polymers used for intracellular drug delivery

(a) Anionic polymers thought to become more hydrophobic and lipophilic in acidic environments. (b) Cationic amine-containing polymers believed to disrupt endo-lysosomes through the proton sponge mechanism.

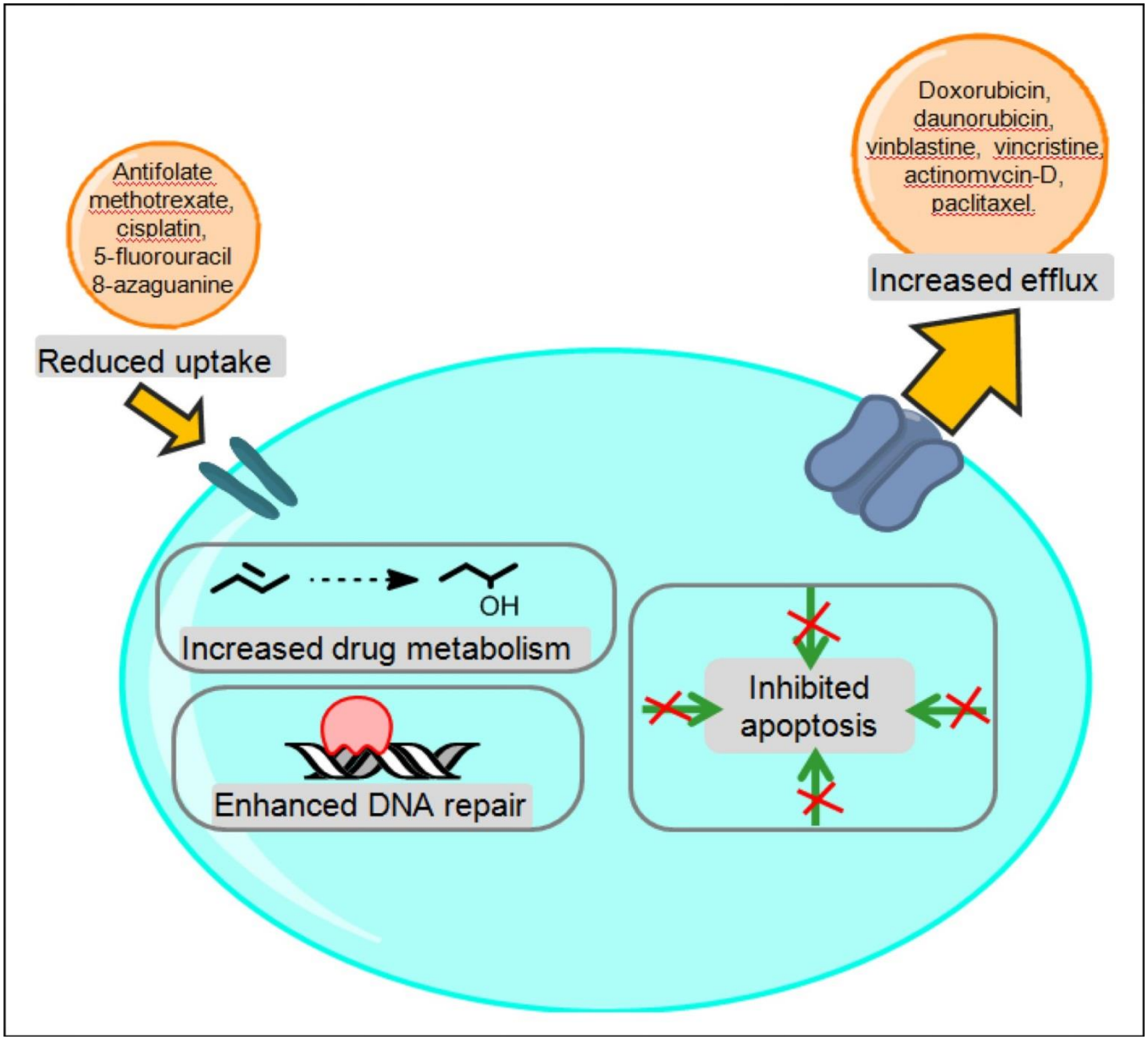

Figure 6. Multidrug Resistance

Examples of cellular characteristics that enable cancer cell multidrug resistance to chemotherapeutics include reduced uptake, increased metabolism, and increased efflux of the drugs. Chemotherapeutics affected are also summarized.

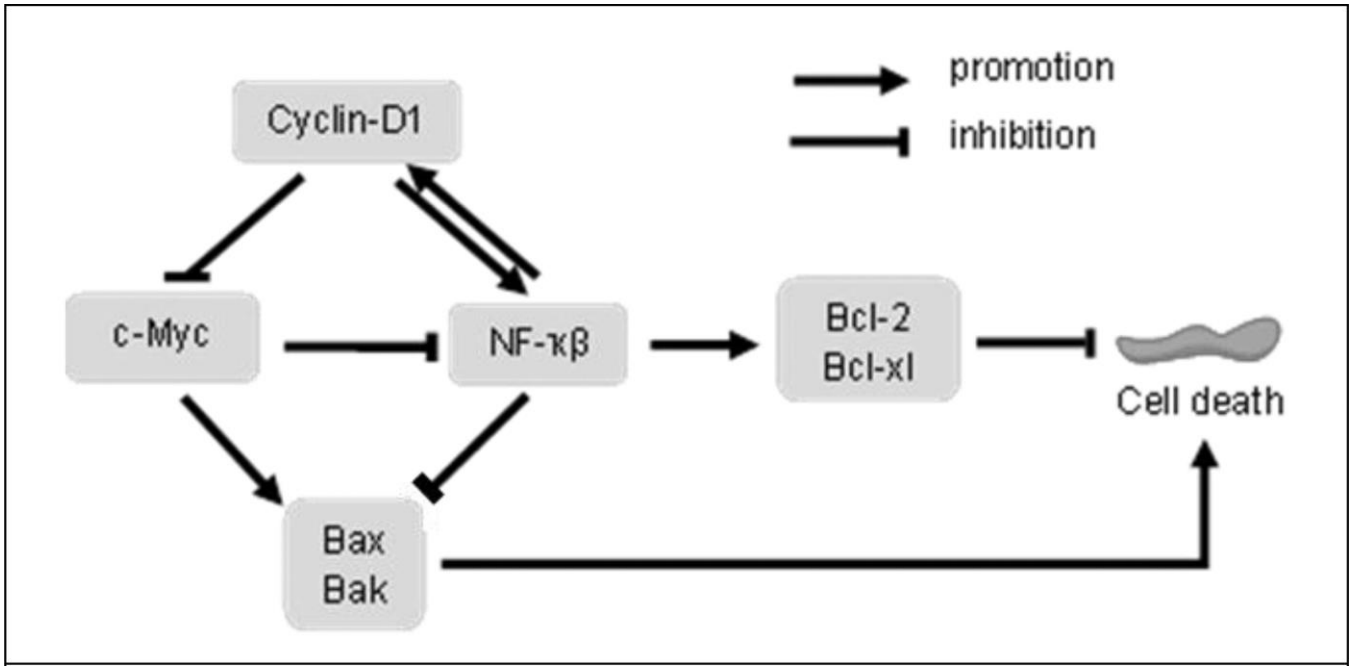

Figure 7. Relationships of some of the genes involved in MDR phenotype

Table 1

Cell Penetrating Peptides

Peptide (abbreviation)	Sequence	Sequence Origin	Ref
Penetratin (PEN, pAntp)	RQIKIWFQNRRMKWKK	Drosophila antennapedia homeodomain	[118]
Trans-activating transcriptional factor (TAT)	GRKKRRQRRRPPQ	Human Immunodeficiency Virus type I (HIV-1)	[118]
pVEC	LLIILRRRIRKQAHAHSK	Murine vascular endothelial cadherin	[118]
Transportan	GWTLNSAGYLLGKINLKALAALAKKIL	Galanin (neuropeptide) and mastoporan (toxic peptide in wasp venom)	[118]
YARA	YARAAARQARA	Optimized TAT transduction domain	[320]
WLR	WLRRIKAWLRRIKAWLRRIK	synthetic	[320]
VP22	MTSRRSVKSGPREVPRDEYEDLYYIPSSGMAS PDSPPDTSRRGALQTRSRQRGEVRFVQYDESD YALYGGSSSEDDEHPEVPRTRRPVSGAVLSGP GPARAPPPPAGSGGAGRTPTTAPRAPRTQRVA TKAPAAPAAETTRGRKSAQPESAALPDAPAST APTRSKTPAQGLARKLHFSTAPPNPDAPWTPR VAGFNKRVFCAAVGRLAAMHARMAAVQLW DMSRPRTDEDLNELLGITTIRVTVCEGKNLLQ RANELVNPDVVQDDAATATRGRSAASRPTER PRAPARSASRPRRPVE	Herpes Simplex Virus type I (HSV-1)	[321]
SynB vector	RGGRLYRRRFVVGR	Protegerin-I analogue without cysteine residues	[322]
Diatos Peptide Vector 3 (DPV3)	RKKRRRESRKKRRRES	Superoxide dismutase	[117]
Diatos Peptide Vector 6 (DPV6)	GRPRESGKKRKRKRLKP	Platelet-derived growth factor (PDGF)	[117]
Diatos Peptide Vector 7 (DPV7)	GKRKKKGKLGKKRDP	Epidermal-like growth factor	[117]
Diatos Peptide Vector 7b (DPV7b)	GKRKKKGKLGKKRPRSR	Epidermal-like growth factor	[117]
Diatos Peptide Vector 3/10 (DPV3/10)	RKKRRRESRRARRSPRHL	Superoxide dismutase and intestinal mucin	[117]
Diatos Peptide Vector 10/6 (DPV10/6)	SRRARRSPRESGKKRKRKR	Intestinal mucin and PDGF	[117]
Diatos Peptide Vector 1047 (DPV1047)	VKRGLKLRHVRPRVTRMDV	Apolipoprotein B and anti-DNA antibody	[117]
Diatos Peptide Vector 10 (DPV10)	SRRARRSPRHLGSG	Intestinal mucin	[117]
Diatos Peptide Vector 15 (DPV15)	LRRERQSRLRRERQSR	Cationic antimicrobial protein 37 (CAP37)	[117]
Diatos Peptide Vector 15b(DPV15b)	GAYDLRRRERQSRLRRRERQSR	Cationic antimicrobial protein 37 (CAP37)	[117]
R8	RRRRRRRR	Oligoarginine (synthetic)	[114]
R12	RRRRRRRRRRRR	Oligoarginine (synthetic)	[120]
IRQ	IRQRRRR	Oligoarginine derivative (synthetic)	[323]
basic fibroblast growth factor 1 (HbFGF-1)	NYKKPKL	Nuclear localization sequence in HbFGF-1	[324]
basic fibroblast growth factor 2 (HbFGF-2)	HFKDPKR	Nuclear localization sequence in HbFGF-2	[324]
MPG	GALFLGFLGAAGSTMGAWSQPKKKRKV	HIV Gp41-SV40 nuclear localization sequence	[121]
Sweet arrow peptide (SAP)	VRLPPPVRLPPPVRLPPP	Proline rich motif	[121]

Peptide (abbreviation)	Sequence	Sequence Origin	Ref
hCT (9–32)	LGTYTQDFNKTFPQTAIGVGAP	Human calcitonin	[121]
Pep-1	KETWWETWWTEWSQPKKKRKV	Trp-rich motif-SV40 nuclear localization sequence	[121]

Table 2

Fusogenic Peptides

Peptide (abbreviation)	Sequence	Sequence Origin	Ref
Model amphipathic peptide (MAP)	KALAKALAKALA	Chimeric	[121]
GALA	WEAALAEALAEALAEHLAEALAEALEALAA	Model amphipathic peptide derivative	[135]
KALA	WEAKLAKALAKALAKHLAKALAKALKACEA	Model amphipathic peptide derivative	[141]
EALA	EALAEALAEALA	Chimeric	[142]
4(6)	Ac-LARLLARLLARLLRALLRALLRAL	Synthetic amphipathic peptide	[143]
Hel 11-7	KLLKLLLKLWKKLLKLLK	Synthetic amphipathic peptide	[143]
INF7	GLFEAIEGFIENGWEGMIWDYG	23 mer Hemagglutinin (HA-2) derivative	[137]
JTS-1	GLFEALLELLESLWELLLEA	INF7 mimic	[137]
ppTG1	GLFKALLKLLKSLWKLLLKA	JTS-1 mimic	[144]
ppTG20	GLFRALLRLLRSLWRLLLRA	JTS-1 mimic	[144]
LAH4 Analogues	KKALLALALHHLAHLALHLALALKK	Histidine rich amphipathic peptide	[145]
β-amyloid (29–42)	GAIIGLMVGGVVIA	Transmembrane β-amyloid protein derivative	[146]
Influenza HA-2	GLFGAIAGFIENGWEGMIDGWYG	N-terminal sequence of influenza hemagglutinin subunit HA-2	[140]
Influenza derivative I	GLFQAIAGFIQNGYQGMIDGGGC	Hemagglutinin (HA-2) mimic	[138]
Influenza derivative II	GLFEAIAEFIEGGWEGLIEGCA	Hemagglutinin (HA-2) mimic	[139]
Mellitin	GIGAVLKVLTTGLPALISWIKRKRQQ	Peptide component of bee venom	[148]
Penetratin (PEN, pAntp)	RQIKIWFQNRRMKWKK	Drosophila antennapedia homeodomain	[118]
Trans-activating transcriptional factor (TAT)	GRKKRRQRRRPPQ	Human Immunodeficiency Virus type I (HIV-1)	[118]
Transportan	GWTLNSAGYLLGKINLKALAALAKKIL	Galanin (neuropeptide) and mastoporan (toxic peptide in wasp venom)	[118]

Table 3

Application of Cationic Polymeric Carriers to Facilitate Endosomal/Lysosomal Escape.

Cationic Polymer	Gene	Cell	Efficacy	Ref
Cationic polymeric nanoparticles				
PEI	STAT3	B16 melanoma	~5% gene silencing (25 nM);~25% gene silencing and 13% cell death (50 nM).	[325]
PEI-StA	STAT3	B16 melanoma	~53% gene silencing (25 nM);~68% gene silencing and 40% cell death (50 nM).	[325]
PDMAEMA	VEGF	PC3 prostate cancer cell	68 % gene silencing (N/P = 2) 97 % gene silencing (N/P = 4)	[173]
PDMAEMA-b-PDbB complex with PSMA	Plk1	MDR Ovarian cancer cell	>70% transfection, 50% gene silencing, and 5%–10% apoptosis	[272]
PEI-b-PEG-RGD	Luciferase gene VEGF-R2	Neuroblastoma In vivo, mice	90% gene silencing Tumor size barely increased (6 fold bigger for untreated and ~12 fold bigger for siRNA negative control	[326]
EHCO	Luciferase	CHO-d1EGFP	84% cellular uptake and 87% gene silencing	[211]
Biodegradable cationic polymeric nanoparticles				
PAMAM dendrimer complexed with PEG-b-P(PrMA-co-MAA	Bcl-2	PC-3 prostate cancer cell	62% gene silencing (50 nM)	[226]
PAMAM dendrimer	Hsp27	PC-3 prostate cancer cell	75% gene silencing (50 nM) and ~45% cell apoptosis	[327]
PEO-b-PBAE	MDR-1	SKOV3 human ovarian adenocarcinoma	Effective gene silencing (100 nM) and 10 – 25% greater cell apoptosis induced in SKOV3 cells, <5% greater cell apoptosis induced in SKOV3 MDR cells	[328]
PBAE	Luciferase gene	Hepatoma, primary hepatocytes	~38%–75% gene inhibition and 10%–20% cell apoptosis in hepatoma 50%–70% gene inhibition in primary hepatocytes	[204]
PHPMA-MPPM TMC	Luciferase gene	H1299 lung cancer cells	30%–40% gene silencing (compared with 50% with PDMAEMA nanoparticle and 60% with lipofectamine)	[329]

EHCO: N-(1-aminoethyl)iminobis[N-(oleicyl-cysteinyl-histinyl-1-aminoethyl)propionamide; RGD: Arg-Gly-Asp; Hsp27: heat-shock protein 27; PHPMA-MPPM: poly((2-hydroxypropyl)methacrylamide 1-methyl-2-piperidine methanol); TMC: O-methyl-free N,N,N-trimethylated chitosan; PBME: Poly(β-amino esters); PDbB: butyl methacrylate; PSMA: poly(styrene-alt-maleic anhydride). Concentrations provided in the "Efficacy" column refer to siRNA.

Table 4

In vitro Success at Inducing Apoptosis through siRNA Knockdown.

Gene Target	Delivery Method	Cell line	Effect	Ref
Anti-Apoptotic				
Bcl-2	siRNA vector Cationic Lipid Lipofectamine™	HeLa HeLa, Lung adenocarcinoma, hepatoma, ovarian carcinoma, ocular melanoma Melanoma, renal carcinoma	Stopped growth Stopped growth 25–35 % apoptosis	[250] [251] [253]
Bcl-xL	X-tremeGENE kit™	PHK, HaCaT	Growth inhibition and apoptosis	[330]
BAXi	Oligofectamine®	Prostate carcinoma	45% apoptotic cells	[331]
Survivin	Oligofectamine® Plasmid	Human sarcoma ovarian carcinoma, ocular melanoma Melanoma, renal carcinoma	10% apoptosis 45–70% apoptosis	[258] [253]
Livin	siRNA vector pSUPER	HeLa HeLa	8% apoptotic cells 4% apoptotic cells	[257] [332]
XIAP	Lipofectamine™	Ovarian cancer	75% apoptosis	[260]
c-myc	Lipofectamine™	MCF-7	50% apoptosis	[267]
Oncogenes				
HER2/neu	Oligofectamine®	SKBr3, MCF7/HER2 tumor cell lines	20–50% apoptosis	[267]
Viral E6 oncogene	pSUPER	HPV+ cervical carcinoma	Massive apoptosis of susceptible cells	[333]
Lyn Kinase (oncoprotein)	electroporation	Chronic Myelogenous Leukemia	40% apoptosis	[334]
PLK1	Oligofectamine® Plasmid vector	Breast cancer, HeLa, colon cancer, lung cancer HeLa, prostate cancer, human glioblastoma, dermal fibroblasts	13–50% apoptosis <5% apoptosis	[271] [335]
Protein kinase B	Lipofectamine™	Bone marrow cells, HEK 293	20% apoptosis	[336]
HDAC3	Oligofectamine®	HeLa	15% apoptosis	[337]
B-RAF	Thymidine	A375 Colo829 WM-266-4	23–52% apoptosis	[338]
OPA1	Oligofectamine®	HeLa NIH-OVCAR-3	38% apoptosis	[339]
m-bcr/abl	siRNA vector	K562 leukemic cell	7.5 fold increase in apoptosis	[340]

Table 5

In vivo Success at Inducing Apoptosis through siRNA Knockdown.

Gene Target	Method	Cell line / Animal Model	Effect	Ref
Anti-Apoptotic				
c-myc	Anisamide-targeted nanoparticles Plasmid polymerase III promoter Protamine-antibody fusion protein	Melanoma in mice MCF-7 in mice B16 melanoma in mice	Tumor growth decreased by 75% relative to control Increased tumor latency Tumor growth decreased by 75% relative to control	[262, 265, 266] [263] [264]
Bcl2	In vivo-jetPEI™	Melanoma in mice	15–50% apoptosis, decrease in tumor growth	[252]
BAXi	Superfect	HT1080 and B16F10 in mice	Reduces cancer metastasis	[341]
Survivin	DharmaFect®	A549/DDP in mice	Tumor growth decreased by 40% relative to control	[259]
XIAP	Lipofectamine™	MCF-7 cells in mice	Tumor growth decreased by 75% relative to control	[261]
Oncogenes				
Coagulation tissue factor mTF	Lipofectamine™ Ex vivo transfection	B-16 cells in Female C57BL/6 mice	Tumor growth did not vary significantly	[342]
PAR-1	Neutral liposomes (DOPC)	A375SM human melanoma cell line Female athymic nude mice (NCr-nu)	Tumor growth decreased by 75% relative to control, reduced invasion of cancer cells	[343]
HIF-1alpha	shRNA – Lipofectamine™ shRNA-Tf-PEI	A375 and A875 cells Nude mice	A375 – 50% reduction in tumor size A875 – no effect	[344]
STAT3	Lipid-substituted PEI	Murine B16.F10 cells Male C57Bl/6 mice	Significant increase in caspase 3 activity, tumor growth decreased by 70% relative to control	[325]
S100A4	pS100A4-shRNA	gastric cancer cell line, BGC823, nude mice	Tumor growth decreased by 75% relative to control	[345]
WT1	Aerosol PEI	B16 F10 mouse melanoma	Tumor growth decreased by 80%, survival time increased	[346]
Plk1	In vivo jetPEI™	C666-1 cells in mice	Increase to 50% multinuclear cells and decrease in tumor growth	[270]

Appendix C: *Ex Vivo* Red Blood Cell Hemolysis Assay for the Evaluation of pH-responsive Endosomolytic Agents for Cytosolic Delivery of Biomacromolecular Drugs

Video Article

Ex Vivo Red Blood Cell Hemolysis Assay for the Evaluation of pH-responsive Endosomolytic Agents for Cytosolic Delivery of Biomacromolecular Drugs

Brian C. Evans*[1,2], Christopher E. Nelson*[1,2], Shann S. Yu*[1,2], Kelsey R. Beavers[2,3], Arnold J. Kim[1], Hongmei Li[1,2], Heather M. Nelson[4], Todd D. Giorgio[1,2,5,6], Craig L. Duvall[1,2]

[1]Department of Biomedical Engineering, Vanderbilt University

[2]Vanderbilt Institute for Nanoscale Science & Engineering, Vanderbilt University

[3]Interdisciplinary Materials Science Program, Vanderbilt University

[4]Monroe Carell Jr. Children's Hospital, Vanderbilt University Medical Center

[5]Department of Chemical & Biomolecular Engineering, Vanderbilt University

[6]Department of Cancer Biology, Vanderbilt University

*These authors contributed equally

Correspondence to: Craig L. Duvall at craig.duvall@vanderbilt.edu

URL: http://www.jove.com/video/50166
DOI: doi:10.3791/50166

Keywords: Immunology, Issue 73, Cellular Biology, Medicine, Biomedical Engineering, Bioengineering, Cancer Biology, Molecular Biology, Erythrocytes, Endosomes, Small Interfering RNA, Gene Therapy, Nanomedicine, Gene delivery, Nanoparticles, Endosome Escape, Intracellular Trafficking, Cytosolic Drug Delivery, red blood cells, assay

Date Published: 3/9/2013

Citation: Evans, B.C., Nelson, C.E., Yu, S.S., Beavers, K.R., Kim, A.J., Li, H., Nelson, H.M., Giorgio, T.D., Duvall, C.L. *Ex Vivo* Red Blood Cell Hemolysis Assay for the Evaluation of pH-responsive Endosomolytic Agents for Cytosolic Delivery of Biomacromolecular Drugs. *J. Vis. Exp.* (73), e50166, doi:10.3791/50166 (2013).

Abstract

Phospholipid bilayers that constitute endo-lysosomal vesicles can pose a barrier to delivery of biologic drugs to intracellular targets. To overcome this barrier, a number of synthetic drug carriers have been engineered to actively disrupt the endosomal membrane and deliver cargo into the cytoplasm. Here, we describe the hemolysis assay, which can be used as rapid, high-throughput screen for the cytocompatibility and endosomolytic activity of intracellular drug delivery systems.

In the hemolysis assay, human red blood cells and test materials are co-incubated in buffers at defined pHs that mimic extracellular, early endosomal, and late endo-lysosomal environments. Following a centrifugation step to pellet intact red blood cells, the amount of hemoglobin released into the medium is spectrophotometrically measured (405 nm for best dynamic range). The percent red blood cell disruption is then quantified relative to positive control samples lysed with a detergent. In this model system the erythrocyte membrane serves as a surrogate for the lipid bilayer membrane that enclose endo-lysosomal vesicles. The desired result is negligible hemolysis at physiologic pH (7.4) and robust hemolysis in the endo-lysosomal pH range from approximately pH 5-6.8.

Video Link

The video component of this article can be found at http://www.jove.com/video/50166/

Introduction

Although there are many potential high-impact therapeutic targets inside the cell, the intracellular delivery of agents poses a significant challenge. Frequently, drugs, especially biologics, are internalized by cells and trafficked into vesicles that either lead to degradation of their contents through the endo-lysosomal pathway, or are shuttled back out of the cell *via* exocytosis.[1] In the latter process, the internal pH of the vesicles is acidified to approximately 5-6, which is the optimal pH for activity of enzymes that function in this compartment, such as lysozyme.[2]

Recently, a number of materials have been specifically engineered to leverage the acidification of endosomes to facilitate cytosolic delivery of their cargo. One example of this approach uses synthetic, polymer micelle nanoparticles whose core is zwitterionic and charge-neutral at physiologic pH (*i.e.* 7.4). However, at pH 6.0 - 6.5, the polymers become protonated and acquire a net positive charge that destabilizes the micelle core, and the exposed polymer segments interact with and disrupt the endosomal membrane. This activity has been shown to promote the endosomal escape of peptide and nucleic acid-based therapeutics, allowing them to access their cytosolic targets.[3,4] Other examples of methods developed to mediate endosomal escape that disrupt the membrane barrier include 'fusogenic' peptides or proteins that can mediate membrane fusion or transient pore formation in the phospholipid bilayer.[5] Homopolymers of anionic alkyl acrylic acids such as poly(propylacrylic acid) are another well-studied approach, and in these polymers, the protonation state of pendant carboxylic acid dictates transition into a hydrophobic, membrane-disruptive state in endo-lysosomal pH ranges.[6,7]

One useful model system for screening endosomolytic behavior is the *ex vivo* pH-dependent hemolysis assay.[8] In this model system, the erythrocyte membrane serves as a surrogate for the lipid bilayer membrane that enclose endo-lysosomal vesicles. This generalizable model has been used by others to evaluate the endosomolytic behavior of cell-penetrating peptides and other polymeric gene delivery systems.[8-11] In this experiment, human red blood cells and test materials are co-incubated in buffers at defined pHs that mimic extracellular (7.4), early endosomal (6.8), and late endo-lysosomal (< 6.8) environments. The amount of hemoglobin released during the incubation period is quantified as a measure of red blood cell lysis, which is normalized to the amount of hemoglobin released in positive control samples lysed with a detergent.

From screening a small library of potentially endosomolytic test materials, one can infer that samples that produce no hemolysis at pH 7.4, but significantly elevated hemolysis at pH < 6.5, will be the most effective and cytocompatible candidates for cytosolic drug delivery. Materials that fit these criteria would be expected to remain inert and not indiscriminately destroy lipid bilayer membranes (*i.e.* that could cause cytotoxicity) until being exposed to a drop in the local pH following internalization into endo-lysosomal compartments.

In this protocol, erythrocytes are isolated from a human donor and co-incubated at pH 5.6, 6.2, 6.8, or 7.4 with experimental endosomolytic drug delivery agents. Intact erythrocytes are pelleted, and the supernatants (containing hemoglobin released from lysed erythrocytes) are analyzed for the characteristic absorbance of hemoglobin *via* a plate reader (**Figure 1**).

Protocol

1. Preparation and Sterilization of Buffers and Test Agents

1. 150 mM NaCl buffer: Dissolve 4.383 g NaCl crystals in 500 ml of nanopure water.
2. pH Buffers: Prepare phosphate buffers at pH 5.6, 6.2, 6.8, and 7.4 by mixing appropriate amounts of monobasic and dibasic sodium phosphate. If samples are to be tested at lower pH values (*i.e.* pH < 5.6) then a more appropriate buffer, such as citrate buffer, should be used. Buffer recipes are readily available, and an example reference has been provided here.[12]
3. Sterilize all buffers noted above through a bottle-top vacuum filtration apparatus and re-check buffer pH's.
4. 20% Triton X-100 (positive control): Mix 20 ml pure Triton X-100 in 80 ml of nanopure water. Vortex vigorously and sonicate to dissolve. Leave at room temperature overnight before use.

2. Preparation of Erythrocytes

1. Obtain 25 ml of blood from an anonymous human donor, drawn directly into K_2-EDTA-coated Vacutainer tubes to prevent coagulation.

NOTE: All procedures must be pre-approved by the appropriate Institutional Review Board (IRB), and venipuncture and blood collection must be performed by a trained phlebotomist in order to minimize the risk to the donor. Standard phlebotomy procedures have been published elsewhere.[13]

2. Centrifuge blood at 500 x g for 5 min, and mark levels of hematocrit (red, lower layer) and plasma (yellowish, upper layer) on tube.
3. Aspirate plasma gently *via* a micropipettor, add into bleach, and discard into biohazardous waste.
4. Fill hematocrit tube to marked line (original level of plasma) with 150 mM NaCl solution. Cap and invert a few times to gently mix. Centrifuge at 500 x g for 5 min.
5. Repeat step 2.3-2.4 to wash blood cells again. Then aspirate supernatant and replace with PBS at pH 7.4. Invert to mix.
6. Split blood evenly into four tubes, corresponding to each pH that will be tested. Label the tubes according to each pH to be tested (5.6, 6.2, 6.8, 7.4).
7. Centrifuge blood tubes at 500 x g for 5 min. Mark levels on tubes, then aspirate supernatant.
8. Fill each tube to marked line with buffer of appropriate pH (as indicated in 2.6).
9. Label four 50 ml conical tubes (one per pH to test), and pipet 49 ml of PBS of appropriate pH into each conical tube.
10. Add 1 ml of erythrocytes (same pH) into corresponding tube for a 1:50 dilution. Visually inspect the diluted blood, which should be turbid and will settle if left undisturbed. If no pellet forms, cells have lysed.

3. Lysis Assay 96 Well Plate Setup and Quantification

1. Prepare stock solutions of all experimental drug delivery agents, at 20x the desired final concentration to be tested (Assay will take 10 µl of drug delivery agent + 190 µl diluted red blood cells, leading to a 1/20 dilution of the original drug delivery agent into the final test mixture). Stocks of 20, 100, and 800 µg/ml are suggested, resulting in final test concentrations of 1, 5, and 40 µg/ml, respectively.
2. Pipet 10 µl of each stock solution into V-bottom 96-well plates. For optimal results, load each sample in triplicate or quadruplicate.

NOTE: For ease, it is recommended that a separate 96-well plate should be prepared for each pH to be tested, with each sample (at each concentration) loaded at n=3-4 per plate.

3. For positive control wells, add 10 µl of 20% Triton X-100.
4. For negative control wells, add 10 µl of phosphate buffer. Use buffer at the same pH to be tested.
5. Pipet 190 µl of diluted erythrocytes (see 2.10) to each well, making sure cell stock solution remains homogenous during transfer. Hint: Use multi-channel pipette to simplify this task.
6. Incubate plates at 37 °C for one hour (Optional: Use an orbital shaker or rocker).
7. Centrifuge plates for 5 min at 500 x g to pellet intact erythrocytes. Note: when removing the plate from the centrifuge and transporting it to the next step, handle with care and be certain not to disrupt the cell pellet.

8. Using a multichannel pipet, transfer 100 µl of supernatant from each well into a clear, flat-bottomed 96-well plate. Note: if the cell pellet is accidentally disturbed for any sample(s), one can re-centrifuge the plate and then proceed with supernatant transfer.
9. Measure absorbance of supernatants with a plate reader. Note that a range of wavelengths can be used (400 - 541 nm).

NOTE: Different plate readers may have different saturation points and sensitivities, so the choice of a wavelength for measurements depends on whether or not hemolysis data from experimental samples can be reliably normalized against maximum hemolysis as induced by detergent treatment. This requires accurate measurement of absorbance values of the positive control samples.

10. Using Microsoft Excel or a similar data analysis software, find the average of the background absorbance readings from the negative control samples set up for each pH (step 3.4). Subtract this background absorbance value from all other samples that were measured at that pH.
11. After background subtraction, find the average absorbance of the positive control detergent-treated samples (step 3.3). Then normalize all experimental data points to this mean absorbance value, which should represent 100% hemolysis. Finally, multiply each well value by 100% to calculate % hemolysis that occurred in each individual well relative to the detergent control.

Representative Results

Typically, the agents that exhibit ideal pH-dependent hemolytic behavior have the highest potential for cytosolic delivery of drugs, nucleic acids, or other bioactive molecules. This is exemplified by Agent #1 as portrayed in **Figure 2**, which exhibits minimal hemolysis at pH 7.4, but a sharp increase in hemolytic behavior at endosomal pH ranges (< 6.5). Some agents may exhibit significant levels of hemolytic behavior at physiological pH ranges (Agent #2 at 40 µg/ml; **Figure 2**), suggesting that these agents may not be hemocompatible and could potentially be cytotoxic at these concentrations.

In most cases, hemolysis is also dose-dependent, as increasing concentrations of the test materials correspond with higher levels of hemolysis, especially at the lower pH ranges tested (5.6 - 6.2).

Figure 1. Schematic Diagram of Red Blood Cell Hemolysis Assay. Human erythrocytes are isolated and incubated with experimental endosomolytic drug delivery agents in a series of buffers simulating the pH range from physiologic (7.4) to late endosomes/lysosomes (5.6). The optimal drug delivery agents will not disrupt the erythrocytes at physiologic pH but will exhibit robust hemolysis in more acidic conditions. To assess percent hemolysis, the release of hemoglobin into the surrounding medium is measured *via* absorbance on a plate reader.

Figure 2. Representative Results of a Hemolysis Assay Demonstrating Behavior of Two Experimental Endosomolytic Agents. First, the average A_{450} of the vehicle (PBS) control was subtracted from the other samples tested at that pH. Afterward, experimental samples were normalized to the A_{450} of Triton X-100-treated erythrocyte samples and multiplied by 100%. Based on these control samples, the ability of experimental transfection agents to lyse erythrocytes can be calculated. Typically, ideal endosomolytic agents exhibit dose-dependent and pH-dependent hemolytic behavior. Ideal agents (such as Agent #1) exhibit minimal hemolysis at pH 7.4, but a sharp increase in hemolytic behavior at endosomal pH ranges (< 6.5). Some agents exhibit substantial hemolytic behavior at physiological pH ranges (Agent #2 at 40 µg/ml), suggesting that these agents may be cytotoxic at these concentrations. Error bars indicate standard deviation of 4 independent measurements.

Discussion

pH-responsive polymers or other agents designed for endosomolytic function can be rapidly and effectively screened based on lysis of red blood cells at pH values encountered in the endosome (**Figure 1**; pH 6.8 - early endosome, pH 6.2 - late endosome, pH 5.6 - lysosome).[14-17] pH-dependent hemolysis has been used to screen the ability of carriers to mediate endosomal release of biomacromolecular therapeutics (*e.g.* peptides, siRNA, ODNs, proteins), and results of this assay can be predictive of performance as an intracellular drug delivery vehicle.[3,4,8,18,19] Thus, this assay represents an effective screen to gauge the ability of polymeric drug carriers to mediate intracellular drug delivery based on their pH-dependent membrane disruption.

As noted in the procedure, hemolysis is detected through spectrophotometric measurement of the supernatants of red blood cells treated with experimental agents. Therefore, in addition to hemoglobin, it is likely to contain other erythrocyte-derived cytosolic components, including proteins and carbohydrates. While these other components may contribute a small amount of signal to the spectrophotometric measurement, 100% hemolysis was calibrated to the erythrocyte lysate resulting from treatment with Triton X-100. Assuming all erythrocytes from the same donor contain similar levels of hemoglobin and other biomolecules, we can safely conclude that the 'contaminating' components will not contribute any artifacts to the hemolysis measurement, especially if the same blood sample is used for all tests. However, this highlights the possibility that, for any given blood donor, there are likely to be small day-to-day variations in blood composition and hematocrit, and therefore, internal control samples (steps 3.3-3.4, 3.10-3.11) should be analyzed for all experiments.

One should also always closely examine the raw absorbance data. Though it cannot be appreciated in the normalized example data shown in **Figure 2**, detergents such as Triton X-100 effectively destabilize erythrocyte membranes regardless of pH, and one should expect to see very little sample to sample variability in positive controls. The absorbance spectrum of Triton X-100 does not include peaks in the 400-600 nm range recommended for this assay, and therefore, should not interfere with the normalization of experimental data.[20] Furthermore, for negative control samples, one should not observe significant hemolysis after the 1 hr incubation in any of the buffers used (*i.e.* even the most acidic buffer does not typically generate hemolysis on this timeframe). Background readings on negative control samples should closely approximate background absorbance readings taken on the fresh buffers.

Ideally, researchers will employ complementary strategies to characterize their experimental drug delivery systems. The hemolysis assay is advantageous for initial endosomolytic agent screening on naturally-occurring biomembranes, but should be considered as only one of the many tools in the drug delivery researcher's armamentarium for testing cytosolic delivery agents. For example, one potential shortcoming of the hemolysis assay is that it utilizes the red blood cell membrane as a biological model for endosomal membranes. However, the make-up and lipid content of endosomal membranes varies by cell-type and may not be accurately recapitulated by the blood cell membrane.[1] A variety of other, complementary assays have been developed to mimic endosomal membrane composition and behavior.[21,22] One alternative to is to utilize liposomes containing fluorescence resonance energy transfer (FRET)-quenched fluorophores, which become unquenched following destabilization of the liposomes and release of the fluorophores to the surrounding media. In studies that employ this method, the quantification of unquenched fluorophores has been found to correlate with the ability of a vehicle to mediate endosomal escape of its payload.[21,23] Microscopy-based measurements can provide a more robust but lower-throughput method that is complementary to the hemolysis assay. For example, it is common to assess colocalization of the carrier or the drug itself with dye-labeled lysosomes (*e.g.* LysoTracker by Life Technologies), or the trafficking pathways can be characterized using pH-sensitive dyes conjugated the carrier or drug (*e.g.* pHrodo by Life Technologies).[24-26]

Once an endosomolytic delivery system has been confirmed to achieve cytosolic cargo delivery, the hemolysis assay can also provide information on the mechanism through which endosomal escape occurs. For example, gene delivery vehicles based on polyethyleneimine (PEI) lack an inherent ability to disrupt phospholipid membranes at neutral or acidic pH's.[11,27] Instead, PEI achieves cytosolic gene delivery through a 'proton sponge' effect. After internalization, PEI buffers the endosome by "absorbing" protons that are pumped across the endosomal membrane to acidify these compartments. Eventually, this leads to buildup of excess protons and their counter-ions inside the endosome. This results in a rise in osmotic pressure, water influx, vesicle swelling, and endosomolysis. Therefore, the success of proton sponge effect necessitates the accumulation of a critical concentration of PEI into an endosome.[27] Delivery vehicles that achieve endosomal disruption through the 'proton sponge' effect will not physically disrupt red blood cells or liposomes, and their efficacy in achieving intracellular drug delivery must be assessed through osmotic pressure calculations, or *in vitro* microscopy, or functional studies.

In conclusion, the hemolysis assay described here is a reliable model for screening pharmaceutical agents designed for intracellular delivery of biologic drugs. This assay provides a high throughput means of drug delivery vehicle screening, enabling the rapid development of formulations that deliver biologics with intracellular targets.

Disclosures

IRB approval: Procedures involving human subjects have been approved by the Vanderbilt University Institutional Review Board (IRB; Protocol #111251). No conflicts of interest declared.

Acknowledgements

The authors acknowledge funding through the Department of Defense Congressionally Directed Medical Research Programs (#W81XWH-10-1-0445), National Institutes of Health (NIH R21 HL110056), and American Heart Association (#11SDG4890030).

References

1. Alberts, B., *et al.* Molecular Biology of the Cell., 4th edn., Garland Science, (2002).
2. Boasson, E.H. On the Bacteriolysis by Lysozyme. *The Journal of Immunology.* **34**, 281-293 (1938).
3. Convertine, A.J., Benoit, D.S., Duvall, C.L., Hoffman, A.S., & Stayton, P.S. Development of a novel endosomolytic diblock copolymer for siRNA delivery. *J. Control. Release.* **133**, 221-229 (2009).
4. Duvall, C.L., Convertine, A.J., Benoit, D.S., Hoffman, A.S., & Stayton, P.S. Intracellular Delivery of a Proapoptotic Peptide via Conjugation to a RAFT Synthesized Endosomolytic Polymer. *Mol. Pharm.* **7**, 468-476 (2010).
5. Varkouhi, A.K., Scholte, M., Storm, G., & Haisma, H.J. Endosomal escape pathways for delivery of biologicals. *Journal of Controlled Release.* **151**, 220-228 (2011).
6. Plank, C., Oberhauser, B., Mechtler, K., Koch, C., & Wagner, E. The influence of endosome-disruptive peptides on gene transfer using synthetic virus-like gene transfer systems. *Journal of Biological Chemistry.* **269**, 12918-12924 (1994).
7. Ratner, A.J., *et al.* Epithelial Cells Are Sensitive Detectors of Bacterial Pore-forming Toxins. *Journal of Biological Chemistry.* **281**, 12994-12998 (2006).
8. Saar, K., *et al.* Cell-penetrating peptides: A comparative membrane toxicity study. *Analytical Biochemistry.* **345**, 55-65 (2005).
9. Kichler, A., Leborgne, C., Coeytaux, E., & Danos, O. Polyethylenimine-mediated gene delivery: a mechanistic study. *The Journal of Gene Medicine.* **3**, 135-144 (2001).
10. Behr, J.-P. The Proton Sponge: a Trick to Enter Cells the Viruses Did Not Exploit. *CHIMIA International Journal for Chemistry*. **51**, 34-36 (1997).
11. Dawson, R.M.C., Elliot, D.C., Elliot, W.H., & Jones, K.M. Data for Biochemical Research 3rd edn., Oxford University Press, (1986).
12. Ernst, D.J. Applied Phlebotomy. 1st edn., Lippincott Williams & Wilkins (2005).
13. Bulmus, V., *et al.* A new pH-responsive and glutathione-reactive, endosomal membrane-disruptive polymeric carrier for intracellular delivery of biomolecular drugs. *Journal of controlled release : official journal of the Controlled Release Society.* **93**, 105-120 (2003).
14. Lackey, C.A., *et al.* Hemolytic Activity of pH-Responsive Polymer-Streptavidin Bioconjugates. *Bioconjugate Chemistry.* **10**, 401-405 (1999).
15. Murthy, N., Campbell, J., Fausto, N., Hoffman, A.S., & Stayton, P.S. Bioinspired pH-responsive polymers for the intracellular delivery of biomolecular drugs. *Bioconjugate chemistry.* **14**, 412-419 (2003).
16. Murthy, N., Robichaud, J.R., Tirrell, D.A., Stayton, P.S., & Hoffman, A.S. The design and synthesis of polymers for eukaryotic membrane disruption. *Journal of controlled release : official journal of the Controlled Release Society*. **61**, 137-143 (1999).

17. Yu, H., *et al.* Overcoming endosomal barrier by amphotericin B-loaded dual pH-responsive PDMA-b-PDPA micelleplexes for siRNA delivery.
ACS nano. **5**, 9246-9255 (2011).
18. Nelson, C.E., *et al.* Sustained local delivery of siRNA from an injectable scaffold. *Biomaterials.* **33**, 1154-1161, (2012).
19. Miozzari, G.F., Niederberger, P., & Hütter, R. Permeabilization of microorganisms by Triton X-100. *Analytical Biochemistry*. **90**, 220-233 (1978).
20. Chen, H., Zhang, H., McCallum, C.M., Szoka, F.C., & Guo, X. Unsaturated Cationic Ortho Esters for Endosome Permeation in Gene Delivery.
Journal of Medicinal Chemistry. **50**, 4269-4278 (2007).
21. Roth, C.M. Quantitative Measurements and Rational Materials Design for Intracellular Delivery of Oligonucleotides. *Biotechnology Progress*.
24, 23-28 (2008).
22. Blumenthal, R., Seth, P., Willingham, M.C., & Pastan, I. pH-dependent lysis of liposomes by adenovirus. *Biochemistry*. **25**, 2231-2237 (1986).
23. Moore, N.M., Sheppard, C.L., Barbour, T.R., & Sakiyama-Elbert, S.E. The effect of endosomal escape peptides on in vitro gene delivery of polyethylene glycol-based vehicles. *The Journal of Gene Medicine*. **10**, 1134-1149 (2008).
24. Panyam, J., Zhou, W.Z., Prabha, S., Sahoo, S.K., & Labhasetwar, V. Rapid endo-lysosomal escape of poly(DL-lactide-co-glycolide)
nanoparticles: implications for drug and gene delivery. *The FASEB Journal.* **16**, 1217-1226 (2002).

Appendix D: Scaling and systems biology for integrating multiple organs-on-a-chip

Lab on a Chip

RSC Publishing

CRITICAL REVIEW

View Article Online
View Journal | View Issue

Scaling and systems biology for integrating multiple organs-on-a-chip

Cite this: Lab Chip, 2013, 13, 3496

John P. Wikswo,*[abc] Erica L. Curtis,[ab] Zachary E. Eagleton,[ab] Brian C. Evans,[ab] Ayeeshik Kole,[ab] Lucas H. Hofmeister[ab] and William J. Matloff[ab]

Coupled systems of in vitro microfabricated organs-on-a-chip containing small populations of human cells are being developed to address the formidable pharmacological and physiological gaps between monolayer cell cultures, animal models, and humans that severely limit the speed and efficiency of drug development. These gaps present challenges not only in tissue and microfluidic engineering, but also in systems biology: how does one model, test, and learn about the communication and control of biological systems with individual organs-on-chips that are one-thousandth or one-millionth of the size of adult organs, or even smaller, i.e., organs for a milliHuman (mHu) or microHuman (μHu)? Allometric scaling that describes inter-species variation of organ size and properties provides some guidance, but given the desire to utilize these systems to extend and validate human pharmacokinetic and pharmacodynamic (PK/PD) models in support of drug discovery and development, it is more appropriate to scale each organ functionally to ensure that it makes the suitable physiological contribution to the coupled system. The desire to recapitulate the complex organ–organ interactions that result from factors in the blood and lymph places a severe constraint on the total circulating fluid (5 mL for a mHu and 5 μL for a μHu) and hence on the pumps, valves, and analytical instruments required to maintain and study these systems. Scaling arguments also provide guidance on the design of a universal cell-culture medium, typically without red blood cells. This review presents several examples of scaling arguments and discusses steps that should ensure the success of this endeavour.

Received 21st February 2013,
Accepted 14th June 2013

DOI: 10.1039/c3lc50243k

www.rsc.org/loc

Introduction

Organ-on-chip (OoC) microphysiological systems (MPS) programs funded by a variety of governmental agencies in the United States, Europe, and Asia are developing individual organs-on-a-chip and, more important, coupling human-cell, multi-organ, organ-on-chip and larger human organ construct (HoC) systems for drug development and studies of drug toxicity and efficacy. While individual OoC technologies have advanced considerably in the past decade,[1–6] significant technical challenges must be met before multiple organs can be integrated into a single system of coupled organs.[1] Only limited reports describe coupled organs,[2,3] and there is not yet a full understanding of how biological scaling laws apply to multiple, coupled OoCs. To replicate human physiology and drug response with interconnected human OoCs/HoCs, it is critical that each OoC/HoC has the correct relative size. Extensive literature describes differences in organ size between animal species whose body mass, M_b, spans 6 orders

[a]Vanderbilt Institute for Integrative Biosystems Research and Education, Vanderbilt University, Nashville, TN 37235, USA. E-mail: john.wikswo@vanderbilt.edu; Fax: +1 615-322-4977; Tel: +1 615-343-4124

[b]Department of Biomedical Engineering, Vanderbilt University, Nashville, TN 37235, USA

[c]Department of Molecular Physiology & Biophysics and Department of Physics & Astronomy, Vanderbilt University, Nashville, TN 37235, USA

} Electronic supplementary information (ESI) available: Discussion of the Shannon-Wiener Index, and a Scaling Spreadsheet that provides an extensive table describing scaling parameters for brain, heart, kidney, liver, lung, and blood. See DOI: 10.1039/c3lc50243k

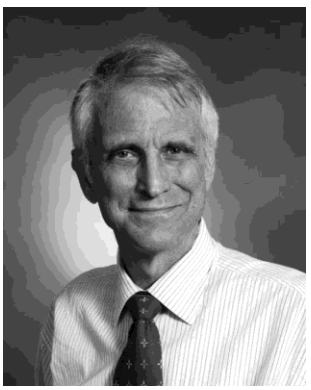

John P. Wikswo

John Wikswo received the B.A. degree from the University of Virginia in 1970 and M.S. and Ph.D. degrees, all in physics, from Stanford University in 1973 and 1975, respectively. He joined the Vanderbilt University faculty in 1977, where he is now the Gordon A. Cain University Professor, the A. B. Learned Professor of Living State Physics, and Professor of Biomedical Engineering, Molecular Physiology and Biophysics, and Physics. He uses novel instrumentation, quantitative measurements, and mathematical models to study and control cellular metabolism and signaling in organs on chips.

Erica L. Curtis

Erica Curtis received the B.E. degree in biomedical engineering from Vanderbilt University in 2013. As a participant in SyBBURE (Systems Biology and Bioengineering Undergraduate Research Experience), a program funded by Gideon Searle at Vanderbilt, she developed and tested a platform for performing quasi-real-time integration of microfluidics with mass spectrometry instrumentation for the purpose of studying yeast systems biology. In 2013 she was awarded a National Science Foundation Graduate Research Fellowship.

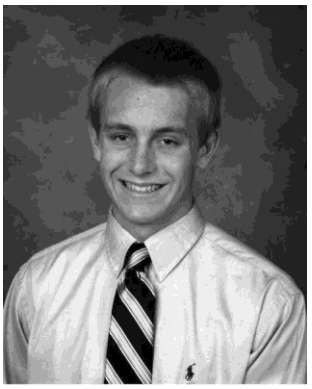

Zachary E. Eagleton

Zachary Eagleton received the B.E. degree in biomedical engineering from Vanderbilt University in 2013. At Vanderbilt he worked on the development of a low resource diagnostic test for malaria. The focus of his research was the use of optical coherence tomography to study flow patterns in small colloidal drops. He is currently a research and development engineer at Philips North America.

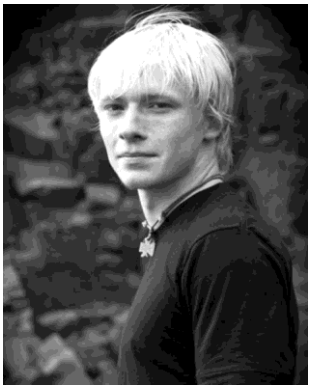

Brian C. Evans

Brian Evans received the B.S.E. degree in biomedical engineering from Case Western Reserve University in 2010 and the M.S. degree in biomedical engineering from Vanderbilt University in 2013. He is currently pursuing his Ph.D. in biomedical engineering at Vanderbilt University and is a National Science Foundation Graduate Research Fellow. At Vanderbilt he works on the development of novel biomaterials to enhance the intracellular delivery of biomacromolecular therapeutics for applications ranging from cardiovascular disease to cancer therapy.

Ayeeshik Kole

Ayeeshik Kole received the B.E. degree in biomedical engineering with honors from Vanderbilt University in 2012. At Vanderbilt his research focused on the use of high-resolution mass spectrometry in conjunction with microfluidics for the demonstration of cell system control. He is currently in the Medical Scientist Training Program at Indiana University School of Medicine, where he will earn a dual degree with a doctorate from the Purdue University Weldon School of Biomedical Engineering.

Lucas H. Hofmeister

Lucas Hofmeister received the B.S. degree in biomedical engineering from the University of Tennessee at Knoxville in 2010. He is currently pursuing his Ph.D. in biomedical engineering at Vanderbilt University, where he is an American Heart Association Graduate Research Fellow. At Vanderbilt Lucas's research is focused on developing targeted nanoparticle drugs to prevent and treat atherosclerosis, and he is a research coordinator for SyBBURE (Systems Biology and Bioengineering Undergraduate Research Experience), a program funded by Gideon Searle.

William J. Matloff

Will Matloff received the B.E. degree in biomedical engineering and mathematics from Vanderbilt University in 2013. As a participant in SyBBURE (Systems Biology and Bioengineering Undergraduate Research Experience), a program funded by Gideon Searle at Vanderbilt, he worked on building automated microfluidic chemical mixing tools for systems biology research.

Table 1 Allometric scaling coefficients and organ masses for a Hu, mHu, and μHu based upon primate data. Coefficients from Stahl, 1965[12]

			Human		milliHuman (mHu)		microHuman (μHu)		Organ mass ratios	
		Body mass:	60 kg		60 g		60 mg			
Organ	A	B	M, g	Organ/Body	M, g	Organ/Body	M, mg	Organ/Body	M_{mHu}/M_{Hu}	$M_{\mu Hu}/M_{Hu}$
Liver	33.2	0.93	1496	2.5%	2.4	4.0%	3.9	6.6%	1.62E-03	2.63E-06
Brain	85	0.66[a]	1268	2.1%	13	22%	139	232%	1.05E-02	1.10E-04
Lungs	9.7	0.94	455	0.76%	0.69	1.2%	1.0	1.7%	1.51E-03	2.29E-06
Heart	5.2	0.97	276	0.46%	0.34	0.57%	0.42	0.70%	1.23E-03	1.51E-06
Kidneys	6.3	0.87	222	0.37%	0.54	0.91%	1.3	2.2%	2.45E-03	6.03E-06
Pancreas	2.0	0.91	83	0.14%	0.15	0.26%	0.29	0.48%	1.86E-03	3.47E-06
Spleen	1.5	0.85	49	0.081%	0.14	0.23%	0.39	0.64%	2.82E-03	7.94E-06
Thyroid	0.15	1.12	15	0.025%	0.0064	0.01%	0.0028	0.0047%	4.37E-04	1.91E-07
Adrenals	0.53	0.7	9.3	0.016%	0.07	0.12%	0.59	0.98%	7.94E-03	6.31E-05
Pituitary	0.03		0.49	0.00081%	0.0044	0.0074%	0.040	0.067%	9.12E-03	8.32E-05

[a] Coefficients for human brain scaling: 80–90. The corresponding number for monkeys is 20–30, and great apes 30–40.

of magnitude from shrew to whale. Organ size does not scale proportionally (isometrically) with M_b, but instead obeys a number of different allometric power laws that describe, for example, how as the animal's linear dimension L increases, its mass increases as L^3, and hence the cross-sectional area of the bones must increase non-linearly.[4] Metabolic rates may exhibit $M_b^{3/4}$ scaling,[5–8] pulmonary and vascular networks exhibit $M_b^{3/4}$ scaling,[9,10] and blood circulation time scales as $M_b^{1/4}$.[11] Table 1 shows the coefficients A and B, derived from primates with body masses of 10 g to 100 kg,[12] to compute organ mass $M = AM_b^B$. When multiple organs are connected, their relative size could be normalized to mass, surface area, volumetric flow, or other geometric measures. The challenge is to specify the appropriate scaling law(s) for specific applications, whether it be to construct a physically functional organ (e.g., a pumping heart), a pharmacodynamic model (3D co-culture systems), or both simultaneously in a MPS.

For convenience we select three scales for our discussion: Human (Hu), milliHuman (mHu), and microHuman (μHu); we assume an adult Hu mass of 70 kg and hence a mHu mass of 70 g and a μHu mass of 70 mg. In theory, a system with multiple organs could be designed to represent any fraction of a human, possibly a nanoHuman (nHu). In this paper we discuss the factors that guide the specification of the size of each organ in a coupled system. We hope that this will provide guidance to the ongoing efforts to design and implement coupled organ systems.

Allometric scaling

i. Principle. Allometric scaling has been of great academic interest, but it is largely unexplored in the design of coupled microphysiological systems. As reviewed elsewhere,[1] allometric scaling formed the early foundation of pharmacokinetic modeling of the delivery and activity of a drug within a human relative to experiments using culture dishes and small mammals, but it has been supplanted by scaling based upon physiology rather than simply mass or body surface area.[13–15]

ii. Pros/cons. In this review, we follow a similar trajectory, beginning with simple allometric scaling to estimate organ size, and then concluding that the requisite OoC and HoC scaling must reflect physiological activity and the efficiency with which engineered tissues can replicate human organ function in vivo. The power of allometric scaling is that there is a rich literature to guide the OoC/HoC designer, as provided in the Scaling Spreadsheet in the Electronic Supplementary Information (ESI†). As we will show, allometric scaling provides an excellent starting point for specifying and validating coupled OoC/HoC systems.

However, this scaling may not produce valid parameters for mHu and μHu systems. The most notable observation from Table 1 is that the large human brain size (a = 85) and its allometric scaling exponent (b = 0.66) would produce a μBrain that has twice the body mass of the μHuman. The nature of this problem can be seen in Fig. 1. The intersections of the allometric scaling lines for each organ with the vertical mHu and μHu lines in Fig. 1A indicate the allometric mass of the mHu and μHu organ in Table 1. The scaling of each organ relative to its mass for a 1.0 Hu is shown in Fig. 1B, which suggests that allometric scaling for the brain, pituitary, and adrenals will produce larger than average organs, while that for the thyroid will be smaller. Given its median position, one might consider using the pancreas scaling as a starting point, with B = 0.91.

There would be similar issues were allometric scaling used to set the heart rates and blood circulation times. The heart rate of a mouse is approximately one hundred times that of an adult human,[11] and hence one would not want to assemble a mHu whose organs and the connecting vasculature would require perfusion at rates that would not be realistic for a human. Human cells might not function properly or for long when placed in organs sized to a mouse.

Simple scaling will also fail for other reasons. A working heart cannot be less than one cardiomyocyte thick. Key endothelial layers must be one cell thick, and only one cell, independent of organ size. Certain immune cells function at such a low density (3000 leukocytes per ml of cerebral spinal

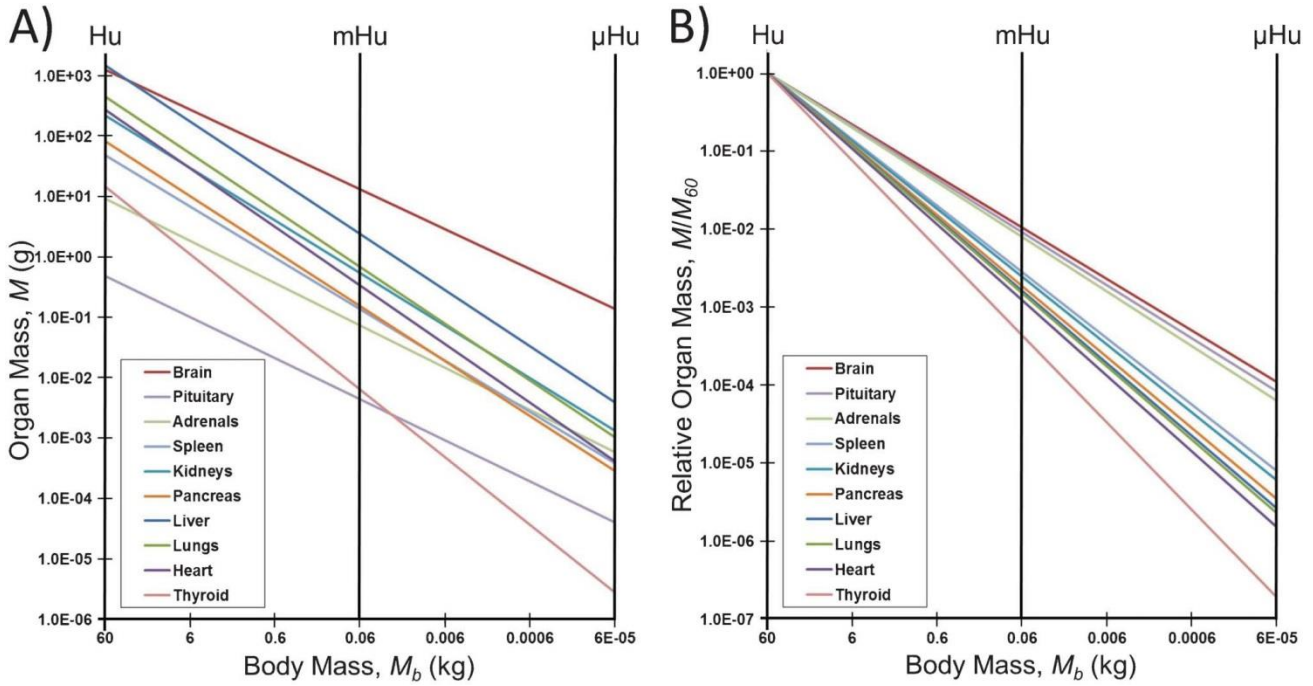

Fig. 1 How allometric scaling might (mis)inform mHu and mHu scaling when known power laws[12] are used to extrapolate from humans. A) Organ mass in grams. B) The mass of each organ relative to that for a 1.0 Hu. Note the range in allometric slopes for different organs, and that a 10^6 reduction in body mass leads to only a 10^4 reduction in the mass of the brain, pituitary, and adrenals, leading to a mBrain with twice the mass of the mHuman.

fluid (CSF)) that the breadth of acquired immune response may not be replicable in a mBrain with a CSF volume of ≯1 mL that would contain about 3 leukocytes. Cellular heterogeneity should not scale.

Interconnected ''histological sections''

i. Principle. Given that cells in OoCs/HoCs may not operate with the same efficiency as cells in vivo, it may be more realistic to construct an OoC/HoC system that reflects a small fraction of an adult human. Don Ingber has described this as creating ''living histological 'sections' of an adult human'' (personal communication).

ii. Pros/cons. This approach is ideal for OoC/HoCs operated in isolation, in that it effectively avoids the need for scaling by simply observing a small portion of an organ. The rate of perfusion can be determined by the number of cells being supported and the section can be studied for as long as it survives. The first challenge occurs if the media is recirculated – what is the correct volume for that media? The rate at which the OoC/HoC consumes nutrients, secretes metabolites, and otherwise conditions that media is determined by this volume, and to overestimate the volume might lead to proportion delays in the appearance, for example, of toxic metabolites, particularly if they have only limited lifetimes. It is necessary, however, to make the ''section'' large enough and sufficiently realistic that the organ functions in a more physiologically realistic manner than a simple monolayer monoculture in a Petri dish or well plate. Building a functional ''section'' from an individual human's cells may have advantages over using real ones[16] in that it may be possible to create ''sections'' of an individual patient's organs that are not readily available.

This approach is advantageous when one desires to recapitulate only a subset of an organ's function, for example, a lung alveolus with epithelial, endothelial, immune, and mechanical interactions but without requiring gas transfer,[17,18] a heart-on-a-chip that elucidates drug effects on cardiac electrophysiology or mechanical activity but doesn't pump blood,[19,20] or a gut-on-a-chip that does not consider bile activity, nutrient and water uptake, or abluminal transport.[21] In this case, the system may scale linearly, and in effect one is creating a local system with inputs, outputs, and selected physiological controls.[22]

However, the situation becomes more complex when two or more ''histological sections'' are coupled in series or parallel. Correct representation of organ-organ interactions is now determined by the size of each section and the volume of their shared fluid. A scaling mismatch of the two organs could make one section either oblivious of the other or dominated by it. Too large a fluid volume would delay or minimize organ-organ interactions. Furthermore, a small histological section may not be representative of the complexity of the organ as a whole and may be missing essential biological features that can alter biological responses to stimuli.

However, engineering all in vivo conditions artificially would fundamentally eliminate the need to couple the organ systems, and the same results could be achieved by running each organ in its own microenvironment. This contradicts the purpose of coupling the organ systems together, in which the goal is to observe the most physiologically accurate response and intra-

organ signaling to perturbations in the system without a priori biases. Hence we need functional scaling of our ''sections''.

Functional scaling

i. Principle. Given the shortcomings of allometric scaling and the uncertainties of how to scale coupled ''histological sections'', it is worthwhile to examine the obvious alternative: functional or physiological scaling of coupled organs. With this approach, one identifies the organ functions that are the most important for the coupled system, e.g., heart: volume pumped; lung: gas exchanged; liver: metabolism; kidney: molecular filtering and transport; brain: blood-brain barrier function and synapse formation. The functional parameters to be achieved for a particular implementation are specified, and then the physical milli- or micro-organ is sized, iteratively if necessary, to achieve the requisite functional activity given the constraints imposed by physical architecture, materials, and available cells.

ii. Pros/cons. This is a rational approach to preserve specific organ functions at their appropriate relative magnitudes, rather than relying on the classical, allometric approach. Given that the chosen functions should be quantifiable, this provides a straightforward approach to designing both the device and the functional readouts of a complete OoC system.

One limitation of the approach is that functional scaling may result in oversimplification of OoCs and limit the translatability of the results achieved. Another is that it may not be possible to create an organ that recapitulates more than one organ function. Just as we saw in Fig. 1, different functions may scale differently with respect, for example, to surface-volume ratio. One could devise two-part organs, e.g., a heart with separate chambers for recapitulating mechanical and electrophysiological functions.[19,20]

iii. Example. Fig. 2 shows an example of a coupled mHu HoC system currently under development by a collaboration between Los Alamos National Laboratory, Vanderbilt University, the University of California San Francisco, Charité Hospital Berlin, Harvard University, and the CFD Research Corporation.[23] The design challenges are to properly size all organs to provide realistic organ-organ interactions, including drug metabolism, and to do so with a low enough volume of blood surrogate that the autocrine and paracrine signaling factors released by each organ are not diluted to below the level of physiological effect for other organs. A working heart and a functional lung are desired. Simple scaling would suggest that given an adult blood volume of γ4.5 liters, a mHu and a mHu would have blood volumes of γ4.5 ml and γ4.5 ml, respectively. A microfluidic cardiopulmonary assist system might be required as the system is assembled and the organs grow and stabilize, e.g., if the lungs and heart have not yet achieved their needed level of gas exchange and pumping. Given that every organ in the body is not being represented, it may be necessary to include a microformulator[1,24,25] to add missing blood components, as well as a means to neutralize ones that are not removed by a missing organ. Finally, in recognition that complex biological systems tend to oscillate, a system for sensing and control[22,26] will be required to maintain organ stability and simulate aspects of neurohumoral physiological control not explicitly included, thereby ensuring both homeostasis and the requisite physiological daily and longer biorhythms.

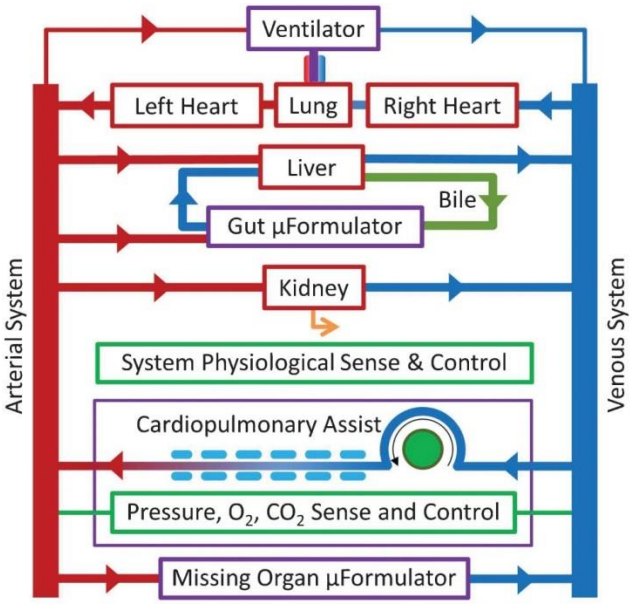

Fig. 2 The mHu Advanced Tissue-engineered Human Ectypal Network Analyzer (ATHENA), a milliHuman (Homo chippus) being developed by Los Alamos National Lab, Vanderbilt University, Charité Universitätsmedizin Berlin, University of California–San Francisco, Harvard University, and CFD Research Corporation with the support of the Defense Threat Reduction Agency (DTRA).[23] Figure from Wikswo et al., 2013, with permission.[1]

Examples of organ scaling

We now present several examples of scaling considerations that might apply to the creation of individual organs. In the ESI} Scaling Spreadsheet, we present an extensive compilation, with appropriate references from a vast and often inconsistent literature, of γ250 anatomical and functional parameters for the brain, heart, kidney, liver, lung, and blood that can be used to guide the design, modeling, and validation of OoCs and HoCs, using either allometric or functional scaling. In the following paragraphs we provide a brief discussion of the importance of several of the parameters for each organ.

Our examples are limited to the major organs that are common therapeutic targets and do not include other significant tissues such as adipose, bone, endocrine, skeletal muscle, or skin tissues. When attempting to recapitulate in vivo metabolic and physiologic demands of a coupled organ system, one must consider that these tissues also play a key role in metabolic demands and biochemical signaling. As a result, design criteria for OoC scaling should take into consideration the presence, absence, and simulation of various organs when scaling certain physiologic parameters. The ESI} Scaling Spreadsheet and the discussion of each example below should provide guidelines for a rational approach to the design of integrated HoC/OoC systems.

Brain

There are a growing number of reports on in vitro, flow-based models of the neurovascular unit (NVU) and blood-brain barrier (BBB),[27–31] and other neural co-cultures.[32–35] For this scaling analysis, we choose to reduce the brain from its extreme structural and functional complexity and focus our analysis on scaling of the NVU, which is the most important functional unit for ADMET (absorption, distribution, metabolism, and excretion toxicity) studies and functionally represents the BBB. The NVU consists of a capillary and its surrounding cell types, including endothelial cells, pericytes, astrocytes, microglia, and neurons. Correct and, importantly, feasible scaling of an NVU will require a unique combination of geometrical and biochemical scaling.

This is important because the brain is particularly complex, and the literature is riddled with inconsistent physiological data. For example, one of the most common misconceptions of brain physiology is that glial cells outnumber neurons by ten to one, where in fact the ratio for neocortical glia to neurons is 1.2, and the ratio of non-neuronal to neuronal cells ranges from 0.2 to 1.5, depending upon the brain region. These ratios are of exquisite importance when constructing a brain-on-a-chip.

Many of these misconceptions arise from the difficulty of studying the brain. Brain tissue is very diverse across species, and therefore studying the physiological parameters of rodent or other brains will not give an accurate representation of human physiology. The best understanding we can gain from non-human studies comes from the primate brain. The architectural complexity of the brain also complicates the analysis of simple parameters such as capillary density and cell numbers. Neurons can traverse multiple brain regions. Significant advances have been made in this regard by Herculano-Houzel et al., with their isotropic fractionator technique,[36] and improvements will continue to be made with more advanced analytical techniques such as the transparent brain recently developed by Chung et al.[37]

As the ESI} Scaling Spreadsheet indicates, gray matter and white matter may also contain different ratios of cell types and orientations. These parameters are important for scaling in brain region-specific ways. The task of assembling these parameters is complicated because most groups studying the brain make empirical measurements on a specific brain region and not the whole-brain scale. In addition, metabolic parameters such as oxygen consumption are difficult to measure for specific brain regions, but capillary density and cell number distribution are far easier to measure for isolated brain regions. To further complicate gathering this information, many of these parameters had to be assembled by studying the control groups from manuscripts investigating a specific disease state. Finally, it is unclear which of these parameters will be most important for the end goal of creating and integrating a brain-on-a-chip. Therefore, in the Scaling Spreadsheet we present our best understanding of the necessary physiological parameters and their sources for the reader to evaluate and employ as necessary. We envision this table of parameters as evolving alongside our understanding of the human brain and the challenges of building HoCs.

Functional scaling of the brain is largely driven by metabolism. In humans the brain represents 20% of the overall metabolic load and 2% of overall body mass.[38,39] Moreover, the relative metabolic demand of the brain grows more slowly than body and brain mass (allometric exponent 0.873).[40,41] The total energy consumption by the brain varies linearly with the number of neurons in the brain at a rate of 5.79×10^{-29} mmol glucose min^{-1} $neuron^{-1}$.[40] However, it is unclear if an in vitro brain-on-a-chip (BoC) can recapitulate the metabolic rate of the in vivo case. Therefore, we believe that a mHu and mHu BoC, for example, should be scaled linearly by the number of neurons in the adult human brain, and the remaining components of the brain should be scaled according to the metabolic demand of the number of neurons in the BoC. Autoregulation of the BBB by all cellular components of the NVU also necessitates correct scaling of the cell numbers in the BoC and capillary surface areas in relation to the metabolic demand of the neurons which they support. According to the cellular composition of the cerebral cortex, the NVU should consist of 1.2 astrocytes/neuron, 0.46 vascular cells/neuron, and 0.2 microglia/neuron.[42]

The greatest challenge in geometrical scaling of the brain is realization of the capillary density of the brain, which has one of the largest capillary densities of any organ. The average human adult has between 12 and 18 m^2 of BBB, or 150 to 200 cm^2 g^{-1} of tissue. The necessity of providing neurons with such a high capillary surface area per neuron (174 mm^2 $neuron^{-1}$) will challenge fabrication techniques and is most feasible in microfluidic systems.[42,43] In association with the vasculature, pericytes cover around 30% (5 m^2, 667 cm^2 g^{-1}) and astrocytes cover around 99% (18 m^2, 200 cm^2 g^{-1}) of the abluminal surface of brain microvasculature.[44–46]

Scaling of blood flow in a BoC relative to other OoCs could present significant challenges. The human brain has a flow rate of 7 L min^{-1}, which accounts for 13% of total blood flow.[47–50] This number should scale functionally with the size and metabolism of the BoC in order to supply sufficient glucose, oxygen, and other nutrients and remove resulting metabolites. Values such as the central metabolic rate for oxygen (CMRO2) of 3.2 mL/100 g min should remain constant with decreased size and will be a useful readout of BoC success.[47] Another critical factor is maintenance of the shear stress at the endothelial barrier. Blood surrogate flow must be supplied to a BoC with a sufficiently small capillary cross-sectional area to maintain a shear of around 1.5 Pa without excessive volumetric flow rates.[51–53] This value will also determine the pharmacokinetic parameters of the brain by influencing the residence time and Péclet number of the BoC capillaries.

In summary, the scaling of a BoC revolves around the NVU and is focused on delivering the correct metabolic demand relative to other organs and the unique transport properties of the BBB. As these technologies develop it will become more clear which of these scaling laws are critical to success, and also where scaling can or must be broken in favor of realistic implementation of these technologies for routine studies.

Heart

The scaling considerations that apply to the development of heart tissue revolve around tissue architecture and composition, electrical conduction, biochemical factors, metabolism, and fluid flow. An important decision that must be addressed early in the development of an OoC/HoC heart is whether it is to be a working heart, i.e., support the flow of blood against a mechanical load (including the pulmonary or peripheral vasculature),[54–58] or serve as an electromechanical sensor of the effects of drugs and their metabolites on cardiac performance.[19,20]

The cardiac parameters in the ESI† Scaling Spreadsheet support several of the major cardiac scaling issues we have discussed. For example, if a heart construct is to be used as the fluidic pump that provides and supports circulation of a blood surrogate through a coupled OoC system, then functional parameters such as transport capacity, ejection fraction, and fractional cell shortening become scaling issues of paramount importance. The ESI† Scaling Spreadsheet is constructed to circumvent the need to look up individual organ parameters, which often vary throughout the literature and species type. Furthermore, a desired organ size can be used to quickly calculate approximate parameter values for an organ of a certain size based upon both allometric and functional scaling. Thus the table is a valuable resource for quickly and efficiently approximating functional and structural parameters for OoC design, and it also highlights a number of the scaling issues that must be considered in terms of design criteria.

Composition and biochemical factors are of significant import in modeling mammalian heart tissue, which is intrinsically heterogeneous, containing cardiomyocytes, fibroblasts, vascular smooth muscle cells, endothelial cells, and neuronal cells among other less abundant non-myocytic cells.[59] These cell types all interact through a variety of biochemical factors and signaling mechanisms to maintain cardiomyocyte phenotype and tissue function.[60–65] In terms of these fundamental signaling pathways, one may need to consider exogenous sources of biochemical factors that are scaled to the targeted tissue construct's mass, volume, and composition. One must also consider that the size of the organ construct will limit the ability to accurately recreate features of the mammalian heart (e.g., if the size of a heart construct is limited to 1–2 cells thick, as would be required for a mHeart, then the realization of an endocardium and the incorporation of all native cell types will not be feasible, whereas this might be possible with a 15-myocyte thick mHeart).

Tissue architecture and metabolism must also be considered. The specialized cells that comprise heart tissue are organized in a highly specific structure that results in a transendothelial biochemical gradient that forms the blood-heart barrier. Furthermore, the fibers in the heart are aligned in anisotropic, helically wound layers that impart unique, spatiotemporally dynamic biomechanical properties to heart tissue. This issue is of key importance when considering the use of a scaffold or substrate as a culture platform, since mismatched substrate and tissue properties can result in a significant reduction in cardiac pump function. In addition to its complex architecture, heart tissue is very metabolically active and requires sufficient oxygenation. Thus, scaling cellular metabolism is another concern, as the balance of energy supply and demand is essential for maintaining cardiac pump function. To meet this demand, native heart tissue contains a dense, complex network of myocardial capillaries that penetrate orthogonally through the myocardium. However, recapitulating a complex network of small diameter capillaries may not yet be feasible in vitro, although recent developments are promising.[66,67] As a result, the utilization of planar diffusion may suffice for now, as the reduced thickness of the cultured myocardium of engineered heart tissue may allow for adequate oxygenation without vascular perfusion.

Fluid flow and other biomechanical stimulation of cardiac tissue are integral to a variety of the heart's intrinsic control mechanisms. Synchronized cardiomyocyte contraction results in complex mechano-electrical feedback mechanisms through the activation of stretch-activated channels and modulation of cellular calcium handling, the endocardium responds to both fluid shear stresses and pulsatile cyclical strain by releasing paracrine and endocrine factors, and baroreceptors transduce sensory feedback into various forms of cellular signaling. Under normal fluid shear conditions, endothelial and vascular smooth muscle cells have relatively low rates of proliferation, whereas abnormal hemodynamic conditions result in pathological cellular phenotypes that are associated with a number of cardiovascular diseases.[68] The proper scaling of biomechanical properties in conjunction with fluid dynamics is therefore crucial to modeling both normal and pathological cardiac tissue. In order to achieve physiologic fluid shear stresses in miniaturized working heart constructs, one must appropriately apply volumetric and resistance scaling by modulating flow rates and blood surrogate/media viscosity in accordance with the geometry of the bioreactor and tissue construct. These scaling issues only gain significance when integrating heart-on-a-chip technologies into multi-organoid constructs, especially if the heart tissue is to be responsible for cardiac output to perfuse the entire organ network. Here, cardiac output (i.e., stroke volume, heart rate, ejection fraction, etc.), tissue size, metabolic and perfusion demands of other tissues, total peripheral resistance, and resident blood surrogate volume are all variables that need to be properly scaled relative to each other. However daunting it may be, the scaling of biological variables for the integration of multiple human organ constructs provides a basis for fabricating functional mHu or mHu constructs that would streamline drug development and discovery and produce a more realistic cellular microenvironment than monolayer monocultures in Petri dishes or well plates.

Overall, each of these scaling issues merits consideration in the design of engineered heart constructs, and optimization of heart-on-a-chip technologies, not to mention all organ-on-a-chip technologies, is a compromise between verisimilitude and a functional abstraction.

Kidney

Building an in vitro kidney model necessitates architectural, functional, and biochemical scaling. The nephron consists of three structurally and functionally distinct subunits – glomerular filtration, proximal reabsorption and secretion, and urine

concentration–which must scale individually as well as relative to one another in order to preserve whole organ functionality.

The ESI† Scaling Spreadsheet provides examples and literature references for a range of functional and structural factors that need to be considered in kidney scaling. First and foremost, the kidney model must scale in order to sufficiently filter the circulating volume of blood in the HoC construct and achieve physiologically relevant rates of the glomerular filtration. Second, the model must be manipulated to facilitate physiological rates of fractional reabsorption, a challenging feat due to the wide discrepancies between in vivo functionality and in vitro performance. The kidney also provides a unique example of an organ in which the preservation of geometrical features, such as the countercurrent mechanism and exchanger, is critical to realizing an accurate model of the human kidney.

Functional scaling begins in the glomerulus. The glomerular filtration rate (GFR) in a 70 kg human produces 125 mL min^{-1} of ultrafiltrate and therefore 125 mL min^{-1} in a functional milliHuman (mHu).[39] The ratio of the surface area of the glomerular hemofilter to porous surface area can be optimized in the model to achieve this rate of filtration, given that a physical filter will be different from a biological one.

Recapitulation and subsequent scaling of the specific transport, metabolic, endocrine, and immune activities of the renal tubules pose formidable fabrication and scaling challenges.[69,70] A potential approach begins with functional scaling of active solute reabsorption rate in the proximal tubule. For example, a 70 kg human normally filters 180 g per day of D-glucose, almost all of which is reabsorbed in the proximal tubule; therefore, a mHu kidney must scale to filter and subsequently reabsorb about 180 mg of glucose per day.[71] Because metabolic activity and active transport abilities of the proximal cells in vitro may differ significantly from in vivo quantities, preliminary in vitro studies must be conducted to characterize the phenotype of human proximal tubule cells in single hollow fibers. From these results, we can predict the number of cells and surface area required for functional scaling of solute reabsorption. Manipulation of geometric dimensions or the use of parallel proximal tubule modules can ensure that the proximal tubule model can receive the appropriate volume of ultrafiltrate from the glomerular unit.

Although the scaling of the urine-concentrating mechanism must encompass functional scaling concepts, the approach must also pay particular attention to scaling the critical architecture of the loop of Henle. Although the relation of absolute loop length and urine-concentrating ability between species is highly debated, the creation of the corticomedullary osmotic gradient is unequivocally linked to active reabsorption of Na^+ as well as the complex geometry of the loop of Henle.[72,73] In an approach similar to that of the proximal tubule model, functional scaling in the loop of Henle can be achieved by scaling the rate of Na^+ reabsorption. Active reabsorption of Na^+ by Na/K-ATPase pumps located in the thick ascending limb of the loop of Henle (TAL) effectively drives the passive H_2O reabsorption in the descending limb. Additionally, the Na/K-ATPase pump has been extensively characterized and is tunable with a variety of solutes, hormones, and drugs, and therefore may serve as a point of modulation for scaling purposes.[74] Successful scaling may be impossible without the preservation of architectural features such as the countercurrent mechanism and exchanger. Computational modeling can be used to optimize the length and surface area to volume ratios needed to establish a physiologically relevant osmotic gradient for a human, 300 to 1200 mOsm regardless of size.[75] Additionally, ''preconditioning'' of long loops with short loops, as seen in vivo in a ratio of 85 short to 15 long in humans, may help to maximize urine-concentrating ability.[73,76]

The kidney is an excellent example of a key OoC/HoC design concept: while functional and biochemical scaling may provide the best approach to scaling a histological section of a human, some organ functionalities cannot be achieved without reproduction and scaling of certain physiological architectures.

Liver

The ESI† Scaling Spreadsheet provides an overview of the available allometric scaling laws for the liver and a basis from which we can evaluate parameters that will scale and those that will not.[77] Intuitively, we can identify certain parameters that will not scale. For example, cellular parameters such as sinusoidal endothelial cell (SEC) fenestration size will remain 100–1000 nm in diameter.[78] Additionally, hepatocyte density (1.39×10^8 cells g^{-1} liver), protein concentration (90 mg g^{-1} liver), and liver density (1.03 g liver mL^{-1}) are not expected to show appreciable scaling in our milli/microliver.[39,79]

There are, however, central design parameters for which there are allometric scaling laws, but from which we can justifiably deviate for functional scaling. For functional scaling, we argue that the hepatic mass will not follow the allometric power law and instead represent $1/10^3$ or $1/10^6$ of what is found in a normal human. For example, although an allometric power law exists for oxygen consumption, we instead use functional scaling given that the metabolic demand per hepatocyte—approximately 0.3 to 0.9 nmol $s^{-1}/10^6$ cells—will be equivalent in our scaled OoC.[80,81] The allometric value for oxygen consumption in the mHu ($O_2 = 0.035\ M_b^{0.69}$, with M_b in g, such that a 60 g mHu would have a hepatic oxygen consumption of 0.59 ml min^{-1}) underestimates consumption when compared to a functional proportion of a normal human (2.06 ml min^{-1}).[9] Note that if oxygen transport through the blood surrogate is insufficient, a system of hydrophobic hollow fibers could be used to increase the interstitial oxygen concentration without affecting interstitial or blood volumes, as has been done quite successfully for liver HoCs.[82,83]

In addition to proper oxygen delivery, there is also a need to seed the appropriate number of cells with sufficient exposure to a blood surrogate. In vivo hepatocytes sit adjacent to the 1.4 μm perisinusoidal space (i.e., the space of Disse), which separates the hepatocytes from the sinusoidal capillary that averages 10 μm in diameter and 275 μm in length. Appropriate concerns are whether a longer and larger in vitro model of a hepatic sinusoid unit via hollow fiber (HF) bioreactors will affect nutrient delivery, create unwanted oxygen gradients, and/or add to necessary volume given the limitations of HF fabrication. Although the number of hepatocytes needed for a

functional mHu is calculated to be 3×10^8 cells, it is unclear if current HF technology can support this.[83–85] Neither 3-D, planar microfabricated, or hollow-fiber livers have yet achieved collection of bile, generated by the liver canaliculi, into bile ducts.

Validation of the milli- and microliver models will primarily occur via iterative in vitro–in vivo correlation of xenobiotic clearance. Several groups have conducted correlation studies, with a general belief that each drug compound, unsurprisingly, may have its own allometric power law across species (due to metabolic variations) and also a different scaling factor (due to assumptions made in their model such as diffusional barriers).[86–93] For example, Naritomi et al. found that they could predict human in vivo clearance rates of eight model compounds from human in vitro data by using an animal scaling factor ($Cl_{in\ vivo}/Cl_{in\ vitro}$) from either a rat or a dog. Scaling factors were similar across species for each of the eight compounds, but varied from 0.3 to 26.6-fold among the compounds.[89]

While this variation may prove to be troublesome in the analysis of unknown compounds during drug evaluation and discovery stages, awareness of the properly scaled input parameters and thorough analysis of a wide range of model compounds (e.g., acetaminophen, diazepam) will assist in building predictive pharmacokinetic/pharmacodynamic (PK/PD) models of the OoC system.

Lastly, Boxenbaum notes in an early paper on allometric scaling of clearance rates that these models may not prove to be accurate, particularly at small masses, as the intercept of the allometric equation predicts a non-zero clearance rate at 0 g. This collapse of allometric theory at the micro- and milliscale gives credence to the necessity to scale based on organ function.[22]

Lung

Within the lung, the bronchial tree and the alveoli can be scaled separately. The main structures in the lung that do not scale with system size are the individual cell parameters, such as cell volume and radius. While one might not expect to scale the percent distribution of cells, this may be necessary if the efficiency of a particular cell type in a mHu or mHu differs from that in a Hu.

The ESI† Scaling Spreadsheet provides a collection of both functional and structural lung variables. Inconsistencies between the allometric exponents show a disconnect between structure and function, illustrating a novel problem when constructing HoCs. As we have discussed, additional support systems, such as assistance from a microformulator, may be necessary to ensure the most accurate structure/function mLung construct incorporated onto a HoC. A robust table of scaling values is therefore a valuable reference tool when making the inevitable compromises while designing a coupled OoC system.

Allometric scaling in the bronchial region is found in the diameters of the trachea and bronchioles. Allometrically, the diameter of the terminal bronchiole scales with an exponent of 0.21, while the radius of the trachea scales with an exponent of 0.39. However, this presents a problem: allometrically scaled, a mHu would have a terminal bronchiole diameter of 30 mm, which is near the limit of current soft-lithographic microfabrication technology; were hollow fibers used for the larger bronchial tubes, with a minimum diameter of 200 mm, the microfluidic network would require approximately six binary splittings to achieve a 240 mm diameter. Either scaling laws must be broken or novel fabrication techniques[94] utilized to accommodate and create a viable mHu trachea/bronchi system.[9]

Allometric scaling in the alveoli is critical as well. The most important function of the alveolus is oxygenation, so scaling should be addressed to meet oxygenation needs, if required for the MPS. The critical parameter to be properly scaled is surface area, as it is the main component of Fick's law and governs diffusion capacity across the alveolar-capillary barrier. Pulmonary diffusing capacity (DL_{O2}) scales linearly with body mass with an exponent of ≈ 1.[95] This means that the DL_{02}/body mass ratio is relatively constant in all mammals. Diffusing capacity is related to alveolar surface area, mean barrier thickness, and capillary blood volume, and the allometric coefficients are 0.95 for surface area, 0.05 for barrier thickness, and about 1 for capillary blood volumes.[95]

To replicate a mHu, alveolar diameter would be 21 mm–an order of magnitude less than the average 200 mm diameter of a human. The diameter of a type 1 epithelial cell is around 20 mm. Thus any individual mHu alveolus would require only a single epithelial cell,[9,96] but the entirety of alveolae for a 0.1 mHu might well be modeled by a rectangular membrane of the appropriate area.[17,18]

Another scaling argument that should be considered is the mass-of-tissue to volume-of-media, in this case lung tissue volume to blood volume. Blood volume is linearly related to body mass in mammals (allometric exponent of 1). Thus scaling lung tissue surface area and blood substitute volume in the HoC depends on the total mass of the system, and if both are scaled correctly then oxygen concentration should be sufficient. If scaling is ignored, problems could arise with the surface area required to supply the blood with sufficient oxygen for metabolic needs.[95]

A mLung would have 184 000 cells in the alveolar region. Around 37% of those (the interstitial cells) could be eliminated, since only endothelial, type I and II cells, and macrophages are needed to create a functional alveolar-capillary unit. The correct percentage breakdown of cells is important to assure sufficient paracrine factors and surfactant production.[97–99]

The scaling factor that appears to present the greatest challenge to a mLung is respiration rate. Were we to use allometric scaling, a mLung would have to inspire 643 times per minute to maintain proper oxygenation. Due to the strain this would put on a 1 mm thick polymer membrane, it is likely that this frequency would have to be slowed to prevent rupture. As a result, more surface area would need to be added or higher oxygen concentrations used to compensate for the loss of rate in order to maintain a minute volume of 0.17977 mL min^{-1} consumption of oxygen. This highlights the challenges of scaling, especially into the micro- and nano-scales, where the limitations imposed by non-biological fabrication technologies prevent meeting design parameters without violating scaling laws,[100] which could result in a less

accurate abstraction. Hence it is critical to specify the desired lung functions and scale the device to achieve them.

Blood

A universal media, or blood surrogate, for HoCs and OoCs must be able to support each cell type in addition to recapitulating the blood's critical role in homeostasis through the transport of dissolved gases, carrier proteins with bound molecules, soluble nutrients, metabolites, and signaling molecules. Since blood ''maintenance'' is dynamic but tightly controlled by several organs and biochemical processes, development of a blood surrogate is non-trivial.

Allometric scaling of blood components gives some insight into how the surrogate should be constructed. The ESI} Scaling Spreadsheet corroborates the scaling issues that must be considered in designing a blood surrogate. First, it can be seen that the concentrations of blood remain virtually the same in organisms of all sizes: conveniently, the concentrations of a remarkably large number of blood components do not scale with body mass.[101] This means that the creation of a blood surrogate can benefit from the large body of work that has been completed on creating cell media. Second, it can be noted that blood volume scales linearly with mass; thus, the total volume of the blood surrogate in an OoC/HoC device should be proportional to the entire size of the device. For all non-aquatic mammals, the blood volume is about 6–7% of the total body volume.[100] Scaling the blood surrogate volume with the size of the OoC/HoC device is necessary to ensure that signaling and other transported molecules are not excessively diluted and that the total mass of transported blood surrogate components is enough to support the organs. Third, the spreadsheet shows the critical functional parameters for ensuring that the cells behave in a physiological manner. The epithelial cells in contact with the blood surrogate must have the same shear stress that cells experience in the body to achieve the requisite polarization. In addition, the cells must experience the same levels of oxygen and carbon dioxide, which are dictated by the gas transport capabilities of the blood surrogate, in order to maintain the physiological metabolism of the cells. The physical properties of a number of different oxygen carriers are also shown. The spreadsheet is based upon the scaling of a complete system; as discussed above, it may be necessary to correct for the hydrodynamic, metabolic, and chemical activity of organs that are not included in the system.

Hence, little should be changed in normal blood to form a blood surrogate. However, there are other scaling issues that must be considered to ensure that the cells in the mHu and mHu behave physiologically.

First, the blood surrogate must recapitulate physiological oxygen transport properties. Experiments have shown that the rate of oxygen delivery to the cells affects the cells' metabolic rate.[102] There are programmatic differences relative to the suitability of serum in an OoC/HoC system: the Defense Threat Reduction Agency (DTRA) program announcement[23] precludes the use of serum, whereas the Defense Advanced Research Projects Agency (DARPA) program[103] does not. If simple serum-free aqueous culture media is used, the low concentration of dissolved oxygen in the media may limit metabolic rates and affect capillary surface-to-volume scaling. Therefore, the level of oxygen transport that cells experience in vivo as enabled by hemoglobin must be functionally mimicked with the blood surrogate. Were erythrocytes not used, perfluorocarbons and hemoglobin-based oxygen carriers may be very effective for achieving this.[104–106] If human or animal serum is not utilized, appropriate concentrations of carrier proteins such as albumin may be required to replicate organ-organ chemical communication.

For the purpose of supporting HoCs, the blood surrogate must maintain multiple cell types while also optimizing physiological processes. While there is no known universal serum-free media, a number of different formulations of minimal media can be used as a starting point for the creation of a medium that can support multiple cell types.[107,108] To achieve optimal cell functionality and longevity, supplements must be added to this minimal medium.[109]

Although a number of effective medium formulations for the growth and maintenance of multiple cell types have been developed, these media mixtures have not been widely tested for interconnected HoCs. For OoC/HoC systems, this represents a significant challenge due to differential scaling, simultaneous maintenance of multiple cell types, and the recirculatory nature of HoCs. Logic dictates that during flow-through of the blood surrogate within a HoC, some components will be absorbed or metabolized, while others will be added to the blood surrogate, with a negative impact on downstream HoCs.

One method that has been successfully used to create a common blood surrogate for a number of different cells in an OoC/HoC first involves combining the established serum-free mediums of each cell type, which can be found in the literature, to create a base medium. Next, various other components, such as growth factors and supplements, are added to optimize for physiological functionality, based on a number of different physiological measures. Finally, since some of the components of the medium support one type of cell but hinder others, one of several different techniques is used to ensure that each organ receives an optimal subset of the components of the blood surrogate. Zhang et al. [108] demonstrated this method by creating a blood surrogate that supported four cultured cell types: liver (C3A), lung (A549), kidney (HK-2), and adipose (HPA). Another option is to grow cells in isolated OoC/HoCs on their preferred media, and then gradually, through controlled valves, wean them slowly from this media to the universal one.

In addition, some properties of blood and related structures that exist physiologically cannot yet be replicated with HoCs. For example, capillaries, which have relatively constant size across species, are too small to be recreated at present, so care must be taken to design the HoCs such that the physical characteristics of the blood surrogate, such as flow, volume, and shear stress, match those found in the tiny capillaries. It is imperative to match the wall shear stress in HoCs to that of microvessels to achieve the same mechanotransduction and gene expression in endothelial cells as in humans.[52] This might be addressed by self-organizing on-chip microvasculature.[66,67]

Furthermore, it is important to understand PK/PD scaling in order to add drugs to the HoC/OoCs at proper levels and to use the HoC/OoCs to predict the pharmacokinetics in humans.[2,3] The classical scaling relationship for drug/signal dosing is that the body's ability to use and metabolize drugs/signals varies with surface area.[110] But these scaling laws are critically dependent on the biochemical mechanisms and physical properties of the organs.[111] If the organs do not functionally mimic physiology, they could fail to predict the PK/PD of humans. Differences in drug transport and metabolism in the HoC can render typical allometric PK/PD scaling useless. This can be seen clearly by the fact that PK/PD varies significantly between infants and adults.[112]

Finally, the blood surrogate will require supporting systems that can provide missing functionality required for blood surrogate and organ maintenance. As required, a microformulator[108] can provide media supplements specific to each organ.[108] The microformulator could be used to locally add media components to a particular organ. A size-exclusion filter or an affinity capture chamber or matrix (Donna Webb, personal communication) could be used to remove any toxic molecules produced by one organ before they reach other organs. Computer-controlled microformulators could also provide the regulated injection of molecules that cannot be maintained by the system alone and those from organs not in the HoC.[24,113]

Cellular heterogeneity

In contrast to the common monocultures and occasional co-cultures used in much of cellular biology, organs present a much richer cellular heterogeneity. Cellular heterogeneity is a key issue to consider when applying scaling laws to OoCs, since downscaling an organ may result in a reduction in the number of cell types present. Furthermore, achieving a complex co-culture system that preserves native cellular heterogeneity in an organ, much less coupled organs, is still far from realization. As a result, in addition to scaling issues, the choice of cell types used to develop an OoC may also be altered in order to focus on a biological response that is specific to a certain cell population in the organ of interest. Table 2 indicates the relative fractions of the most common cells in each of the organs considered. In the ESI}, we present these data in terms of Shannon-Wiener Index (SWI),[114,115] a useful method to quantify cellular heterogeneity. We were unable to identify from the literature a self-consistent set of cell distributions for the kidney. One could also argue that the erythrocytes and leukocytes could be treated separately.

Table 2 Heterogeneity of cell types in different organs

Organ	# of cell types, N	Cell type	%
Brain (neocortex)[42]	4	Glia	41%
		Neurons	33%
		Vascular	17%
		Microglia	8%
		Total	100%
Heart[59,60]	5	Cardiomyocytes	55%
		Fibroblasts	25%
		Vascular smooth muscle	10%
		Endothelial	7.0%
		Neuronal	3.0%
		Total	100%
Liver[116]	4	Hepatocyte	60%
		Sinusoidal endothelial	20%
		Kupffer	15%
		Hepatic stellate	5.0%
		Total	100%
Lung (alveolar) [97]	5	Endothelial	39%
		Interstitial	29%
		Type II epithelial	18%
		Type I epithelial	11%
		Alveolar macrophages	3%
		Total	100%
Blood[117]	6	Erythrocytes	99%
		Neutrophils	0.50%
		Lymphocytes	0.30%
		Monocytes	0.050%
		Eosinophils	0.025%
		Basophils	0.007%
		Total	99.9%

Engineering challenges

We have discussed a number of criteria for scaling mHu and mHu organs as required to design and validate realistic, coupled HoC/OoC systems. That said, there are also a number of engineering challenges that must be met before it is possible to construct a realistic mHu as shown in Fig. 2 or a mHu as shown schematically in Fig. 3. These challenges are cataloged in detail elsewhere,[1] and include determining the proper size of each organ, fluidic control of mL and mL volumes, analytical chemistry in mL and nL volumes, including comprehensive molecular characterization in real time, maintaining and controlling coupled organ systems, vascularizing organs with appropriate surface-to-volume ratios, developing a universal blood surrogate, accounting for missing organs and the adjustment of blood surrogate, modeling coupled organ systems, characterization of organ health and disease, and minimizing organ cost to enable high-content screening. Several of these can be revisited based upon our detailed scaling analysis.

The circulating volume of perfusate of an OoC/HoC must match organ size, lest metabolites, hormones, and paracrine signals be diluted to the point that each organ operates in a large reservoir independent of the other organs, thereby precluding accurate study of the desired organ-organ interaction so necessary for PK/PD,[120] ADMET,[121] and drug safety/toxicity studies.[122,123] The aforementioned γ4.5 mL and γ4.5 mL blood volumes for a mHu and mHu will place severe constraints on not only the fraction of an organ bioreactor that must be occupied by cells, but also limits the size of in-system sensors and the volume that can be withdrawn for analysis of the system's state and subsequent control adjustments. The

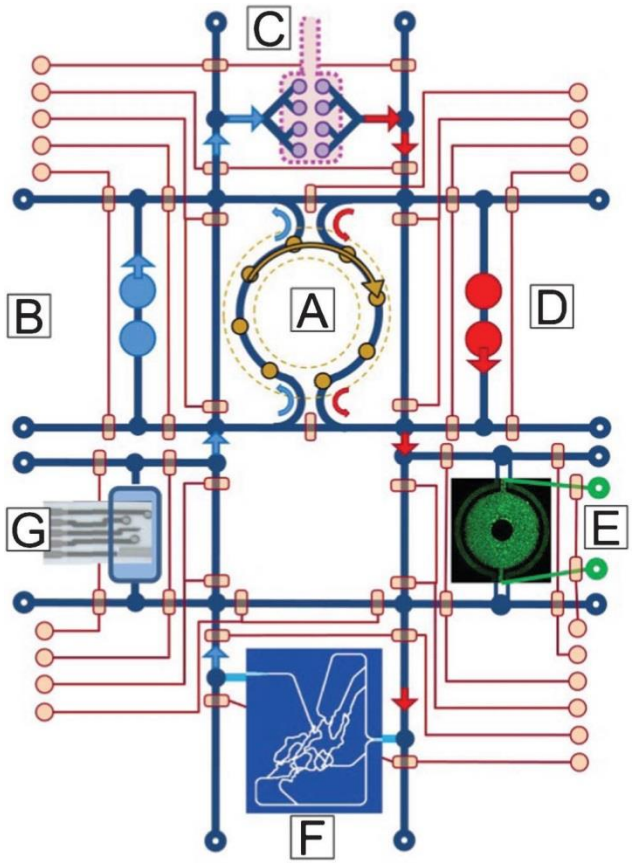

Fig. 3 A concept drawing of a four-organ mHu (Homo chippiens). A) An on-chip peristaltic ventricular assist, B) Right heart, C) Lung, D) Left heart, E) Liver (courtesy of Kapil Pant), F) Peripheral circulation[118] (courtesy of Kapil Pant), G) Microchemical analyzer of metabolic activity.[119] The system would operate on a single microfluidic chip, with on-chip pneumatic valves controlling system functions and connections.

scaling arguments applied to the organs also apply to the instruments that will analyze their performance.

One might also wonder whether the ratio of cell-to-perfusate volumes alone precludes the use of conventional well plate cell culture in creating properly coupled HoC/OoC systems: blood and interstitial fluid volumes for organs in vivo are a small fraction of the volume of the organ itself. Well-plate tissue cultures without internal vascularization can seldom support tissues thicker than 100 to 300 mm without necrosis, so the height of fluid above such tissues grown in a well plate would have to be a small fraction of the thickness of the cell layer to maintain the proper tissue-fluid volume ratios. Because of surface tension effects, it is difficult to pipette fluid from such a thin layer of fluid without damaging the underlying cells. This argues for flow-based HoC/OoC systems that can function within the aforementioned volume constraints. The capabilities of microfluidic systems will be critical to produce compact organs with both appropriate temporal responses and the ability to produce and react to circulating cytokines,[124–126] and to work with small quantities of rare or expensive human cells.[127]

Another issue that has been largely overlooked yet is critical to consider in OoC/HoC design is temporal scaling in reference to disparate cell growth and turnover rates between tissues and between in vivo and in vitro conditions, particularly when studying drugs with slow kinetics. It is well recognized that cellular co-cultures are subject to being overrun by one of the two cell types, although components can be added to culture media to retard proliferation of one species[128] or accelerate the growth of the other. It may be possible to design a mechanical means to address cellular turnover, for example by adding or removing sections of cells from an organ as the entire MPS ages.

While fluorescence sensors can be used to record metabolic signals such as acidification and oxygenation, it may be wise to reserve optical bandwidth for intracellular fluorescent probes, and instead utilize miniature, wide-bandwidth electrochemical sensors matched to small cell populations[129–131] or single cells.[132–135] It is a great advantage that, typically, the signal-to-noise ratio of electrochemical sensors does not increase as the electrodes are miniaturized,[136] and it has been shown possible to make electrochemical measurements of single cells and small cell populations.[134,135,137,138]

A larger problem is to characterize the circulating molecules either consumed or produced by each organ, given the small volumes and the need to track concentrations of many molecules over long periods of time. Nanospray injection, ion mobility-mass spectrometry (nESI-IM-MS) may prove to be the key technique for rapid OoC state monitoring, given that IM separations require milliseconds rather than the hour or so of high pressure liquid chromatography,[139,140] with the recognition that nESI requires desalting of the media that can now be done on-line.[141] Ultimately, the sensors and controllers might be interconnected in a way that would lead to automated inference of model-based control algorithms.[22,142]

An additional implication of the small fluid volumes in a mHu or mHu is that adjustment of the chemical concentrations of the perfusion media, for example to simulate humoral control of organ function, requires injection of small volumes of precisely mixed fluids. While a high-throughput screening fluidic robot or droplet injector can handle nl to pl volumes, it is a non-trivial to connect one of these into a closed, circulating system of coupled HoCs/OoCs. It is yet another problem to achieve the dynamic range of concentrations of different chemical species found in typical cell culture media without the use of large volumes of media and serial dilution techniques. It will also be necessary to provide the signaling molecules and metabolites from missing organs, as well as apply localized biochemical perturbations to assess the response of the other organs, but note that this has to be done as a small perturbation of the mL to mL volume of the blood surrogate with a temporal resolution guided by the requisite controller bandwidth. A microfluidic microformulator as we discussed earlier may meet these needs.

As the complexity of a coupled OoC system increases with the number of organs integrated, organ scaling will become more complicated, since the metabolic demands and relative

scaling between organs will undoubtedly be affected. We also believe that the scaling in multi-organ OoC/HoC systems, particularly for dynamic metabolic phenomena, will require systematic design such that the functional scaling of any organ system is not significantly altered by another organ, and no single organ receives a substantial, unintended scaling priority.

Coupled non-linear biological systems can spontaneously oscillate and may require external stabilization, which in turn will require the use of sensors and controllers, possibly at the level of each organ. The neurohumoral control of human homeostasis may in fact be simulated by a properly configured sensor and control system, which in turn will benefit from both properly scaled sensors and the ability to rapidly reformulate the perfusion media. That said, regulatory noise may contain useful information about system interconnections.

It will be interesting to determine whether cellular heterogeneity in mixed cultures, critical to cellular signaling mechanisms in vivo, can be maintained for long times in vitro in coupled HoC/OoC systems. Given the regulatory role of the cellular microenvironment in vivo,[143,144] there would be reason to expect that it might in fact become easier to maintain heterogeneity as multiple cell types are grown together in balanced environments with self-conditioned media. The Shannon-Wiener Index may prove important in assessing and controlling this.

We have not yet addressed in detail the scaling issues associated with microfluidics, oxygen carrying capacity of the blood surrogate, and the distributed hydraulic impedance of both the individual organs and the coupled system. This is of particular significance for mHu and mHu systems with working hearts. One would expect that designing around these constraints would benefit greatly from multiphysics, computational biology modeling tools.[145,146] Optimized microfluidic design using a first-principles optimization of vascular branching[147–149] may be better suited than approaches that assume a particular scaling law.[9]

Ultimately, there may be significant technical and economic advantages to creating a mHuman on a single microfluidic chip as shown schematically in Fig. 3. Simpler implementations are already being developed.[108] The total volume of fluidic interconnects is minimized. On-chip valves can be utilized to bypass individual organs while the organs are being seeded and grown to a stable state, and to adjust the duty cycle by which they are connected to the entire system so that conditioning of media can be gradual rather than sudden, providing time for cellular up- and down-regulation of signaling and control genes. Multi-organ integration is not, however, a practical approach until each organ has been perfected individually, albeit at the correct size. Hence as we gain experience in this field, we need to make our HoCs and OoCs small, but not too small.

Conclusions

It is reasonable to assume that the many issues addressed in this review can be resolved through careful attention to engineering and physiological details, particularly with the large number of well-funded investigators now working on this worldwide. Clearly, this does represent a Lab-on-a-Chip challenge of unprecedented complexity and significance. It is most important to recognize that there are obvious trade-offs between realism and simplicity, since the ability to sense and control the microscale environment in microfabricated organs-on-a-chip may provide a solution to the current impasse in extending existing in vitro models, most of which are based upon single-layer cellular monoculture, to greater realism and utility.[150]

There will undoubtedly be requests to make these OoC/HoC systems ever-more realistic, and to criticize them for their shortcomings. There have been similar drives for perfect reductionist representations, particularly in the regulatory networks and systems biology communities, where computational models continue to grow in complexity and may operate at a very small rate compared to real time. It is important to realize that OoC/HoC systems reside in a niche of abstraction that will improve constantly with technology but will never exactly recreate a full human, which represents $\gamma 10^{9}$ years of evolutionary engineering. It may be most useful if OoCs and HoCs are viewed as simplified model systems for PK/PD and systems biology studies, not small humans.

The drive to perfect reductionism is put in perspective by both Jorge Luis Borges and Lewis Carroll, in which a map of an empire/country the size of an empire/country is not found useful.[151,152] Just as a perfect map resolves few problems and produces others, the creation of a near-to-perfect in vitro replica of a human may accomplish little at great expense. We believe that with the proper application of scaling and a balance between abstraction and realism, we should be able to learn much about the complexity of human biology[153] and its interaction with drugs from each implementation of a HoC/OoC. Ultimately, we may be able to create OoC/HoC surrogates for specific genetic or disease subgroups for drug development or for individual patients to optimize their treatment.

Acknowledgements

We thank Rashi Iyer and Kapil Pant for their contributions to Fig. 2 and 3, and Allison Price and Don Berry for their editorial assistance. We have benefitted from extensive discussions with Frank E. Block, Jr., Frank E. Block III, David Cliffel, William Fissell, Geraldine Hamilton, Donald Ingber, Rashi Iyer, Daniel Levner, John McLean, Kapil Pant, Kevin Kit Parker, Andrzej Przekwas, and Philip Samson regarding microfluidic devices and organs-on-a-chip. This research has been funded in part by Defense Threat Reduction Agency grants HDTRA1-09-1-00-13 and DTRA100271A-5196; NIH grants R01GM092218, RC2DA028981, and, through the NIH Common Fund, NCATS grant 1UH2-TR000491-01; DARPA grant W911NF-12-2-0036;

the NSF Graduate Research Fellow Program (BCE); and the Vanderbilt Institute for Integrative Biosystems Research and Education (VIIBRE), the Systems Biology and Bioengineering Undergraduate Research Experience (SyBBURE) funded by Gideon Searle, and a Vanderbilt University Discovery Grant. The content is solely the responsibility of the authors and does not necessarily represent the official views of the funding agencies and institutions.

References

1 J. P. Wikswo, F. E. Block III, D. E. Cliffel, C. R. Goodwin, C. C. Marasco, D. A. Markov, D. L. McLean, J. A. McLean, J. R. McKenzie, R. S. Reiserer, P. C. Samson, D. K. Schaffer, K. T. Seale and S. D. Sherrod, IEEE Trans. Biomed. Eng., 2013, 60, 682.
2 M. B. Esch, T. L. King and M. L. Shuler, Annu. Rev. Biomed. Eng., 2011, 13, 55.
3 M. Shuler, Ann. Biomed. Eng., 2012, 40, 1399.
4 K. Schmidt-Nielsen, J. Exp. Zool., 1975, 194, 287.
5 M. Kleiber, Hilgardia, 1932, 6, 315.
6 M. Kleiber, Proceedings of the Society for Experimental Biology and Medicine. Society for Experimental Biology and Medicine (New York, N.Y.), 1941, 48, 419.
7 K. Schmidt-Nielsen, in Scaling: Why is animal size so important?, Cambridge University Press, New York, 1984, ch. 8, pp. 90–98.
8 P. S. Dodds, D. H. Rothman and J. S. Weitz, J. Theor. Biol., 2001, 209, 9.
9 G. B. West, J. H. Brown and B. J. Enquist, Science, 1997, 276, 122.
10 J. H. Brown, V. K. Gupta, B. L. Li, B. T. Milne, C. Restrepo and G. B. West, Philos. Trans. R. Soc. London, Ser. B, 2002, 357, 619.
11 S. L. Lindstedt and W. A. Calder, Quart. Rev. Biol., 1981, 56, 1.
12 W. R. Stahl, Science, 1965, 150, 1039.
13 T. N. Johnson, A. Rostami-Hodjegan and G. T. Tucker, Clin. Pharmacokinet., 2006, 45, 931.
14 M. Danhof, J. de Jongh, E. C. M. De Lange, O. Della Pasqua, B. A. Ploeger and R. A. Voskuyl, Annu. Rev. Pharmacol. Toxicol., 2007, 47, 357.
15 H. W. Leung, in General, Applied and Systems Toxicology, John Wiley & Sons, Ltd, 2009.
16 M. Hadi, I. M. Westra, V. Starokozhko, S. Dragovic, M. T. Merema and G. M. M. Groothuis, Chem. Res. Toxicol., 2013, 26, 710.
17 D. Huh, D. C. Leslie, B. D. Matthews, J. P. Fraser, S. Jurek, G. A. Hamilton, K. S. Thorneloe, M. A. Mcalexander and D. E. Ingber, Sci. Transl. Med., 2012, 4, 159ra147.
18 D. Huh, B. D. Matthews, A. Mammoto, M. Montoya-Zavala, H. Y. Hsin and D. E. Ingber, Science, 2010, 328, 1662.
19 A. Grosberg, P. W. Alford, M. L. McCain and K. K. Parker, Lab Chip, 2011, 11, 4165.
20 P. W. Alford, A. W. Feinberg, S. P. Sheehy and K. K. Parker, Biomaterials, 2010, 31, 3613.
21 H. J. Kim, D. Huh, G. Hamilton and D. E. Ingber, Lab Chip, 2012, 12, 2165.
22 P. R. LeDuc, W. C. Messner and J. P. Wikswo, Annu. Rev. Biomed. Eng., 2011, 13, 369.
23 Chemical and Biological Defense Innovations and Technologies, Grants.gov, 12 Dec. 2011. http://www.grants.gov/search/search.do?mode=VIEW&oppId=133833.
24 C. L. Hansen, M. O. A. Sommer and S. R. Quake, Proc. Natl. Acad. Sci. U. S. A., 2004, 101, 14431.
25 C. L. Hansen, Caltech, 2004.
26 R. Yang, M. Zhang and T. J. Tarn, in Life science automation fundamentals and applications, ed. M. Zhang, B. Nelson and R. Felder, Artech House, Norwood, MA, 2007, ch. 6, pp. 153–196.
27 L. Cucullo, N. Marchi, M. Hossain and D. Janigro, J. Cereb. Blood Flow Metab., 2011, 31, 767.
28 R. Booth and H. Kim, Lab Chip, 2012, 12, 1784.
29 A. K. H. Achyuta, A. J. Conway, R. B. Crouse, E. C. Bannister, R. N. Lee, C. P. Katnik, A. A. Behensky, J. Cuevas and S. S. Sundaram, Lab Chip, 2013, 13, 542.
30 L. M. Griep, F. Wolbers, B. de Wagenaar, P. M. ter Braak, B. B. Weksler, I. A. Romero, P. O. Couraud, I. Vermes, A. D. van der Meer and A. van den Berg, Biomed. Microdevices, 2013, 15, 145.
31 B. Prabhakarpandian, M. C. Shen, J. B. Nichols, I. R. Mills, M. Sidoryk-Wegrzynowicz, M. Aschner and K. Pant, Lab Chip, 2013, 13, 1093.
32 Y. Gao, D. Majumdar, B. Jovanovic, C. Shaifer, P. Lin, A. Zijlstra, D. Webb and D. Li, Biomed. Microdevices, 2011, 13, 539.
33 D. Majumdar, Y. Gao, D. Li and D. J. Webb, J. Neurosci. Methods, 2011, 196, 38.
34 J. Park, H. Koito, J. Li and A. Han, Lab Chip, 2012, 12, 3296.
35 M. Shi, D. Majumdar, Y. Gao, B. M. Brewer, C. R. Goodwin, J. A. McLean, D. Li and D. J. Webb, Lab Chip, 2013, DOI: 10.1039/C3LC50249J.
36 S. Herculano-Houzel, P. Ribeiro, L. Campos, A. V. da Silva, L. B. Torres, K. C. Catania and J. H. Kaas, Brain Behav. Evol., 2011, 78, 302.
37 K. Chung, J. Wallace, S. Y. Kim, S. Kalyanasundaram, A. S. Andalman, T. J. Davidson, J. J. Mirzabekov, K. A. Zalocusky, J. Mattis, A. K. Denisin, S. Pak, H. Bernstein, C. Ramakrishnan, L. Grosenick, V. Gradinaru and K. Deisseroth, Nature, 2013, 497, 332.
38 S. Herculano-Houzel, Front. Hum. Neurosci., 2009, 3, Article 31.
39 B. Davies and T. Morris, Pharm. Res., 1993, 10, 1093.
40 S. Herculano-Houzel, PLoS One, 2011, 6, Article e17514.
41 J. Karbowski, BMC Biol., 2007, 5, Article 18.
42 L. Lyck, I. D. Santamaria, B. Pakkenberg, J. Chemnitz, H. D. Schroder, B. Finsen and H. J. G. Gundersen, J. Neurosci. Methods, 2009, 182, 143.
43 P. Kreczmanski, H. Heinsen, V. Mantua, F. Woltersdorf, T. Masson, N. Ulfig, R. Schmidt-Kastner, H. Korr, H. W. M. Steinbusch, P. R. Hof and C. Schmitz, Acta Neuropathol., 2009, 117, 409.
44 A. Armulik, G. Genove and C. Betsholtz, Dev. Cell, 2011, 21, 193.
45 T. M. Mathiisen, K. P. Lehre, N. C. Danbolt and O. P. Ottersen, Glia, 2010, 58, 1094.
46 D. E. Sims, Tissue Cell, 1986, 18, 153.

47 H. Ito, I. Kanno, C. Kato, T. Sasaki, K. Ishii, Y. Ouchi, A. Iida, H. Okazawa, K. Hayashida, N. Tsuyuguchi, K. Ishii, Y. Kuwabara and M. Senda, Eur. J. Nucl. Med. Mol. Imaging, 2004, 31, 635.
48 L. C. Mchenry, N. Engl. J. Med., 1966, 274, 82.
49 L. C. Mchenry, N. Engl. J. Med., 1965, 273, 562.
50 P. Lebrungrandie, J. C. Baron, F. Soussaline, C. Lochh, J. Sastre and M. G. Bousser, Arch. Neurol., 1983, 40, 230.
51 L. Cucullo, M. Hossain, V. Puvenna, N. Marchi and D. Janigro, BMC Neurosci., 2011, 12, 40.
52 A. G. Koutsiaris, S. V. Tachmitzi, N. Batis, M. G. Kotoula, C. H. Karabatsas, E. Tsironi and D. Z. Chatzoulis, Biorheology, 2007, 44, 375.
53 J. M. Tarbell, Cardiovasc. Res., 2010, 87, 320.
54 Y. Tanaka, K. Morishima, T. Shimizu, A. Kikuchi, M. Yamato, T. Okano and T. Kitamori, Lab Chip, 2006, 6, 362.
55 J. Park, I. C. Kim, J. Baek, M. Cha, J. Kim, S. Park, J. Lee and B. Kim, Lab Chip, 2007, 7, 1367.
56 J. C. Nawroth, H. Lee, A. W. Feinberg, C. M. Ripplinger, M. L. McCain, A. Grosberg, J. O. Dabiri and K. K. Parker, Nat. Biotechnol., 2012, 30, 792.
57 E. J. Lee, D. E. Kim, E. U. Azeloglu and K. D. Costa, Tissue Eng. A, 2008, 14, 215.
58 G. A. Giridharan, M. D. Nguyen, R. Estrada, V. Parichehreh, T. Hamid, M. A. Ismahil, S. D. Prabhu and P. Sethu, Anal. Chem., 2010, 82, 7581.
59 I. Banerjee, J. W. Fuseler, R. L. Price, T. K. Borg and T. A. Baudino, Am. J. Physiol. Heart, 2007, 293, H1883.
60 D. L. Brutsaert, Physiol. Rev., 2003, 83, 59.
61 M. Horackova and J. A. Armour, Cardiovasc. Res., 1995, 30, 326.
62 M. Horackova and Z. Byczko, Exp. Cell Res., 1997, 237, 158.
63 M. Horackova, M. H. Huang, J. A. Armour, D. A. Hopkins and C. Mapplebeck, Cardiovasc. Res., 1993, 27, 1101.
64 K. Lemmens, V. F. M. Segers, M. Demolder and G. W. De Keulenaer, J. Biol. Chem., 2006, 281, 19469.
65 T. M. Leucker, M. Bienengraeber, M. Muravyeva, I. Baotic, D. Weihrauch, A. K. Brzezinska, D. C. Warltier, J. R. Kersten and P. F. Pratt, J. Mol. Cell. Cardiol., 2011, 51, 803.
66 Y. H. Hsu, M. L. Moya, P. Abiri, C. C. W. Hughes, S. C. George and A. P. Lee, Lab Chip, 2013, 13, 81.
67 M. L. Moya, Y.-H. Hsu, A. P. Lee, C. C. W. Hughes and S. C. George, Tissue Eng. Pt. C, 2013, DOI: 10.1089/ten.tec.2012.0430.
68 T. G. Papaioannou, E. N. Karatzis, M. Vavuranakis, J. P. Lekakis and C. Stefanadis, Int. J. Cardiol., 2006, 113, 12.
69 W. H. Fissell, J. Kimball, S. M. Mackay, A. Funke and H. D. Humes, Ann. N. Y. Acad. Sci., 2001, 944, 284.
70 H. D. Humes, S. M. Mackay, A. J. Funke and D. A. Buffington, Kidney Int., 1999, 55, 2502.
71 E. M. Wright, Am. J. Physiol. Renal, 2001, 280, F10.
72 S. Abrahams, L. Greenwald and D. L. Stetson, Am. J. Physiol., 1991, 261, R719.
73 C. A. Beuchat, J. Theor. Biol., 1990, 143, 113.
74 R. Greger, Physiol. Rev., 1985, 65, 760.
75 S. Kurbel, K. Dodig and R. Radic, Adv. Physiol. Educ., 2002, 26, 278.
76 C. A. Beuchat, Am. J. Physiol-Reg. I., 1996, 271, R157.
77 J. W. Prothero, Comparative Biochemistry and Physiology Part A: Physiology, 1982, 71, 567.
78 Y. Nahmias, F. Berthiaume and M. L. Yarmush, Adv. Biochem. Eng. Biotechnol., 2007, 103, 309.
79 A. K. Sohlenius-Sternbeck, Toxicol. in Vitro, 2006, 20, 1582.
80 B. D. Foy, A. Rotem, M. Toner, R. G. Tompkins and M. L. Yarmush, Cell. Transplant., 1994, 3, 515.
81 U. J. Balis, K. Behnia, B. Dwarakanath, S. N. Bhatia, S. J. Sullivan, M. L. Yarmush and M. Toner, Metab. Eng., 1999, 1, 49.
82 S. C. Balmert, D. McKeel, F. Triolo, B. Gridelli, K. Zeilinger, R. Bornemann and J. C. Gerlach, Int. J. Artif. Organs, 2011, 34, 410.
83 K. Zeilinger, T. Schreiter, M. Darnell, T. Soderdahl, M. Lubberstedt, B. Dillner, D. Knobeloch, A. K. Nussler, J. C. Gerlach and T. B. Andersson, Tissue Eng., Part C, 2011, 17, 549.
84 J. M. Piret and C. L. Cooney, Biotechnol. Bioeng., 1991, 37, 80.
85 W. G. Whitford and J. J. S. Cadwell, BioProcess Int., 2009, 7, 54.
86 I. Mahmood, J. Pharm. Sci., 2005, 94, 883.
87 T. Lave, S. Dupin, C. Schmitt, R. C. Chou, D. Jaeck and P. Coassolo, J. Pharm. Sci., 1997, 86, 584.
88 Y. Naritomi, S. Terashita, A. Kagayama and Y. Sugiyama, Drug Metab. Dispos., 2003, 31, 580.
89 Y. Naritomi, S. Terashita, S. Kimura, A. Suzuki, A. Kagayama and Y. Sugiyama, Drug Metab. Dispos., 2001, 29, 1316.
90 H. Boxenbaum, J. Pharmacokinet. Biopharm., 1980, 8, 165.
91 D. J. Carlile, K. Zomorodi and J. B. Houston, Drug Metab. Dispos., 1997, 25, 903.
92 G. Ghibellini, L. S. Vasist, E. M. Leslie, W. D. Heizer, R. J. Kowalsky, B. F. Calvo and K. L. R. Brouwer, Clin. Pharmacol. Ther., 2007, 81, 406.
93 R. J. Riley, D. F. McGinnity and R. P. Austin, Drug Metab. Dispos., 2005, 33, 1304.
94 J. S. Miller, K. R. Stevens, M. T. Yang, B. M. Baker, D. H. Nguyen, D. M. Cohen, E. Toro, A. A. Chen, P. A. Galie, X. Yu, R. Chaturvedi, S. N. Bhatia and C. S. Chen, Nat. Mater., 2012, 11, 768.
95 E. R. Weibel, Annu. Rev. Physiol., 1987, 49, 147.
96 C. Hou and M. Mayo, Phys. Rev. E, 2011, 84, 061915.
97 J. D. Crapo, B. E. Barry, P. Gehr, M. Bachofen and E. R. Weibel, Am. Rev. Respir. Dis., 1982, 126, 332.
98 W. A. H. Wallace, M. Gillooly and D. Lamb, Thorax, 1992, 47, 437.
99 A. O. S. Fels and Z. A. Cohn, J. Appl. Physiol., 1986, 60, 353.
100 W. R. Stahl, J. Appl. Physiol., 1967, 22, 453.
101 M. Kjeld and O. Olafsson, Can. J. Zool., 2008, 86, 890.
102 M. F. Brown, T. P. Gratton and J. A. Stuart, Am. J. Physiol-Reg. I., 2007, 292, R2115.
103 Microphysiological Systems, Solicitation no. DARPA-BAA-11-73 FedBizOpps.gov, 11 Sept. 2011. https://www.fbo.gov/index?s=opportunity&mode=form&id=956b160c42aaa386cf5762f12c21be9f&tab=core&_cview=0.
104 G. Chen and A. F. Palmer, Biotechnol. Prog., 2009, 25, 1317.
105 D. R. Spahn, Crit. Care, 1999, 3, R93.
106 M. Yamazaki, R. Aeba, R. Yozu and K. Kobayashi, Circulation, 2006, 114, I220.

107 V. Jager, J. Lehmann and P. Friedl, Cytotechnology, 1988, 1, 319.
108 C. Zhang, Z. Q. Zhao, N. A. A. Rahim, D. van Noort and H. Yu, Lab Chip, 2009, 9, 3185.
109 J. van der Valk, D. Brunner, K. De Smet, A. F. Svenningsen, P. Honegger, L. E. Knudsen, T. Lindl, J. Noraberg, A. Price, M. L. Scarino and G. Gstraunthaler, Toxicol. in Vitro, 2010, 24, 1053.
110 D. Pinkel, Cancer Res., 1958, 18, 853.
111 C. Hall, E. Lueshen, A. Mosat and A. A. Linninger, J. Pharm. Sci., 2012, 101, 1221.
112 V. Sharma and J. H. McNeill, Br. J. Pharmacol., 2009, 157, 907.
113 A. H. Diercks, A. Ozinsky, C. L. Hansen, J. M. Spotts, D. J. Rodriguez and A. Aderem, Anal. Biochem., 2009, 386, 30.
114 L. Jost, Oikos, 2006, 113, 363.
115 C. J. Keylock, Oikos, 2005, 109, 203.
116 D. E. Malarkey, K. Johnson, L. Ryan, G. Boorman and R. R. Maronpot, Toxicol. Pathol., 2005, 33, 27.
117 L. Sherwood, in Human physiology: from cells to systems, Cengage-Brooks/Cole, Belmont, CA, 7th edn, 2010.
118 B. Prabhakarpandian, Y. Wang, A. Rea-Ramsey, S. Sundaram, M. F. Kiani and K. Pant, Microcirculation, 2011, 18, 380.
119 L. A. Hiatt, J. R. McKenzie, L. F. Deravi, R. S. Harry, D. W. Wright and D. W. Cliffel, Biosens. Bioelectron., 2012, 33, 128.
120 J. H. Sung, C. Kam and M. L. Shuler, Lab Chip, 2010, 10, 446.
121 K. Viravaidya and M. L. Shuler, Biotechnol. Prog., 2004, 20, 590.
122 F. D. Sistare and J. J. DeGeorge, Biomarkers Med., 2011, 5, 497.
123 B. Ma, G. Zhang, J. Qin and B. Lin, Lab Chip, 2009, 9, 232.
124 J. P. Wikswo, A. Prokop, F. Baudenbacher, D. Cliffel, B. Csukas and M. Velkovsky, IEE Proc.: Nanobiotechnol., 2006, 153, 81.
125 A. Prokop, Z. Prokop, D. Schaffer, E. Kozlov, J. P. Wikswo, D. Cliffel and F. Baudenbacher, Biomed. Microdevices, 2004, 6, 325.
126 S. Faley, K. Seale, J. Hughey, D. K. Schaffer, S. VanCompernolle, B. McKinney, F. Baudenbacher, D. Unutmaz and J. P. Wikswo, Lab Chip, 2008, 8, 1700.
127 S. L. Faley, M. Copland, D. Wlodkowic, W. Kolch, K. T. Seale, J. P. Wikswo and J. M. Cooper, Lab Chip, 2009, 9, 2659.
128 A. Suzumura, S. Bhat, P. A. Eccleston, R. P. Lisak and D. H. Silberberg, Brain Res., 1984, 324, 379.
129 S. E. Eklund, D. E. Cliffel, E. Kozlov, A. Prokop, J. P. Wikswo Jr and F. J. Baudenbacher, Anal. Chim. Acta, 2003, 496, 93.
130 S. E. Eklund, R. M. Snider, J. Wikswo, F. Baudenbacher, A. Prokop and D. E. Cliffel, J. Electroanal. Chem., 2006, 587, 333.
131 S. E. Eklund, R. G. Thompson, R. M. Snider, C. K. Carney, D. W. Wright, J. Wikswo and D. E. Cliffel, Sensors, 2009, 9,2117.
132 I. A. Ges and F. Baudenbacher, Biosens. Bioelectron., 2010, 26, 828.
133 I. A. Ges and F. Baudenbacher, Biosens. Bioelectron., 2010, 25, 1019.
134 I. A. Ges, I. A. Dzhura and F. J. Baudenbacher, Biomed. Microdevices, 2008, 10, 347.
135 I. A. Ges and F. Baudenbacher, J. Exp. Nanosci., 2008, 3,63.
136 D. Grieshaber, R. MacKenzie, J. Voeroes and E. Reimhult, Sensors, 2008, 8, 1400.
137 M. Ciobanu, D. E. Taylor, J. P. Wilburn and D. E. Cliffel, Anal. Chem., 2008, 80, 2717.
138 J. R. McKenzie, A. M. Palubinsky, J. E. Brown, B. McLaughlin and D. E. Cliffel, ACS Chem. Neurosci., 2012, 3, 510.
139 J. R. Enders, C. C. Marasco, A. Kole, B. Nguyen, S. Sundarapandian, K. T. Seale, J. P. Wikswo and J. A. Mclean, IET Syst. Biol., 2010, 4, 416.
140 J. R. Enders, C. R. Goodwin, C. C. Marasco, K. T. Seale, J.P. Wikswo and J. A. Mclean, Spectroscopy Supp. Curr. Trends Mass Spectrometry, 2011, July, 18.
141 J. R. Enders, C. C. Marasco, J. P. Wikswo and J. A. Mclean, Anal. Chem., 2012, 84, 8467.
142 M. D. Schmidt, R. R. Vallabhajosyula, J. W. Jenkins, J. E. Hood, A.S. Soni, J. P. Wikswo and H. Lipson, Phys. Biol., 2011, 8, 055011.
143 L. G. Griffith and M. A. Swartz, Nat. Rev. Mol. Cell Biol.,2006, 7, 211.
144 D. E. Ingber, Semin. Cancer Biol., 2008, 18, 356.
145 R. Kannan and A. Przekwas, Int. J. Numer. Methods Biomed. Eng., 2011, 27, 13.
146 A. J. Przekwas, M. R. Somayaji and Z. J. Chen, CoBi Tools for model Guided Manufacturing of Biologics from Synthetically Stimulated Biofactories, 2011.
147 A. Bejan and S. Lorente, Phys. Life Rev., 2011, 8, 209.
148 S. Lorente, W. Wechsatol and A. Bejan, Int. J. Heat MassTransfer, 2002, 45, 3299.
149 W. Wechsatol, S. Lorente and A. Bejan, Int. J. Heat MassTransfer, 2002, 45, 4911.
150 A. D. van der Meer and A. van den Berg, Integr. Biol., 2012,4, 461.
151 J. L. Borges and N. T. tr- Di Giovanni, in A Universal History of Infamy, Penguin, London, 1975.
152 L. Carroll, in The complete Sylvie and Bruno, Mercury House, San Francisco, 1991, ch. 11, pp. 262–267.
153 S. Huang and J. Wikswo, in Reviews of Physiology, Biochemistry and Pharmacology, ed. S. G. Amara, E. Bamberg, T. Gudermann, S. C. Hebert, R. Jahn, W. J. Lederer, R. Lill, A. Miyajima and S. Offermanns, 157 edn, 2007, vol. 157, pp. 81-104.

Appendix E: Presentations

1. **Evans BC**, Beamish JA, Marchant RE. *Design, Synthesis, and Characterization of PEGDA hydrogels for tissue engineering applications*. **Accepted Poster:** University Hospitals Medical Center Research Showcase (2009). Nashville, Tennessee, USA.
2. **Evans BC**, Duvall CL. *Development of a novel cell-internalized smart polymer platform for intracellular peptide delivery.* **Accepted Poster:** University of Memphis Biomaterials Day (2011). Memphis, Tennessee, USA.
3. Dunn MF, **Evans BC**, Duvall CL. *Delivery of a MK2 Inhibitor Utilizing Peptide Stapling.* **Accepted Poster:** Vanderbilt Summer Research Symposium (2011). Nashville, Tennessee, USA.
4. Beavers K, Mares J, **Evans BC**, Duvall CL, Weiss S. *Surface functionalization of Porous Silicon Nanoparticles for siRNA Delivery.* **Accepted Poster:** Vanderbilt Nanoscience and Nanotechnology Forum (2011). Nashville, Tennessee, USA.
5. **Evans BC**, Gupta MK, Duvall CL. *Cell-permeant, pH-responsive Nano-carriers for Intracellular Peptide Delivery to Prevent Graft Failure.* **Accepted Poster:** University of Memphis Biomaterials Day (2012). Memphis, Tennessee, USA.
6. **Evans BC**, Gupta MK, Duvall CL. *A novel pH responsive, cell penetrating micelle for intracellular delivery of a peptidic MAPKAP kinase II inhibitor.* **Accepted Poster:** Hilton Head Regenerative Medicine Conference (2012). Hilton Head, South Carolina, USA.
7. **Evans BC**, Hocking KM, Brophy CM, Duvall CL. *Enhanced intracellular peptide delivery with pH-responsive, endosomolytic Nano-polyplexes to prevent intimal hyperplasia in human saphenous vein grafts*. **Accepted oral presentation**: Society for Biomaterials Annual Meeting & Exposition (2013). Boston Massachussettes, USA. **Award:** Drug Delivery SIG Star award honorable mention.
8. **Evans BC**, Hocking KM, Brophy CM, Duvall CL. *MK2 Inhibitory Peptide Delivery with Endosomolytic Nano-Polyplexes Prevents Vasoconstriction and Intimal Hyperplasia in Human Saphenous Vein Bypass Grafts.* **Accepted Poster:** 40th Annual Meeting & Exposition of the Controlled Release Society (CRS), (2013). Honolulu, Hawaii, USA.
9. Beavers KR, Mares JW, **Evans BC**, Weiss SM, Duvall CL. *An improved strategy for the loading, characterization, and controlled delivery of peptide nucleic acid therapies.* **Accepted poster:** Biomedical Engineering Society Annual meeting (2013). Seattle, Washington.
10. **Evans BC**, Hocking KM, Osgood MJ, Voskresensky I, Brophy CM, Duvall CL. *MK2 inhibitory nano-polyplexes prevent intimal hyperplasia ex vivo in human vein and in vivo in a rabbit transplant model.* **Accepted oral presentation:** TERMIS-AM Annual Conference and Exposition (2013) Atlanta, Georgia, USA.
11. **Evans BC**, Hocking KM, Osgood MJ, Voskresensky I, Dmowska J, Brophy CM, Duvall CL. *Nano-polyplexes for enhanced intracellular delivery and retention of a MK2i inhibitory peptide inhibit vascular graft intimal hyperplasia* **Accepted poster:** VISE Annual surgery and engineering symposium (2013) Nashville, TN, USA.
12. Page JM, **Evans BC**, Gupta MK, Guelcher S, Duvall CL. *pH-responsive, hydrolytically degradable nanoparticles for cytosolic drug delivery.* **Accepted Oral Presentation:** Society for Biomaterials Annual Meeting & Exposition (2014). Denver, Colorado, USA.
13. **Evans BC**, Hocking KM, Brophy CM, Duvall CL. *A Novel Platform for Enhanced Intracellular Delivery of Therapeutic Peptides to Promote Tissue Vasorelaxation.* **Accepted Oral Presentation:** Society for Biomaterials Annual Meeting & Exposition (2014). Denver, Colorado, USA.
14. **Evans BC**, Nelson CE, Hocking KM, Brophy CM, Duvall CL. *GrafDefense: Nanopolyplexes for Improving Saphenous Vein Graft Patency.* **Accepted Oral Presentation:** Society for Biomaterials Annual Meeting & Exposition (2014) Business plan Competition. Denver, Colorado, USA.
15. Hocking KM, **Evans BC**, Duvall CL, Brophy CM, Cheung-Flynn J. *Modulation of HSP20 Influences Vasoreactivity independent of [Ca2+]i.* **Accepted Poster:** Atherosclerosis Thrombosis and Vascular Biology (2014). Toronto, Ontario, Canada.
16. **Evans BC**, Hocking KM, Osgood MJ, Voskresensky I, Brophy CM, Duvall CL. *Nano-polyplexes for enhanced intracellular delivery of a MK2 inhibitory peptide inhibit vascular graft intimal hyperplasia.* **Accepted Poster:** Hilton Head Regenerative Medicine Conference (2014). Hilton Head, South Carolina, USA.
17. **Evans BC**, Hocking KM, Brophy CM, Duvall CL. *Electrostatically-complexed, pH-responsive nanoparticles as a platform for intracellular peptide delivery.* **Invited Oral Presentation:** Vanderbilt

Institute of Nanoscale Science and Engineering Summer NanoSeminar (2014). Nashville, Tennessee, USA.

18. **Evans BC**, Hocking KM, Osgood MJ, Voskresensky I,Dmowska J, Brophy CM , Duvall CL. *Nano-polyplex MK2 Inhibitory Peptide Delivery Inhibits Vascular Graft Intimal Hyperplasia.* **Accepted Poster:** Gordon Research Conference: Drug Carriers in Medicine and Biology (2014). Waterville Valley, New Hampshire, USA.
19. **Evans BC**, Hocking KM, Osgood MJ, Voskresensky I,Dmowska J, Brophy CM , Duvall CL. *Nano-polyplex MK2 Inhibitory Peptide Delivery Inhibits Vascular Graft Intimal Hyperplasia.* **Invited Oral Presentation:** Gordon Research Conference: Drug Carriers in Medicine and Biology (2014). Waterville Valley, New Hampshire, USA.
20. **Evans BC**, Hocking KM, Kilchrist KV, Brophy CM, Duvall CL. *A Novel Platform Technology for Cytosolic Peptide Delivery with Endosomolytic Nano-Polyplexes Applied to Vasospasm*. **Accepted Oral Presentation:** University of Kentucky Biomaterials Day (2014). Lexington, KY, USA. **Award:** 3rd Place Student Oral Presentation Competition
21. **Evans BC**, Hocking KM, Osgood MJ, Voskresensky I, Dmowska J, Kilchrist KV, Brophy CM, Duvall CL. *A Novel Platform Technology for Cytosolic Peptide Delivery with Endosomolytic Nano-Polyplexes Applied to Vascular Graft Intimal Hyperplasia*. **Accepted Poster:** Life Science Tennessee Annual Conference & Venture Forum (2014). Nashville, TN, USA.
22. **Evans BC**, Hocking KM, Osgood MJ, Voskresensky I, Dmowska J, Kilchrist KV, Brophy CM, Duvall CL. *A Novel Platform Technology for Cytosolic Peptide Delivery with Endosomolytic Nano-Polyplexes Applied to Vascular Graft Intimal Hyperplasia*. **Accepted Poster:** 15th Annual Vanderbilt Nanoscience and Nanotechnology Forum (2014). Nashville, Tennessee, USA. **Award:** 2nd Place Poster Presentation Competition.
23. **Evans BC**, Hocking KM, Osgood MJ, Voskresensky I, Dmowska J, Kilchrist KV, Brophy CM, Duvall CL. *A Novel Platform Technology for Cytosolic Peptide Delivery with Endosomolytic Nano-Polyplexes Applied to Vascular Graft Intimal Hyperplasia*. **Accepted Poster:** VISE Annual surgery and engineering symposium (2014) Nashville, TN, USA.
24. **Evans BC**, Hocking KM, Osgood MJ, Voskresensky I, Dmowska J, Kilchrist KV, Brophy CM, Duvall CL. *Nano-polyplex MK2 Inhibitory Peptide Delivery Inhibits Vascular Graft Intimal Hyperplasia by Blocking Inflammation and Maintaining the Contractile VSMC Phenotype*. **Submitted Abstract:** 2015 Annual Meeting & Exposition of the Controlled Release Society (CRS). Edinburgh, Scotland.

Appendix F: Patents

1. Duvall CL, **Evans BC**, Brophy CM, Hocking KM. *Polyplexes*. US Patent Application Serial No. PCT/US14/33873 filed April 11, 2014 (VU13109PCT1).

Appendix G: Awards

1. 2nd Place Vanderbilt Nanoscience and Nanotechnology Forum Poster Competition (November 2014)
2. 3rd Place University of Kentucky Biomaterials Day Student Oral Presentation Competition (September 2014)
3. National Science Foundation Graduate Research Fellowship (2012-2015)
4. Drug Delivery SIG Star award honorable mention (SFB Annual meeting 2013).
5. Biomedical Engineering Academic Award (2010 Case Western Reserve University)
6. Biomedical Engineering Honor Society (2009-2010 Case Western Reserve University)
7. Howard Hughes Medical Institute Fellowship (Summer 2009)

REFERENCES

1. Brian C. Evans, K.M.H., Kameron V. Kilchrist, Eri S. Wise, Colleen M. Brophy, Craig L. Duvall., *An Endosomolytic Nano-polyplex Platform Technology for Cytosolic Peptide Delivery Applied to Inhibit Pathological Vasoconstriction.* ACS Nano, 2015.
2. Brian C. Evans, K.M.H., Michael J. Osgood, Igor Voskresensky, Julia Dmowska, Kameron V. Kilchrist, Colleen M. Brophy, Craig L. Duvall., *MK2 Inhibitory Peptide Delivered in Nano-polyplexes Inhibits Vascular Graft Intimal Hyperplasia.* Science Translational Medicine, 2015.
3. Krupnick, A.S., et al., *Orthotopic mouse lung transplantation as experimental methodology to study transplant and tumor biology.* Nat Protoc, 2009. **4**(1): p. 86-93.
4. Li, H., et al., *Delivery of intracellular-acting biologics in pro-apoptotic therapies.* Curr Pharm Des, 2011. **17**(3): p. 293-319.
5. Al-Taei, S., et al., *Intracellular traffic and fate of protein transduction domains HIV-1 TAT peptide and octaarginine. Implications for their utilization as drug delivery vectors.* Bioconjug Chem, 2006. **17**(1): p. 90-100.
6. Belting, M., S. Sandgren, and A. Wittrup, *Nuclear delivery of macromolecules: barriers and carriers.* Adv Drug Deliv Rev, 2005. **57**(4): p. 505-27.
7. Duvall, C.L., et al., *Intracellular delivery of a proapoptotic peptide via conjugation to a RAFT synthesized endosomolytic polymer.* Mol Pharm, 2010. **7**(2): p. 468-76.
8. Flynn, C.R., et al., *Internalization and intracellular trafficking of a PTD-conjugated anti-fibrotic peptide, AZX100, in human dermal keloid fibroblasts.* J Pharm Sci, 2010. **99**(7): p. 3100-21.
9. Chorev, M., et al., *Partially Modified Retro-Inverso-Peptides - Novel Modification of Biologically-Active Peptides.* Federation Proceedings, 1979. **38**(3): p. 363-363.
10. Taylor, J.W., *The synthesis and study of side-chain lactam-bridged peptides.* Biopolymers, 2002. **66**(1): p. 49-75.
11. Kritzer, J.A., *STAPLED PEPTIDES Magic bullets in nature's arsenal.* Nature Chemical Biology, 2010. **6**(8): p. 566-567.
12. Cahill, K., *Cell-penetrating peptides, electroporation and drug delivery.* Iet Systems Biology, 2010. **4**(6): p. 367-378.
13. De Coupade, C., et al., *Novel human-derived cell-penetrating peptides for specific subcellular delivery of therapeutic biomolecules.* Biochemical Journal, 2005. **390**: p. 407-418.
14. Efremov, R.G., et al., *Factors important for fusogenic activity of peptides: molecular modeling study of analogs of fusion peptide of influenza virus hemagglutinin.* Febs Letters, 1999. **462**(1-2): p. 205-210.
15. Ayame, H., N. Morimoto, and K. Akiyoshi, *Self-assembled cationic nanogels for intracellular protein delivery.* Bioconjugate Chemistry, 2008. **19**(4): p. 882-890.
16. Ko, Y.T., C. Falcao, and V.P. Torchilin, *Cationic Liposomes Loaded with Proapoptotic Peptide D-(KLAKLAK)(2) and Bcl-2 Antisense Oligodeoxynucleotide G3139 for Enhanced Anticancer Therapy.* Molecular Pharmaceutics, 2009. **6**(3): p. 971-977.
17. Yamada, Y., et al., *Mitochondrial drug delivery and mitochondrial disease therapy - An approach to liposome-based delivery targeted to mitochondria.* Mitochondrion, 2007. **7**(1-2): p. 63-71.
18. Zhao, P.Q., et al., *Paclitaxel-Loaded, Folic-Acid-Targeted and TAT-Peptide-Conjugated Polymeric Liposomes: In Vitro and In Vivo Evaluation.* Pharmaceutical Research, 2010. **27**(9): p. 1914-1926.
19. El-Sayed, A., et al., *Octaarginine- and octalysine-modified nanoparticles have different modes of endosomal escape.* Journal of Biological Chemistry, 2008. **283**(34): p. 23450-23461.

20. Kuai, R., et al., *Efficient Delivery of Payload into Tumor Cells in a Controlled Manner by TAT and Thiolytic Cleavable PEG Co-Modified Liposomes.* Molecular Pharmaceutics, 2010. **7**(5): p. 1816-1826.
21. Lackey, C.A., et al., *A biomimetic pH-responsive polymer directs endosomal release and intracellular delivery of an endocytosed antibody complex.* Bioconjugate Chemistry, 2002. **13**(5): p. 996-1001.
22. Henry, S.M., et al., *pH-responsive poly(styrene-alt-maleic anhydride) alkylamide copolymers for intracellular drug delivery.* Biomacromolecules, 2006. **7**(8): p. 2407-2414.
23. Murthy, N., et al., *Design and synthesis of pH-responsive polymeric carriers that target uptake and enhance the intracellular delivery of oligonucleotides.* Journal of Controlled Release, 2003. **89**(3): p. 365-74.
24. Li, H.M., et al., *Matrix Metalloproteinase Responsive, Proximity-Activated Targeting Polymeric Nanoparticles for siRNA Delivery to Tumor Metastases.* Molecular Therapy, 2012. **20**: p. S266-S266.
25. Gupta, M.K., et al., *Poly(PS-b-DMA) micelles for reactive oxygen species triggered drug release.* Journal of Controlled Release, 2012. **162**(3): p. 591-598.
26. Go, A.S., et al., *Heart disease and stroke statistics--2013 update: a report from the American Heart Association.* Circulation, 2013. **127**(1): p. e6-e245.
27. Alexander, J.H., et al., *Efficacy and safety of edifoligide, an E2F transcription factor decoy, for prevention of vein graft failure following coronary artery bypass graft surgery: PREVENT IV: a randomized controlled trial.* JAMA, 2005. **294**(19): p. 2446-54.
28. Slomp, J., et al., *Formation of intimal cushions in the ductus arteriosus as a model for vascular intimal thickening. An immunohistochemical study of changes in extracellular matrix components.* Atherosclerosis, 1992. **93**(1-2): p. 25-39.
29. Wallitt, E.J., M. Jevon, and P.I. Hornick, *Therapeutics of vein graft intimal hyperplasia: 100 years on.* Ann Thorac Surg, 2007. **84**(1): p. 317-23.
30. Kent, K.C. and B. Liu, *Intimal hyperplasia--still here after all these years!* Ann Vasc Surg, 2004. **18**(2): p. 135-7.
31. Conte, M.S., et al., *Results of PREVENT III: a multicenter, randomized trial of edifoligide for the prevention of vein graft failure in lower extremity bypass surgery.* J Vasc Surg, 2006. **43**(4): p. 742-751; discussion 751.
32. Saunders, P.C., et al., *Vein graft arterialization causes differential activation of mitogen-activated protein kinases.* J Thorac Cardiovasc Surg, 2004. **127**(5): p. 1276-84.
33. Bakin, A.V., et al., *p38 mitogen-activated protein kinase is required for TGFbeta-mediated fibroblastic transdifferentiation and cell migration.* J Cell Sci, 2002. **115**(Pt 15): p. 3193-206.
34. Hedges, J.C., et al., *A role for p38(MAPK)/HSP27 pathway in smooth muscle cell migration.* J Biol Chem, 1999. **274**(34): p. 24211-9.
35. Rousseau, S., et al., *Inhibition of SAPK2a/p38 prevents hnRNP A0 phosphorylation by MAPKAP-K2 and its interaction with cytokine mRNAs.* EMBO J, 2002. **21**(23): p. 6505-14.
36. Dambach, D.M., *Potential adverse effects associated with inhibition of p38 alpha/beta MAP kinases.* Current Topics in Medicinal Chemistry, 2005. **5**(10): p. 929-939.
37. Engel, K., A. Kotlyarov, and M. Gaestel, *Leptomycin B-sensitive nuclear export of MAPKAP kinase 2 is regulated by phosphorylation.* EMBO J, 1998. **17**(12): p. 3363-71.
38. Chen, H.F., L.D. Xie, and C.S. Xu, *Role of heat shock protein 27 phosphorylation in migration of vascular smooth muscle cells.* Mol Cell Biochem, 2009. **327**(1-2): p. 1-6.
39. Molnar, P., et al., *The cyclic AMP response element-binding protein (CREB) mediates smooth muscle cell proliferation in response to angiotensin II.* J Cell Commun Signal, 2014. **8**(1): p. 29-37.

40. Ward, B., et al., *Design of a bioactive cell-penetrating peptide: when a transduction domain does more than transduce.* Journal of Peptide Science, 2009. **15**(10): p. 668-674.
41. Hayess, K. and R. Benndorf, *Effect of protein kinase inhibitors on activity of mammalian small heat-shock protein (HSP25) kinase.* Biochem Pharmacol, 1997. **53**(9): p. 1239-47.
42. Lopes, L.B., et al., *A novel cell permeant peptide inhibitor of MAPKAP kinase II inhibits intimal hyperplasia in a human saphenous vein organ culture model.* J Vasc Surg, 2010. **52**(6): p. 1596-607.
43. Roger, V.L., et al., *Heart Disease and Stroke Statistics-2012 Update A Report From the American Heart Association.* Circulation, 2012. **125**(1): p. E2-E220.
44. Baek, J.H., S.S. Han, and D.H. Lee, *Native Coronary Artery and Grafted Artery Spasm Just after Coronary Artery Bypass Grafting: A Case Report.* Journal of Korean Medical Science, 2010. **25**(4): p. 641-643.
45. Lorusso, R., et al., *Refractory Spasm of Coronary Arteries and Grafted Conduits After Isolated Coronary Artery Bypass Surgery.* Annals of Thoracic Surgery, 2012. **93**(2): p. 545-551.
46. Keller, K.B. and L. Lemberg, *Prinzmetal's angina.* Am J Crit Care, 2004. **13**(4): p. 350-4.
47. Harding, M.B., et al., *Ergonovine maleate testing during cardiac catheterization: a 10-year perspective in 3,447 patients without significant coronary artery disease or Prinzmetal's variant angina.* J Am Coll Cardiol, 1992. **20**(1): p. 107-11.
48. Sueda, S., et al., *Frequency of provoked coronary spasms in patients undergoing coronary arteriography using a spasm provocation test via intracoronary administration of ergonovine.* Angiology, 2004. **55**(4): p. 403-11.
49. Feigin, V.L., et al., *Risk factors for subarachnoid hemorrhage: an updated systematic review of epidemiological studies.* Stroke, 2005. **36**(12): p. 2773-80.
50. van Gijn, J., R.S. Kerr, and G.J. Rinkel, *Subarachnoid haemorrhage.* Lancet, 2007. **369**(9558): p. 306-18.
51. Kassell, N.F., et al., *Treatment of ischemic deficits from vasospasm with intravascular volume expansion and induced arterial hypertension.* Neurosurgery, 1982. **11**(3): p. 337-43.
52. Dreiza, C.M., et al., *Transducible heat shock protein 20 (HSP20) phosphopeptide alters cytoskeletal dynamics.* FASEB J, 2005. **19**(2): p. 261-3.
53. Guay, J., et al., *Regulation of actin filament dynamics by p38 map kinase-mediated phosphorylation of heat shock protein 27.* Journal of Cell Science, 1997. **110**: p. 357-368.
54. Furnish, E.J., et al., *Treatment with transducible phosphopeptide analogues of the small heat shock-related protein, HSP20, after experimental subarachnoid hemorrhage: prevention and reversal of delayed decreases in cerebral perfusion.* J Neurosurg, 2010. **112**(3): p. 631-9.
55. Flynn, C.R., et al., *Transduction of phosphorylated heat shock-related protein 20, HSP20, prevents vasospasm of human umbilical artery smooth muscle.* Journal of Applied Physiology, 2005. **98**(5): p. 1836-1845.
56. Muto, A., et al., *Inhibition of Mitogen Activated Protein Kinase Activated Protein Kinase II with MMI-0100 reduces intimal hyperplasia ex vivo and in vivo.* Vascul Pharmacol, 2012. **56**(1-2): p. 47-55.
57. Patel, L.N., J.L. Zaro, and W.C. Shen, *Cell penetrating peptides: Intracellular pathways and pharmaceutical perspectives.* Pharmaceutical Research, 2007. **24**(11): p. 1977-1992.
58. El-Sayed, A., S. Futaki, and H. Harashima, *Delivery of Macromolecules Using Arginine-Rich Cell-Penetrating Peptides: Ways to Overcome Endosomal Entrapment.* Aaps Journal, 2009. **11**(1): p. 13-22.
59. Frankel, A.D. and C.O. Pabo, *Cellular Uptake of the Tat Protein from Human Immunodeficiency Virus.* Cell, 1988. **55**(6): p. 1189-1193.

60. Elliott, G. and P. O'Hare, *Intercellular trafficking and protein delivery by a herpesvirus structural protein.* Cell, 1997. **88**(2): p. 223-33.
61. Fuchs, S.M. and R.T. Raines, *Pathway for polyarginine entry into mammalian cell.* Biochemistry, 2004. **43**(9): p. 2438-2444.
62. Kyriakides, T.R., et al., *pH-sensitive polymers that enhance intracellular drug delivery in vivo.* Journal of Controlled Release, 2002. **78**(1-3): p. 295-303.
63. Lackey, C.A., et al., *Hemolytic activity of pH-responsive polymer-streptavidin bioconjugates.* Bioconjugate Chemistry, 1999. **10**(3): p. 401-405.
64. Convertine, A.J., et al., *Development of a novel endosomolytic diblock copolymer for siRNA delivery.* Journal of Controlled Release, 2009. **133**(3): p. 221-229.
65. Li, H.M., et al., *Matrix Metalloproteinase Responsive, Proximity-Activated Polymeric Nanoparticles for siRNA Delivery.* Advanced Functional Materials, 2013. **23**(24): p. 3040-3052.
66. Thomas, J. and D.A. Tirrell, *Polyelectrolye-sensitized phospholipid vesicles.* Accounts of Chemical Research, 1992. **25**: p. 336-342.
67. Thomas, J.L., S.W. Barton, and D.A. Tirrell, *Membrane solubilization by a hydrophobic polyelectrolyte: surface activity and membrane binding.* Biophys J, 1994. **67**(3): p. 1101-6.
68. Kyriakides, T.R., et al., *pH-sensitive polymers that enhance intracellular drug delivery in vivo.* J Control Release, 2002. **78**(1-3): p. 295-303.
69. Murthy, N., et al., *The design and synthesis of polymers for eukaryotic membrane disruption.* J Control Release, 1999. **61**(1-2): p. 137-43.
70. Shi, L.B., et al., *Heterogeneity in ATP-dependent acidification in endocytic vesicles from kidney proximal tubule. Measurement of pH in individual endocytic vesicles in a cell-free system.* Biophysical journal, 1991. **59**(6): p. 1208-17.
71. Van Dyke, R.W., *Na+/H+ exchange modulates acidification of early rat liver endocytic vesicles.* The American journal of physiology, 1995. **269**(4 Pt 1): p. C943-54.
72. Yamashiro, D.J., S.R. Fluss, and F.R. Maxfield, *Acidification of endocytic vesicles by an ATP-dependent proton pump.* The Journal of cell biology, 1983. **97**(3): p. 929-34.
73. Moad, G., et al., *Advances in RAFT polymerization: the synthesis of polymers with defined end-groups.* Polymer, 2005. **46**(19): p. 8458-8468.
74. Ferrito M, T.D., *Poly(2-ethylacrylic acid).* Macromol Synth, 1992(11): p. 59-62.
75. Evans, B.C., Nelson, C. E., Yu, S. S., Beavers, K. R., Kim, A. J., Li, H., et al., *Ex Vivo Red Blood Cell Hemolysis Assay for the Evaluation of pH-responsive Endosomolytic Agents for Cytosolic Delivery of Biomacromolecular Drugs.* J. Vis. Exp., 2013. **(73)**.
76. San Martin, A., et al., *Dual regulation of cofilin activity by LIM kinase and Slingshot-1L phosphatase controls platelet-derived growth factor-induced migration of human aortic smooth muscle cells.* Circ Res, 2008. **102**(4): p. 432-8.
77. Murthy, N., et al., *The design and synthesis of polymers for eukaryotic membrane disruption.* Journal of Controlled Release, 1999. **61**(1-2): p. 137-143.
78. Foster, S., et al., *Intracellular delivery of a protein antigen with an endosomal-releasing polymer enhances CD8 T-cell production and prophylactic vaccine efficacy.* Bioconjug Chem, 2010. **21**(12): p. 2205-12.
79. Edwards, D.C., et al., *Activation of LIM-kinase by Pak1 couples Rac/Cdc42 GTPase signalling to actin cytoskeletal dynamics.* Nat Cell Biol, 1999. **1**(5): p. 253-9.
80. Kapopara, P.R., et al., *Deficiency of MAPK-activated protein kinase 2 (MK2) prevents adverse remodelling and promotes endothelial healing after arterial injury.* Thromb Haemost, 2014. **112**(6): p. 1264-76.
81. Bitler, B.G. and J.A. Schroeder, *Anti-cancer therapies that utilize cell penetrating peptides.* Recent Pat Anticancer Drug Discov, 2010. **5**(2): p. 99-108.

82. Heitz, F., M.C. Morris, and G. Divita, *Twenty years of cell-penetrating peptides: from molecular mechanisms to therapeutics.* British Journal of Pharmacology, 2009. **157**(2): p. 195-206.
83. Wadia, J.S. and S.F. Dowdy, *Protein transduction technology.* Curr Opin Biotechnol, 2002. **13**(1): p. 52-6.
84. Madani, F., et al., *Mechanisms of cellular uptake of cell-penetrating peptides.* J Biophys, 2011. **2011**: p. 414729.
85. Bolte, S. and F.P. Cordelieres, *A guided tour into subcellular colocalization analysis in light microscopy.* Journal of Microscopy-Oxford, 2006. **224**: p. 213-232.
86. Humphries, W.H.t. and C.K. Payne, *Imaging lysosomal enzyme activity in live cells using self-quenched substrates.* Anal Biochem, 2012. **424**(2): p. 178-83.
87. Ruttekolk, I.R., et al., *The Intracellular Pharmacokinetics of Terminally Capped Peptides.* Molecular Pharmaceutics, 2012. **9**(5): p. 1077-1086.
88. Taniyama, Y., et al., *Role of p38 MAPK and MAPKAPK-2 in angiotensin II-induced Akt activation in vascular smooth muscle cells.* American Journal of Physiology-Cell Physiology, 2004. **287**(2): p. C494-C499.
89. Ronkina, N., et al., *The mitogen-activated protein kinase (MAPK)-activated protein kinases MK2 and MK3 cooperate in stimulation of tumor necrosis factor biosynthesis and stabilization of p38 MAPK.* Molecular and Cellular Biology, 2007. **27**(1): p. 170-181.
90. Zarubin, T. and J.H. Han, *Activation and signaling of the p38 MAP kinase pathway.* Cell Research, 2005. **15**(1): p. 11-18.
91. Kalra, M. and V.M. Miller, *Early remodeling of saphenous vein grafts: proliferation, migration and apoptosis of adventitial and medial cells occur simultaneously with changes in graft diameter and blood flow.* J Vasc Res, 2000. **37**(6): p. 576-84.
92. Stark, V.K., et al., *Monocyte chemotactic protein-1 expression is associated with the development of vein graft intimal hyperplasia.* Arteriosclerosis Thrombosis and Vascular Biology, 1997. **17**(8): p. 1614-1621.
93. Richard, J.P., et al., *Cellular uptake of unconjugated TAT peptide involves clathrin-dependent endocytosis and heparan sulfate receptors.* J Biol Chem, 2005. **280**(15): p. 15300-6.
94. Nelson, C.E., et al., *Balancing Cationic and Hydrophobic Content of PEGylated siRNA Polyplexes Enhances Endosome Escape, Stability, Blood Circulation Time, and Bioactivity in Vivo.* ACS Nano, 2013. **7**(10): p. 8870-80.
95. Mietus-Snyder, M., et al., *Regulation of scavenger receptor expression in smooth muscle cells by protein kinase C: a role for oxidative stress.* Arterioscler Thromb Vasc Biol, 1997. **17**(5): p. 969-78.
96. Li, H., M.W. Freeman, and P. Libby, *Regulation of smooth muscle cell scavenger receptor expression in vivo by atherogenic diets and in vitro by cytokines.* J Clin Invest, 1995. **95**(1): p. 122-33.
97. Saric, T., C.I. Graef, and A.L. Goldberg, *Pathway for degradation of peptides generated by proteasomes - A key role for thimet oligopeptidase and other metallopeptidases.* Journal of Biological Chemistry, 2004. **279**(45): p. 46723-46732.
98. Motwani, J.G. and E.J. Topol, *Aortocoronary saphenous vein graft disease: pathogenesis, predisposition, and prevention.* Circulation, 1998. **97**(9): p. 916-31.
99. Zhang, L., et al., *Graft-extrinsic cells predominate in vein graft arterialization.* Arterioscler Thromb Vasc Biol, 2004. **24**(3): p. 470-6.
100. Cooley, B.C., et al., *TGF-beta Signaling Mediates Endothelial-to-Mesenchymal Transition (EndMT) During Vein Graft Remodeling.* Science Translational Medicine, 2014. **6**(227).
101. Whitehead, K.A., et al., *In vitro-in vivo translation of lipid nanoparticles for hepatocellular siRNA delivery.* ACS Nano, 2012. **6**(8): p. 6922-9.

102. Ruifrok, A.C. and D.A. Johnston, *Quantification of histochemical staining by color deconvolution.* Anal Quant Cytol Histol, 2001. **23**(4): p. 291-9.
103. Jiang, Z., et al., *A novel vein graft model: adaptation to differential flow environments.* Am J Physiol Heart Circ Physiol, 2004. **286**(1): p. H240-5.
104. Hitti, E., et al., *Mitogen-activated protein kinase-activated protein kinase 2 regulates tumor necrosis factor mRNA stability and translation mainly by altering tristetraprolin expression, stability, and binding to adenine/uridine-rich element.* Mol Cell Biol, 2006. **26**(6): p. 2399-407.
105. Ronkina, N., et al., *MAPKAP kinases MK2 and MK3 in inflammation: complex regulation of TNF biosynthesis via expression and phosphorylation of tristetraprolin.* Biochem Pharmacol, 2010. **80**(12): p. 1915-20.
106. Rensen, S.S., P.A. Doevendans, and G.J. van Eys, *Regulation and characteristics of vascular smooth muscle cell phenotypic diversity.* Netherlands Heart Journal, 2007. **15**(3): p. 100-8.
107. Ono, H., et al., *cAMP-response element-binding protein mediates tumor necrosis factor-alpha-induced vascular smooth muscle cell migration.* Arteriosclerosis Thrombosis and Vascular Biology, 2004. **24**(9): p. 1634-1639.
108. Huang, Z.S., et al., *Differential gene expression in vein graft endothelial and smooth muscle cells isolated by laser capture microdissection.* Journal of the American College of Surgeons, 2009. **209**(3): p. S137-S137.
109. Staal, F.J.T., et al., *DNA microarrays for comparison of gene expression profiles between diagnosis and relapse in precursor-B acute lymphoblastic leukemia: choice of technique and purification influence the identification of potential diagnostic markers (vol 17, pg 1324, 2003).* Leukemia, 2004. **18**(5): p. 1041-1041.
110. Beamish, J.A., et al., *Molecular regulation of contractile smooth muscle cell phenotype: implications for vascular tissue engineering.* Tissue Eng Part B Rev, 2010. **16**(5): p. 467-91.
111. Schleimer, K., et al., *Training a sophisticated microsurgical technique: interposition of external jugular vein graft in the common carotid artery in rats.* J Vis Exp, 2012(69).
112. Rensen, S.S.M., P.A.F.M. Doevendans, and G.J.J.M. van Eys, *Regulation and characteristics of vascular smooth muscle cell phenotypic diversity.* Netherlands Heart Journal, 2007. **15**(3): p. 100-108.
113. Mueller, L., et al., *TNF-alpha similarly induces IL-6 and MCP-1 in fibroblasts from colorectal liver metastases and normal liver fibroblasts.* Biochem Biophys Res Commun, 2010. **397**(3): p. 586-91.
114. Mitchell, R.N. and P. Libby, *Vascular remodeling in transplant vasculopathy.* Circ Res, 2007. **100**(7): p. 967-78.
115. Zwolak, R.M., M.C. Adams, and A.W. Clowes, *Kinetics of vein graft hyperplasia: association with tangential stress.* J Vasc Surg, 1987. **5**(1): p. 126-36.
116. Reusch, J.E., *Beyond phosphorylation: nuclear export in vascular remodeling.* Arterioscler Thromb Vasc Biol, 2011. **31**(9): p. 1955-6.
117. Dambach, D.M., *Potential adverse effects associated with inhibition of p38alpha/beta MAP kinases.* Current Topics in Medicinal Chemistry, 2005. **5**(10): p. 929-39.
118. Pichon, S., M. Bryckaert, and E. Berrou, *Control of actin dynamics by p38 MAP kinase - Hsp27 distribution in the lamellipodium of smooth muscle cells.* Journal of Cell Science, 2004. **117**(12): p. 2569-2577.
119. Chen, L., et al., *Differential targeting of prosurvival Bcl-2 proteins by their BH3-only ligands allows complementary apoptotic function.* Mol Cell, 2005. **17**(3): p. 393-403.
120. Dharap, S.S. and T. Minko, *Targeted proapoptotic LHRH-BH3 peptide.* Pharmaceutical Research, 2003. **20**(6): p. 889-96.
121. Ellerby, H.M., et al., *Anti-cancer activity of targeted pro-apoptotic peptides.* Nat Med, 1999. **5**(9): p. 1032-8.

122. Finnegan, N.M., et al., *Induction of apoptosis in prostate carcinoma cells by BH3 peptides which inhibit Bak/Bcl-2 interactions.* Br J Cancer, 2001. **85**(1): p. 115-21.
123. Holinger, E.P., T. Chittenden, and R.J. Lutz, *Bak BH3 peptides antagonize Bcl-xL function and induce apoptosis through cytochrome c-independent activation of caspases.* Journal of Biological Chemistry, 1999. **274**(19): p. 13298-304.
124. Lopes, L.B., et al., *Inhibition of HSP27 phosphorylation by a cell-permeant MAPKAP Kinase 2 inhibitor.* Biochemical and Biophysical Research Communications, 2009. **382**(3): p. 535-539.
125. Lopes, L.B., et al., *Enhanced skin penetration of P20 phosphopeptide using protein transduction domains.* European Journal of Pharmaceutics and Biopharmaceutics, 2008. **68**(2): p. 441-445.
126. Shroff, E.H., et al., *BH3 peptides induce mitochondrial fission and cell death independent of BAX/BAK.* PLoS One, 2009. **4**(5): p. e5646.
127. Ferrito, M.a.T., D. A., *Poly(2-ethylacrylic acid).* Macromolecular Syntheses, 1992. **11**: p. 59-62.
128. Convertine, A.J., et al., *Development of a novel endosomolytic diblock copolymer for siRNA delivery.* Journal of Controlled Release, 2009. **133**(3): p. 221-9.
129. Elosegui-Artola, A., et al., *Image Analysis for the Quantitative Comparison of Stress Fibers and Focal Adhesions.* PLoS One, 2014. **9**(9).
130. Liu, X.Y. and F. Fagotto, *A Method to Separate Nuclear, Cytosolic, and Membrane-Associated Signaling Molecules in Cultured Cells.* Science Signaling, 2011. **4**(203).
131. Hocking, K.M., et al., *Detrimental effects of mechanical stretch on smooth muscle function in saphenous veins.* Journal of Vascular Surgery, 2011. **53**(2): p. 454-460.
132. Jaiswal, J.K., N.W. Andrews, and S.M. Simon, *Membrane proximal lysosomes are the major vesicles responsible for calcium-dependent exocytosis in nonsecretory cells.* Journal of Cell Biology, 2002. **159**(4): p. 625-635.
133. Hevey, R. and C.C. Ling, *Global financial challenge: opportunities for strengthening R&D research in targeted drug delivery.* Future Medicinal Chemistry, 2012. **4**(1): p. 1-5.
134. Wang, C.J., et al., *Alteration of basilar artery rho-kinase and soluble guanylyl cyclase protein expression in a rat model of cerebral vasospasm following subarachnoid hemorrhage.* Biomed Res Int, 2014. **2014**: p. 531508.
135. Merdan, T., et al., *PEGylation of poly(ethylene imine) affects stability of complexes with plasmid DNA under in vivo conditions in a dose-dependent manner after intravenous injection into mice.* Bioconjug Chem, 2005. **16**(4): p. 785-92.
136. Lin, N., et al., *A novel system enhancing the endosomal escapes of peptides promotes Bak BH3 peptide inducing apoptosis in lung cancer A549 cells.* Target Oncol, 2013.
137. Holm, T., et al., *Studying the uptake of cell-penetrating peptides.* Nat Protoc, 2006. **1**(2): p. 1001-5.
138. Saha, K., et al., *Surface functionality of nanoparticles determines cellular uptake mechanisms in mammalian cells.* Small, 2013. **9**(2): p. 300-5.
139. Vranic, S., et al., *Deciphering the mechanisms of cellular uptake of engineered nanoparticles by accurate evaluation of internalization using imaging flow cytometry.* Part Fibre Toxicol, 2013. **10**: p. 2.
140. Frohlich, E., *The role of surface charge in cellular uptake and cytotoxicity of medical nanoparticles.* Int J Nanomedicine, 2012. **7**: p. 5577-91.
141. Yue, Z.G., et al., *Surface charge affects cellular uptake and intracellular trafficking of chitosan-based nanoparticles.* Biomacromolecules, 2011. **12**(7): p. 2440-6.
142. Gratton, S.E., et al., *The effect of particle design on cellular internalization pathways.* Proc Natl Acad Sci U S A, 2008. **105**(33): p. 11613-8.
143. Selinka, H.C., T. Giroglou, and M. Sapp, *Analysis of the infectious entry pathway of human papillomavirus type 33 pseudovirions.* Virology, 2002. **299**(2): p. 279-287.

144. Doherty, G.J. and H.T. McMahon, *Mechanisms of endocytosis.* Annu Rev Biochem, 2009. **78**: p. 857-902.
145. Tsubamoto, Y., et al., *Dextran sulfate, a competitive inhibitor for scavenger receptor, prevents the progression of atherosclerosis in Watanabe heritable hyperlipidemic rabbits.* Atherosclerosis, 1994. **106**(1): p. 43-50.
146. Lysko, P.G., et al., *Identification of a small-molecule, nonpeptide macrophage scavenger receptor antagonist.* J Pharmacol Exp Ther, 1999. **289**(3): p. 1277-85.
147. Stephen, S.L., et al., *Scavenger receptors and their potential as therapeutic targets in the treatment of cardiovascular disease.* Int J Hypertens, 2010. **2010**: p. 646929.
148. Garcia-Arguinzonis, M., et al., *Low-density lipoproteins induce heat shock protein 27 dephosphorylation, oligomerization, and subcellular relocalization in human vascular smooth muscle cells.* Arterioscler Thromb Vasc Biol, 2010. **30**(6): p. 1212-9.
149. Zhao, W., et al., *Tristetraprolin regulates interleukin-6 expression through p38 MAPK-dependent affinity changes with mRNA 3' untranslated region.* J Interferon Cytokine Res, 2011. **31**(8): p. 629-37.
150. Rousseau, S., et al., *Inhibition of SAPK2a/p38 prevents hnRNP A0 phosphorylation by MAPKAP-K2 and its interaction with cytokine mRNAs.* EMBO J, 2002. **21**(23): p. 6505-6514.
151. Kobayashi, M., et al., *MAPKAPK-2-mediated LIM-kinase activation is critical for VEGF-induced actin remodeling and cell migration.* EMBO J, 2006. **25**(4): p. 713-26.
152. Cheng, J.C., R.D. Vigil, and R.O. Fox, *A competitive aggregation model for flash nanoprecipitation.* J Colloid Interface Sci, 2010. **351**(2): p. 330-42.
153. Han, J., et al., *A simple confined impingement jets mixer for flash nanoprecipitation.* J Pharm Sci, 2012. **101**(10): p. 4018-23.
154. Margulis, K., et al., *Formation of curcumin nanoparticles by flash nanoprecipitation from emulsions.* J Colloid Interface Sci, 2014. **434**: p. 65-70.
155. Pustulka, K.M., et al., *Flash nanoprecipitation: particle structure and stability.* Mol Pharm, 2013. **10**(11): p. 4367-77.
156. Zhu, Z., *Flash nanoprecipitation: prediction and enhancement of particle stability via drug structure.* Mol Pharm, 2014. **11**(3): p. 776-86.
157. Zhu, Z., et al., *Polyelectrolyte stabilized drug nanoparticles via flash nanoprecipitation: a model study with beta-carotene.* J Pharm Sci, 2010. **99**(10): p. 4295-306.